Mixed Valent Metal Pincer Complexes and Reactivity of Metal Complexes of Extended Pincer Ligands

Jeewantha Sampath Hewage
Marquette University

MIXED VALENT METAL PINCER COMPLEXES AND REACTIVITY OF METAL COMPLEXES OF EXTENDED PINCER LIGANDS

by

Jeewantha S. Hewage, B.Sc., M.Sc.

A Dissertation submitted to the Faculty of the Graduate School,
Marquette University,
in Partial Fulfillment of the Requirements for
the Degree of Doctor of Philosophy

Milwaukee, Wisconsin

December 2015

ABSTRACT

MIXED VALENT METAL PINCER COMPLEXES AND REACTIVITY OF METAL COMPLEXES OF EXTENDED PINCER LIGANDS

Jeewantha S. Hewage, B.Sc., M.Sc.

Marquette University, 2015

Historically, the study of mixed valence complexes has been critical for advancing our understanding of electron transfer processes in biological and abiological systems. The recent use of mixed valence complexes in electrochromic materials, and the promise of their use in future technological or molecular electronic applications, has spurred further interest in this class of compound. Previous studies by our research group have shown that gallium(III) or tricarbonylrhenium(I) complexes of pincer-type ligands with diarylamido anchors and either pyrazol-1-yl (pz) or diarylphosphino (PAr_2) flanking donors are electroactive species with quasi reversible ligand-centered oxidations. Moreover, the one-electron oxidized derivative with pz flankers, $[Ga(L)(L^{+})]^{2+}$ was found by both spectroscopic and electrochemical means to be a Robin Day Class II species with weak electronic communication occurring between pincers across the main group metal bridge. Cursory electrochemical studies suggested that stronger interactions occurred on replacing gallium(III) with other metal centers. This dissertation elaborates on these initial, prior, findings by describing more detailed synthetic protocol to various $[M(L)_2]^{n+}$ complexes where M = Ni, Co, Rh, Ir, n = 0-3 (depending on M), and where L has different organic groups decorating the periphery. Electrochemical measurements and in-depth spectroscopic analyses of oxidized and reduced forms of the complexes were used to better quantify the effects of metal and ligand substitution on their electronic properties including the extent of electronic communication in mixed valence derivatives. Another goal of the work was to prepare in multimetallic pincer complexes via both covalent and self-assembly approaches and study their electronic properties. Thus, the preparation and properties of $[Re(CO)_3]_2(\mu\text{-L-L})$ with dinucleating pincers (L-L) is described. Initial successes and difficulties with the preparation and characterization of coordination networks based on these pincers and those with different Lewis donors at the *para*- aryl position are outlined next. Finally, 'Extended Pincers' (EP), ligands comprised of an N,N'-diarylformamidinate anchor with flanking pz and/or PAr_2 *ortho*-aryl donors were prepared since they should support multimetallic complexes with unusual metal-metal bonds or reactivity due to proximity of the metal centers. Their group 1 and group 11 metal complexes may serve as useful reagents for future chemistry.

ACKNOWLEDGEMENTS

Jeewantha S. Hewage, B.Sc., M.Sc.

I take immense pleasure in thanking my advisor, Professor James R. Gardinier, for his guidance, help, patience, and time through my entire period of graduate studies at Marquette University. Without his close guidance, I would not have completed my graduate studies. It is a great privilege for me to work under such an elite professor. I would like to thank my graduate advisory committee Professor Rajendra Rathore, Professor Chae S. Yi, and Professor Adam Fiedler for being a part of my graduate committee and being so generous in devoting their valuable time for my success.

I would like to thank the Gardinier research group for their invaluable support. My acknowledgement would be incomplete without a word to Dr. Sarath Wanniarachchi. I am utterly grateful for him sharing his knowledge and prior experience throughout the research, which made the uphill battle much easier. I would also like to thank Alexander Treleven for his valuable academic discussions.

I am also grateful to the Department of Chemistry for providing me unrestricted facilities during my entire course of study. I take this opportunity to thank all the professors in the Department of Chemistry who directly or indirectly contributed to my academic progress. I would like to convey my sincere gratitude to Dr. Sergey V. Lindeman who provided X-ray crystallography experiments, Dr. Sheng Cai for helping special NMR experiments and Dr. Brien Bennett for EPR spectroscopy guidance. Also I would like to thank the Graduate School and the Marquette University administration.

Finally, my humble gratitude to my parents and my wife, Manjula, for being excessively supportive and standing by me at every step of the way. I also credit my son, Sandila, and daughter, Sanuli, for inspiring me every day. This whole journey would not have been possible without your love and support.

TABLE OF CONTENTS

LIST OF TABLES

LIST OF FIGURES

LIST OF SCHEMES

CHAPTER 1

INTRODUCTION

1.1. Conductive Metal Organic Frameworks.

Porous, crystalline, metal-organic frameworks (MOFs) have gained substantial interest in the past few decades as promising candidates for gas sorption, separation, storage and catalytic applications.[1-7] Many research groups have dedicated resources in finding means to increase porosity or selectivity in gas sorption and reactivities. There has been a very recent push for conducting and semiconducting MOFs because such materials would allow for incorporation into devices technology or even the design of new photocatalysts for alternative energy conversions.[8-19]

Traditionally MOFs are electrically insulating and means to increase electric conductivity by incorporation of ions or chemical oxidants often sacrifice porosity or structural integrity, thus there are inherent challenges in this pursuit. A successful strategy for electrically conductive or semi conductive MOFs is to incorporate redox active groups as part of the organic framework that allows an efficient pathway for hole or electron hopping. Despite the field's infancy, a number of groups recently demonstrated various strategies to make conducting MOFs with permanent porosity. Dinca and co-workers have recently reported that tetrathiafulvalene-tetrabenzoate (H_4TTFTB) assembled MOF with $Zn(NO_3)_2$ (Figure 1.1) exhibits charge mobility commensurate with some of the best organic semiconductors and confirmed conductivity measurements.[8] The carboxylate donor groups coordinated to Zn^{2+} to make the MOF, and

π-stacking of the TTFTB units facilitate charge mobility through space. They have further shown that the electrical conductivity of this MOF can be tuned by changing the metal ion.

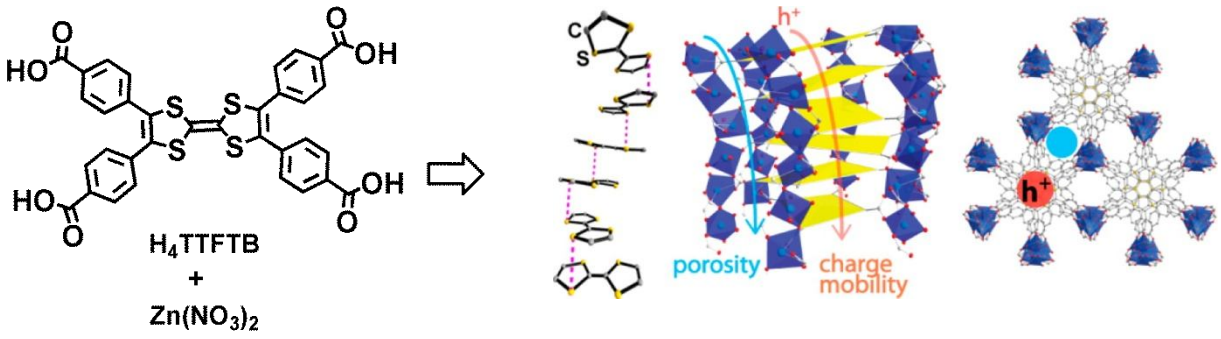

Figure 1.1. Left: Structure of redox active tetrathiafulvalene-tetrabenzoate ligand (H_4TTFTB), Right: Side view of TTF stack, charge mobility and a view down the c axis from ref. 8.

Allendorf and co-workers have reported a $Cu_3(BTC)_2$ (BTC : benzene-1,3,5-tricarboxylic acid) derived conductive MOF, which is air stable.[10] Alvaro et al. reported that a MOF prepared by coordination of Zn_4O nodes with terephthalate linkers behaves as a semiconductor.[9] A secondary challenge for many conducting MOFs suitable for alternative energy schemes is that most of the MOFs are made of hydrolytically unstable metal carboxylate linkages. Means to improve hydrolytic stability have been explored but generally limited to few metal $Fe(O_2C)_n$ nodes. Thus there is an impetus to find new motifs that will improve hydrolytic stability to MOF structures, and at the same time impart desired reactivity or electronic properties to the materials.

It is well known that metal pincer complexes exhibit remarkable stability as a result of the terdentate nature of the ligand. Furthermore, many pincer complexes also

exhibit remarkable reaction chemistry by supporting low coordination number metal centers, by chemical non innocence (metal ligand cooperativity) or by tunable redox behavior. This established behavior prompted an exploration into the possibility of constructing MOFs that incorporate metal pincers as either part of a linear, node, or both. For the development of conducting polymers and MOFs, a hypothetical structure such as Figure 1.2, was envisioned.

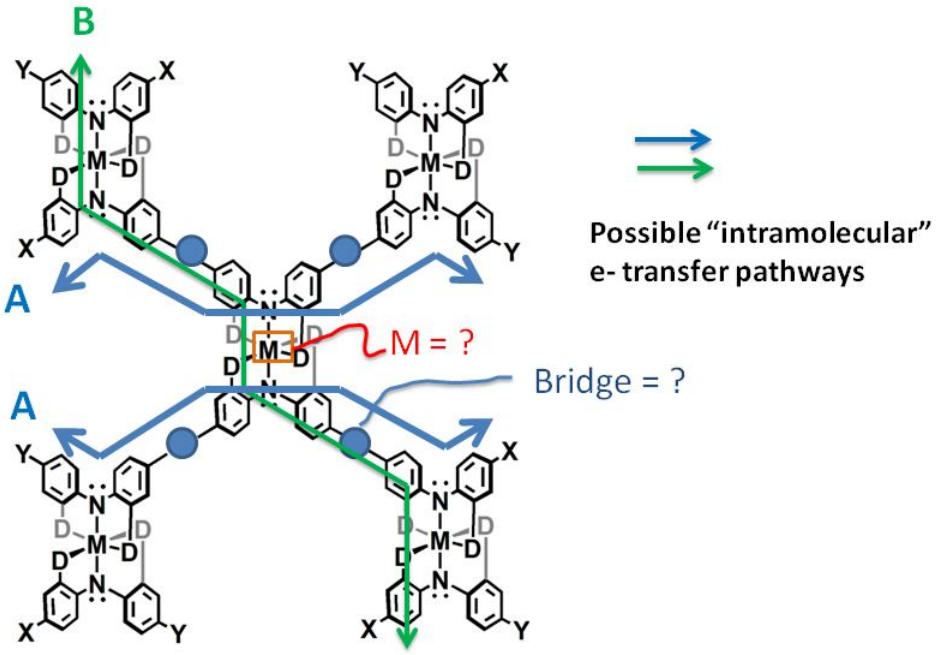

Figure 1.2. Proposed coordination polymer of redox active metal pincer complexes.

Here the metal pincer with redox active diarylamido units would serve as the node and the spacer bridge could be verified to have either redox properties, void spaces, or both. In this way one might anticipate e^- or $hole^+$ transfer could occur along polymer chain A (Figure 1.2). However, it was unknown whether it would also be possible to have electronic pathways across N-M-N units as in path B, Figure 1.2. Thus this study set out

to test such possibilities by synthesizing individual fragments and examining their properties. The aim was to evaluate the strength of electronic communication across various bridges or nodes by methods outlined in the next section. Then, studies on making assembles of pincer complexes such as in Figure 1.2 were explored.

1.2. Mixed Valence Compounds.

Mixed valence (MV) compounds are typically chemical species which have two or more otherwise identical redox centers with different oxidation states. These compounds were recognized by scientists several decades ago as the colorful compounds that were used as pigments in artworks (Prussian blue, PB: $Fe^{III}[Fe^{III}Fe^{II}(CN)_{6\cdot}xH_2O]$). The color results from an intervalence electron transfer process of these MV compounds which absorb energy from the visible light. Thus, the blue color of PB results from charge transfer arising from e^- transfer between Fe^{II}/Fe^{III} sites. More recently, MV compounds have gained increased attention in the study of electron transfer (ET) processes, which are fundamental to most chemical and biological systems.[20-26] A recent trend of using redox active molecules as the basis for materials in electronic devices has accelerated this attention among scientists.[27-38] As a consequence, the study of electronic communication between redox centers (in MV compounds) provides a sound foundation for building future molecular wires or other electronic materials.

The role model for MV compounds is the well known Creutz-Taube ion $[(NH_3)_5(\mu\text{-pyz})Ru(NH_3)_5]^{5+}$ (Figure 1.3.a), metals that are formally in the +2 and +3 oxidation states, linked by a pyrazine ligand.[39,40] The odd electron transverses the bridging organic ligand but unevenly occupies both metal sites over time.[41] The discovery of this complex initiated investigation of other mixed valence complexes for

fundamental studies. The efficiency of charge delocalization in MV compounds is mainly dependent on the nature of the bridging ligand. If the bridge can facilitate good electronic communication between two metal ions, the charge would be fully delocalized over the entire molecule. In 1990, Reimers and Hush investigated the effect of the bridge on the electronic communication, using different oligovinyl-linked dipyridyl bridges shown in Figure 1.3.b.[42] There was electronic communication between the two metal ions over the bridge proven by spectroscopic, electrochemical, and theoretical studies. The strength was highly dependent on the length of the bridge, a moderate communication for n = 0 to a weak communication for n = 3.

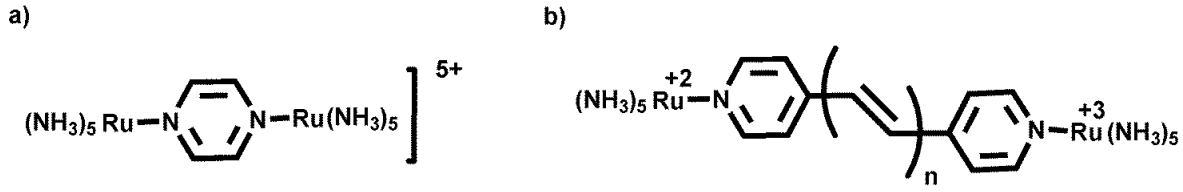

Figure 1.3. a) Creutz-Taube ion. b) Complexes made by Reimers and Hush to investigate the effect of the bridge to the charge delocalization, n = 0 – 3.[42]

1.3. Classification of Mixed-Valence Compounds.

The Creutz-Taube ion described above has an overall +5 charge from ruthenium(II) and ruthenium(III) ions. Later investigations confirmed that there is good electronic communication between the two metal ions, but the charge is not fully delocalized.[39-41] Investigations by Reimers and Hush (Figure 1.3.b)[42] found that the delocalization or localization of the extra charge is mainly dependent on the nature of the bridge. The delocalization and localization of the charge through the bridge of MV

compounds became such an important issue that Robin and Day introduced a classification for these systems, now referred to as the Robin-Day classification.[60] MV systems can be classified into three categories based on the extent of electronic communication or electron delocalization between two redox centers; Robin-Day class I, II, and III. The molecules in the Robin-Day class I have essentially separate redox sites and they do not have any electronic interactions. In class III systems, the interaction of the two redox sites is so great that it has full electron delocalization. Therefore, Robin-Day class II MV systems have moderate electron delocalization between class I and class III.

Mixed valence systems, especially Robin-day class II and class II/III borderline, show interesting optical properties because of the significant electronic coupling between two redox sites separated by a bridge.[61,62] Electronic coupling between two redox-active subunits across the common bridge leads to an avoided crossing of the individual potential hypersurfaces. It results in a potential hypersurface with double minima (Figure 1.4.b). The shape of the resulting potential energy hypersurface depends on the ratio between the electronic coupling parameter, H_{ab}, and the reorganization energy, λ. This λ is the energy required for necessary structural adjustment of individual redox centers and solvents.[63] The Robin-Day class II mixed-valence systems have $2H_{ab}$ values larger than 0 but smaller than the reorganization energy, λ. Intramolecular electron transfer can then occur by photochemical excitation from one local minimum into the excited state hypersurface, from which the system can relax to the ground state with an inversion of redox states. The underlying absorption band is called an intervalence charge transfer (IVCT) absorption band, which usually appears in the NIR region.

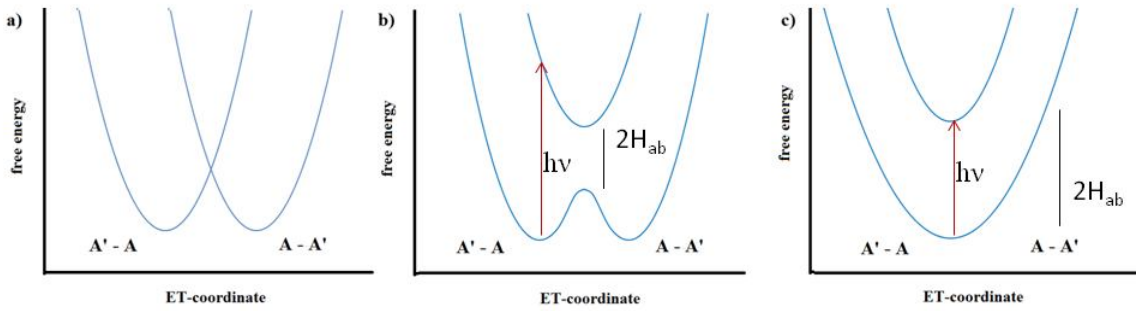

Figure 1.4. Potential energy curves for electron transfers in MV complexes. a) Robin-Day class I, b) Robin-Day class II, c) Robin-Day class III.

The electronic coupling element H_{ab}, can be obtained by analysis of the IVCT band. The Hush relations given in the Equations 1 and 2 can be used to calculate this electronic coupling element of weakly to moderately delocalized systems.[63,64] E_{OP} is the energy of

$$E_{OP} = \lambda \qquad (1)$$

$$H_{ab}\,(\mathrm{cm}^{-1}) = [(4.2\mathrm{x}10^{-4})\varepsilon_{max}\Delta\tilde{\nu}_{1/2}E_{OP}]^{1/2}/d \qquad (2)$$

the absorption maxima, λ is the Marcus reorganization energy, ε_{max} is the molar extinction coefficient, $\Delta\tilde{\nu}_{1/2}$ is the full-width-at-half-maximum in cm^{-1}, and d is the separation between two redox centers in Å. Class II systems have H_{ab} values greater than zero but lower than $\lambda/2$, and it is highly dependent on the solvent. The interaction of two redox centers of class III systems is very strong and the ground state has only a single minimum (Figure 1.4.c). The energy of IVCT band of class III systems is independent of the solvent. This is the delocalized system, and the electronic coupling element is half of the energy of the absorbance maxima.

The Marcus reorganization energy, λ, of mixed-valence class II and class II/III systems is highly dependent on the nature of the solvent used in the spectroscopic measurements, while λ of class III systems is independent on the nature of the solvent.[71] Furthermore, the IVCT bands of class II and class II/III systems are Gaussian shaped but the band of class III generally is asymmetric.[43,72] Data gathered from IVCT band analysis can be used to calculate the thermal energy barrier to electron transfer, ΔG, and the rate constant for electron transfer, k_{et} using classical Marcus Theory (eqn 3 and 4).[65]

$$\Delta G = (\lambda - 2H_{ab})^2 / 4\lambda \ \ cm^{-1} \qquad (3)$$

$$k_{et} = (2H_{ab}^2/h)[\pi^3 / \lambda k_B T]^{1/2} \exp-(\Delta G/k_B T) \qquad (4)$$

The MV compounds can be synthesized by the comproportionation of the doubly-oxidized derivative (both redox centers are in the oxidation state n+1), with the non-oxidized derivative (both redox centers are in the oxidation state n) as shown in Equation 5. A MV system can be represented as M^{n+}-B-$M^{(n+1)+}$ where the Ms are the redox centers or the metal ions with different oxidation states connected by the bridge B. The equilibrium constant for the comproportionation of this MV compound can be written as Equation 6. The electrochemical properties of the compound can be used to determine K_{com} as shown in Equation 7, where F = 96485 $Cmol^{-1}$, R = 8.31441 $JK^{-1}mol^{-1}$. The value of ΔE depends in part on the electronic communication of the two redox centers, and generally the closer the redox centers or the higher the electronic delocalization, the higher the values for the redox potential splitting (ΔE) and K_{com}.

$$M^{n+}\text{–}\mathbf{B}\text{–}M^{n+} + M^{(n+1)+}\text{–}\mathbf{B}\text{–}M^{(n+1)+} \longleftrightarrow 2\ M^{n+}\text{–}\mathbf{B}\text{–}M^{(n+1)+} \qquad (5)$$

$$K_{com} = [M^{n+}\text{–}\mathbf{B}\text{–}M^{(n+1)+}]^2 / [M^{n+}\text{–}\mathbf{B}\text{–}M^{n+}][\ M^{(n+1)+}\text{–}\mathbf{B}\text{–}M^{(n+1)+}] \qquad (6)$$

$$K_{com} = e^{(\Delta E \cdot F/R \cdot T)} \quad (7)$$

Robin-Day class I MV species have non-interacting redox centers, therefore the oxidation of one redox center would not affect the oxidation of the other redox center and technically results in one two-electron oxidation or reduction wave. Consequently, the equilibrium constant for the comproportionation (K_{com}) is very low, and it has been accepted that Robin-Day class I MV systems have K_{com} values from zero to 10^2.[73] Robin-Day class III MV species have full electron delocalization over the two redox centers and large K_{com} values greater than 10^6. The K_{com} value of class II species lies in between these two values ($10^2 < K_{com} < 10^6$). Electrochemical measurements (cyclic voltammetry, differential pulse voltammetry, etc.) provide a convenient method to estimate the strength of the electronic communication in MV compounds, but are not sufficient to establish the nature of electronic communication in weakly interacting systems, as this redox potential splitting (ΔE) might be due to simple Coulombic interactions. In addition, resolution of the line width of peaks and the concentration of the electrolyte would affect the separation of redox waves. Therefore the electrochemical and the spectroscopic investigations can be used to classify mixed-valence compounds.

Not all MV compounds have M-B-M frameworks. Therefore, purely organic MV compounds have replaced metal centers with redox active organic centers such as triarylamines,[43-52] tetrathiafulvalenes,[53] carbazoles,[54] dihydrazines,[55-56] quinones,[57] nitro groups[58] and nitrobenzene derivatives.[59] Bis(triarylamine)s with phenylene or other bridges (Figure 1.5) are one of the most popular classes of MV compounds to have been studied extensively[43-52] This might be due to the stability of the radical cation formed and convenient synthetic possibilities of bis(triarylamine)s. Lambert and co-workers have

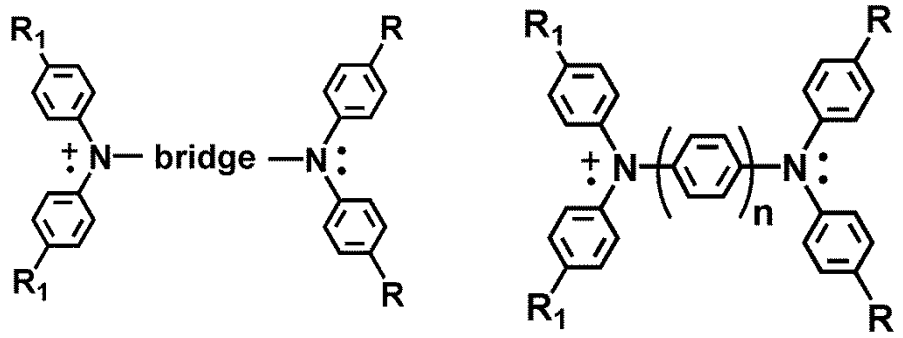

Figure 1.5. Mixed-valence bis(triarylamine) compounds. R, R_1: alkyl group, OMe.

studied extensively electronic communication of two redox centers of bis(triarylamine)s with a series of compounds that have OMe as the R (Figure 1.5) and different bridges.[43] They have shown that the electron delocalization in bis(triarylamine)s with R = OMe (Figure 1.5 Right) is highly dependent on the nature and length of the bridge. Also there are inverted organometallic type L-M-L systems with redox active organic ligands connected by metal bridges.[74-76]

1.4. Initial Studies of Electronic Communication of Mixed Valence Metal Pincer Complexes.

Our research group has been interested in metal complexes of uninegative, tridentate pincer ligands based on di(2-pyrazolyl-aryl) amines (Figure 1.6).[66,67] These ligands will be described herein by shorthand notation H(X,Y): X and Y denote substitution at the *para*-aryl positions. These ligands are redox active, because di(arylamine)s are electron donors. Electrochemical, EPR, and spectroscopic studies of gallium(III), rhenium(I) and rhodium(III) complexes of these ligands have outlined many properties.[66,70] An investigation of the carbonylrhodium(I) chemistry of this class of ligand revealed that the electronic properties and the reactivity of these complexes can be

predictably tuned by changing the *para*-aryl groups (X and Y, Figure 1.6).[68] Six membered chelate rings formed by the amido and pyrazolyl donors binding with metals

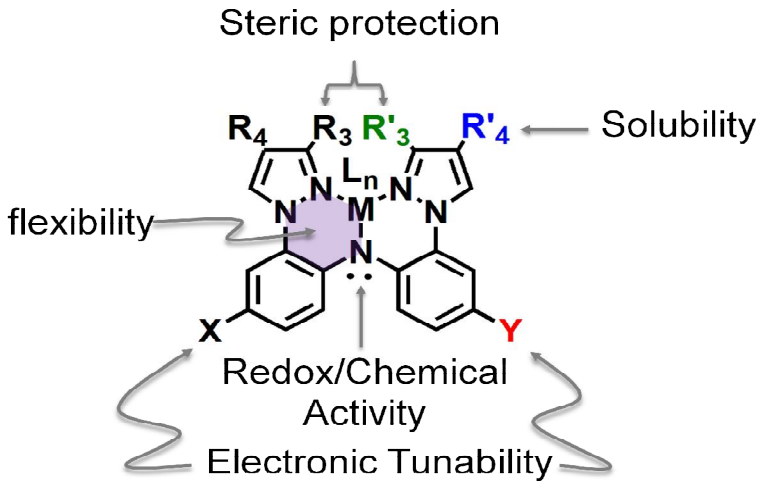

Figure 1.6. Generic depiction of a metal complex of the di(2-pyrazolyl-aryl)amino NNN-pincer.

give structural flexibility allowing either *fac*- or *mer*- binding modes. Also, substituents on the pyrazole groups (R_3 and R_4) further control steric, electronic, and structural properties of complexes.[68]

As described in my M.Sc. thesis, a gallium(III) complex, $[Ga(Me,Me)_2]^+$ and oxidized derivatives (Figure 1.7) were prepared and studied. The cyclic voltammogram of $[Ga(Me,Me)_2]^+$ showed two, reversible, one-electron oxidation waves that were assigned as the ligand-based oxidations because gallium(III) cannot be further oxidized to gallium(IV). The equilibrium constant for comproportionation (K_{com} = 1.62 x 10^3) from electrochemical data indicates the mono-oxidized complex is a Robin-Day Class II mixed valence complex. This observation was supported by means of spectroscopic studies, where band shape analysis of the intervalence charge transfer (IVCT) band of the

$[Ga(Me,Me)_2]^{2+}$ gave E_{OP} 1565 nm and H_{ab} 264 cm^{-1} in CH_2Cl_2 and E_{OP}1444 nm and H_{ab} 223 cm^{-1} in CH_3CN. The solvent dependence and small H_{ab} indicated a Robin-Day class

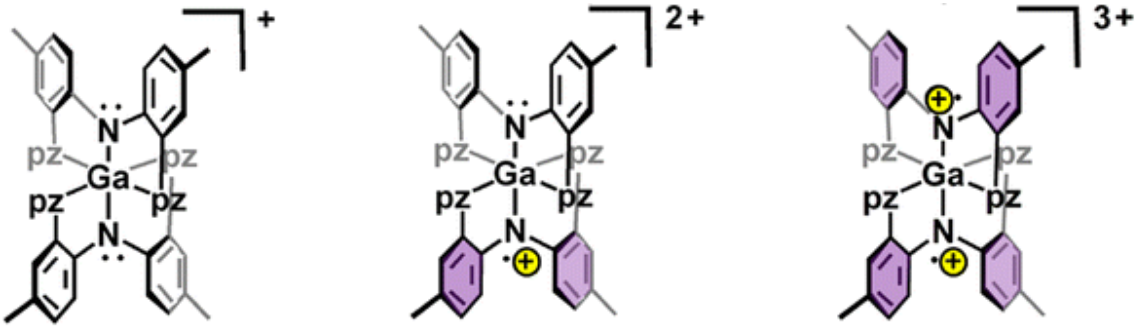

Figure 1.7. Left: Gallium(III) pincer ligand complex, Middle: mono-oxydized gallium(III) complex, Right: di-oxydized gallium(III) complex.

II species in accord with CV measurements. The electronic communication must occur by hopping across the metal bridge as there are no energetically accessible orbitals in gallium(III).

1.5. Overview of the Dissertation.

In this Dissertation, the effect of replacing gallium with other metals and of replacing groups about the ligand on electronic properties is explored. The transition metal counterparts of $[Ga(Me,Me)_2]^{2+}$ are expected to have greater electronic communication between ligands because interacting d-orbitals of transition metals must be energetically accessible to allow dπ-pπ interaction with the magnetic orbital on the ligand. Also, synthetic methods that give "linked" or dinucleating pincer ligands and their complexes are described. Then methods to make coordination polymers and networks

using numerous metal pincers are outlined. Specifically this dissertation consists of the following chapters.

Chapter 2 describes the syntheses and electronic properties of homoleptic nickel (II) complexes of this ligand and other related ones with different *para*-aryl substituents. In Chapter 3 the group 9 complexes were prepared to detail and quantify the increasing electronic communication on increasing atomic number, Z. Chapter 4 describes syntheses of di-nucleating pincer ligands, where two pincer fragments are connected by phenylene bridges. Bis(tricarbonylrhenium(I)) complexes, $[(CO)_3Re(\mu\text{-}L)Re(CO)_3]^{n+}$ n = 0, 1,2 , were prepared and characterized to study effect of spacer length on electronic communication in singly oxidized derivatives (n = +1).

Chapter 5 focuses on attempts to incorporate metal pincer complexes into 1D, 2D, and 3D assembles. Both success and difficulties in such pursuits are described.

Finally, Chapter 6 describes initial efforts of developing "Extended" pincer ligands that have formamidinate anchors which can bind multiple metals with the aid of different flanking donors (Figure 1.8).

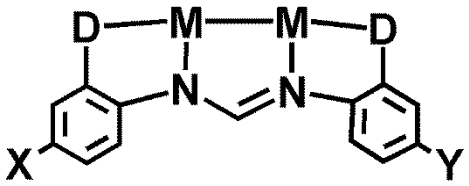

Figure 1.8. Generic depiction of an extended pincer ligand.

These ligands have diarylformamidinate anchors with either pyrazolyl or diarylphosphine flanking donors. The preparations of both symmetric and asymmetric derivatives are outlined. The group 1 and group 11 complexes are also described; these are envisioned to be starting materials for future studies. The coinage metal complexes provided opportunity to explore potential metallophilic interactions. The luminescent behavior and catalytic activity of various derivatives were explored.

CHAPTER 2

HOMOLEPTIC NICKEL(II) COMPLEXES OF REDOX-TUNABLE PINCER-TYPE LIGANDS

The following chapter was published in: Hewage, J. S.; Wanniarachchi, S.; Morin, T. J.; Liddle, B. J.; Banaszynski, M.; Lindeman, S. V.; Bennett, B.; Gardinier, J. R. *Inorg. Chem*. **2014**, *53* (19), 10070-10084.

2.1. INTRODUCTION

There has been long-standing interest in metal complexes of redox-active "noninnocent" ligands[1] that persists because of the enticing prospects for advancing fundamental knowledge of electronic structure and bonding,[2] for discovering new reactivity that may arise from both metal and ligand-centered electron transfer,[3] or for the development of new technological applications that rely on electron (or hole) transfer.[4] Control over the syntheses and electrochemical properties of new classes of redox-active ligands and their metal complexes is important for making advances in either fundamental or applied areas of study. While a majority of such studies have focused on metal complexes of bidentate noninnocent ligands,[5] those involving terdentate "pincer" ligands are gaining prominence.[6−18] Among these, the chemical and redox noninnocence of metal complexes of the bis(imino)pyridine "pincer" ligand has been exploited to produce a number of remarkable chemical transformations.[7] Metal pincer complexes with redox-active diarylamido anchors are also gaining popularity for their spectacular reaction chemistry.[6,8−18]

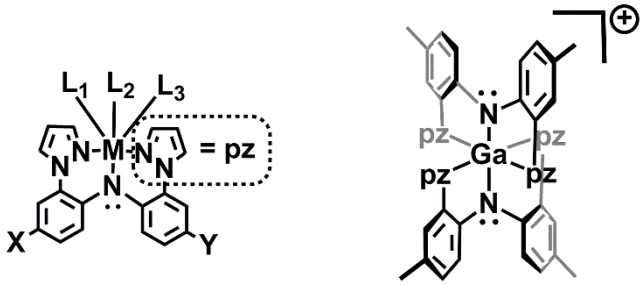

Figure 2.1. Metal complexes of pyrazolyl-containing redox-active pincer ligands.

We have been studying the properties of metal complexes of a new class of redox-active pincer-type ligand that has pyrazolyl flanking donors attached to a diarylamido anchor, as in Figure 2.1.[19] These uninegative pincer-type ligands will be described herein by the shorthand notation $(X,Y)^{-}$ that denotes the substitution at the *para*-aryl positions (X and Y, left of Figure 2.1) of the diarylamido backbone. In rhodium chemistry, complexes (Me,Me)Rh(L_1)(L_2)(L_3) showed ligand-centered oxidations that occurred at potentials that depended on the charge of the complex and the Lever parameter (E_L) of nonpincer ligands L_1, L_2, and L_3.[19b] Also, for a series of carbonylrhodium(I) complexes, (X,Y)Rh(CO), the reactivity toward a given alkyl halide increased predictably with the electron-donating ability of the X and Y groups as indicated by the groups' Hammett σ_p parameter.[19c] More recently, the homoleptic gallium(III) complex $[Ga(Me,Me)_2]^{+}$ was reported, which showed two reversible one-electron oxidations in its voltammogram.[19a] The entire valence series was structurally and spectroscopically characterized. On the basis of electrochemical and spectroscopic studies, the one-electron oxidized $[Ga(Me,Me)_2]^{2+}$ was found to be a Robin−Day class II species where weak electronic communication between oxidized and nonoxidized ligands was thought to occur via superexchange through the empty orbitals on gallium. It was conjectured that replacing

the gallium(III) center with a transition metal would greatly strengthen the electronic communication because the 3d-orbitals should be energetically accessible and allow for dπ−pπ interactions with the magnetic orbitals on the ligand. In addition to changing metals, we were also interested in determining whether changing the electronic properties (without changing the steric profile) of the redox-active pincer ligands would provide a means to alter the strength of electronic communication. Although we previously observed that changing *para*-aryl substituents can affect electronic properties in rhodium complexes, it was unclear whether this translated to first-row metals, and, more importantly, how much could the electronic properties be tuned. Could this tuning be enough to switch from a ligand- to a metal-centered redox process, or vice versa? This contribution discloses our first efforts in this vein, where eight new pincer ligands of the type H(X,Y) were prepared to allow a systematic study of the electronic properties of 12 nickel(II) complexes, $Ni(X,Y)_2$, with diverse *para*-aryl substituents. The electrochemical, spectroscopic properties, and computational studies on the complete valence series $[Ni(Me,Me)_2]^{n+}$ are documented. Comparison of properties between mixed-valent complexes $[M(Me,Me)_2]^{n+}$ (n = 1 for M = Ni and n = 2 for M = Ga) was made to elucidate the role of the metal center in mediating electronic communication.

2. 2. RESULTS AND DISCUSSION

2.2.1. Syntheses. Eight new and four known[19] NNN-pincer ligands, H(X,Y), with pyrazolyl flanking donors attached to diarylamine anchors with different *para*-aryl (X- and Y-) substituents have been prepared by a variety of synthetic routes as summarized in

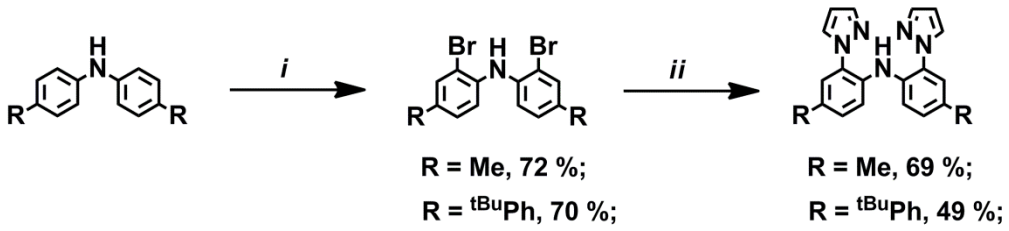

Scheme 2.1. Synthesis of H(Me,Me) and H(^{tBu}Ph,^{tBu}Ph) by sequential bromination and amination reactions. Key: i) 2 eq. Br_2, 1:1 (v/v) CH_2Cl_2:MeOH, 0^{o}C, 1 h; ii) 3.5 eq. pyrazole, 3.5 equiv. K_2CO_3, 10 mol% CuI, 40 mol% DMED, xylenes, reflux 36 h.

Schemes 2.1-4. In the first method (Scheme 2.1), bromination of a diarylamine followed by CuI-catalyzed coupling of pyrazole was used to produce H(Me,Me) or H(^{tBu}Ph,^{tBu}Ph). This route is not suitable for reactions involving unsubstituted diarylamines such as diphenylamine (for instance, in attempts to give H(H,H)) since bromination first occurs at the *para*-aryl position of the diarylamine. Instead, a second versatile synthetic approach can be used whereby the arms of the pincer ligand are attached via an amination reaction between a 2-halo-5-Y-aryl-*1H*-pyrazole and a 2-(pyrazolyl)-4-X-aniline, exemplified by the seven derivatives in Scheme 2.2. It is noted that the reactions in Scheme 2.2 are optimized routes. The asymmetric derivatives H(X,Y) can be prepared by using the opposite combination of reagents (interchanging X and Y of the pyrazolyl-containing reagents in Scheme 2.2) but the yields were found to be lower. As shown in Scheme 2.3, two ligands with bromide groups at the *para*-aryl position of the diarylamido backbone, H(Br,Br) and H(Me,Br), were easily accessed by bromination reactions between *N*-bromosuccinimide and either H(H,H) or H(Me,H) in CH_3CN. The use of other solvents for the bromination reactions was also successful but generally resulted in lower yields than when using CH_3CN. Finally, the derivative H(Br,Br) was amenable to Suzuki

coupling reactions to give H(^{tBu}Ph,^{tBu}Ph) or H(^{CN}Ph,^{CN}Ph) in modest to good yields, as per Scheme 2.4.

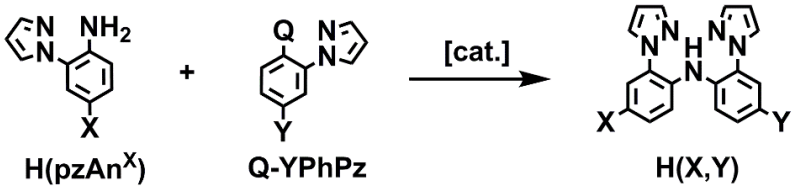

entry	X =	Q =	Y =	[cat.]	Product	Yield (%)
1	Me	Br	H	*a*	H(Me,H)	73
2	H	Br	H	*a*	H(H,H)	68
3	CO_2Et	I	Me	*b*	H(Me,CO_2Et)	73
4	Me	Br	CF_3	*a*	H(Me,CF_3)	83
5	CN	I	Me	*b*	H(Me,CN)	51
6	CF_3	Br	CF_3	*a*	H(CF_3,CF_3)	90
7	CN	Br	CN	*a*	H(CN,CN)	50

a) CuI, Cs_2CO_3, dioxane, reflux, 15h;
b) $Pd(OAc)_2$, BINAP, Cs_2CO_3, toluene, reflux 3-4 d

Scheme 2.2. Convergent synthetic route to H(X,Y) ligands.

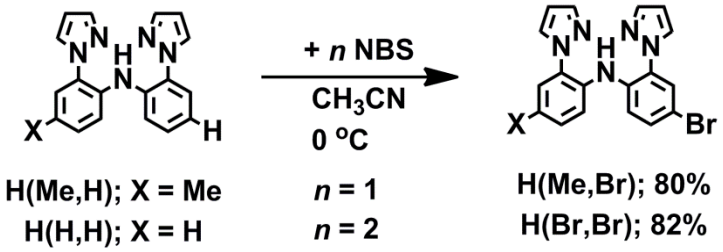

Scheme 2.3. Preparation of H(Me,Br) and H(Br,Br) by bromination reactions.

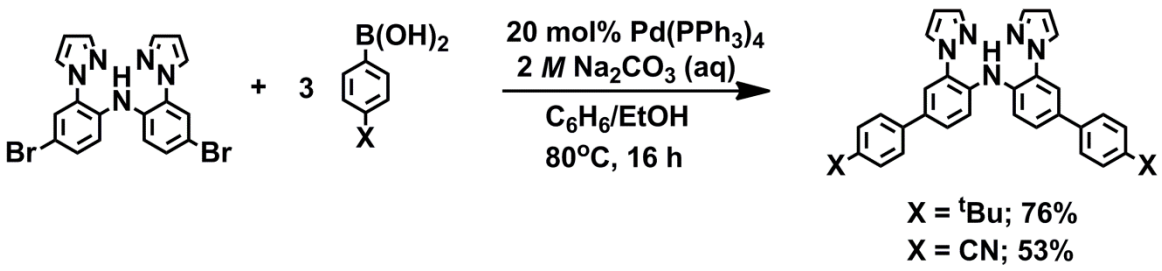

Scheme 2.4. Preparation of H(^{tBu}Ph,^{tBu}Ph) and H(^{CN}Ph,^{CN}Ph) by Suzuki reactions.

The one-pot reaction between $NiCl_2 \cdot 6H_2O$ and 2 mol equiv[24] of each of the 12 H(X,Y) ligands followed by 2 mol equiv of $(NEt_4)(OH)$ in MeOH rapidly afforded precipitates of "Ni(X,Y)$_2$"; the soluble byproducts (H_2O, NEt_4Cl) were removed by filtration. If the precipitates are collected by suction filtration, washed with Et_2O (minimal in the cases of **2**, **9**, and **11**, vide infra), and air-dried, then samples analyze as either hemihydrates, hydrates, a dimethanol solvate (for Ni(Me,$CO_2Et)_2$), or are solvent-free (Ni(Me,Br)$_2$, **4**, and Ni(Br,Br)$_2$, **7**) as detailed in the Experimental Section. Heating these samples under vacuum over the course of hours is sufficient to remove solvent in seven of the cases (see Scheme 2.5), but solvent could not be completely removed in the remaining cases. Solvate molecules are retained by complexes with Lewis donor X- or Y-groups and derivatives with hydrogen at the *para*-aryl position. While the former cases are easily understood, the reason why water is retained in the latter cases (**2**·0.5 H_2O and **3**·0.5 H_2O) is not clear, as it has not yet been possible to grow single crystals for X-ray structural studies.[25] The yields shown in Scheme 2.5 (>80%) correspond to samples after washing and heating under vacuum. The characterization data were acquired from samples that analyzed as shown in Scheme 2.5. The Ni(X,Y)$_2$ complexes are generally

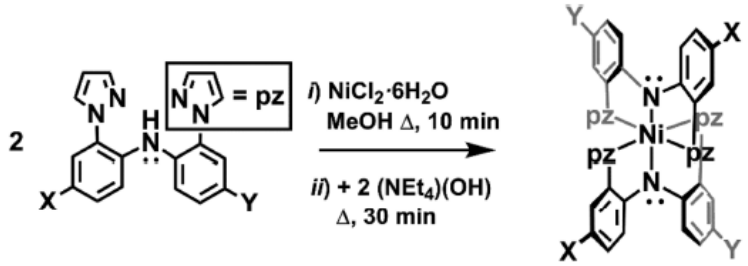

Ni(Me,Me)$_2$ (1), 95%
Ni(Me,H)$_2$·0.5H$_2$O (2·0.5H$_2$O), 87%
Ni(H,H)$_2$·H$_2$O (3·H$_2$O), 82%
Ni(Me,Br)$_2$ (4), 97%
Ni(Me,CO$_2$Et)$_2$·2MeOH (5·2MeOH), 98%
Ni(Me,CF$_3$)$_2$ (6), 97%

Ni(Br,Br)$_2$ (7), 85%
Ni(Me,CN)$_2$ (8), 88%
Ni(CF$_3$,CF$_3$)$_2$ (9), 93%
Ni(CN,CN)$_2$·0.5H$_2$O (10·0.5H$_2$O), 86%
Ni(^{tBu}Ph,^{tBu}Ph)$_2$ (11), 95%
Ni(^{CN}Ph,^{CN}Ph)$_2$·H$_2$O (12·H$_2$O), 88%

Scheme 2.5. Preparation of Ni(X,Y)$_2$ Complexes.

soluble in halogenated solvents, moderately soluble in aromatic solvents, THF, acetone, CH_3CN, and nitromethane, very slightly soluble in alcohols, but insoluble in alkanes and Et_2O. Exceptions occur for Ni(Me,H)$_2$·0.5 H_2O, Ni(CF$_3$,CF$_3$)$_2$, and Ni(^{tBu}Ph,^{tBu}Ph)$_2$, which show appreciable solubility in Et_2O. In these cases, the methanol precipitates were washed with either minimal Et_2O or with hexanes to remove any inadvertent excess ligand prior to drying. In contrast, the Ni(X,Y)$_2$ complexes with cyano substituents (**8**, **10**, and **12**) are noticeably less soluble in organic solvents than the other nine derivatives. All complexes appear to be air stable both in the solid state and in solution. Each of the **12** complexes is paramagnetic with a solid-state room-temperature magnetic moment in the range of 2.7−3.2 μ_B, as expected for nickel(II) with a significant spin−orbit coupling contribution to the magnetic moment.[26] The solids are also noticeably thermochromic (Figure 2.3). At room temperature, the complexes range in color from brown to yellow-brown to orange-brown to red (Figure 2.2). However, the complexes become bright

orange or red (depending on the complex) upon cooling to −196 °C. The origin of the solid-state thermochromic behavior of these $Ni(X,Y)_2$ complexes remains unclear but is likely due to the known temperature dependence of charge transfer bands.[26,27]

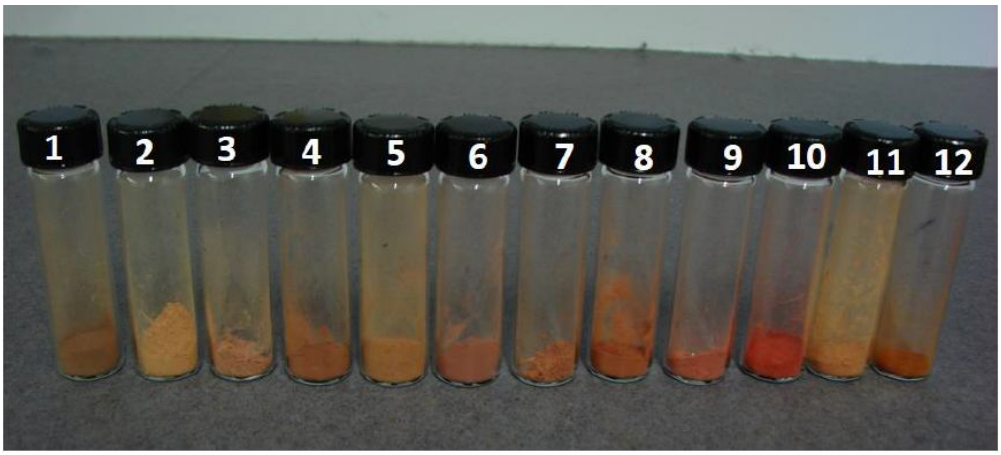

Figure 2.2. Photographs of compounds **1-12** as powders at room temperature.

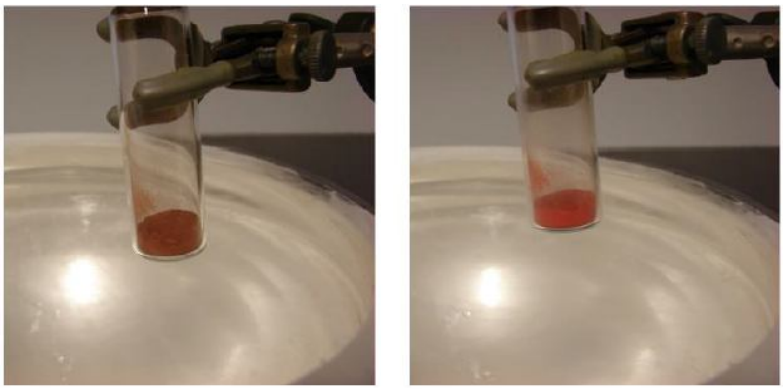

Figure 2.3. Photographs of compound **4** before and after cooling to 77 K showing thermochromic behavior.

2.2.2. Solid State. The solid-state structures of six $Ni(X,Y)_2$ derivatives have been determined by single-crystal X-ray diffraction. The structure of $Ni(Me,CN)_2$ is given in Figure 2.4, while selected bond distances and angles are given in Table 2.1; structures of other complexes are given in Figures 2.5-2.9 and the crystallographic data collections are given in Tables 2.2-2.3. All $Ni(X,Y)_2$ complexes have six coordinate nickel(II) with an average Ni−N bond distance of 2.07 ± 0.01 Å, in line with other nickel(II) complexes containing NiN_6 kernels.[28] With the exception of *cis*-$Ni(Me,CN)_2$ described later, the nickel center in each complex resides in a compressed octahedral environment where the diarylamido $Ni-N_{Ar}$ bonds are shorter (avg 2.05 ± 0.02 Å) than the pyrazolyl $Ni-N_{pz}$ bonds (avg 2.09 ± 0.02 Å). For asymmetric derivatives $Ni(X,Y)_2$ where $X \neq Y$, there are two possible isomers where the X groups are either *cis*- or *trans* with respect to the central $N_{Ar}-Ni-N_{Ar}$ axis (left and right of Figure 2.4, respectively). In the case of $Ni(Me,CN)_2$, both isomers are found in a 1:1 ratio as crystallographically independent molecules in the single crystal. The *cis*-$Ni(Me,CN)_2$ isomer differs from all other structurally characterized $Ni(X,Y)_2$ complexes in that the average $Ni-N_{Ar}$ distance of 2.08 ± 0.01 Å is statistically identical to or slightly longer than the average of the $Ni-N_{pz}$ bond distances of 2.07 ± 0.01 Å. For the other structurally characterized asymmetric $Ni(X,Y)_2$ derivatives **4** and **6**, the isomers cocrystallize as (superimposed) disordered pairs (Figure 2.7). It is also noteworthy that for symmetric derivatives $Ni(X,Y)_2$ where X = Y such as in **1**, **3**, and **10**, the molecules have approximate D_2 symmetry and are chiral. Because of the modest dihedral angle between the mean planes of the pyrazolyl and aryl rings (avg 37 ± 3°), the tridentate ligands are nonplanar. As such, two enantiomers exist that can be differentiated by the relative skew of a line formed by the centroids pyrazolyl rings and a

line conjoining centroids of aryl rings of the same ligand (Figure 2.10). Both possible isomers are found in the crystal of each **1**, **3**, and **10**. Similarly, all four isomers of the nominally C_2-symmetric $Ni(X,Y)_2$ complexes **4** and **6** are found in their solid state structures, as in Figure 2.11.

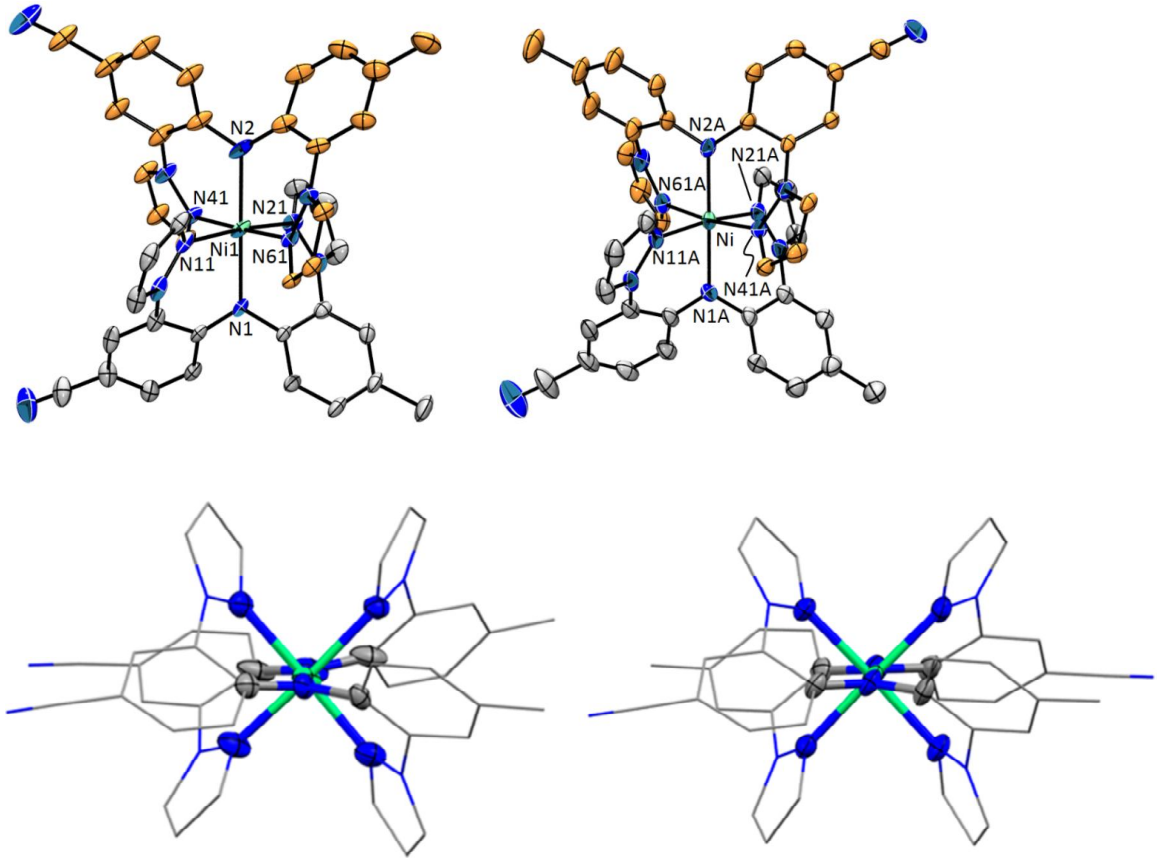

Figure 2.4. Top: Structures of the two isomers (*cis*- isomer, left; *trans*- isomer, right) of $Ni(Me,CN)_2$ found in the crystal with partial atom labeling. Hydrogen atoms have been removed and carbon atoms of the top ligand on each complex have been colored gold for clarity. Bottom: Views approximately down N1-Ni-N2 bonds showing the nearly coplanar amido "$N_{Ar}NiC_2$" moieties.

Table 2.1. Selected Distances (Å) and Angles (deg) for the Isomers of $Ni(Me,CN)_2$.

atom/bond label[a]	Bond Distances (Å) *trans*-isomer	*cis*-isomer
Ni1−N1	2.070(4)	2.050(4)
Ni1−N2	2.082(4)	2.057(4)
Ni1−N11	2.073(4)	2.088(4)
Ni1−N21	2.067(4)	2.101(4)
Ni1−N41	2.059(4)	2.082(3)
Ni1−N61	2.084(4)	2.103(4)
Bond Angles (deg)		
N1−Ni1−N2	179.14(15)	178.62(16)
N1−Ni1−N11	86.86(15)	85.80(15)
N1−Ni1−N61	90.54(14)	93.30(15)
N2−Ni1−N61	88.63(15)	87.35(15)
N11−Ni1−N2	92.88(17)	92.97(16)
N11−Ni1−N61	85.91(15)	91.39(15)
N21−Ni1−N1	87.52(15)	86.59(15)
N21−Ni1−N2	92.77(17)	94.66(15)
N21−Ni1−N11	174.22(17)	172.10(15)
N21−Ni1−N61	95.46(15)	86.92(15)
N41−Ni1−N1	92.03(15)	93.14(14)
N41−Ni1−N2	88.79(16)	86.25(14)
N41−Ni1−N11	91.22(16)	90.82(14)
N41−Ni1−N21	87.66(17)	91.72(14)
N41−Ni1−N61	176.04(15)	173.33(15)

[a]Those of *trans*-isomer have an additional "A" after the atom number; thus Ni1−N1 in the *cis*-isomer is Ni1A−N1A in the *trans*-isomer.

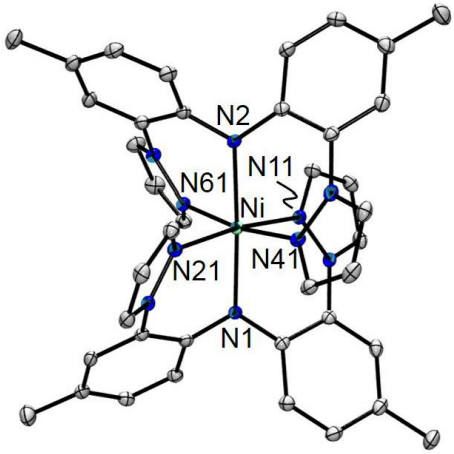

Figure 2.5. Molecular structure of **1** with hydrogen atoms removed for clarity. Selected bond distances (Å): Ni1-N1 2.0520(12), Ni1-N2 2.0377(12), Ni1-N11 2.0829(13), Ni1-N21 2.0880(13), Ni1-N41 2.1007(13), Ni1-N61 2.0886(13). Selected bond angles (deg.): N1-Ni1-N11 86.56(5), N1-Ni1-N21 87.56(5), N1-Ni1-N41 95.92(5), N1-Ni1-N61 91.90(5), N2-Ni1-N1 177.09(5), N2-Ni1-N11 95.73(5), N2-Ni1-N21 90.28(5), N2-Ni1-N41 85.97(5), N2-Ni1-N61 86.36(5), N11-Ni1-N21 172.93(5), N11-Ni1-N41 87.94(5), N11-Ni1-N61 88.99(5), N21-Ni1-N41 88.77(5), N21-Ni1-N61 95.12(5), N61-Ni1-N41 171.41(5).

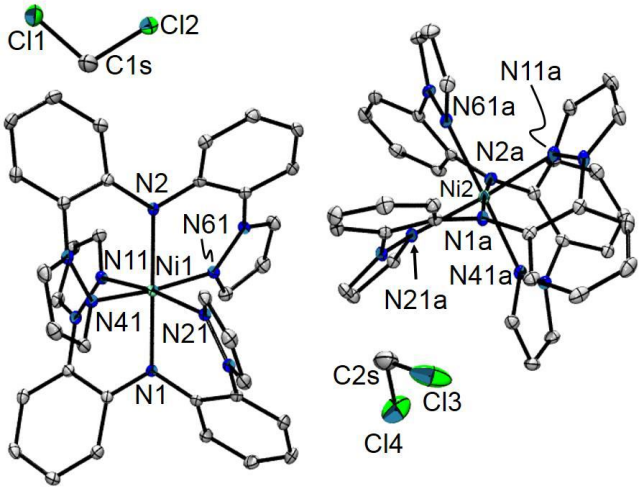

Figure 2.6. Molecular structure of crystallographically-independent units in **3**·CH_2Cl_2 with hydrogen atoms removed for clarity. Selected bond distances (Å): Ni1-N1 2.0307(15), Ni1-N2 2.0364(16), Ni1-N11 2.0870(16), Ni1-N21 2.1249(16), Ni1-N41 2.1061(16), Ni1-N61 2.0902(16), Ni2-N1A 2.0427(16), Ni2-N2A 2.0497(16), Ni2-N11A 2.0791(16), Ni2-N21A 2.0933(16), Ni2-N41A 2.0878(16), Ni2-N61A 2.0868(16). Selected bond angles (deg.): N1-Ni1-N2 179.95(8), N1-Ni1-N11 86.74(6), N1-Ni1-N21

86.35(6), N1-Ni1-N41 92.70(6), N1-Ni1-N61 93.40(6), N2-Ni1-N11 93.26(6), N2-Ni1-N21 93.65(6), N2-Ni1-N41 87.24(6), N2-Ni1-N61 86.66(6), N1A-Ni2-N2A 175.90(6), N1A-Ni2-N11A 87.53(6), N1A-Ni2-N21A 89.09(6), N1A-Ni2-N41A 89.05(6), N1A-Ni2-N61A 94.84(6), N2A-Ni2-N11A 90.41(6), N2A-Ni2-N21A 93.23(6), N2A-Ni2-N41A 87.61(6), N2A-Ni2-N61A 88.57(6), N11A-Ni2-N21A 174.51(6), N11A-Ni2-N41A 95.14(6), N11A-Ni2-N61A 86.59(6), N41A-Ni2-N21A 89.12(6), N61A-Ni2-N21A 89.39(6), N61A-Ni2-N41A 175.82(6).

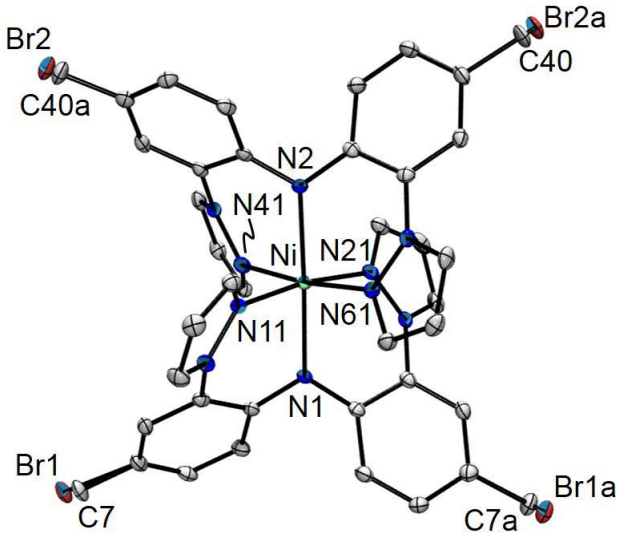

Figure 2.7. Molecular structure of **4** with both disorder components shown but with hydrogen atoms removed for clarity. Selected bond distances (Å): Ni1-N1 2.037(3), Ni1-N2 2.050(3), Ni1-N11 2.088(3), Ni1-N21 2.101(3), Ni1-N41 2.087(3), Ni1-N61 2.077(3). Selected bond angles (deg.): N1-Ni1-N2 177.86(11), N1-Ni1-N11 86.96(11), N1-Ni1-N21 86.23(11), N1-Ni1-N41 90.48(11), N1-Ni1-N61 95.05(11), N2-Ni1-N11 91.82(11), N2-Ni1-N21 95.09(11), N2-Ni1-N41 87.87(11), N2-Ni1-N61 86.67(11), N11-Ni1-N21 172.40(11), N41-Ni1-N11 94.54(11), N41-Ni1-N21 88.87(11), N61-Ni1-N11 88.68(11), N61-Ni1-N21 88.58(11), N61-Ni1-N41 173.75(11).

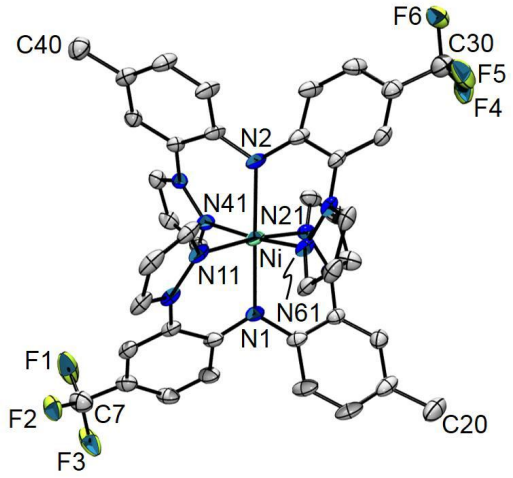

Figure 2.8. Molecular structure of one disorder component of **6** with hydrogen atoms removed for clarity. Selected bond distances (Å): Ni1-N11 2.093(2), Ni1-N21 2.086(2), Ni1-N1 2.0464(18), Ni1-N61 2.0849(19), Ni1-N41 2.0736(19), Ni1-N2 2.0534(18). Selected bond angles (deg.): N21-Ni1-N11 172.96(7), N1-Ni1-N11 86.38(8), N1-Ni1-N21 86.80(7), N1-Ni1-N61 91.57(8), N1-Ni1-N41 93.92(8), N1-Ni1-N2 179.02(8), N61-Ni1-N11 88.31(8), N61-Ni1-N21 93.63(8), N41-Ni1-N11 89.66(8), N41-Ni1-N21 89.06(8), N41-Ni1-N61 174.02(7), N2-Ni1-N11 94.37(8), N2-Ni1-N21 92.46(8), N2-Ni1-N61 87.84(7), N2-Ni1-N41 86.71(7).

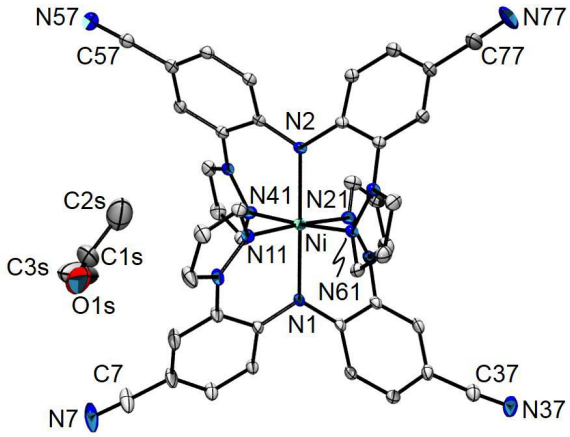

Figure 2.9. Structure of **10**·acetone with hydrogen atoms removed for clarity. Selected bond distances (Å): Ni1-N1 2.0481(17), Ni1-N2 2.0489(18), Ni1-N11 2.064(2), Ni1-N21 2.075(2), Ni1-N41 2.0789(19), Ni1-N61 2.0858(19). Selected bond angles (deg.): N1-Ni1-N2 179.33(8), N1-Ni1-N11 87.17(7), N1-Ni1-N21 88.84(7), N1-Ni1-N41 92.15(7), N1-Ni1-N61 91.47(7), N2-Ni1-N11 92.21(7), N2-Ni1-N21 91.79(7), N2-Ni1-N41 88.09(7), N2-Ni1-N61 88.28(7), N11-Ni1-N21 175.79(7), N11-Ni1-N41 91.27(8), N11-

Ni1-N61 87.74(7), N21-Ni1-N41 87.54(8), N21-Ni1-N61 93.70(8), N41-Ni1-N61 176.20(7).

Table 2.2. Crystallographic Data Collection and Structure Refinement for Ni(Me,Me)$_2$, **1**, Ni(H,H)$_2$·CH_2Cl_2, **3**·CH_2Cl_2, Ni(Me,Br)$_2$, **4**, and Ni(Me,CF_3)$_2$,**6.**

Compound	**1**	**3**·CH_2Cl_2	**4**	**6**
Formula	$C_{40}H_{36}N_{10}Ni$	$C_{37}H_{30}Cl_2N_{10}Ni$	$C_{38}H_{30}Br_2N_{10}Ni$	$C_{40}H_{34}F_6N_{10}Ni$
Formula weight	715.50	744.32	845.25	823.458
Crystal system	triclinic	monoclinic	triclinic	triclinic
Space group	P -1	P 2_1/n	P -1	P -1
Temperature [K]	100(2)	100(2)	100(2)	100(2)
a [Å]	8.7592(2)	9.55338(11)	8.7709(3)	8.9877(2)
b [Å]	12.8293(3)	17.50145(18)	12.8252(4)	13.0879(2)
c [Å]	16.0382(3)	40.5845(5)	16.1692(5)	16.3390(3)
α[°]	79.7090(10)	90.00	80.012(2)	79.7450(10)
β[°]	84.0790(10)	93.2065(12)	83.860(2)	84.0600(10)
γ [°]	75.7380(10)	90.00	76.027(2)	74.1850(10)
V [Å^3]	1715.33(6)	6775.02(13)	1734.24(10)	1816.60(6)
Z	2	8	2	2
$D_{calcd.}$ [gcm^{-3}]	1.385	1.459	1.619	1.505
λ[Å] (Cu or Mo Kα)	1.54178	1.54178	1.54178	1.54178
μ [mm^{-1}]	1.179	2.635	3.866	1.442
Abs. Correction	numerical	multi-scan	numerical	numerical
F(000)	748	3072	852	844
θ range [°]	2.81 to 67.98	3.34 to 70.67	2.78 to 67.55	2.75to 67.91
Reflections collected	14299	53167	14217	6167
Indep. reflns	5860	12822	5894	6167
T_min/max	0.6603/ 0.9034	0.63724/1.0	0.3161/ 0.8995	0.6492/0.8021
Data/restraints/	5860/0/464	12822/0/902	5894/4/478	6167/0/571
Goodness-of-fit on F^2	1.000	1.037	1.244	1.054
$R1^a$/$wR2^b$ [$I>2\sigma(I)$]	0.0308/0.0788	0.0373/0.0860	0.0454/0.0963	0.0431/0.1095
$R1^a$ /$wR2^b$ (all data)	0.0331/0.0804	0.0467/0.0895	0.0491/0.0977	0.0447/0.1107
Largest diff.	0.236/-0.310	0.673/-0.634	0.310/-0.348	0.620/-0.360

[a] $R1 = \Sigma||F_o| - |F_c||/\Sigma|F_o|$ [b] $wR2 = [\Sigma w(|F_o| - |F_c|)^2/\Sigma w|F_o|^2]^{1/2}$.

Table 2.3. Crystallographic Data Collection and Structure Refinement for $Ni(Me,CN)_2 \cdot 1.29\ CH_2Cl_2$, **8**$\cdot 1.29\ CH_2Cl_2$, $Ni(CN,CN)_2 \cdot 2$ acetone, **10**$\cdot 2$ acetone, and $Ni(CN,CN)_2 \cdot$acetone, **10**$\cdot$acetone.

Compound	**8**$\cdot 1.29\ CH_2Cl_2$	**10**$\bullet$2 acetone	**10**$\bullet$acetone
Formula	$C_{41.3}H_{32.6}Cl_{2.6}N_{12}$	$C_{46}H_{36}N_{14}NiO_2$	$C_{43}H_{30}N_{14}NiO$
Formula weight	847.49	875.60	817.52
Crystal system	monoclinic	triclinic	monoclinic
Space group	P 2_1/n	P -1	P 2_1/n
Temperature [K]	100(2)	100.0(1)	100.0(1)
a [Å]	17.3591(3)	9.8514(2)	14.21320(17)
b [Å]	27.8741(5)	13.9696(3)	15.60318(16)
c [Å]	17.7477(3)	16.7096(4)	17.3945(2)
α[°]	90.00	100.8347(18)	90.00
β[°]	102.7148(19)	98.0479(18)	103.6602(13)
γ [°]	90.00	91.2391(18)	90.00
V [Å^3]	8376.9(3)	2233.64(8)	3748.49(8)
Z	8	2	4
$D_{calcd.}$ [gcm^{-3}]	1.344	1.302	1.449
λ[Å] (Cu or Mo	0.7107	0.7107	0.7107
μ [mm^{-1}]	0.674	0.489	0.575
Abs. Correction	numerical	numerical	numerical
F(000)	3491	908	1688
θ range [°]	3.46 to 32.80	2.97 to 29.14	2.88 to 29.20
Reflections	268199	35371	42291
Independent Rflns	29874	10555 (R_{Int}=0.0355)	9159
T_min/max	0.723/0.962	0.834/0.941	0.922/0.958
Data/restr./param.	29874/84/1111	10555/40/563	9159/0/534
Goodness-of-fit	1.022	1.037	1.047
*R*1[a] /*wR*2[b]	0.1005/0.2599	0.0663/0.1963	0.0476/0.1128
*R*1/*wR*2 (all data)	0.1939/0.2906	0.0814/0.2108	0.0592/0.1201
peak/hole / e Å^{-3}	1.930/-0.843	1.821/-0.780	0.747/-0.792

[a] $R1 = \Sigma||F_o| - |F_c||/\Sigma|F_o|$ [b] $wR2 = [\Sigma w(|F_o| - |F_c|)^2/\Sigma w|F_o|^2]^{1/2}$.

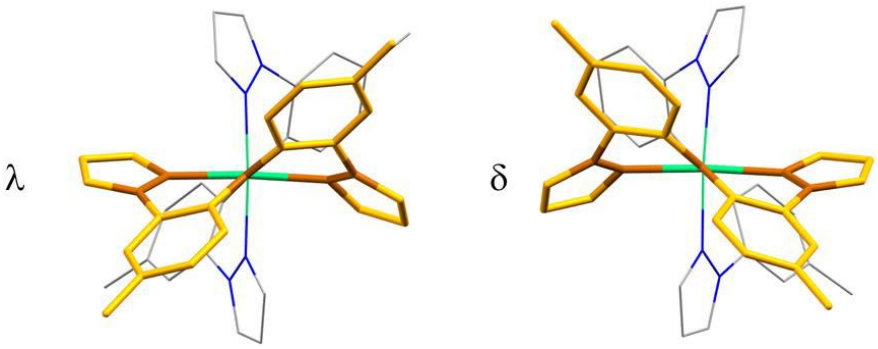

Figure 2.10. Isomers of Ni(Me,Me)$_2$.

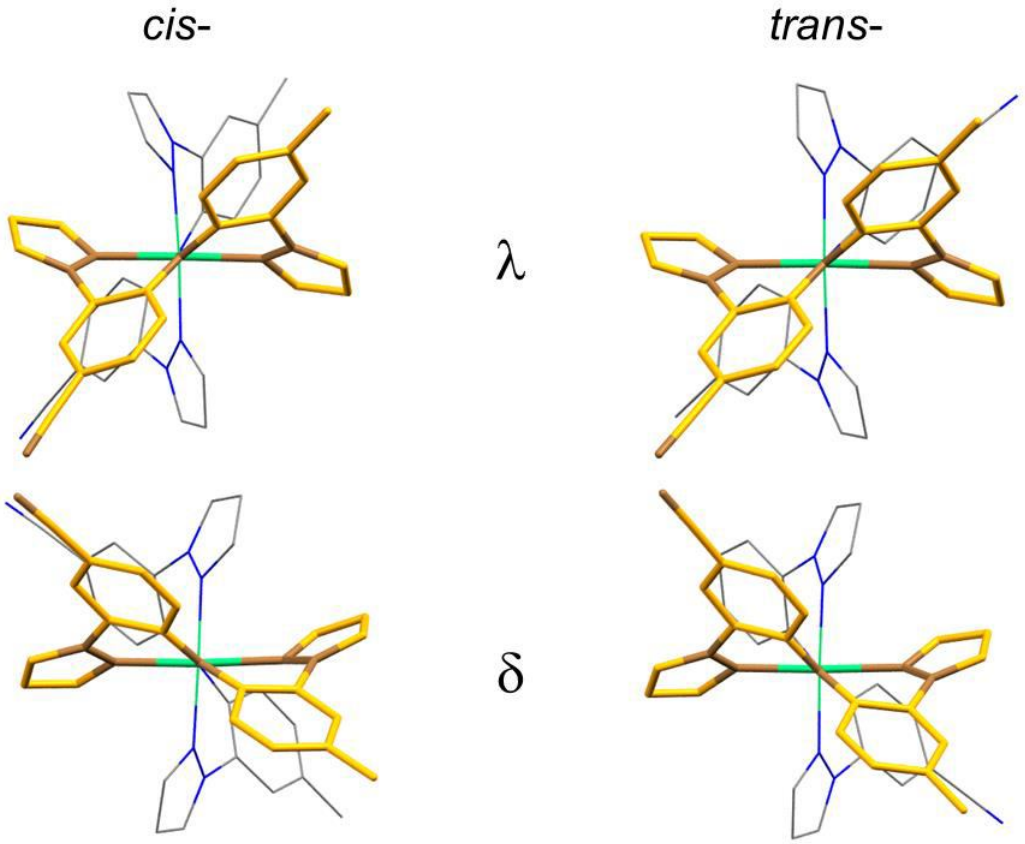

Figure 2.11. Isomers of Ni(Me,CN)$_2$. *Cis*- and *trans*- refer to the relative disposition of cyano- groups with respect to the central N_{Ar}-Ni-N_{Ar} bonds.

It will be useful to examine a qualitative MO diagram of **1** derived from DFT calculations, to facilitate discussion of the electronic properties of the complexes. As detailed in the Experimental Section, a later section, we examined several different theoretical models and all gave qualitatively similar results. Figure 2.12 provides representative "spin-down" β-frontier orbitals of **1** obtained at the M06/def2-SV(P) level of theory. First, each pair of the β-HOMO(−N) (N = 0, 1) or the β-LUMO(+N) (N = 0, 1), although not degenerate by symmetry, are essentially energetically degenerate. These four frontier orbitals are mostly ligand centered with the exception of the β-HOMO that is weakly mixed with a nickel orbital (vide infra). There are two main types of ligand π- (or π*-) orbitals; those like β-HOMO(−N) (N = 0, 1) that have significant contributions from the nitrogen p-orbitals and those like β-LUMO(+N) (N = 0, 1) that do not. We label the former as π_L-orbitals as per Kasha's convention[24] because these presumably involve the electronically active lone pair of electrons on nitrogen, whereas the latter are more conventional π- (or π*-) orbitals. Second, for simplicity, it is convenient to relabel the axes to swap the usual geometries of the d_{xy} and d_{x2-y2} orbitals. Thus, the z-axis is taken to be coincident with the N_{Ar}−Ni−N_{Ar} vector, while the x- and y-axes bisect *cis*-disposed Ni−N_{pz} bonds. As such, the lobes of the d_{xy} orbital are directed along the Ni−N_{pz} bonds (β-LUMO(+8), Figure 2.12) while the lobes of the d_{x2-y2} orbital are between these bonds (β-HOMO(−6), Figure 2.12). The d_{xz} orbital is then normal to the C_2N_{Ar}Ni planes (with a central amido N_{Ar} atom, see β-HOMO(0, −8, and −21) of Figure 2.12), and the d_{yz} orbital resides in the C_2N_{Ar}Ni plane (β-HOMO(−10), Figure 2.12). Thus, the d_{xz} orbital is

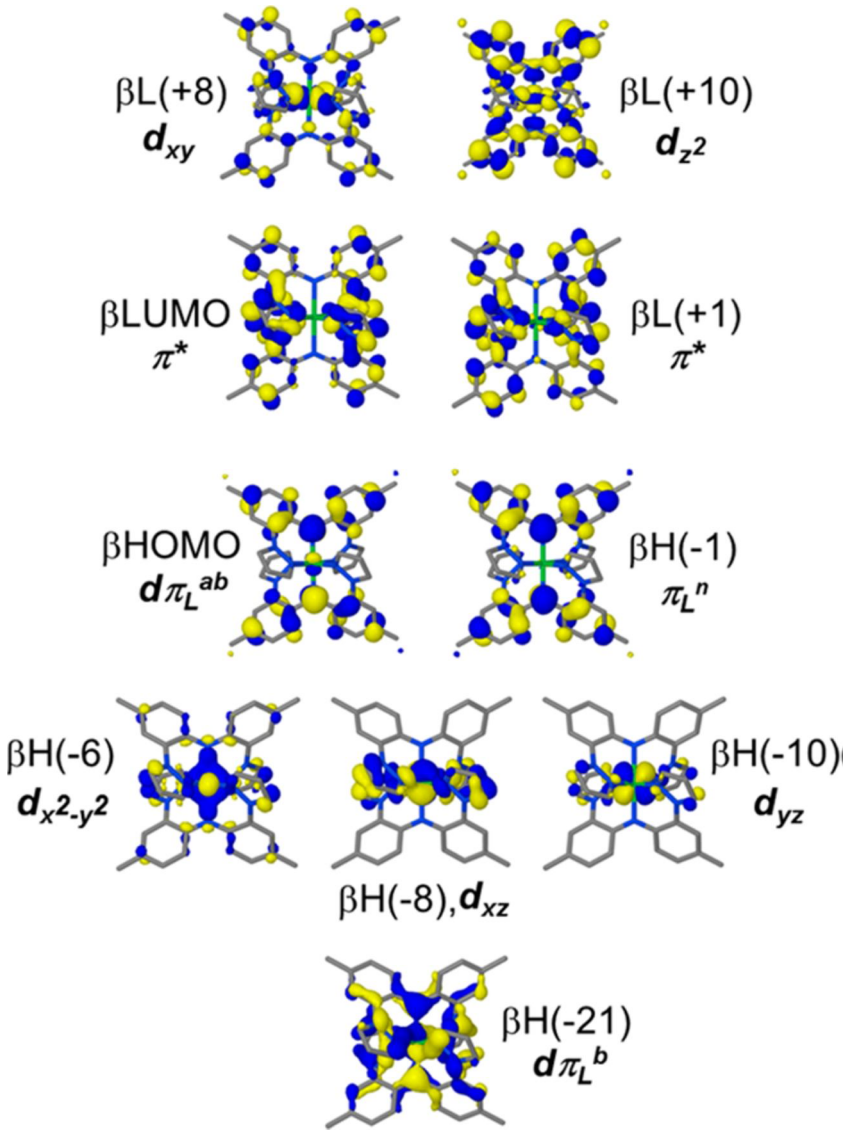

Figure 2.12. *β*-Frontier orbitals of Ni(Me,Me)$_2$ calculated at the M06/ def2-SV(P) level.

mainly nonbonding, but there is a small amount of mixing with a π_L-orbital that has out-of-phase nitrogen p_x-orbitals to give a (presumably weak) dπ−pπ interaction (labeled $d\pi_L^{ab}$ or $d\pi_L^{b}$, in Figure 2.12, where the superscript describes the antibonding or bonding-type of overlap between the d_{xz} and nitrogen p_x-orbitals). Moreover, the nonbonding d_{yz}, d_{x2-y2}, and d_{xz} orbitals are degenerate (or nearly so depending on the level of theory). The

d_{xy} and d_{z2} orbitals are extensively mixed with various π*-orbitals, but those with highest metal character such as *β*-LUMO(+8 or +10), Figure 2.12, are nearly degenerate (by energy considerations) with the latter being slightly higher in energy than the former. Thus, the calculations suggest that despite the low (D_2) symmetry of **1**, the complex behaves electronically like an isolated nickel(II) center in a NiN_6 environment (i.e., with local octahedral symmetry) that only weakly interacts with a ligand π-system. This latter point will be elaborated on in a later section.

2.2.3. Solution Properties. The electronic absorption spectra of **1**−**12** are similar to each other. Exceptions arise from the extended π-systems in **8**, **10**−**12** that shift bands to lower energy (and give higher extinction coefficients) and/or the presence of functional groups in **5**, **8**, **10**, **12** that give more complex bands due to the introduction of added n−π* transitions. Thus, the spectrum of each compound has two main sets of bands in the visible to NIR region (Table 2.4 and Figure 2.13). First, there is a set of high intensity (ε > 10 000 $M^{-1}cm^{-1}$) variably overlapping bands in the higher-energy 300−450 nm range that are due to π_L−π* and ligand-to-metal charge transfer (LMCT) transitions. Such assignments are based on energy and intensity considerations, by spectral comparisons between series of complexes, and by results of time-dependent density functional (TD-DFT) calculations (Computational work). Figure 2.14 shows an overlay of the higher energy bands for a related series of compounds $Ni(Me,Me)_2$, **1**, $Ni(Me,CF_3)_2$, **6**, and $Ni(CF_3,CF_3)_2$, **9**. The bands in the 325−425 region of the spectra of **1**, **6**, and **9** (and in

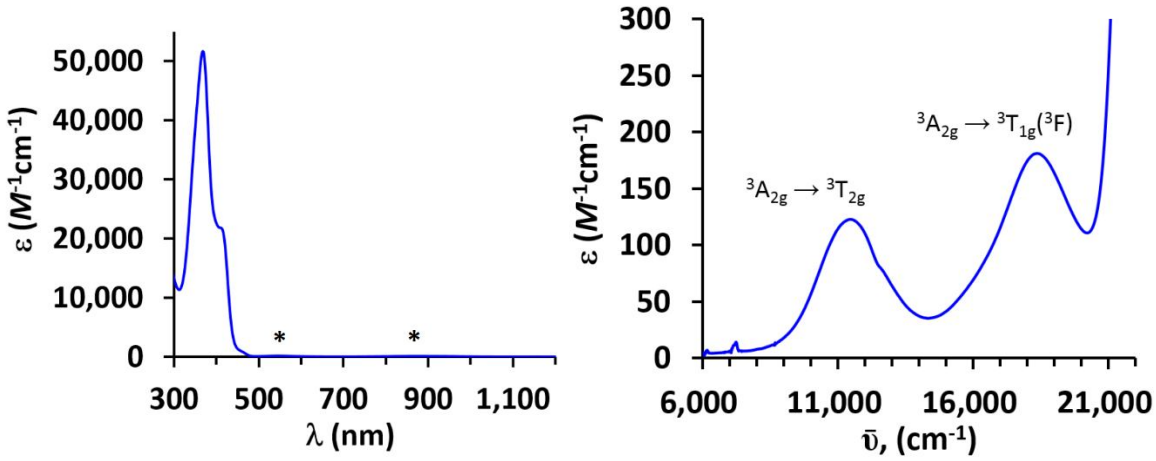

Figure 2.13. Left: The electronic spectrum of Ni(Me,Me)$_2$ in CH_2Cl_2 with asterisks denoting *d-d* bands Right: Close-up view of the spectrum highlighting the *d-d* transitions. The weak peak near 7,100 cm^{-1} is an instrumental artifact.

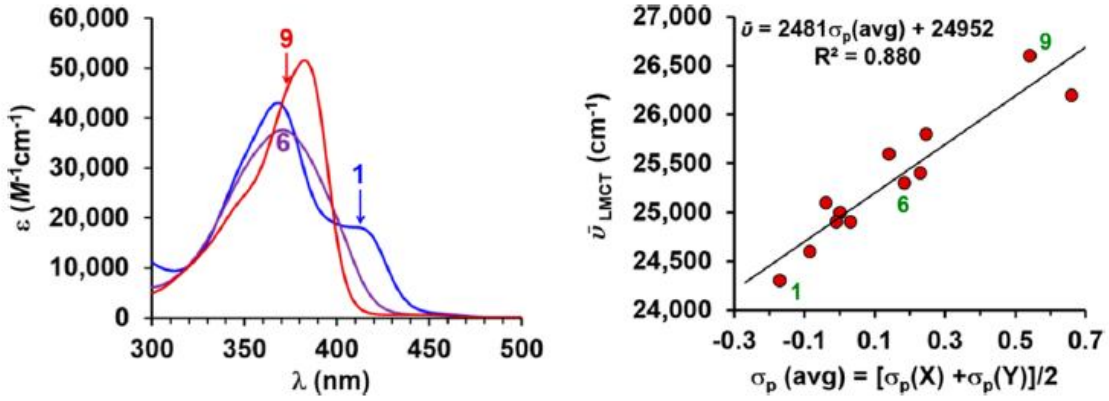

Figure 2.14. Left: Overlay of higher energy portion of the UV−vis spectrum of **1** (blue), **6** (violet), and **9** (red). Right: Plot showing correlation between energy (cm^{-1}) of LMCT transition and the average of the Hammett σ_p parameter of X and Y *para*-aryl substituents in Ni(X,Y)$_2$ complexes **1**−**12**.

most other cases) can be deconvoluted into three main Gaussian components: a band invariantly found at 350 nm, a band that progresses from 368 to 384 nm along the series **1** to **6** to **9**, and a band that appears as a shoulder at 413 nm in the spectrum of **1** that shifts

to 397 nm in **6**, and to 374 in **9**. The hypsochromic shift of the latter band with increasing electronegativity of the *para*-aryl substituent is a hallmark of a LMCT transition. In fact, the energy of this transition scales linearly with the average of the Hammett σ_p parameters[30] of *para*-aryl substituents (X and Y) in $Ni(X,Y)_2$ complexes, right of Figure 2.14. TD-DFT calculations suggest the LMCT transitions in this region are between the ligand's π_L^n orbital (the superscript "n" refers to an in-phase combination of nitrogen p-orbitals on a π_L orbital that is nonbonding by symmetry with respect to any metal d-orbital) and orbitals with significant d_{z2} or d_{xy} character similar to β-LUMO(+8 or +10), Figure 2.12. The slight bathochromic shift of the middle band in the spectra along the series **1**, **6**, and **9** is suggestive of some MLCT character. TD-DFT calculations suggest that this band is indeed due to an admixture of $d\pi_L^{ab}$–π^* (the $d\pi_L^{ab}$ has some metal character) and π_L^n–π^* transitions, while the invariant band component is an admixture of ligand-based π_L^n–π^* and π–π^* transitions. As exemplified by the overlay of spectra for **1**, **6**, and **9** in the left of Figure 2.15 and as collected in Table 2.4, the second common set of bands in the spectra of **1**–**12** are lower energy bands that are of similar shape and occur in the normal range (500 nm < λ_{max} < 1000 nm) for d–d transitions of many other nickel(II) complexes with NiN_6 coordination.[31] The relatively high intensity ($\varepsilon \approx 100$–400 $M^{-1}cm^{-1}$) of these lower energy bands as compared to typical d–d bands ($\varepsilon \approx 1$–100 M^{-1} cm^{-1}) is suggestive of partial charge transfer character. TD-DFT calculations of **1** (right of Figure 2.15 and Table 2.12) support the assertion of partial charge transfer character in these bands. For instance, the lowest energy band is calculated to be the sum of three excitations (at 1033, 1051, and 1170 nm) that are each complex admixtures of transitions involving chiefly the five orbitals in the right of Figure 2.15. The calculated excitation at

Table 2.4. Summary of d−d, LMCT, and $\pi_L-\pi^*$ Bands in the Electronic Absorption Spectra of $Ni(X,Y)_2$ Complexes in CH_2Cl_2.

	$\bar{\upsilon}$, cm^{-1} (ε, M^{-1} cm^{-1})				
compound	$^3A_{2g}\rightarrow{}^3T_{2g}$	$^3A_{2g}\rightarrow{}^3T_{1g}(^3F)$	$^3A_{2g}\rightarrow{}^3T_{1g}(^3P)$[a]	**LMCT**[b]	$\pi_L-\pi^*$
$Ni(Me,Me)_2$, **1**	11 470 (100)	18 400 (180)	29 800	24 300 (18 000)	27 500 (22 300)
$Ni(Me,H)_2$, **2**[e]	11 520 (110)	18 480 (180)	30 130	24 600 (13 100)	27 400 (31 800)
$Ni(H,H)_2$, **3**[e]	11 510 (110)	18 595 (170)	30 700	25 000 (16 000)	24 900 (14 400)
$Ni(Me,Br)_2$, **4**	11 490 (120)	18 550 (210)	30 560	24 900 (16 100)	27 100 (43 000)
$Ni(Me,CO_2Et)_2$, **5**[e]	11 640 (150)	18 900 (430)[c]	31 530	25 100 (50 100)	25 100 (50 100)
$Ni(Me,CF_3)_2$, **6**	11 500 (100)	18 700 (170)	31 260	25 300 (32 000)	26 500 (36 200)
$Ni(Br,Br)_2$, **7**	11 480 (140)	18 670 (250)	31 210	25 400 (23 000)	26 800 (48 100)
$Ni(Me,CN)_2$, **8**	11 590 (195)[d]	18 800 (380)[c]	31 280	25 800 (57 600)	25 800 (57 600)
$Ni(CF_3,CF_3)_2$, **9**	11 640 (120)[d]	18 900 (210)	31 530	26 700 (45 000)	26 100 (51 500)
$Ni(CN,CN)_2$, **10**[e]	11 600 (170)[d]	na		26 200 (47 000)	24 600 (11 800)
$Ni(^{tBu}Ph,^{tBu}Ph)_2$, **11**	11 520 (240)	na		24 900 (69 900)	24 000 (91 800)
$Ni(^{CN}Ph,^{CN}Ph)_2$, **12**[e]	11 650 (350)	na		25 100 (47 000)	22 000 (11 000)

[a]Estimated from Tanabe−Sugano diagram with C/B = 4.71. [b]Occurring as a shoulder or obtained by deconvolution; ε reported as found in spectrum. [c]From deconvolution of spectra. [d]From the average of split bands. [e]As the solvate shown in Scheme 2.5. na = not available, masked by intense ligand-based transitions.

Table 2.5. Ligand Field and nephelauxetic parameters for $Ni(X,Y)_2$ complexes.

Compound	$\bar{\upsilon}$, cm^{-1} (ε, $M^{-1}cm^{-1}$) $^3A_{2g}\rightarrow{}^3T_{2g}$	$^3A_{2g}\rightarrow{}^3T_{1g}$ (^3F)	$^3A_{2g}\rightarrow{}^3T_{1g}(^3P)$[a]	Δ_o/B[a]	B (cm^{-1})[b]	β (cm^{-1})[c]
$Ni(Me,Me)_2$, **1**	11,470(100)	18,400 (180)	29,800	12.6	913	0.84
$Ni(Me,H)_2$, **2**	11,520 (110)	18,480 (180)	30,130	12.3	937	0.87
$Ni(H,H)_2$, **3**	11,510 (110)	18,595(170)	30,700	11.7	985	0.91
$Ni(Me,Br)_2$, **4**	11,490 (120)	18,550 (210)	30,560	12.0	976	0.90
$Ni(Me,CO_2Et)_2$, **5**	11,640 (150)	18,900 (430)[d]	31,530	11.3	1034	0.96
$Ni(Me,CF_3)_2$, **6**	11,500 (120)	18,700 (190)	31,260	11.2	1030	0.95
$Ni(Br,Br)_2$, **7**	11,480 (140)	18,670 (250)	31,210	11.2	1029	0.95
$Ni(Me,CN)_2$, **8**	11,590 (195)[e]	18,800 (380)[d]	31,280	11.4	1020	0.94
$Ni(CF_3,CF_3)_2$, **9**	11,640 (120)[e]	18,900 (210)	31,530	11.3	1034	0.96
$Ni(CN,CN)_2$, **10**	11,600 (170)[e]	*na*	---	---	---	---
$Ni(^{tBu}Ph,^{tBu}Ph)_2$, **11**	11,520 (240)	*na*	---	---	---	---
$Ni(^{CN}Ph,^{CN}Ph)_2$, **12**	11,650 (350)	*na*	---	---	---	---

[a] Estimated from Tanabe Sugano diagram with C/B = 4.71. [b] estimated from $15B = E(^3A_{2g}\rightarrow{}^3T_{1g}(^3F))+E(^3A_{2g}\rightarrow{}^3T_{1g}(^3P))-30Dq$.[53] [c] $\beta = B/(B_{ion} = 1082\ cm^{-1})$. [d] from deconvolution of spectra [e]from the average of split bands. *na* = not available, masked by intense ligand-based transitions.

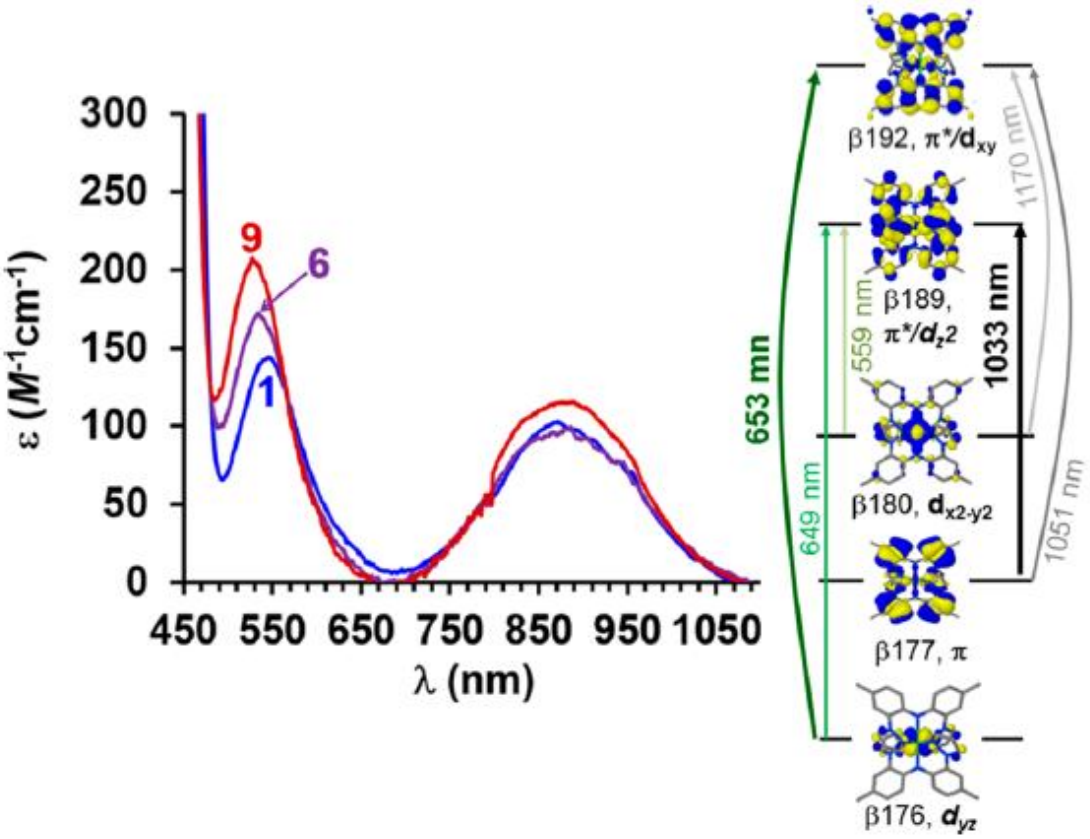

Figure 2.15. Left: Overlay of the lower energy portion of the UV−vis spectrum of **1** (blue), **6** (violet), and **9** (red) in CH_2Cl_2. Right: Summary of results of TD-DFT calculations (M06/def2-SV(P)) for **1**.

1033 nm has the highest oscillator strength of the three components and is bolded most strongly in Figure 2.15. If one only considers the dominant transition (which is at best 25−50% of the total character) of each excitation, the main component of that at the 1030 or 1051 nm excitation is essentially a π−π* transition where the π* has significant metal character from d_{z2} and d_{xy} orbitals. The third excitation calculated at 1170 nm originates from a nearly pure metal orbital (d_{x2-y2}) to a π* orbital with partial d_{xy} character. The less dominant transitions of the three excitations occur between orbitals with a diverse range of d-, π-, π_L-, or π*- character. Finally, as with most other nickel(II) complexes with distorted NiN_6 kernels, it is possible to evaluate the ligand field strength from the energy

of the d−d bands with the aid of Tanabe−Sugano diagrams because the electronic effects arising from distortion from octahedral symmetry are generally small or negligible in room-temperature solution, especially for weaker-field ligands.[31] Notably the 12 current $Ni(X,Y)_2$ complexes have a nearly constant 10Dq value of 11 480(60) cm^{-1}, which is comparable to that found for nickel(II) complexes of other pyrazolyl-based ligands such as the tris(pyrazolyl)borates: $Ni(Tp)_2$ (10Dq = 11 900 cm^{-1}), Ni(Tp*= tris(3,5-dimethylpyrazolyl)borate)$_2$ (10Dq = 11 400 cm^{-1}), or [Ni(Tpm* = tris(3,5-dimethylpyrazolyl)-methane)$_2$]$^{2+}$ (10Dq = 11 700 cm−1).[32] Importantly, the constant value of 10Dq regardless of ligand substitution in these complexes reflects the weakness of any dπ−pπ interactions, in accord with the theoretical calculations.

2.2.4. Cyclic voltammetry. The electrochemical properties of the 12 $Ni(X,Y)_2$ complexes in dichloromethane solution were measured by cyclic voltammetry. A representative set of voltammograms for **1** in CH_2Cl_2 is given in Figure 2.16, and a summary of results is given in table 2.6. Each complex exhibits two one-electron oxidation waves as assessed by comparisons of current intensities with equimolar solutions of ferrocene and by spectrophotometric titrations with various oxidants. With the exception of $Ni(CN,CN)_2 \cdot H_2O$, the oxidation waves were quasi-reversible because the ratios of current peak intensities were unity, but the separation between anodic and cathodic peaks was greater than 59 mV and increased with scan rate (Figure 2.16). For $Ni(CN,CN)_2 \cdot H_2O$, $10 \cdot H_2O$, the voltammograms showed waves characteristic of adsorption processes, because the cathodic current peaks were

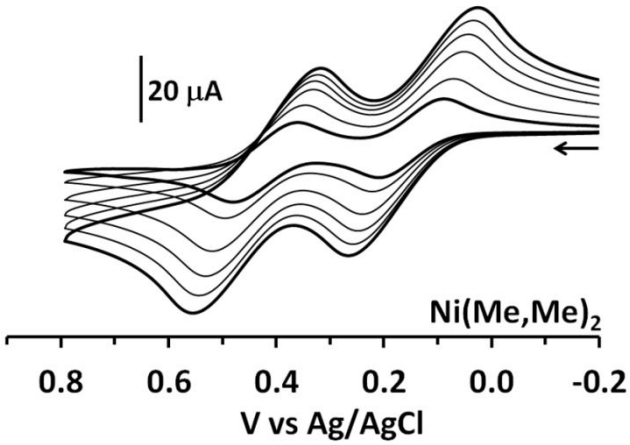

Figure 2.16. Overlay of cyclic voltammograms of $Ni(Me,Me)_2$ in CH_2Cl_2 obtained at scan rates of 50 (inner), 100, 200, 300, 400, and 500 mV/s (outer).

unexpectedly large but decreased on increasing scan rate or after addition of a few drops of CH_3CN (Figure 2.17). As shown in Table 6, the first and second oxidation potentials for $Ni(X,Y)_2$ complexes varied over about 700 mV by simply replacing *para*-aryl ligand substituents. There is a strong linear correlation between the average of the Hammett σ_p parameter of the four *para*-aryl substituents of the $Ni(X,Y)_2$ complexes and either the first or the second oxidation potential (Figure 2.18) where complexes with electron-donating groups are the easiest to oxidize. Such a trend also provides an indication that there is substantial ligand character to the HOMO in both $Ni(X,Y)_2$ and their mono-oxidized counterparts,[33] a feature corroborated by DFT calculations (vide infra). The linear relationship between oxidation potential and Hammett σ_p parameter was useful for establishing the Hammett parameter for the C_6H_4-4-CN group ($\sigma_p = 0.14 \pm 0.03$), which, to the best of our knowledge, was unknown. These electrochemical results also parallel

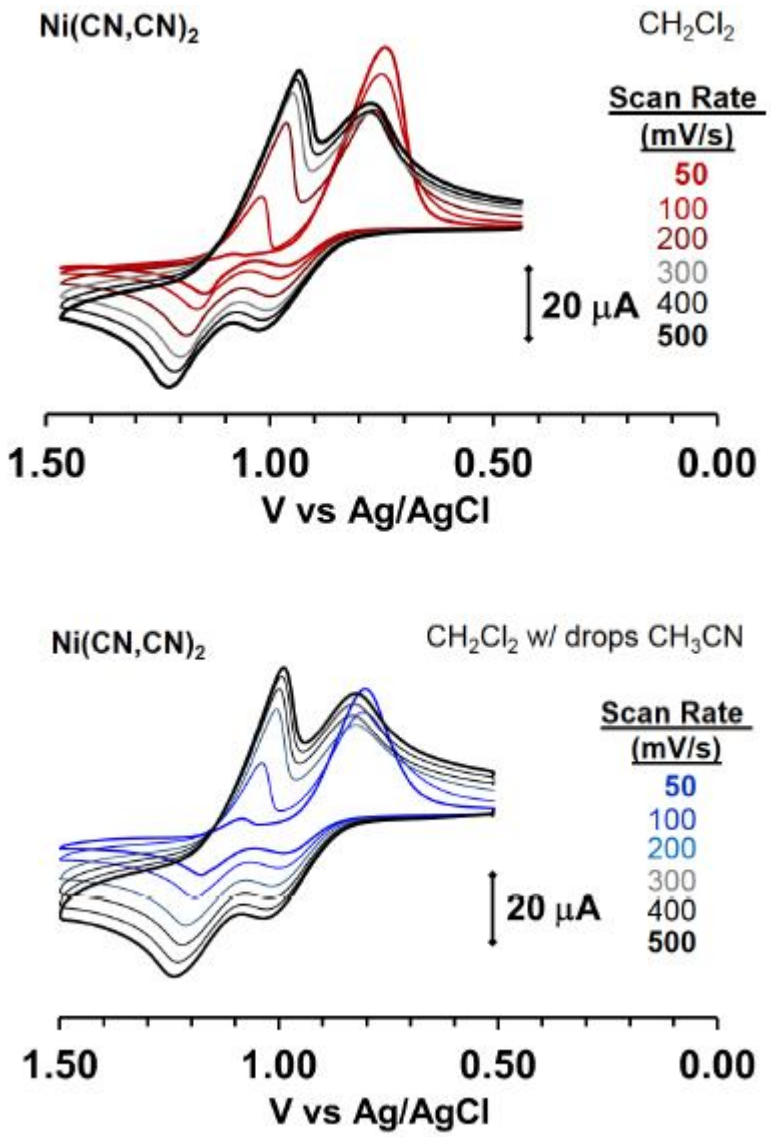

Figure 2.17. Cyclic voltammograms obtained for $Ni(CN,CN)_2$ in CH_2Cl_2 (top) and in CH_2Cl_2 with a few drops of CN_3CN added (bottom). In each case, NBu_4PF_6 is the supporting electrolyte.

those from a recent report by the Heyduk group demonstrating that it was possible to tune the redox potential of tungsten(V) complexes of a trianionic triamido ligand over a 270 mV range by changing groups along the ligand periphery without greatly altering the structures or nitrene transfer reactivity of the complexes.[11a] The separation between the two oxidation potentials of the 12 $Ni(X,Y)_2$ complexes ranges between 200 and about

300 mV. Accordingly, the equilibrium constant for comproportionation (K_{com}, eq 1) varies between 10^4 and 10^6 depending on the complex, but without any obvious trend. Regardless, these values indicate that, on the electrochemical time scale, the mono-oxidized complexes $[Ni(X,Y)_2]^+$ are either Robin−Day class II or are nearing the Robin−Day class II/III borderline of mixed valence species.[34] Because the separation of

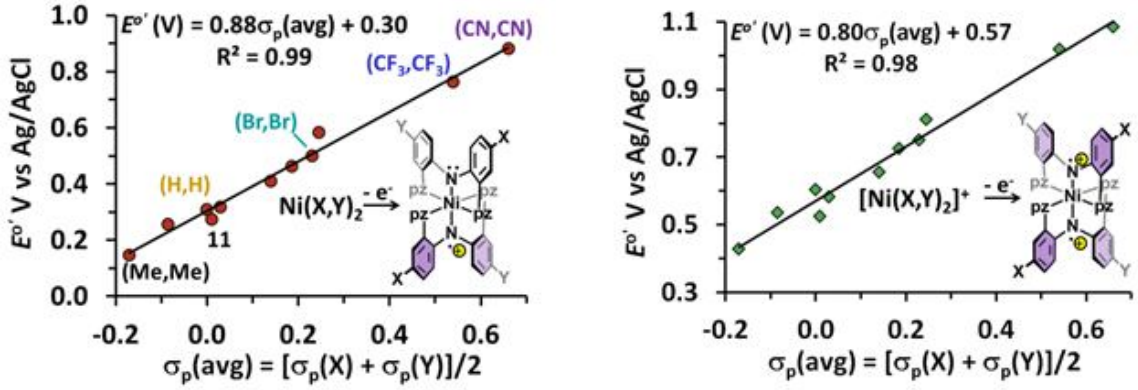

Figure 2.18. Correlations between oxidation potentials and the average of the Hammett σ_p parameter of para-substituents of aryl groups in $Ni(X,Y)_2$ complexes.

Table 2.6. Electrochemical Data from Cyclic Voltammetry Experiments of **1**−**12** and Reference Compounds in CH_2Cl_2.

	$E^{o'}$, V vs Ag/AgCl[a]			
Compound	$E_{1/2,ox1}$ (Δ, mV)	$E_{1/2,ox2}$ (Δ,mV)	K_{com}[b]	σ_p(avg.)[ref]
Ni(Me,Me)$_2$, **1**	0.146 (188)	0.428 (187)	$6.57x10^5$	-0.17
Ni(Me,H)$_2$, **2**[d]	0.257 (154)	0.536 (156)	$5.84x10^5$	-0.085
Ni(H,H)$_2$, **3**[d]	0.311 (187)	0.604 (192)	$1.01x10^6$	0.0
Ni(Me,Br)$_2$, **4**	0.318 (163)	0.582 (165)	$3.24x10^5$	0.03
Ni(Me,CO_2Et)$_2$, **5**[d]	0.409 (230)	0.656 (208)	$1.66x10^5$	0.14
Ni(Me,CF_3)$_2$, **6**	0.464 (174)	0.724 (173)	$2.77x10^5$	0.185
Ni(Br,Br)$_2$, **7**	0.500 (161)	0.751 (153)	$1.94x10^5$	0.23
Ni(Me,CN)$_2$, **8**	0.584 (175)	0.810 (176)	$7.26x10^4$	0.245
Ni(CF_3,CF_3)$_2$, **9**	0.763 (170)	1.019 (168)	$2.36x10^5$	0.54
Ni(CN,CN)$_2$, **10**[d]	0.882 (232)	1.085 (208)	$2.94x10^4$	0.66
Ni(^{tBu}Ph,^{tBu}Ph)$_2$,	0.274 (136)	0.524 (138)	$1.87x10^5$	0.01
Ni(^{CN}Ph,^{CN}Ph)$_2$, **12**	0.455 (153)	0.657 (151)	$2.82x10^4$	0.14[c]
[Ga(Me,Me)$_2$]$^{+3,c}$	1.165 (207)	0.977(223)	$1.62x10^3$	-0.17
Ferrocene	0.522 (180)	---	---	---

[a]Average values obtained for scan rates of 50, 100, 200, 300, 400, and 500 mV/s with 0.1 M NBu_4PF_6 as supporting electrolyte. [b]$K_{com} = e^{(\Delta E \cdot F/RT)}$, T = 295 K. [c] from this work. [d] As the solvate listed in Scheme 1. $\Delta = E_{pa} - E_{pc}$.

oxidation waves alone is insufficient to establish the strength of electronic communication (and hence unambiguous assignment of Robin−Day class)[35] since the separation could be due to simple Coulombic effects rather than or in addition to electronic communication via superexhange or hopping mechanisms, further verification was established by spectroscopic and computational means.

$$Ni(X,Y)_2 + [Ni(X,Y)_2]^{2+} \rightleftarrows 2[Ni(X,Y)_2]^{+}$$

$$K_{com} = [M^{+}]^2/[(M^0)][(M^{2+})] \quad (1)$$

The reactions of $Ni(Me,Me)_2$ with ferrocenium tetrafluoroborate, $Fc(BF_4)$, were investigated, as in Scheme 2.6, to learn more about the properties of the oxidized $[Ni(X,Y)_2]^{n+}$ (n = 1, 2) complexes. The oxidation potentials of $Ni(Me,Me)_2$, **1** (0.15, 0.43 V vs Ag/AgCl), are sufficiently low to permit twoelectron oxidation with the ferrocenium ion, Fc^+ (0.52 V vs Ag/AgCl). Thus, titrations monitored by UV−visible spectroscopy showed that the violet dioxidized complex $[Ni(Me,Me)_2](BF_4)_2$, $(\mathbf{1})(BF_4)_2$, was quantitatively formed in solution by the reaction of **1** with 2 equiv of $FcBF_4$ in dichloromethane, as in the top of Scheme 2.6. On a preparative scale, the sample crystallizes with 2 equiv of CH_2Cl_2 (vide infra), but loses some solvent on drying under vacuum to give a species that analyzes as $(\mathbf{1})(BF_4)_2 \cdot 0.5CH_2Cl_2$. Complex $(\mathbf{1})(BF_4)_2$, prepared in situ or synthetically as the solvate, is stable in air as a solid or as a solution in CH_2Cl_2 or CH_3CN, but slowly decomposes over the course of hours in THF or propylene carbonate. The solid state structures of two solvates of $(\mathbf{1})(BF_4)_2$ were determined by single-crystal X-ray diffraction (Figure 2.19 and 2.20). A comparison of bond distances in the solvates with those in charge-neutral **1** shows two main structural differences. First, the average Ni−N distance in $(\mathbf{1})^{2+}$ is 0.02 Å shorter than that in **1**. This effect is most pronounced in the pyrazolyl groups where the average $Ni-N_{pz}$ distance is 2.065(2) Å in $(\mathbf{1})^{2+}$ but is 2.090(8) Å in **1**. The Ni−N distances involving the aryl amido groups exhibit a lesser or statistically negligible shortening on oxidation; the average $Ni-N_{Ar}$ distance is 2.036(2) Å in $(\mathbf{1})^{2+}$ but is 2.045(7) Å in **1**. This latter observation is opposite of that found for the gallium complexes where oxidation caused a lengthening of the $Ga-N_{Ar}$ bonds (the $Ga-N_{pz}$ bonds shortened upon oxidation, however). A second difference in structures of $(\mathbf{1})^{2+}$ and **1** is manifest in various intraligand C−C and C−N

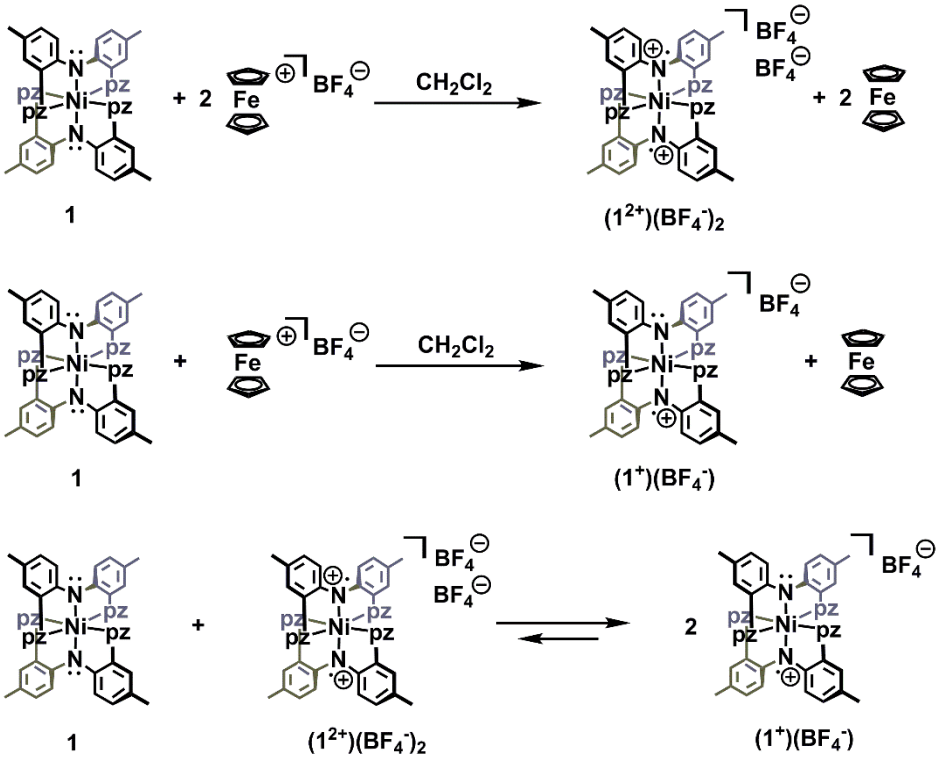

Scheme 2.6. Preparation of oxidized $[Ni(Me,Me)_2]^{n+}$ (n = 1, 2) complexes.

bond distance alterations as well as a decrease in pyrazolyl-aryl dihedral angles on oxidation that are indicative of ortho- quinoidal distortions (Figure 2.21 and Table 2.7) similar to those previously observed in the oxidized ligands of $[Ga(Me,Me)_2]^{n+}$ (n = 2,3) complexes.[19a]

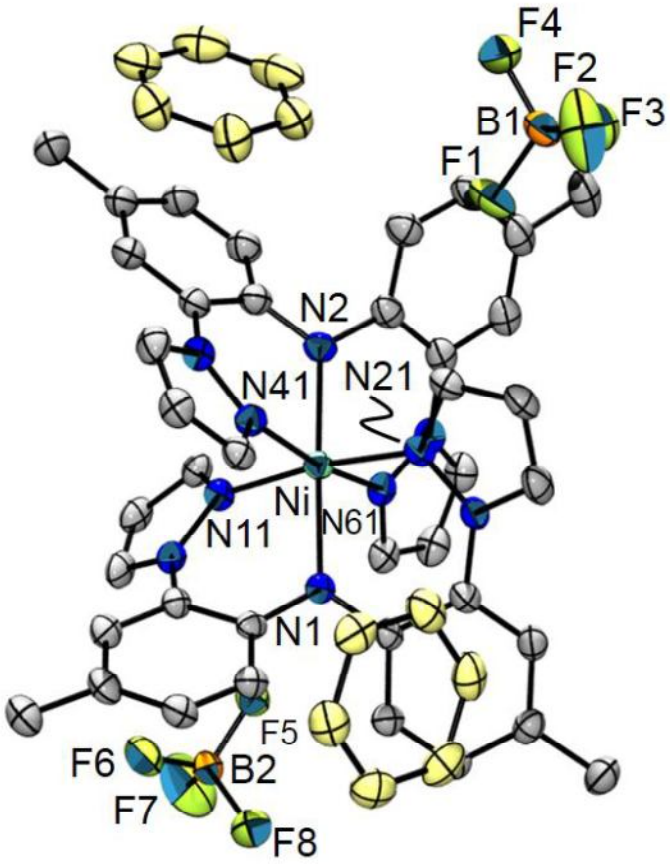

Figure 2.19. Structure of (**1**)$(BF_4)_2 \cdot 2C_6H_6$ with benzene solvent molecules colored goldenrod and with hydrogen atoms removed for clarity. Selected bond distances (Å): Ni1-N1 2.048(3), Ni1-N2 2.020(3), Ni1-N11 2.067(3), Ni1-N21 2.052(3), Ni1-N41 2.076(3), Ni1-N61 2.073(3). Selected bond angles (deg.): N1-Ni1-N11 86.69(12), N1-Ni1-N21 85.65(12), N1-Ni1-N41 95.57(12), N1-Ni1-N61 93.50(13), N2-Ni1-N1 178.25(15), N2-Ni1-N11 94.61(13), N2-Ni1-N21 93.07(13), N2-Ni1-N41 85.61(13), N2-Ni1-N61 85.33(14), N11-Ni1-N41 90.55(12), N11-Ni1-N61 89.66(12), N21-Ni1-N11 172.31(12), N21-Ni1-N41 89.53(13), N21-Ni1-N61 91.47(12), N61-Ni1-N41 170.93(12).

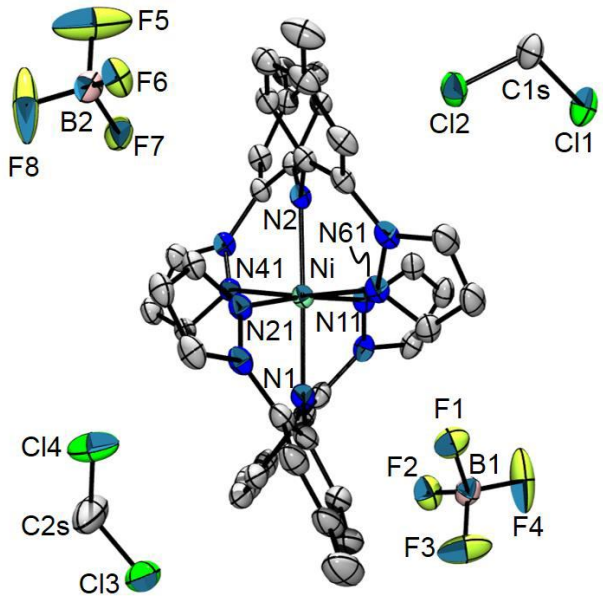

Figure 2.20. Structure of (**1**)$(BF_4)_2 \cdot 2CH_2Cl_2$ with hydrogen atoms removed for clarity. Selected bond distances (Å): Ni1-N1 2.042(3), Ni1-N2 2.033(3), Ni1-N11 2.074(3), Ni1-N21 2.066(3), Ni1-N41 2.057(3), Ni1-N61 2.053(3). Selected bond angles (deg.): N1-Ni1-N11 86.40(11), N1-Ni1-N21 85.79(11), N1-Ni1-N41 92.68(10), N1-Ni1-N61 95.14(11), N2-Ni1-N1 177.56(11), N2-Ni1-N11 92.83(10), N2-Ni1-N21 95.03(10), N2-Ni1-N41 85.05(10), N2-Ni1-N61 87.15(10), N21-Ni1-N11 172.05(10), N41-Ni1-N11 93.08(10), N41-Ni1-N21 88.77(10), N61-Ni1-N11 88.80(11), N61-Ni1-N21 90.43(11), N61-Ni1-N41 172.06(11).

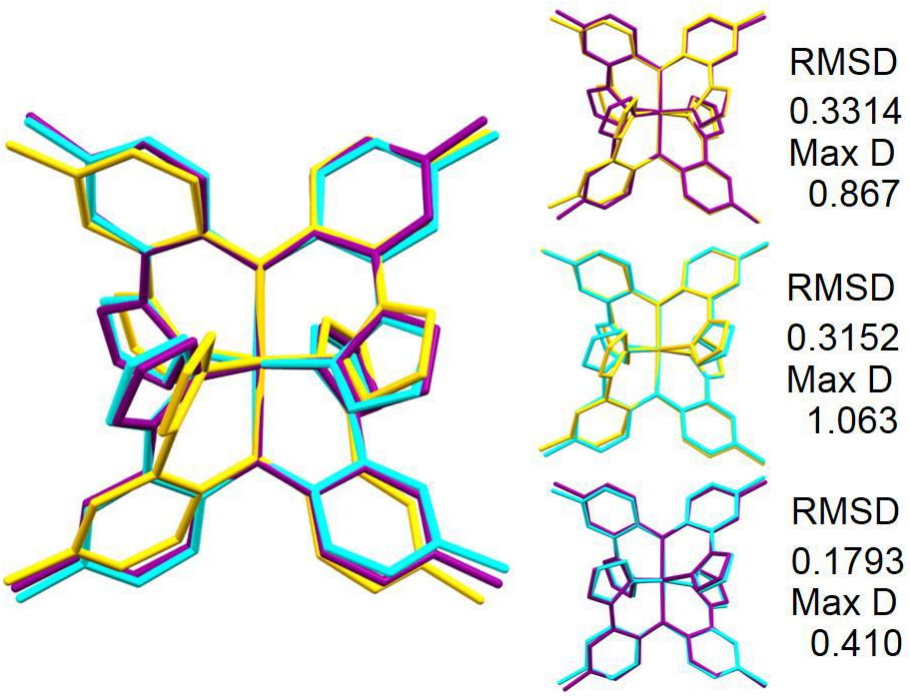

Figure 2.21. Overlays of nickel complexes in **1** (orange), (**1**)$(BF_4)_2 \cdot 2C_6H_6$ (cyan), and (**1**)$(BF_4)_2 \cdot 2CH_2Cl_2$ (violet).

Table 2.7. Intraligand bond labeling scheme and summary of important average bond distances in Å (std dev.) and angles in degrees (std dev.) in **1** and (**1**)$(BF_4)_2$.

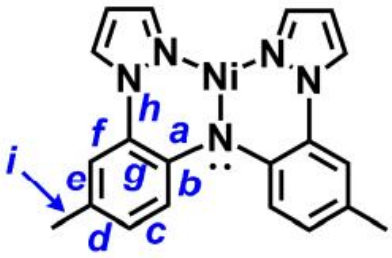

	1	(**1**)$(BF_4)_2 \cdot 2C_6H_6$	(**1**)$(BF_4)_2 \cdot 2CH_2Cl_2$	Avg. (**1**)$(BF_4)_2$	**1**-avg(**1**)$^{2+}$
Ni-N_{Ar}	2.045(7)	2.038(5)	2.034(9)	2.036(12)	0.009
Ni-N_{pz}	2.090(8)	2.063(10)	2.067(9)	2.065(10)	0.025
Ni-N_{all}	2.075	2.054	2.056	2.055	0.02
Bond					
A	1.382(6)	1.383(4)	1.378(11)	1.381(8)	0.001
Bond	1.416(5)	1.412(2)	1.415(5)	1.413(4)	0.002
C	1.376(1)	1.379(5)	1.367(5)	1.373(8)	0.003
D	1.396(2)	1.391(2)	1.394(17)	1.392(11)	0.004
E	1.388(2)	1.390(7)	1.390(3)	1.390(5)	-0.002
F	1.393(3)	1.396(5)	1.385(7)	1.391(8)	0.002
G	1.413(3)	1.422(4)	1.420(9)	1.421(7)	-0.008
H	1.432(6)	1.414(3)	1.423(8)	1.419(8)	0.013
I	1.508(5)	1.510(7)	1.506(8)	1.508(8)	0
Pz-Ar(°)[a]	37(6)	30(7)	27(9)	28(8)	9

[a]dihedral angle between mean planes of pyrazolyl ring and the aryl group to which it is bound

The visible spectrum of (**1**)$(BF_4)_2$ (Figure 2.22) provides another experimental indicator that oxidation is significantly ligand-centered. The spectrum shows modestly intense ($2000 < \varepsilon < 18\,000\ M^{-1}cm^{-1}$) bands in the region of 400−900 nm that are characteristic of π-radical transitions similar to those found in the spectra of mono- and dioxidized $[Ga(Me,Me)_2]^{n+}$ (n = 2,3) complexes, where oxidation is exclusively ligand-

based. The lowest energy d−d band was observed for (**1**)$(BF_4)_2$ (8806 cm^{-1}, ε = 160 $M^{-1}cm^{-1}$) but was not found in the spectrum of (**1**)(BF_4) because it was masked by the IVCT band (vide infra). The room temperature (295 K) solid-state magnetic moment of (**1**)$(BF_4)_2 \cdot 0.5CH_2Cl_2$, μ_{eff} = 4.7 μ_B, is close to but a little lower than μ_{eff} = 4.9−5.2 μ_B expected for an S = 2 species. In contrast to complex **1**, which was EPR silent, the EPR spectrum of the dioxidized complex (**1**)$(BF_4)_2 \cdot 0.5CH_2Cl_2$ in frozen (10 K) CH_2Cl_2 shows a 4S signal near g = 8 in both perpendicular and parallel modes (Figure 2.23) indicative of an S = 2 spin system. While we do not have access to a SQUID magnetometer that would allow for unambiguous assignment of the ground state multiplicity, the S = 2 state appears to be significantly populated even at 10 K. Broken-symmetry[36] DFT calculations of $(\mathbf{1})^{2+}$ at the M06-2X/Def2-TZVP level (computation work) suggest that lower multiplicity states such as the S = 1, $[L(\uparrow)-Ni(\uparrow\uparrow)-L(\downarrow)]^{2+}$, and the S = 0, $L(\downarrow)-Ni(\uparrow\uparrow)-L(\downarrow)]^{2+}$, are much higher in energy than the quintet state.

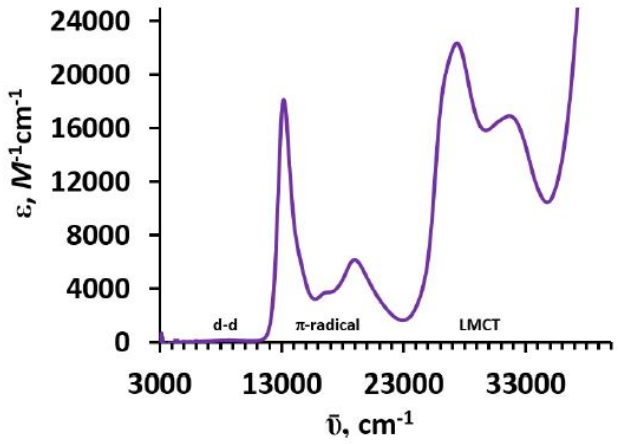

Figure 2.22. Visible/NIR spectrum of $[Ni(Me,Me)_2](BF_4)_2 \cdot 0.5CH_2Cl_2$ in CH_2Cl_2.

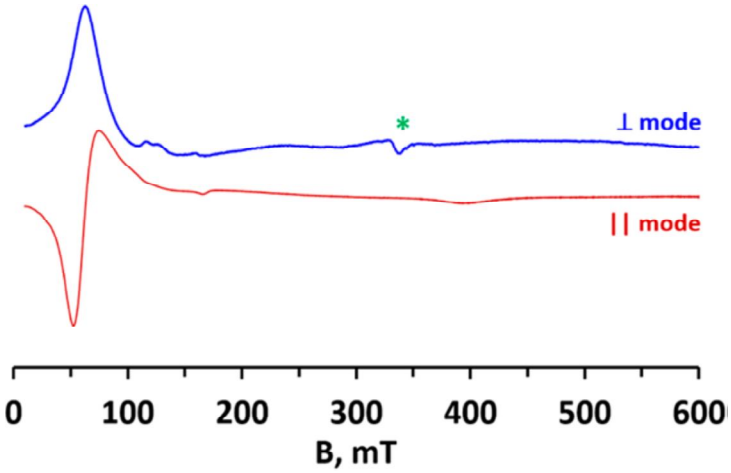

Figure 2.23. X-band EPR spectrum of (**1**)$(BF_4)_2 \cdot 0.5CH_2Cl_2$ in frozen (10 K) CH_2Cl_2 acquired in both perpendicular (blue line) and parallel (red line) modes. The signal near 330 mT from a paramagnetic impurity in the sample chamber is demarcated with a green asterisk. Instrumental parameters: parallel mode, freq = 9.387 GHz; power = 10.0 mW, modulation 10 G; perpendicular mode, freq = 9.632 GHz, power = 2.0 mW, modulation 10 G.

The UV−visible spectrum of (**1**)(BF_4) (Figure 2.24) is sufficiently distinct from either **1** or (**1**)$(BF_4)_2$ to allow spectroscopic monitoring of its formation. UV−visible spectrophotometric titrations show that the blue-violet monooxidized complex (**1**)(BF_4) is formed quantitatively by the comproportionation reaction between **1** and $(\mathbf{1})^{2+}$ in CH_2Cl_2, as in the bottom of Scheme 2.6. On the synthetic scale, a species that analyzes as (**1**)$(BF_4)\cdot 0.5CH_2Cl_2$ is isolated from the comproportionation reaction. While UV−visible spectroscopic monitoring indicates that reaction between **1** and 1 equiv of $FcBF_4$ in CH_2Cl_2 affords (**1**)(BF_4) (as in the middle of Scheme 2.6), the isolation of pure (**1**)(BF_4) by this route is complicated by the need to separate ferrocene without disrupting the disproportionation/comproportionation equilibrium. For example, washing the mixture of (**1**)(BF_4) and ferrocene with toluene or hexanes in an attempt to remove ferrocene also removed some **1** and contaminated the product with (**1**)$(BF_4)_2$ due to disproportionation (i.e., the reverse reaction in the bottom of Scheme 2.6). As with the dioxidized derivative,

(**1**)(BF_4) is stable in air as a solid and as solutions in either CH_2Cl_2 or CH_3CN, but solutions in THF or propylene carbonate degrade over the course of hours.

The absorption spectrum of (**1**)(BF_4) shows medium intensity bands in the visible region (450−900 nm, left of Figure 2.24) for π-radical transitions. In addition, a weaker intensity but broad band is found in the near- to mid-IR region that is absent in the spectrum of either **1** or (**1**)$(BF_4)_2$. This new band is attributed to the intervalence charge transfer (IVCT) transition, which is expected of a Robin−Day class II or III mixed valence species. Typically, band-shape analysis of the IVCT band is used to obtain information regarding the strength of electronic communication in mixed-valence complexes. In the current case, the limited spectral range of the absorption spectrometer and the difficulties inherent in obtaining molar absorptivity data from IR spectra hinder highly accurate band shape analyses, so an estimate was made by averaging multiple attempts at Gaussian fits of the partial band found in the NIR absorption spectral data. A summary of the data for (**1**)(BF_4) and the related gallium complex, $[Ga(Me,Me)_2]^{2+}$, is given in Table 2.8. The use of the Hush relations[37] in eqs 2 and 3 to estimate the electronic coupling element H_{ab} revealed that there is stronger electronic communication between oxidized and nonoxidized ligands in (**1**)(BF_4) than found for $Ga(Me,Me)_2](PF_6)(SbCl_6)$, in qualitative agreement with the electrochemical data. In these relations, E_{OP} is the energy of the absorption maximum in cm^{-1}, λ is the Marcus reorganization energy, ε_{max} is the molar extinction coefficient, $\Delta\tilde{\nu}_{1/2}$ is the full-width-at-half-maximum in cm^{-1}, and d is the separation between redox centers in Å. The value of d = 4.088 was the nitrogen−nitrogen distance between amido groups found in the geometry-optimized structure of $[Ni(Me,Me)_2]^+$ from DFT calculations (M06/def2-SV(P)) and gives the upper limit for

the strength of electronic communication.[38] Spectroscopic evidence in support of the assignment of (**1**)(BF_4) as a Robin−Day class II mixed Table 2.8; valence species includes: (i) the solvent dependence of the IVCT band, as summarized in (ii) Gaussian fits of the IVCT band had an experimental $\Delta\tilde{\nu}_{1/2}$ that was larger than the theoretical value[34a,40] $\Delta\tilde{\nu}_{1/2}(\mathrm{HTL}) = [16\ \ln(2)kBT\lambda]^{1/2}$; and (iii) the calculated values of H_{ab} (466 cm^{-1}) and λ (3050) cm^{-1} fall within the accepted limits of $0 < H_{ab} < \lambda/2$ or $0 < 2H_{ab}/\lambda <(1 - [\Delta\tilde{\nu}_{1/2}(\mathrm{HTL})]/2\lambda)$ for class II or class IIA species, respectively.[40] The thermal energy barrier to electron transfer$\Delta G^* = 378\ cm^{-1}$ calculated using eq 4 from classical Marcus theory[41] is lower than $\Delta G^* = 1344\ cm^{-1}$ found for the gallium complex, which is understandable because it was anticipated that the 3d-orbitals of the nickel center would engage in dπ−pπ interactions with the ligand (vide infra), whereas the 3d-orbitals in the gallium complex are expected to be energetically inaccessible. As such, the rate constant for electron transfer, $k_{et} = 6.8 \times 10^{13}\ s^{-1}$, calculated using eq 5 (where Planck's constant, h = $3.336 \times 10^{-11}\ cm^{-1}$ s, Boltzmann's constant, $k_B = 0.695\ cm^{-1}\ K^{-1}$, and T = 295 K) is about 3 orders of magnitude greater in (**1**)(BF_4) than in $[Ga(Me,Me)_2]^{2+}$.

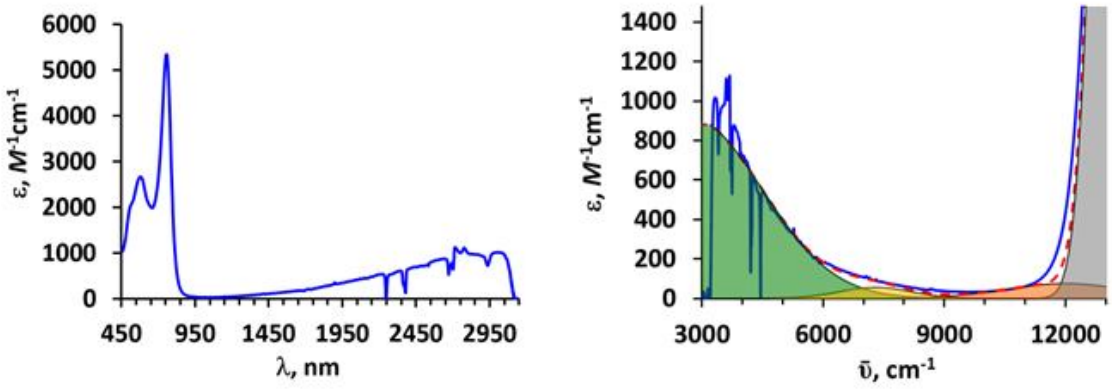

Figure 2.24. Left: Visible/NIR spectrum of $[Ni(Me,Me)_2]^+$ in CH_2Cl_2. Right: Close-up view of NIR region (in cm^{-1} units) with one attempt at spectral deconvolution shown (Gaussian curves are color-shaded; the sum of curves is the red dashed line).

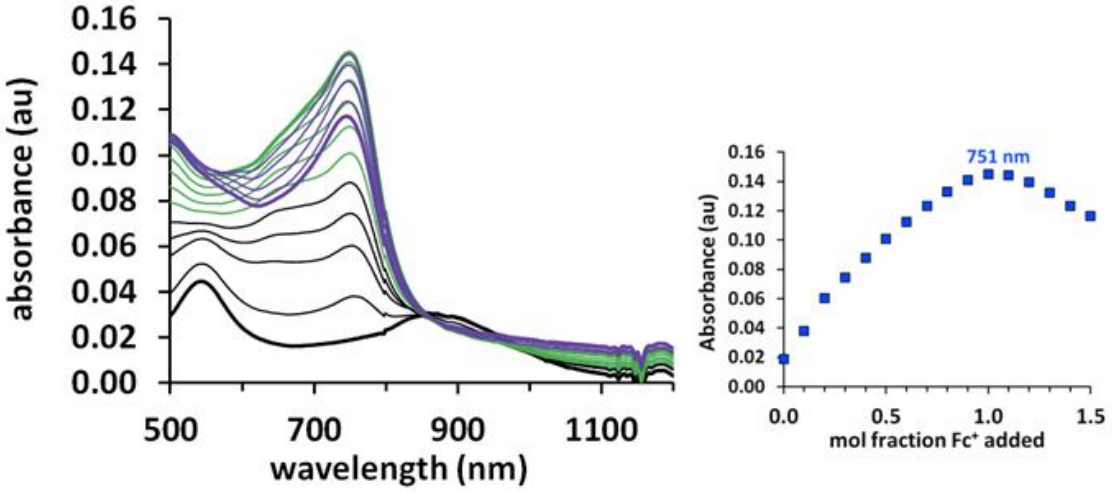

Figure 2.25. Spectroscopic titration of Ni(Me,Me)$_2$ with Fc(PF_6) in CH_2Cl_2.

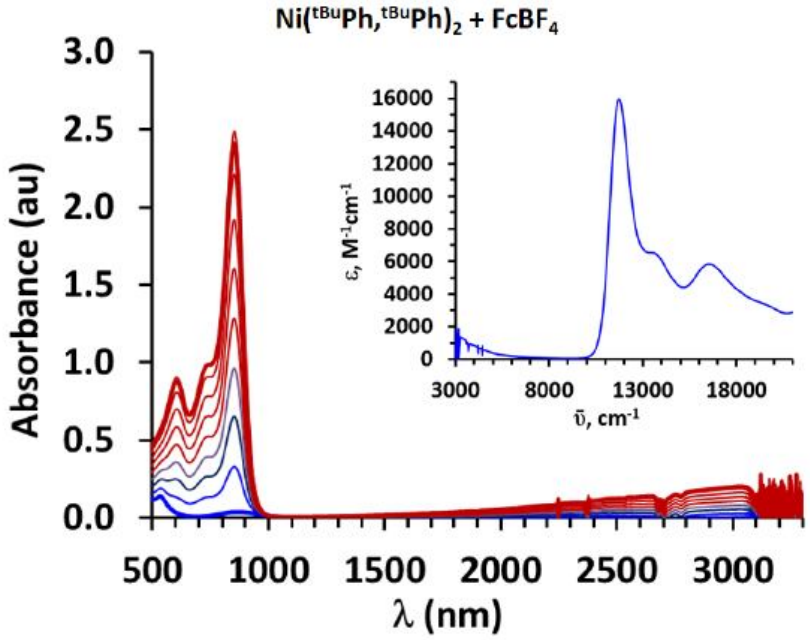

Figure 2.26. Vis-NIR spectra from incremental addition of $FcBF_4$ to solution of Ni(^{tBu}Ph,^{tBu}Ph)$_2$ in CH_2Cl_2. Inset: Spectra of Ni(^{tBu}Ph,^{tBu}Ph)$_2$(BF_4) in wavenumber units.

$$E_{OP} = \lambda \qquad (2)$$

$$H_{ab}\,(cm^{-1}) = [(4.2x10^{-4})\varepsilon_{max}\Delta\tilde{\nu}_{1/2}E_{OP}]^{1/2}/d \qquad (3)$$

$$\Delta G^* = (\lambda - 2H_{ab})^2/4\lambda\ cm^{-1} \qquad (4)$$

$$k_{et} = (2H_{ab}^2/h)[\pi^3/\lambda k_B T]^{1/2}\exp-(\Delta G^*/k_B T) \qquad (5)$$

Table 2.8. Summary of IVCT band shape fitting and ET parameters of (**1**)(BF_4) and $[Ga(Me,Me)_2](PF_6)(SbCl_6)$ in CH_2Cl_2 and CH_3CN.

	(**1**)(BF_4)		$[Ga(Me,Me)_2]^{2+}$ [b]	
	CH_2Cl_2[a]	CH_3CN[a]	CH_2Cl_2	CH_3CN
$E_{OP} = \lambda$ (cm^{-1}), Eq. 2	3050 (173)	3450 (250)	6390	6925
ε_{max} ($M^{-1}cm^{-1}$)	988 (14)	730 (30)	79	55
$\Delta\tilde{\nu}_{1/2}$ (cm^{-1})	2875 (479)	4600 (400)	5192	4900
oscillator strength[c], f_{obs}	1.3 (2) $x10^{-2}$	1.5 (1) $x10^{-2}$	$1.9x10^{-3}$	$1.2x10^{-3}$
H_{ab} (cm^{-1}), see Eq. 3	466 (26)	539 (15)	264	223
$\Delta\tilde{\nu}_{1/2}$ *(HTL)*[d]	2633 (76)	2800 (100)	3812	3968
$\Theta = \Delta\tilde{\nu}_{1/2}/\Delta\tilde{\nu}_{1/2}$ *(HTL)*	1.1 (2)	1.6 (2)	1.36	1.23
$\alpha = 2H_{ab}/\lambda$	0.30 (2)	0.231 (3)	0.083	0.064
ΔG^* (cm^{-1}), see Eq. 4	378 (32)	408 (67)	1344	1515
k_{et} (s^{-1}), see Eq. 5	1.4 (2) $x10^{13}$	1.6(4) $x10^{13}$	2.9 $x10^{10}$	8.6 $x10^{9}$

[a] Standard deviation given in parantheses. [b]see ref 19a. [c]$f_{obs} = (4.6x10^{-9})\lambda_{max}\Delta\tilde{\nu}_{1/2}$; [d]$\Delta\tilde{\nu}_{1/2}$ *(HTL)* $= [16\ln(2)k_B T\lambda]^{1/2}$ where $k_B = 0.695\ cm^{-1}K^{-1}$ and T = 295 K.

2.2.5. EPR. The EPR spectra of (**1**)(BF_4) and (**11**)(BF_4) in frozen CH_2Cl_2 (10−70 K) were recorded. Each gave a similar rhombic spectra characteristic of an S = 3/2 species. The spectra of the latter complex at 70 and 10 K are shown in Figure 2.27, while the spectrum of (**1**)(BF_4) is shown in Figure 2.28.

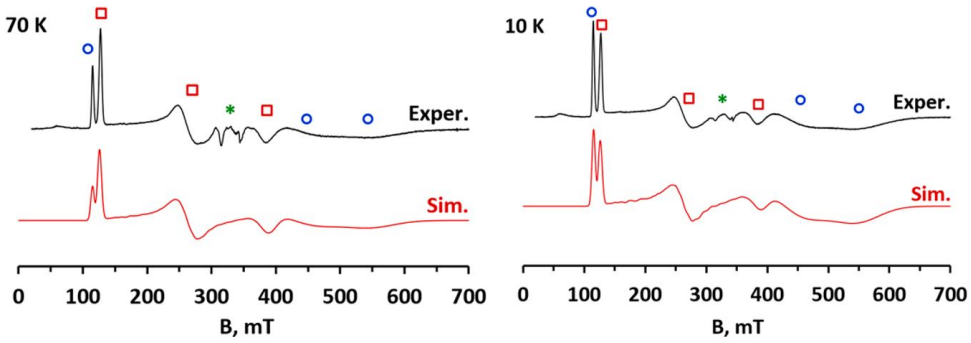

Figure 2.27. Experimental (black line, top) and simulated (red line, bottom) X-band (9.632 GHz) spectrum of [Ni(^{tBu}Ph,^{tBu}Ph)$_2$](BF$_4$) in CH_2Cl_2 at 70 K (left) and 10 K (right). A paramagnetic impurity in the experimental spectra near 330 mT is demarcated with a green asterisk. The simulated spectra were obtained using g_{real} = 2.10; D = 3.34 cm^{-1}, *E/D* = 0.245, and a D-strain of 0.5 cm^{-1}. Signals due to ms = |±3/2⟩ and |±1/2⟩ transitions are marked with blue "○" and red "□", respectively. Instrumental parameters: 70 K, power = 5.0 mW, modulation 10 G; 10 K, power = 2.0 mW, modulation 10 G.

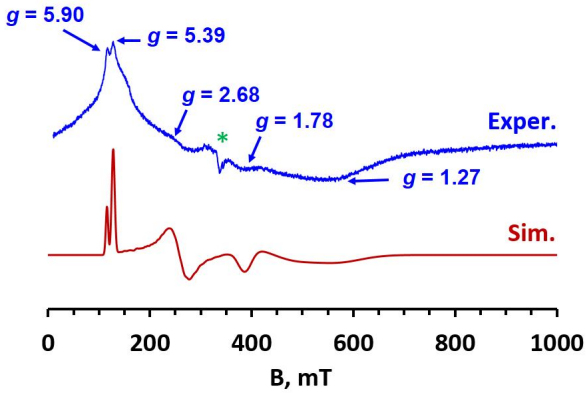

Figure 2.28. X-Band EPR spectrum of [Ni(Me,Me)$_2$](BF$_4$)·0.5CH_2Cl_2 in CH_2Cl_2 at 10 K. Instrumental parameters: Freq. = 9.632 GHz; Power = 0.2 mW, modulation 10 G.

The spectrum of (**11**)(BF$_4$) is a superposition of signals from an S = 3/2 species and a small paramagnetic impurity from the sample chamber (green asterisks, Figure 2.27). The signals from the S = 3/2 species were successfully simulated[42] by using g_{real} = 2.10, a zero-field splitting parameter, *D*, of 3.3 cm^{-1}, and a rhombicity, *E/D*, of 0.245. The small value of *D* ensures that the intra doublet transitions of both the m_s = |±3/2⟩ ground state

(blue ○, Figure 2.27) and the $m_s = |\pm 1/2\rangle$ excited state (red □, Figure 2.27) are populated even at 10 K. Upon warming to 70 K, the signals due to the $m_s = |\pm 1/2\rangle$ component ($g_z^{eff} = 1.682$, $g_y^{eff} = 5.194$, $g_x^{eff} = 2.488$) grow in intensity at the expense of the signals for the $m_s = |\pm 3/2\rangle$ component ($g_z^{eff} = 5.682$, $g_y^{eff} = 1.194$, $g_x^{eff} = 1.512$). Similarly, simulations of the spectra of (**1**)(BF_4) afforded $g_{real} = 2.09$, $D = 2.3$ cm^{-1}, and $E/D = 0.236$.

2.2.6. Computational. To more clearly ascertain the electronic structure of (**1**)(BF_4), the cation (**1**)$^+$ was studied computationally. Five salient features arose from the DFT and TD-DFT calculations on (**1**)$^+$ and comparisons with those on its $[Ni(Me,Me)_2]^{n+}$ (n = 0, 2) relatives. First, the calculated gas-phase structures of **1** and (**1**)$^{2+}$ produced Ni−N bond distances that were only 0.02 Å longer than those in the solid state, and the experimental structural trend of shortening Ni−N_{pz} distances for deoxidized complexes held for the calculated structures, observations that give confidence to the findings for (**1**)$^+$. Importantly, because it was not possible to grow single crystals of $[Ni(Me,Me)_2]^+$ for structural studies, the theoretical geometry optimization showed that (**1**)$^+$ has disparate Ni−N_{Ar} bond distances of 2.063 and 2.025 Å and an estimated $N_{Ar}\cdots N_{Ar}$ distance of 4.088 Å (this latter distance was used in the Hush analysis, vide supra). Moreover, the relative coplanarity of pyrazolyl and aryl rings as well the intraligand bond distances that show orthoquinoidal distortions indicate that the ligand with the longer Ni−N_{Ar} bond was oxidized, whereas the other ligand is not oxidized. That is, the nonoxidized ligand has an average dihedral angle close to 40°, whereas an oxidized ligand has an average dihedral angle near 30° (Table 2.9). Also, the *ortho*-quinoidal distortion in an oxidized ligand of (**1**)$^+$ or (**1**)$^{2+}$ is characterized by shorter C−N_{pz} bonds and a longer C−C bond located between the pyrazolyl and amido nitrogens (Table 2.9, Figure 2.29) versus those bonds in

an unoxidized ligand. Second, despite the lack of solvated anions, the difference in calculated first- and second-reduction potentials, ΔE^0_{calc} = 144 mV (M06-2X/TZVP), associated with the $[Ni(Me,Me)_2]^{n+}$ (n = 0, 1, 2) redox series was aligned with the experimental result, ΔE^0_{exp} = 282 mV. Third, the second oxidation is ligand-centered as suggested by the β-HOMO of $(\mathbf{1})^+$, which has only small contribution from the metal d_{xz} as shown in the bottom of Figure 2.30. The lower symmetry of $(\mathbf{1})^+$ complicates its MO diagram versus that of **1** or $(\mathbf{1})^{2+}$ because it allows mixing of orbitals that is not permitted by the higher symmetry structures of **1** or $(\mathbf{1})^{2+}$. This point can be illustrated by the β-HOMO of $(\mathbf{1})^+$ shown in Figure 2.30. Here, the orbital is mainly ligand-based and is similar to the π_L^n orbital in **1** ((like β-HOMO(−1), Figure 2.12, with inphase nitrogen p_x orbitals), but the lobes of the "bottom-half" of the orbital are larger than those in the "top half". The asymmetry the "distorted" π_L^n orbital allows some mixing with the d_{xz} orbital to give partial (π-)antibonding character to the N−Ni−N interaction, an interaction that is not allowed by symmetry in **1** or $(\mathbf{1})^{2+}$. The fourth salient point from the calculations then is that the lowest energy electronic excitation of $(\mathbf{1})^+$, β-HOMO → β-LUMO, is an intervalence charge transfer transition predicted to be in the NIR to IR region. This transition occurs at an energy that depends on solvent, which is characteristic of a Robin−Day class II species and is fully consistent with the experimental observations.

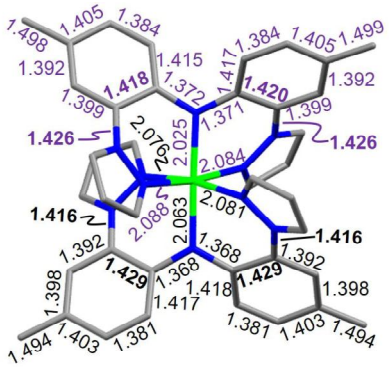

Figure 2.29. Calculated bond distances (Å) within $[Ni(Me,Me)_2]^+$. The values in black represent distances associated with an oxidized ligand whereas those in violet are typical of a non-oxidized ligand. The values in bold are C-C and C-N bonds that show greatest discrepency.

Moreover, several intense (oscillator strength, $f > 0.01$) β-HOMO(−N) (where $N \geq 1$ and that are essentially aryl-based π orbitals) to β-LUMO ($d\pi_L^{ab}$) electronic (π-radical) transitions are predicted to be found in the far red to green regions of visible region in the spectra of $(\mathbf{1})^+$ and $(\mathbf{1})^{2+}$, in accord with experiment. The fifth and final point is that the broken symmetry calculations showed that the quartet state of $(\mathbf{1})^+$ was only 1.64 kcal/mol lower in energy than the doublet, $[L(\uparrow\downarrow)-Ni(\uparrow\uparrow)-L(\downarrow)]^+$, state. Thermal population of the doublet state may account for the lower than expected magnetic moment of each (1)+ and (11)+ measured in the solid state at room temperature.

Table 2.9. Bond Labeling diagram and calculated (M06/Def2-SV(P)) bond distances and angles in $Ni(Me,Me)_2$, $[Ni(Me,Me)_2]^+$, and $[Ni(Me,Me)_2]^{2+}$. Average experimental values are given for comparison.

	Calculated Average (std. dev.)[a]			**Experimental**	
	$Ni(Me,Me)_2$	$Ni(Me,Me)_2^+$	$Ni(Me,Me)_2^{2+}$	**1**	Avg.
Ni-N_{Ar}	2.061(1)	2.044(19)	2.060(1)	2.045(7)	2.036(12)
Ni-N_{pz}	2.108(1)	2.082(6)	2.072(1)	2.090(8)	2.065(10)
Ni-N_{all}	2.092	2.07	2.068	2.075	2.055
Bond					
A	1.373	1.37	1.367	1.382(6)	1.381(8)
Bond	1.419	1.417	1.418	1.416(5)	1.413(4)
C	1.384	1.383	1.381	1.376(1)	1.373(8)
D	1.404	1.404	1.404	1.396(2)	1.392(11)
E	1.391	1.395	1.4	1.388(2)	1.390(5)
F	1.400	1.396	1.39	1.393(3)	1.391(8)
G	1.418	1.424	1.429	1.413(3)	1.421(7)
H	1.425	1.421	1.417	1.433(6)	1.419(8)
I	1.499	1.496	1.493	1.508(5)	1.508(8)
Pz-Ar(°)[a]	41(1)	34(3)	32(1)	37(6)	28(8)

[a]bond distances in Å; [b]dihedral angle between the mean plane of a pyrazolyl ring and that of the aryl group to which it is bound

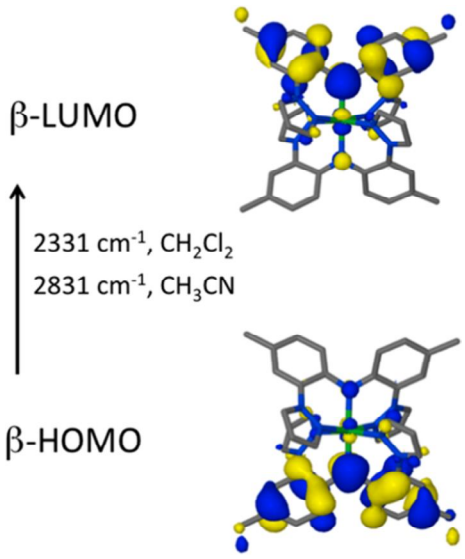

Figure 2.30. Frontier orbitals of $[Ni(Me,Me)_2]^+$ with the calculated energies of the intervalence charge transfer band (TD-DFT, M06/Def2-SV(P)).

2.3. SUMMARY AND CONCLUSIONS

We used four synthetic approaches to prepare eight new and four known pincer-type ligands that have pyrazolyl flanking donors attached to a diarylamine anchor. The 12 pincer variants differ only by the *para*-aryl substituents of the anchor, substituents that dominate the electronic properties of the ligands. As we will report in due course, the synthetic methods reported here are useful because they allow access to a variety of pincer ligands that have different flanking donors and diverse electronic properties. In the current case, we used the 12 ligands to prepare a series of charge-neutral nickel(II) complexes, $Ni(X,Y)_2$, via a simple, high yielding, one-pot reaction that only required filtration for purification of the very poorly soluble desired product. A survey of the electrochemistry of the complexes showed that the first and second oxidation potentials varied linearly over a remarkable 700 mV range with the average of the Hammett σ_p parameters of the ligand's para-aryl substituents. Such a finding may be useful for

"custom-designing" future reagents for redox-titrations or synthetic single-electron transfer reactions. Importantly, it was found that the oxidation waves were ligand-based regardless of *para*-aryl substituents. This finding was aided by the detailed spectroscopic and computational studies of the singly and doubly oxidized complexes $[Ni(Me,Me)_2]^{n+}$ (n = 1, 2). These studies showed that the unpaired electron(s) on the ligand and those on the nickel center remain essentially uncoupled; the magnetic and EPR spectral data for $[Ni(Me,Me)_2](BF_4)_2$ and $[Ni(Me,Me)_2](BF_4)$ are consistent with S = 2 and S = 3/2 species, respectively. The magnetic orbitals on the oxidized ligands (essentially the amido nitrogen p_x-orbitals directed between molecular axes) are orthogonal to those partly filled orbitals on the metal (d_{z2} and d_{xy} that are directed along the Ni−N_{Ar} bonds), which allows ferromagnetic-type interactions. A comparison of the spectroscopic properties of mono-oxidized complex $[Ni(Me,Me)_2](BF_4)$ and the previously known monooxidized gallium(III) complex $[Ga(Me,Me)_2]^{2+}$ afforded insight into the potential role that a bridging metal center can play in mediating electronic communication between its bound unoxidized and oxidized ligands. Such information will be important for making astute decisions about the future design of molecular wires based on covalent or noncovalent assemblies of metal complexes of redox-active pincer complexes. In this vein, the gallium(III) complex $[Ga(Me,Me)_2]^{2+}$ was previously found to be a Robin−Day class II mixed valence species with weak electronic coupling likely occurring via superexchange across the metal bridge facilitated by the energetically accessible empty orbitals. It was originally anticipated that the replacement of gallium with a transition metal would ensure much stronger electronic communication because the metal dorbitals would allow for dπ−pπ interactions with the ligand's π-system. The electrochemical and

spectroscopic studies indeed demonstrated electronic communication exists between oxidized and unoxidized ligands in the mono-oxidized nickel complex $[Ni(Me,Me)_2]^+$. However, both the nickel and the gallium complexes are Robin−Day class II(A) mixed valence compounds; the late first-row transition metal only modestly strengthened the communication between ligands as compared to the diamagnetic p-block metal. The theoretical studies revealed that the dπ−pπ interaction in the nickel complex arises from partial mixing of energetically mismatched ligand and (mainly) nonbonding d_{xz} orbitals. It is noted that nickel has the highest spectroscopic electronegativity (1.88 Pauling units) and one of the lowest d-orbital energies (−12.93 eV) of the first row transition metals.[43] Because the energies of the 3d-orbitals in gallium(III) are expected to be much lower than those in nickel(II), there was no dπ−pπ interaction (*β*-HOMO, Figure 2.12). For complexes of the type $[M(Me,Me)_2]^{n+}$, the strength of the dπ−pπ interaction is expected to scale with an increase in d orbital energies until an energetic match is made with the nearly degenerate set of (noncomplexed) ligand orbitals: the symmetric (nonbonding) combination, π_L^n (like *β*-HOMO(−1), Figure 2.12), and its asymmetric counterpart that participates in the dπ−pπ interaction. Better energetic matches with the ligand are expected to occur with the early transition metals, or with second row and third row metals. For such complexes, it is also expected that one electron-oxidation should lead to species that traverse the Robin−Day class II/III border. A future report will detail the effects of replacing metals on the strength of electronic communication and on the relative stability of electronic states in oxidized homoleptic pincer complexes. We will also detail our endeavors at making assemblies from these electroactive units.

2.4 EXPERIMENTAL

General Considerations. The compounds CuI, ^{t}BuONO, $CuBr_2$, CuI, M_2CO_3 (M = Na, K, Cs), *N*-Bromosuccinimide (NBS), Pd(acetate = $OAc)_2$, 2,2'-Bis(diphenylphosphino)-1,1'-binaphthyl (BINAP), 1-bromo-2-fluorobenzene, pyrazole, N,N'-dimethylethylenediamine (DMED), (Fc = ferrocenium)(BF_4), 4-cyanophenylboronic acid, 4-*tert*-butylphenylboronic acid, anhydrous DMF, $NiCl_2 \cdot 6H_2O$ and the 1.47 *M* [25% (w/w)] solution of (NEt_4)(OH) in CH_3OH were purchased commercially and used as received. The compounds HN(*p*-biphenyl^{t}Bu)$_2$,[16] 1-(2-bromophenyl)-1H-pyrazole (BrPhpz),[5] H(pzAn^{X}) (X = Me, H, CN, or CO_2Et; see Scheme 4.2),[5] H(Me,Me),[4] H(Me,H),[5] H(Me,CF_3),[5] H(CF_3,CF_3),[5] and Pd($PPh_3)_4$[17] were prepared according to literature procedures. Dioxane, Et_2O, and THF were dried over sodium/benzophenone ketyl. Toluene, *p*-xylene, CH_2Cl_2, and CH_3CN were dried over CaH_2. Solvents used in reactions were distilled under argon prior to use.

Physical Measurements. Midwest MicroLab, LLC, Indianapolis, Indiana 45250, performed all elemental analyses. Melting point determinations were made on samples contained in glass capillaries using an Electrothermal 9100 apparatus and are uncorrected. ^{1}H, ^{13}C, and ^{19}F NMR spectra were recorded on a Varian 400 MHz spectrometer. Chemical shifts were referenced to solvent resonances at δ_H 7.27, δ_C 77.23 for $CDCl_3$. Abbreviations for NMR and UV-Vis br (broad), sh (shoulder), m (multiplet), ps (pseudo-), s (singlet), d (doublet), t (triplet), q (quartet), p (pentet), sept (septet). Electrochemical measurements were collected under a nitrogen atmosphere for samples as 0.1 m*M* solutions in CH_2Cl_2 with 0.1 M NBu_4PF_6 as the supporting electrolyte. A three-electrode cell comprised of an Ag/AgCl electrode (separated from the reaction

medium with a semipermeable polymer membrane filter), a platinum working electrode, and a glassy carbon counter electrode was used for the voltammetric measurements. Data were collected at scan rates of 50, 100, 200, 300, 400, and 500 mV/s. With this set up, the ferrocene/ferrocenium couple had an $E_{1/2}$ value of +0.52 V in CH_2Cl_2 at a scan rate of 200 mV/s, consistent with the literature values.[18] Solid state magnetic susceptibility measurements were performed using a Johnson-Matthey MSB-MK1 instrument. Diamagnetic corrections were applied using tabulated values of Pascal's constants.[19] Electronic absorption (UV-Vis/NIR) measurements were made on a Cary 5000 instrument. EPR spectra were obtained on both solid powder samples and as solutions ~0.2 m*M* in 1:1 CH_2Cl_2:toluene mixtures using a Bruker ELEXYS E600 equipped with an ER4116DM cavity resonating at 9.63 GHz, an Oxford instruments ITC503 temperature controller and a ESR-900 helium flow cryostat. The spectra were recorded using 100 kHz field modulation unless otherwise specified.

2.4.1 Ligand Precursor Syntheses.

2-Bromo-5-cyanophenyl-1H-pyrazole, Br-CNPhPz. A deep green solution of 2.4 mL (20.0 mmol) ^{t}BuONO and 2.23 g (10.0 mmol) $CuBr_2$ in 30 mL CH_3CN was purged with argon 20 min, then 1.85 g (10.0 mmol) H(pzAn^{CN}) was added as a solid. After the resulting violet solution had been heated at reflux 2 h, the mixture was added to 100 mL distilled H_2O. The resulting brown precipitate was collected by filtration and then was further purified by column chromatography on silica gel. Elution with 3:1 hexanes ethyl acetate (R_f 0.50) afforded 1.94 g (78%) of the desired compound as a pale yellow solid, after removing solvent and drying under vacuum. Mp, 114-116 ^{o}C. ^{1}H NMR ($CDCl_3$): δ_H 7.93 (d, *J* = 2.4 Hz, 1 H, H_5pz), 7.87 (d, *J* = 2.0 Hz, 1 H, H_3pz), 7.85 (d, *J* = 8.3 Hz, 1

H, Ar), 7.79 (d, *J* = 1.3 Hz, 1 H, Ar), 7.55 (dd, *J* = 8.3, 1.3 Hz, 1 H, Ar), 6.53 (dd, *J* = 2.4, 2.0 Hz, 1 H, H_4pz). ^{13}C NMR ($CDCl_3$): δ_C 142.1, 140.9, 135.3, 132.2, 131.6, 131.4, 23.6, 117.2, 112.8, 107.7. IR (KBr) ν_{CN} 2233 cm^{-1}.

2-Iodo-5-methylphenyl-1H-pyrazole, I-MePhPz. A solution of 3.18 g (46.1 mmol) $NaNO_2$ in 45 mL H_2O was slowly added to a cold (0^{o}C) solution of 5.32 g (30.7 mmol) H(pzAn^{Me}) in 100 mL 7 *M* H_2SO_4. After the solution had been stirred 15 min at 0^{o}C, a solution of 7.65 g (46.1 mmol) KI in 25 mL H_2O was added slowly. After complete addition, the reaction mixture was heated at 80^{o}C for 45 min using an external oil bath. The product mixture was neutralized with a 7 *M* KOH (aq) solution and then was extracted with three 50 mL portions of ethyl acetate. The combined organic fractions were dried over $MgSO_4$ and solvent was removed by rotary evaporation to leave a dark oily residue. The residue was subjected to column chromatography on silica gel. Solvent was removed from the second band (R_f 0.47) when eluting the column with 6:1 hexanes:ethyl acetate to give 5.91 g (68%) of the desired product as a brown oil of sufficient purity to be used successfully in subsequent coupling reactions. ^{1}H NMR ($CDCl_3$): δ_H 7.77 (d, *J* = 8.1 Hz, 1 H, Ar), 7.71 (d, *J* = 1.7 Hz, 1 H, H_3pz), 7.69 (d, *J* = 2.4 Hz, 1 H, H_5pz), 7.22 (d, *J* = 2.2 Hz, 1 H, Ar), 6.93 (dd, *J* = 8.1, 2.2 Hz, 1 H, Ar), 6.43 (dd, *J* = 2.4, 1.7 Hz, 1 H, H_5pz), 2.32 (s, 3 H, CH_3). ^{13}C NMR ($CDCl_3$): δ_C 143.2, 140.8, 139.7, 139.6, 131.24, 131.17, 129.0, 106.6, 89.9, 20.9.

3-bromo-4'-(1,1-dimethylphenyl)-*N*-(3-Bromo-4'-(1,1-dimethylphenyl)-[1,1'-biphenyl]-4-yl)-[1,1'-biphenyl]-4-amine, HN(Br-biphenyl^{t}Bu)$_2$. A solution of 0.45 mL (7.83 mmol) Br_2 dissolved in 30 mL of a 1:1 (v/v) mixture of MeOH:CH_2Cl_2 was added dropwise (1 mL/min) to a cold (0 ^{o}C), magnetically stirred solution of 1.69 g (3.91

mmol) HN(*p*-biphenyl^{t}Bu)$_2$ in 150 mL of a 1:1 (v/v) mixture of MeOH:CH_2Cl_2. After the resulting orange solution had been stirred 1 h at 0 ^oC, 150 mL of a saturated $Na_2S_2O_3$ solution was added whereupon the orange color disappeared. The aqueous and organic layers were separated. The aqueous layer was extracted with two 25 mL portions CH_2Cl_2. The combined organic layers were dried over $MgSO_4$, filtered and solvent was removed by vacuum distillation to leave a dark oil. The oil was subject to flushed through a short pad of silica gel using 4:1 hexanes:CH_2Cl_2 (R_f 0.65) as an eluent. Removal of solvent by vacuum distillation gave 1.66 g (70%) of the desired product as a colorless crystalline solid. Mp, 138-140 ^oC. ^1H NMR ($CDCl_3$) δ_H 7.86 (d, J = 2 Hz, 2 H), 7.47 (m, 12 H, Ar), 6.56 (br s, 1 H, NH), 1.39 (s, 18 H, CH_3). ^{13}C NMR ($CDCl_3$) δ_C 150.5, 138.9, 136.6, 135.7, 131.6, 126.7, 131.6, 126.7, 126.4, 125.9, 118.1, 114.6, 34.7, 31.5.

2.4.2 Ligand Syntheses.

H(H,H). A Schlenk flask charged with 3.18 g (20.0 mmol) H(pzAn^H), 4.45 g (20.0 mmol) BrPhpz, 7.80 g (23.9 mmol) Cs_2CO_3 was deoxygenated by three evacuation and argon back-fill cycles. Next, 15 mL dry, argon-purged dioxane was added by syringe and then 0.762 g (4.00 mmol) CuI was added as a solid under an argon blanket. After the reaction mixture had been heated at reflux for 15 h under argon, it was cooled to room temperature. Dioxane was removed by vacuum distillation. The solid residue was dissolved in a mixture of 50 mL ethyl acetate and 100 mL H_2O. The aqueous and organic layers were separated. The aqueous fraction was extracted with three 30 mL portions of ethyl acetate. The combined organic fractions were dried over $MgSO_4$, filtered, and solvent was removed under vacuum by rotary evaporation to leave a brown oily residue.

The residue was then subjected to column chromatography on silica gel. A beige solid mixture (4.5 g) of the desired product along with a trace of H(pzAn^{H}) was obtained by collecting the second band (R_f 0.56) when eluting with 8:1 hexanes:ethyl acetate and removing solvent under vacuum. The H(pzAn^{H}) impurity was removed by washing with EtOH in the following manner. A 20 mL aliquot of absolute EtOH was added to the 4.5 g beige solid mixture, the mixture dissolved on heating to reflux 2 min. The orange solution was cooled to room temperature which deposited 3.81 g (63 %) colorless crystals of pure H(H,H) that were collected by filtration and dried under vacuum. An additional crop of crystals (0.300 g, 5 %) was obtained by cooling the mother liquor to -30 ^{o}C for 15 h, filtering, and drying under vacuum. Total yield of pure H(HH) as colorless prism crystals: 4.11 g (68 %). Mp, 124 - 126 ^{o}C. ^{1}H NMR ($CDCl_3$): δ_H 8.77 (s, 1 H, NH), 7.72 (d, *J* = 2 Hz, 2 H, H_5pz), 7.71 (d, *J* = 2 Hz, 2 H, H_3pz), 7.46 (dd, *J* = 8, 1 Hz, 2 H, Ar), 7.32 (dd, *J* = 8, 1 Hz, 2 H, Ar), 7.23 (td, *J* = 8, 1 Hz, 2 H, Ar), 6.96 (td, *J* = 8, 1 Hz, 2 H, Ar), 6.44 (pst, *J* = 2 Hz, 2 H, H_4pz). ^{13}C NMR ($CDCl_3$): δ_C 140.8, 137.1, 130.4, 130.1, 128.4, 125.5, 121.1, 118.7, 106.9.

H(Me,Br). A solution of 0.548 g (3.08 mmol) NBS in 20 mL CH_3CN was added dropwise to a cold (0 ^{o}C) solution of 0.971 g (3.08 mmol) H(Me,H) in 20 mL CH_3CN. After the mixture had been stirred at 0^{o}C 2 h, a 10 mL aliquot of saturated aqueous $Na_2S_2O_3$ solution was added. The aqueous and organic layers were separated. The aqueous layer was extracted with three 10 mL portions ethyl acetate. The combined organic layers were washed with a saturated aqueous Na_2CO_3 solution, and then were dried over $MgSO_4$, filtered, and volatiles were removed under vacuum to leave an oily residue. The residue was subjected to column chromatography on silica gel using 4:1

hexanes:ethyl acetate as the eluent. The desired product (0.969 g, 80%) was isolated as a colorless solid after removing solvent from the band near the solvent front (R_f 0.8). Mp, 105 – 107 °C. ^{1}H NMR ($CDCl_3$): δ_H 8.70 (s, 1 H, NH), 7.79 (d, *J* = 1.6 Hz, 1 H, pz), 7.73 (d, *J* = 2.4 Hz, 1 H, pz), 7.71 (d, *J* = 2.4 Hz, 1 H, pz), 7.69 (d, *J* = 1.7 Hz, 1 H, pz), 7.43 (d, *J* = 2.2 Hz, 1 H, Ar), 7.32 (d, *J* = 8.3 Hz, 1 H, Ar), 7.27 (dd, *J* = 8.8, 2.2 Hz, 1 H, Ar), 7.21 (s, 1 H, Ar), 7.19 (d, *J* = 6.7 Hz, 1 H, Ar), 7.08 (dd, *J* = 8.1, 1.5 Hz, 1 H, Ar), 6.47 (pst, *J* = 2.1 Hz, 1 H, pz), 6.41 (pst, *J* = 2.3 Hz, 1 H, pz), 2.35 (s, 3 H, CH_3). ^{13}C NMR ($CDCl_3$): δ_C 141.1, 140.7, 137.1, 133.2, 132.3, 131.4, 131.1, 130.3, 130.1, 130.0, 129.0, 127.8, 126.0, 120.6, 118.6, 111.1, 107.2, 106.9, 20.8.

H(Me,CO_2Et). In an argon-filled drybox, a Schlenk flask was charged with 1.02 g (4.39 mmol) H(pzAn^{CO2Et}), 1.72 g (5.27 mmol) Cs_2CO_3, 0.059 g (0.26 mmol) $Pd(OAc)_2$, and 0.109 g (0.176 mmol) BINAP. The flask was removed from the drybox and was attached to a Schlenk line. A solution of 1.50 g (5.27 mmol) I-MePhPz in 20 mL toluene was purged with argon 20 min and then was transferred via cannula to the reaction flask containing aniline, base, and catalyst. After the reaction mixture had been heated at reflux 3 d, toluene was removed by vacuum distillation. The residue was dissolved in a biphasic mixture of 50 mL distilled water and 50 mL ethyl acetate. The organic and aqueous phases were separated. The aqueous phase was extracted with two 50 mL portions ethyl acetate. The combined organic layers were dried over $MgSO_4$, filtered, and solvent was removed by rotary evaporation to leave an oily residue. The residue was subjected to column chromatography on silica gel using 4:1 hexanes:ethyl acetate as the eluent. The desired product 1.24 g (73%) was obtained as a pale yellow gum after removing solvent from the third band (R_f 0.4). ^{1}H NMR ($CDCl_3$): δ_H 9.15 (s, 1 H, NH),

7.94 (d, *J* = 2.5 Hz, 1 H, pz), 7.83 (d, *J* = 8.5 Hz, 1 H, Ar), 7.79 (d, *J* = 2.5 Hz, 1 H, pz), 7.77 (d, *J* = 2.1 Hz, 1 H, pz), 7.71 (d, *J* = 3.0 Hz, 1 H, pz), 7.67 (s, 1 H, Ar), 7.44 (d, *J* = 8.3 Hz, 1 H, Ar), 7.27 (s, 1 H, Ar), 7.26 (d, *J* = 8.1 Hz, 1 H, Ar), 7.14 (d, *J* = 8.2 Hz, 1 H, Ar), 6.51 (pst, *J* = 3.1 Hz, 1 H, pz), 6.39 (pst, *J* = 3.0 Hz, 1 H, pz), 4.34 (q, *J* = 7.1 Hz, 2 H, CH_2), 2.38 (s, 3 H, Ar-CH_3), 1.37 (t, *J* = 7.1 Hz, 3 H, Et-CH_3). ^{13}C NMR ($CDCl_3$): δ_C 166.1, 142.6, 141.1, 140.8, 133.9, 132.7, 131.9, 130.3, 130.2, 130.0, 129.0, 127.6, 126.5, 126.1, 122.7, 120.9, 114.6, 107.1, 107.0, 60.9, 20.9, 14.6. IR (KBr) ν_{CO} 1706 cm^{-1}.

H(Br,Br). A solution of 1.20 g (6.76 mmol) NBS in 45 mL CH_3CN was added dropwise to a cold (0 ^{o}C) solution of 1.02 g (3.38 mmol) H(H,H) in 30 mL CH_3CN. After complete addition, the mixture was stirred at 0 ^{o}C until the solution noticeably darkened (ca. 1 h). Then, 50 mL of a saturated $Na_2S_2O_3$ solution was added. The biphasic mixture was poured into 100 mL H_2O and the layers were separated. The aqueous layer was extracted with three 50 mL portions ethyl acetate. The combined organic layers were washed with 20 mL of saturated Na_2CO_3 solution, dried over $MgSO_4$, and filtered. Solvent was removed by vacuum distillation to leave an oily residue that was subjected to column chromatography on silica gel using 6:1 hexanes:ethyl acetate as the eluent. The desired product (1.26 g, 82 %) was isolated as a colorless solid after removing solvent from the second band (R_f 0.62). Mp, 95-97 ^{o}C. ^{1}H NMR ($CDCl_3$): δ_H 9.04 (s, 1 H, NH), 7.73 (m, 4 H, pz), 7.48 (d, *J* = 2.2 Hz, 2 H, Ar), 7.33 (dd, *J* = 8.8, 2.2 Hz, 2 H, Ar), 7.27 (d, *J* = 8.8 Hz, 2 H, Ar), 6.47 (pst, *J* = 2.1 Hz, 2 H, pz). ^{13}C NMR ($CDCl_3$): δ_C 141.1, 135.6, 131.1, 130.0, 127.9, 120.1, 112.7, 107.4.

H(Me,CN). Under an argon atmosphere a Schlenk flask was charged with 0.759 g (4.12 mmol) H(pzAn^{CN}), 1.61 g (4.94 mmol) Cs_2CO_3, 0.0585 g (0.261 mmol) $Pd(OAc)_2$, 0.135

g (0.217 mmol) BINAP. A solution of 1.29 g (4.53 mmol), I-MePhPz in 15 mL dry toluene was purged with argon 15 min and then was transferred via cannula to the flask containing the base and catalyst mixture. The reaction mixture was heated at reflux 48 h under argon. After cooling to room temperature toluene was removed by vacuum distillation. The solid product mixture was dissolved in a biphasic mixture of 50 mL H_2O and 50 mL ethyl acetate. The aqueous and organic layers were separated. The aqueous layer was extracted with two 50 mL portions of ethyl acetate. The combined organic layers were dried over $MgSO_4$, filtered, and volatiles were removed under vacuum by rotary evaporation. The remaining brown oil was subjected to column chromatography on silica gel using 1:2 Et_2O:hexane. A 0.719 g (51%) sample of pure H(Me,CN) as a colorless solid was obtained after removing solvent from the second band (R_f 0.52) and drying under vacuum. Mp, 93-94 ^oC. ^1H NMR ($CDCl_3$): δ_H 9.31 (s, 1 H, NH), 7.80 (d, *J* = 1.4 Hz, 1 H, pz), 7.74 (d, *J* = 1.9 Hz, 1 H, pz), 7.70 (d, *J* = 2.4 Hz, 1 H, pz), 7.65 (d, *J* = 1.4 Hz, 1 H, pz), 7.51 (d, *J* = 1.9 Hz, Ar), 7.40 (d, *J* = 8.1 Hz, 1 H, Ar), 7.38 (dd, *J* = 8.6, 1.9 Hz, 1 H, Ar), 7.28 (d, *J* = 1.4 Hz, 1 H, Ar), 7.23 (d, *J* = 8.7 Hz, 1 H, Ar), 7.16 (dd, *J* = 8.2, 1.8 Hz, 1 H, Ar), 6.53 (dd, *J* = 2, 1 Hz, 1 H, pz), 6.39 (dd, *J* = 2, 1 Hz, 1 H, pz), 2.39 (s, 3 H, CH_3). ^{13}C NMR ($CDCl_3$): δ_C 142.7, 141.5, 140.9, 134.9, 133.1, 132.5, 131.0, 130.2, 129.8, 129.1, 128.5, 127.8, 126.1, 123.4, 119.2, 115.2, 107.6, 107.2, 101.0, 21.0. IR (KBr) ν_{CN} 2225 cm^{-1}.

H(CN,CN). A Schlenk flask was charged with 0.755 g (4.10 mmol) H($pzAn^{CN}$), 1.017 g (4.10 mmol) Br-CNPhPz, 1.603 g (4.92 mmol) Cs_2CO_3 and then was deoxygenated by three evacuation and argon back-fill cycles. Next, 15 mL of argon-purged, dry dioxane was added by syringe and then 0.156 g (0.820 mmol) CuI was added under an argon

blanket. After the reaction mixture had been heated at reflux 15 h under argon, it was cooled to room temperature and dioxane was removed by vacuum distillation. The resulting solid was dissolved in a biphasic mixture of 50 mL H_2O and 50 mL ethyl acetate. The aqueous and organic fractions were separated. The aqueous fraction was extracted with three 30 mL portions ethyl acetate. The combined organic fractions were dried over $MgSO_4$, filtered and volatiles were removed under vacuum with the aid of a rotary evaporator. The resulting brown oil was subjected to column chromatography on silica gel using 1:1 ethyl acetate:hexanes. The desired product was obtained as a yellowish solid after removing solvent from the second band (R_f 0.37). Recrystallization by cooling a boiling absolute ethanol solution to room temperature over the course of hours and then to -30 ^oC overnight afforded 0.72 g (50%) H(CN,CN) as pale yellow crystals. Mp, 178-180 ^oC. ^1H NMR ($CDCl_3$): δ_H 10.32 (s, 1 H, NH), 7.79 (d, *J* = 1.9 Hz, 2 H, H_3pz), 7.77 (d, *J* = 2.5 Hz, H_5pz), 7.64 (d, *J* = 1.6 Hz, 2 H, Ar), 7.56 (s, 2 H, Ar), 7.55 (d, *J* = 1.6 Hz, Ar), 6.55 (dd, *J* = 2.5, 1.9 Hz, 2 H, H_4pz). ^{13}C NMR ($CDCl_3$): δ_C 141.8, 139.5, 132.2, 130.5, 130.1, 128.8, 118.9, 118.3, 108.1, 104.9. IR (KBr) ν_{CN} 2226 cm^{-1}.

H(^{tBu}Ph,^{tBu}Ph). *Method A.* In an argon-filled drybox, a Schlenk flask was charged with 0.408 g (0.889 mmol) H(Br,Br), 0.475 g (2.67 mmol), 4-*tert*-butylphenylboronic acid, and 0.206 g (0.178 mmol) $Pd(PPh_3)_4$. The flask was removed from the drybox and attached to a Schlenk line. A solution of 30 mL C_6H_6 and 10 mL absolute ethanol was purged with argon 15 min and was transferred to the reaction flask under argon via cannula. Next, 10 mL of an argon-purged 2 *M* aqueous Na_2CO_3 solution was transferred via cannula to the reaction flask. After the magnetically-stirred biphasic mixture had

been heated at 80°C for 16 h with the aid of an external oil bath, the mixture was cooled to room temperature and poured into 100 mL H_2O. The aqueous and organic fractions were separated. The aqueous layer was extracted with two 50 mL portions ethyl acetate. The combined organic layers were dried over $MgSO_4$ and filtered. The oily residue that was obtained after removing solvents under vacuum was subjected to column chromatography on silica gel using 1:6 ethyl acetate:hexanes as the eluent. The desired product (0.383 g, 76%) H(^{tBu}Ph,^{tBu}Ph) was obtained as a colorless solid after removing solvent from the second band (R_f 0.45) and drying under vacuum 1 h.

Method B. A Schlenk flask charged with 2.61 g (4.41 mmol) HN(Br-biphenyl^{t}Bu)$_2$ 1.06 g (15.4 mmol) pyrazole, 2.16 g (15.4 mmol) K_2CO_3 and 0.19 mL (0.16 g, 1.8 mmol) DMED was deoxygenated by three evacuation and argon back-fill cycles. A 10 mL aliquot of dry, distilled, and argon-purged *p*-xylenes was added by syringe. Then, 0.0840 g (0.441 mmol) CuI was added under an argon blanket. After the resulting mixture had been heated at reflux 3 d under argon, the mixture was cooled to room temperature. Then 30 mL each H_2O and CH_2Cl_2 were added to dissolve the solids. The aqueous and organic layers were separated. The aqueous layer was extracted with three 25 mL portions CH_2Cl_2. The combined organic layers were dried over $MgSO_4$ and filtered. Volatiles were removed under vacuum to give a dark oil. The oil was subjected to flash chromatography on silica gel. First, elution with hexanes removed residual xylene. Then, elution with 8:1 hexane:ethyl acetate afforded 1.22 g (49 %) of H(^{tBu}Ph,^{tBu}Ph) as a colorless solid after removing solvent from the second band (R_f 0.39) and drying under vacuum. Mp, 138-140 °C. ^{1}H NMR ($CDCl_3$): δ_H 8.94 (s, 1 H, NH), 7.78 (d, J = 2.4 Hz, 2 H, H_5pz), 7.77 (d, J = 1.7 Hz, 2 H, H_3pz), 7.59 (d, J = 6.4 Hz, 2 H, Ar), 7.58 (s, 2 H,

Ar), 7.53 (d, *J* = 8.5 Hz, 4 H, Ar), 7.51 (dd, *J* = 8.7, 2.2 Hz, 2 H, Ar), 7.47 (d, *J* = 8.5 Hz, 4 H, Ar), 6.49 (dd, *J* = 2.4, 1.7 Hz, 2 H, H_4pz), 1.37 (s, 18 H, CH_3). ^{13}C NMR ($CDCl_3$): δ_C 150.4, 140.9, 137.2, 136.0, 134.1, 130.7, 130.2, 126.8, 126.4, 126.0, 123.8, 119.0, 107.0, 34.7, 31.6.

H(^{CN}Ph,^{CN}Ph). In an argon-filled drybox, a Schlenk flask was charged with 0.252 g (0.548 mmol) H(Br,Br), 0.242 g (1.64 mmol), 4-cyanophenyl boronic acid, and 0.127 g (0.110 mmol) $Pd(PPh_3)_4$. The flask was removed from the drybox and attached to a Schlenk line. A solution of 15 mL C_6H_6 and 5 mL absolute ethanol was purged with argon 15 min and was transferred to the reaction flask under argon via cannula. Next, 5 mL of an argon-purged 2 *M* aqueous Na_2CO_3 solution was transferred via cannula to the reaction flask. After the magnetically-stirred biphasic mixture had been heated at 80^{o}C for 16 h with the aid of an external oil bath, the mixture was cooled to room temperature and poured into 100 mL H_2O. The aqueous and organic fractions were separated. The aqueous layer was extracted with three 50 mL portions ethyl acetate. The combined organic layers were dried over $MgSO_4$ and filtered. The oily residue that was obtained after removing solvents under vacuum was subjected to column chromatography on silica gel using 1:1 ethyl acetate:hexanes as the eluent. The product which eluted in the pale pink-orange band (R_f 0.39) was recrystallized from absolute ethanol to give 0.146 g (53%) H(^{CN}Ph,^{CN}Ph) as a yellow solid. Mp, 200-202 ^{o}C. ^{1}H NMR ($CDCl_3$): δ_H 9.28 (s, 1 H, NH), 7.82 (d, *J* = 2.4 Hz, 2 H, H_5pz), 7.79 (d, *J* = 1.7 Hz, 2 H, H_3pz), 7.73 (d, *J* = 8.4 Hz, 4H, Ar), 7.68 (d, *J* = 8.4 Hz, 4 H, Ar), 7.62 (d, *J* = 8.9 Hz, 2 H, Ar), 7.61 (d, *J* = 2.2 Hz, 2 H, Ar), 7.53 (dd, *J* = 8.9, 2.3 Hz, 2 H, Ar), 6.53 (dd, *J* = 2.4, 1.7 Hz, 2H, H_4pz).

^{13}C NMR ($CDCl_3$): δ_C 144.2, 141.3, 137.0, 132.9, 132.2, 130.9, 130.2, 127.2, 127.1, 124.2, 119.2, 119.1, 110.9, 107.4. IR (KBr) ν_{CN} 2227 cm^{-1}.

2.4.3 Nickel Complex Syntheses.

Ni(Me,Me)$_2$, 1 An emerald green solution of 1.06 g (3.22 mmol) H(Me,Me) and 1.23 g (1.61 mmol) $NiCl_2 \cdot 6H_2O$ in 15 mL MeOH was heated at reflux 10 min. Then, 0.70 mL of a 1.47 *M* (1.61 mmol) solution of $(NEt_4)(OH)$ in MeOH was injected to the hot reaction mixture by syringe. The solution became dark forest green immediately upon mixing and within one minute copious orange-brown solid precipitated. After the orange-brown suspension had been heated at reflux 30 min, the mixture was allowed to cool to room temperature. The insoluble portion was collected by filtration, was washed with two 5 mL portions Et_2O, and was dried under vacuum to leave 1.10 g (95% yield) of **1** as a brown-orange solid. Mp, 350^{o}C dec. to black liq. Anal. Calcd. (found) for $C_{40}H_{38}N_{10}Ni$: C, 67.15 (66.07); H,5.07 (5.16); N,19.58 (19.15). μ_{eff} (solid, 295 K) = 2.9 μ_B. UV-Vis (CH_2Cl_2) λ_{max}, nm (ε, $M^{-1}cm^{-1}$): 368 (51,600), 415 (21,200), 467 sh (640), 543 (180), 791 sh (77), 872 (123). Crystals suitable for single crystal X-ray diffraction were grown by layering a CH_2Cl_2 solution with MeOH and allowing solvents to diffuse.

Except where noted, the following compounds were prepared in a similar manner where the heating time, amount of solvent, and subsequent work-up procedure were identical to that described for **1**. The amounts of ligand, nickel salt, and base that were used varied in the preparation of each complex and are given below along with the yield and characterization data.

Ni(Me,H)$_2$•0.5H$_2$O, 2•0.5H$_2$O. A mixture of 0.447 g (1.42 mmol) H(Me,H), 0.169 g (0.709 mmol) $NiCl_2 \cdot 6H_2O$, and 1.4 mmol $(NEt_4)(OH)$ (0.97 mL of a 1.47 *M* solution in MeOH) gave 0.406 g (87%) **2** as a yellow-brown powder. Mp, >350°C. Samples that were collected and washed as above but then were air-dried rather than heated under vacuum analysed as **2**•1.5CH_2Cl_2•0.5H_2O $C_{39.5}H_{36}Cl_3N_{10}NiO_{0.5}$: C, 57.59 (57.70); H,4.40 (4.67); N,17.00 (17.05). μ_{eff} (solid, 295 K) = 2.7 μ_B. UV-Vis (CH_2Cl_2) λ_{max}, nm (ε, $M^{-1}cm^{-1}$): 243 (50,500), 365 (31,800), 408 sh (14,000), 456 sh (640), 541 (180), 791 sh (77), 868 (110).

Ni(H,H)$_2$•H$_2$O, 3•H$_2$O. A mixture of 0.204 g (0.675 mmol) H(H,H), 0.0803 g (0.338 mmol) $NiCl_2 \cdot 6H_2O$, and 0.68 mmol $(NEt_4)(OH)$ (0.46 mL of a 1.47 *M* solution in MeOH) gave 0.183 g (82%) **3** as a tan solid. Mp, >350°C. Anal. Calcd. (found) $C_{36}H_{30}N_{10}NiO$: C, 63.83 (63.57); H,4.78 (4.91); N,20.68 (20.49). μ_{eff} (solid, 295 K) = 3.2 μ_B. UV-Vis (CH_2Cl_2) λ_{max}, nm (ε, $M^{-1}cm^{-1}$): 243 (48,000), 364 (30,100), 401 (14,400), 447 sh (760), 538 (166), 798 sh (77), 872 (113). Crystals suitable for single crystal X-ray diffraction were grown by layering a CH_2Cl_2 solution with hexane and allowing solvents to diffuse.

Ni(Me,Br)$_2$, 4. A mixture of 0.343 g (0.869 mmol) H(Me,Br), 0.103 g (0.435 mmol) $NiCl_2 \cdot 6H_2O$, and 0.87 mmol $(NEt_4)(OH)$ (0.59 mL of a 1.47 *M* solution in MeOH) gave 0.355 g (97%) **4** as an orange-brown solid. Mp, 320°C dec. to black liq. Anal. Calcd. (found) for $C_{38}H_{30}N_{10}Br_2Ni$: C, 54.00 (53.69); H, 3.58 (3.67); N, 16.57 (16.37). μ_{eff} (solid, 295 K) = 2.8 μ_B. UV-Vis (CH_2Cl_2) λ_{max}, nm (ε, $M^{-1}cm^{-1}$): 247 (59,300), 369 (43,000), 410 sh (15,500), 460 sh (725), 539 (214), 794 sh (72), 870 (120). Crystals suitable for single crystal X-ray diffraction were grown by layering a CH_2Cl_2 solution with hexane and allowing solvents to diffuse.

Ni(Me,CO_2Et)$_2$•2MeOH, 5•2MeOH. A mixture of 0.500 g (1.29 mmol) H(Me,CO_2Et), 0.153 g (0.645 mmol) $NiCl_2 \cdot 6H_2O$, and 1.29 mmol (NEt_4)(OH) (0.88 mL of a 1.47 *M* solution in MeOH) gave 0.526 g (98%) **5** as a dark orange solid. Mp, 330°C dec. to black liq. Anal. Calcd. (found) for $C_{46}H_{48}N_{10}NiO_6$: C,61.69 (61.34); H, 5.40 (5.13); N, 15.64 (15.78). μ_{eff} (solid, 295 K) = 2.8 μ_B. IR (KBr) $\nu_{C=O}$ 1699 cm^{-1}. UV-Vis (CH_2Cl_2) λ_{max}, nm (ε, $M^{-1}cm^{-1}$): 240 (53,500), 300 (9,800), 356 sh (17,400), 399 (50,100), 490 sh (510), 529 (430), 798 sh (122), 869 (154).

Ni(Me,CF_3)$_2$, 6. A mixture of 0.489 g (1.28 mmol) H(Me,CF_3), 0.152 g (0.638 mmol) $NiCl_2 \cdot 6H_2O$, and 1.28 mmol (NEt_4)(OH) (0.87 mL of a 1.47 *M* solution in MeOH) gave 0.417 g (97%) **6** as an orange-brown solid. Mp, 345°C dec. to black liq. Anal. Calcd. (found) for $C_{40}H_{30}N_{10}F_6Ni$: C, 58.35 (57.98); H, 3.67 (3.72); N, 17.01 (16.88). μ_{eff} (solid, 295 K) = 2.9 μ_B. UV-Vis (CH_2Cl_2) λ_{max}, nm (ε, $M^{-1}cm^{-1}$): 246 (54,700), 377 (36,200), 453 sh (570), 536 (190), 798 sh (78), 871 (120). Crystals suitable for single crystal X-ray diffraction were grown by layering a CH_2Cl_2 solution with hexane and allowing solvents to diffuse.

Ni(Br,Br)$_2$, 7. A mixture of 0.242 g (0.526 mmol) H(Br,Br), 0.0625 g (0.263 mmol) $NiCl_2 \cdot 6H_2O$, and 0.529 mmol (NEt_4)(OH) (0.36 mL of a 1.47 *M* solution in MeOH) gave 0.219 g (85%) **7** as an orange-brown solid. Mp, >350°C. Anal. Calcd. (found) for $C_{36}H_{24}N_{10}Br_4Ni$: C, 44.35 (44.43); H, 2.48 (2.59); N, 14.37 (14.22).μ_{eff} (solid, 295 K) = 3.0 μ_B. UV-Vis (CH_2Cl_2) λ_{max}, nm (ε, $M^{-1}cm^{-1}$): 247 (63,400), 373 (48,100), 463 sh (650), 536 (250), 788 sh (78), 873 (140).

Ni(Me,CN)$_2$, 8. A mixture of 0.302 g (0.887 mmol) H(Me,CN), 0.105 g (0.443 mmol) $NiCl_2 \cdot 6H_2O$, and 0.89 mmol (NEt_4)(OH) (0.61 mL of a 1.47 *M* solution in MeOH) gave 0.288 g (88%) **8** as an orange-brown solid. Mp, >350^{o}C. A sample that was collected and washed with ether but then was air dried rather than heated under vacuum analyzed as **8**•0.5H_2O. Anal. Calcd. (found) for $C_{40}H_{31}N_{12}NiO_{0.5}$: C, 64.36 (64.40); H, 4.19 (4.07); N, 22.52 (22.31). μ_{eff} (solid, 295 K) = 2.9 μ_B. IR (KBr) ν_{CN} 2206 cm^{-1}. λ_{max}, nm (ε, M^{-1}cm^{-1}): 238 (75,500), 293 sh (13,300), 388 (57,600), 473 sh (580), 520 (410), 790 sh (130), 877 (195). X-ray quality crystals of **8** were grown by layering hexanes over a CH_2Cl_2 solution and allowing solvents to diffuse 2 d.

Ni(CF$_3$,CF$_3$)$_2$, 9. A mixture of 0.413 g (0.943 mmol) H(CF_3,CF_3), 0.112 g (0.472 mmol) $NiCl_2 \cdot 6H_2O$, and 0.94 mmol (NEt_4)(OH) (0.64 mL of a 1.47 *M* solution in MeOH) gave 0.410 g (93%) **9** as a dark orange solid. Mp, >350^{o}C. Anal. Calcd. (found) for $C_{40}H_{24}N_{10}F_{12}Ni$: C,51.09 (51.14); H, 2.68 (2.73); N, 14.72 (14.89). μ_{eff} (solid, 295 K) = 3.1 μ_B. λ_{max}, nm (ε, M^{-1}cm^{-1}): 244 (56,000), 282 sh (11,100), 347 sh (23,600), 382 (51,500), 448 sh (670), 527 (210), 794 sh (55), 880 (120).

Ni(CN,CN)$_2$•0.5H$_2$O, 10•0.5H$_2$O. Owing the relatively lower solubility of the ligand in MeOH versus other ligands, the mixture of 0.240 g (0.682 mmol) H(CN,CN), 0.0810 g (0.341 mmol) $NiCl_2 \cdot 6H_2O$, and 0.68 mmol (NEt_4)(OH) (0.46 mL of a 1.47 *M* solution in MeOH) was heated at reflux 6h and was filtered hot. After washing with Et_2O and drying under vacuum 0.222 g (86%) **10** as an orange-brown solid was obtained. Mp, >350^{o}C. Anal. Calcd. (found) for $C_{40}H_{25}N_{14}NiO_{0.5}$: C, 62.52 (62.60); H, 3.28 (3.34); N, 25.52 (25.56). μ_{eff} (solid, 295 K) = 3.2 μ_B. IR (KBr) ν_{CN} 2214 cm^{-1}. λ_{max}, nm (ε, M^{-1}cm^{-1}): 242 (99,200), 303 (22,300), 346 (27,300), 407 (118,000), 491 (930), 512 (982), 792

sh (81), 841 (159) , 893 (160). A mixture of X-ray quality dark red-brown blocks of **10**·2acetone and red prisms of **10**·acetone were grown by layering an acetone solution with hexane and allowing solvents to diffuse over 1d.

Ni(^{tBuPh}Ph,^{tBuPh}Ph)$_2$, 11. A mixture of 0.339 g (0.599 mmol) H(^{tBu}Ph,^{tBu}Ph), 0.0712 g (0.300 mmol) $NiCl_2 \cdot 6H_2O$, and 0.60 mmol $(NEt_4)(OH)$ (0.41 mL of a 1.47 *M* solution in MeOH) gave 0.339 g (95%) **11** as an orange-brown solid. Mp, 345°C dec. to black liq. Anal. Calcd. (found) for $C_{76}H_{76}N_{10}Ni$: C, 76.82 (76.68); H, 6.45 (6.51); N, 11.79 (11.85). μ_{eff} (solid, 295 K) = 2.8 μ_B. λ_{max}, nm (ε, $M^{-1}cm^{-1}$): 250 (91,800), 290 sh (29,300), 331 (24,800), 371 sh (33,300), 417 (91,800), 491 sh (720), 535 (800), 791 sh (150), 866 (235).

Ni(^{CN}Ph,^{CN}Ph)$_2$•H$_2$O, 12•H$_2$O. This procedure differs slightly from the others because of the relatively low solubility of the ligand in MeOH. A few drops of benzene were added to completely dissolve a turbid mixture of 0.146 g (0.289 mmol) H(^{CN}Ph,^{CN}Ph) and 0.0343 g (0.144 mmol) $NiCl_2 \cdot 6H_2O$ in 25 mL EtOH. The resulting solution was then heated at reflux and 0.29 mmol $(NEt_4)(OH)$ (0.20 mL of a 1.47 *M* solution in MeOH) was added by syringe. After heating the resulting orange suspension at reflux 6h, the insoluble product was collected by filtration, was washed with Et_2O (2 x 5 mL) and was dried under vacuum overnight to give 0.136 g (88%) of **12** as an orange brown solid. Mp, >350°C. Anal. Calcd. (found) for $C_{64}H_{42}N_{14}NiO$: C, 71.06 (71.34); H, 3.91 (4.01); N, 18.13 (18.46). μ_{eff} (solid, 295 K) = 2.5 μ_B. IR (KBr) ν_{CN} 2222 cm^{-1}. λ_{max}, nm (ε, $M^{-1}cm^{-1}$): 257 (89,100), 313 sh (16,700), 398 (47,000), 454 (110,000), 543 sh (2,100), 793 sh (280), 866 (360).

2.4.4 Chemical Oxidations.

$[Ni(Me,Me)_2](BF_4)_2$, $(1)(BF_4)_2$. A solution of 0.128 g (0.468 mmol) $FcBF_4$ in 10 mL CH_2Cl_2 was added to a solution of 0.168 g (0.234 mmol) **1** in 20 mL CH_2Cl_2. To ensure quantitative transfer, the flask originally containing the ferrocenium solution was washed with an additional 5 mL CH_2Cl_2 solution and the washings were transferred via cannula to the reaction mixture. After the resulting violet solution had been stirred 30 min at room temperature, solvent was removed under vacuum. The violet solid was washed sequentially with four 10 mL portions of toluene and one 10 mL portion hexane, and then was dried under vacuum for 12 h to leave 0.185 g (89%) of **$(1)(BF_4)_2$** as a violet solid. Mp, >350°C. μ_{eff} (solid, 295 K) = 4.7 μ_B. UV-Vis (CH_2Cl_2) λ_{max}, nm (ε, M^{-1}, cm^{-1}), 312 (16132), 364 (21494), 527 (5921), 603 (3560), 760 (17456). X-ray quality crystals of **$(1)(BF_4)_2$**·$2CH_2Cl_2$ were grown by layering hexanes over a CH_2Cl_2 solution and allowing solvents to diffuse over 20 h.

$[Ni(Me,Me)_2](BF_4)$, $(1)(BF_4)$. Under an argon atmosphere, a solution of 0.1013g (0.1139 mmol) **$(1)(BF_4)_2$** in 10 mL CH_2Cl_2 was added via cannula transfer to a solution of 0.0815g (0.1139 mmol) **1** in 10 mL CH_2Cl_2. After the resulting blue-violet solution had been stirred 30 min at room temperature, solvent was removed under vacuum and then was dried under vacuum for 12 h to leave 0.153 g (84%) of **$(1)(BF_4)$** as a blue-violet solid. Mp, >350°C. μ_{eff} (solid, 295 K) = 3.7 μ_B. UV-Vis (CH_2Cl_2) λ_{max}, nm (ε, M^{-1}, cm^{-1}), 348 (21300), 506 (1955), 576 (2661), 756 (5332). An attempt to grow single crystals by layering a CH_2Cl_2 solution with benzene and allowing solvents to diffuse 1 d, produced violet needles of **$(1)(BF_4)_2$**·C_6H_6 by disproportionation

[Ni(^{tBu}Ph,^{tBu}Ph)$_2$](BF$_4$), (11)(BF$_4$). Under an argon atmosphere, a solution of 0.0459 g (0.168 mmol) FcBF$_4$ in 20 mL CH_2Cl_2 was added via cannula transfer to a solution of 0.200 g (0.168 mmol) **11** in 20 mL CH_2Cl_2. After the resulting green solution had been stirred 1h at room temperature, solvent was removed under vacuum. The green solid was washed sequentially with one 10 mL portion of toluene, three 10 mL portions hexane, and then was dried under vacuum for 2 h to leave 0.150 g (70%) of **(11)(BF$_4$)** as a green solid. Mp, >350^{o}C. μ_{eff} (solid, 295 K) = 2.5 μ_B. UV-Vis (CH_2Cl_2) λ_{max}, nm (ε, M^{-1}, cm^{-1}), 254 (96300), 350sh (34600), 404 (55200), 602 (5900), 725sh (5800), 854 (16200).

2.5 CRYSTALLOGRAPHY.

X-ray intensity data from a brown prism of **1**, a brown needle of **3**·CH_2Cl_2, a brown plate of **4**, a red block of **6**, a brown needle of **8**·1.29 CH_2Cl_2, a brown block of **10**·2 acetone, a red prism of **10**·acetone, a violet needle of [Ni(Me,Me)$_2$](BF$_4$)$_2$·2CH_2Cl_2, (**1**)(BF$_4$)$_2$•2CH_2Cl_2, and a violet needle of (**1**)(BF$_4$)$_2$•·2C_6H_6 were collected at 100.0(1) K with an Oxford Diffraction Ltd. Supernova diffractometer equipped with a 135 mm Atlas CCD detector using Mo(Kα) radiation for **8**·1.29 and both solvates of **10** but using Cu(Kα) for the other experiments. Raw data frame integration and Lp corrections were performed with either CrysAlis Pro (Oxford Diffraction, Ltd.)[20] or SAINT+ (Bruker).[21] Final unit cell parameters were determined by least-squares refinement of 9389, 28800, 6900, 9976, 51210, 15532, 18121, 15224, and 8870 reflections of **1**, **3**·CH_2Cl_2, **4**, **6**, **8**·1.29 CH_2Cl_2, **10**·2 acetone, **10**·acetone, (**1**)(BF$_4$)$_2$•2CH_2Cl_2, and (**1**)(BF$_4$)$_2$•·2C_6H_6, respectively, with $I > 2\sigma(I)$ for each. Analysis of the data showed negligible crystal decay during collection in each case. Direct methods structure solutions, difference Fourier calculations and full-matrix least-squares refinements against F^2 were performed

with SHELXTL.[22] An empirical absorption correction using spherical harmonics, implemented in SCALE3 ABSPACK scaling algorithm was applied to the data for **3**·CH_2Cl_2 while numerical absorption corrections based on gaussian integration over a multifaceted crystal model were applied to the data for the remaining crystals. Hydrogen atoms were placed in geometrically idealized positions and included as riding atoms. The X-ray crystallographic parameters and further details of data collection and structure refinements are given in Tables 2.1-3 and 2.10.

Computational Work.

General Considerations. DFT calculations were performed with either M06 or M06-2X meta-hybrid GGA functionals[44] because these have been found to be useful for affording accurate solutions to a wide variety of computation problems at low computational expense.[45,46] Geometry optimizations used the combination of the M06 functional and the def2-SV(P) double-zeta basis set[47] because we previously found (and find again here) that this method provides excellent agreement (within 0.2 Å) with solid state structures. Solvent (dichloromethane and acetonitrile) effects were accounted for by using the polarizable continuum model IEFPCM,[48] as implemented in Gaussian 09.[49] Analytical vibrational frequency calculations were carried out to verify that optimized geometries were stationary points. Time-dependent DFT methodology was used for excitation energy calculations.[50] For instances where improved accuracy of SCF energies and thermodynamic parameters was warranted such

Table 2.10. Crystallographic Data Collection and Structure Refinement for $[Ni(Me,Me)_2](BF_4)_2 \cdot 2CH_2Cl_2$, (**1**)$(BF_4)_2 \bullet 2CH_2Cl_2$ and $[Ni(Me,Me)_2](BF_4)_2 \cdot 2C_6H_6$, (**1**)$(BF_4)_2 \bullet\cdot 2C_6H_6$.

Compound	**(1)**$(BF_4)_2 \bullet 2CH_2$	**(1)**$(BF_4)_2 \bullet 2C_6H_6$
Formula	$C_{42}H_{40}B_2Cl_4F_8N$	$C_{52}H_{48}B_2F_8N_{10}Ni$
Formula weight	1058.97	1045.33
Crystal system	monoclinic	monoclinic
Space group	P 2_1/c	C c
Temperature [K]	100.0(1)	100.0(1)
a [Å]	24.8291(6)	9.2835(2)
b [Å]	9.5433(2)	25.5403(7)
c [Å]	20.5730(5)	20.4839(6)
α[°]	90.00	90.00
β[°]	108.734(3)	98.748(3)
γ [°]	90.00	90.00
V [Å^3]	4616.52(19)	4800.3(2)
Z	4	4
$D_{calcd.}$ [gcm^{-3}]	1.524	1.446
λ[Å] (Cu Kα)	1.5418	1.5418
μ [mm^{-1}]	3.407	1.272
Abs. Correction	numerical	numerical
F(000)	2160	2160
θ range [°]	3.76 to 73.76	4.09 to 73.78
Reflections	38581	17439
Independent Rflns	9154	8984 (R_{Int}=0.0447)
T_min/max	0.336/0.868	0.738/0.962
Data/restr./param.	9154/0/608	8984/2/662
Goodness-of-fit	1.049	1.037
$R1^a$ /$wR2^b$	0.0639/0.1830	0.0596/0.1618
*R*1/*wR*2 (all data)	0.0732/0.1949	0.0632/0.1672
peak/hole / e Å^{-3}	1.254/-0.809	1.254/-0.809

[a] $R1 = \Sigma||F_o| - |F_c||/\Sigma|F_o|$ [b] $wR2 = [\Sigma w(|F_o| - |F_c|)^2/\Sigma w|F_o|^2]^{1/2}$.

as in broken-symmetry calculations[51] or the determination of reduction potentials, the optimized structures were subject to single-point energy calculations using the def2-TZVP basis set[47] that had the polarization functions on hydrogen removed (for computational time-saving reasons). The calculation of reduction potentials at the double-zeta quality def2-SV(P) level followed Truhlar's methodology[52] and used

recommendations outlined recently by Rulíšek.[46] For estimation of reduction potentials at the triple zeta level, which would be prohibitively costly on our computational cluster, the zero-point energy and thermal corrections for each **1**, (**1**)+, and (**1**)2+ were taken from the calculations performed at the def2-SV(P) level and were applied to the SCF energies obtained from single point calculations at the def2-TZVP level.

Table 2.11. Summary of SCF energies and thermochemical data from theoretical calculations (M06/Def2-SV(P)).

	$Ni(Me,Me)_2$	**$[Ni(Me,Me)_2]^+$**	**$[Ni(Me,Me)_2]^{2+}$**
multiplicity	3	4	5
$<S^2>$	2.0081/2.000	3.7907/3.7508	6.0774/6.0025
ESCF (hartree)	-3598.484935	-3598.314711	-3598.131557
E+ZPE (hartree)	-3597.797706	-3597.626693	-3597.442173
H (hartree)	-3597.753662	-3597.582026	-3597.397927
G (hartree)	-3576.87396	-3597.704346	-3597.517799

Table 2.12. TDDFT/TDA Excitation Energies and Transitions of Ni(Me,Me)$_2$, **1** in CH_2Cl_2 (PCM).

Total Energy First Excited state, E(TD-HF/TD-KS) = -3598.44615144

Excited State	Excitation energy (eV)	Oscillator Strength	Origin[a]	Amplitude[a]	Transition moment			Dipole Strength
					X	Y	Z	(AU)
1	1.0554	0.0000	180 β →192 β	-0.72715	-0.0044	0.0032	0.0150	0.0003
		$<S^2>$=2.005	180 β →187 β	-0.46781				
			170 β →192 β	-0.25366				
			165 β →192 β	-0.25362				
2	1.1765	0.0001	186 β →192 β	0.34359	0.0411	0.0437	0.0095	0.0037
		$<S^2>$=2.009	186 β →187 β	0.25747				
			177 β →192 β	0.50379				
			177 β →187 β	0.32145				
			176 β →189 β	-0.32030				
3	1.2012	0.0009	186 β →189 β	0.32798	-0.0845	-0.1563	-0.0139	0.0318
		$<S^2>$=2.009	177 β →197 β	-0.27048				
			177 β →189 β	0.42708				
			176 β →192 β	-0.39998				
			176 β →187 β	-0.25701				
4	1.8986	0.0011	186 β →189 β	0.26625	-0.0847	-0.1249	-0.0170	0.0231
		$<S^2>$=2.013	177 β →189 β	0.27254				
			176 β →192 β	0.60064				
			176 β →187 β	0.39568				
5	1.9092	0.0002	177 β →192 β	0.25757	-0.0082	0.0628	-0.0082	0.0041
		$<S^2>$=2.011	176 β →197 β	0.34510				
			176 β →194 β	0.30219				
			176 β →189 β	0.57709				

[a]Key: 186 β = β-HOMO, 177 β = β-HOMO(-9), 187 β = β-LUMO, 192 β = β-LUMO (+5), etc. [b] only those transitions with |amplitude| greater than 0.25 are given.

CHAPTER 3

ELECTRONIC COMMUNICATION IN HOMOLEPTIC GROUP 9 METAL PINCER-TYPE COMPLEXES

3.1. INTRODUCTION

The concept of electronic communication through molecular bridges gets attention in chemistry because electron transfer is a feature of many biological and chemical systems.[1-7] The bridge plays a very important role in mediating electronic communication between two ends. Mixed-valence compounds may delocalize their electron density through or over the bridge between redox centers, and, therefore, the bridge plays a central role in the properties of mixed-valence compounds.

In previous chapters, the preparation of the redox-active di(2-pyrazolyl-*p*-tolyl)amine, H(Me,Me)[8-11] (Figure 3.1.a) has been described. The redox-active nature of this ligand and its metal complexes was established by the examination of the features of gallium(III) (Figure 3.1.b), nickel(II) (Figure 3.1.c), rhenium(I), and rhodium(III/I) complexes.[8-11] The electrochemical and spectroscopic data of gallium(III) complexes proved a weak electronic communication between redox active motifs over the diamagnetic metal bridge. The mono-oxidized complex was assigned to be a Robin-Day Class II mixed-valence compound by both electrochemical and spectroscopic methods.[8] As we described in chapter 2 the substitution of Ni(II) in the place of Ga(III) modestly increased the electronic communication of two ligands over the metal bridge in singly oxidized derivative increasing the electronic coupling element H_{ab} = 466(26) cm^{-1} vs 264 cm^{-1} in CH_2Cl_2. The small H_{ab} and solvent dependent IVCT band indicates $[Ni(Me,Me)]^+$

is a Robin-Day class II mixed valence system. Nickel(II) has the highest spectroscopic electronegativity and the lowest d-orbital energy of 1st row transition metals. Therefore, the energetic mismatch of magnetic orbitals of the ligands with the metal d_{xz} orbital might be one reason for the poor strength of any dπ-pπ interaction.

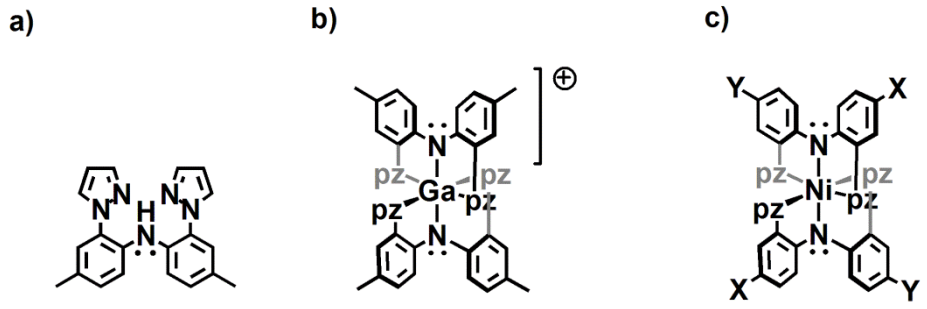

Figure 3.1.a) di(2-pyrazolyl-*p*-tolyl)amine, H(CH_3,CH_3) ligand, **b)** Homoleptic Ga(III) complex of H(CH_3,CH_3) ligand, **c)** Homoleptic Ni(II) complexes of H(X,Y) ligands with different X and Y groups.

In this chapter we will further probe the effects of changing metal bridges on electronic communication in mixed valent $[M(Me,Me)]^{n+}$ species by examining group 9 complexes, both +2 and +3 oxidation states are available these metals. Also, d-orbitals should raise in energy and become more diffuse on increasing Z, so it must be expected to strengthen electronic communication with Z. It may then be possible to transverse Robin-Day classes and obtain a class III mixed valence derivative. Metal bridged class III mixed valence species not yet been reported in the literature.

3.2. RESULTS AND DISCUSSION

3.2.1. Syntheses.

Homoleptic group 9 metal complexes of H(Me,Me)[10] (Figure 3.1.a), have been synthesized by three different synthetic strategies (Schemes 3.1 – 3.3). First, $Co(Me,Me)_2$, **1**, a yellow solid, precipitated immediately in high yield (82%) from one pot reaction between solutions of anhydrous $CoCl_2$, 2 mol equivalents of H(Me,Me) in degassed MeOH, followed by addition of 2 mol equivalents of $(NEt_4)(OH)$ in MeOH (Scheme 3.1). The compound **1** is best stored in a dry-box under an argon atmosphere, as it oxidizes slowly in air, even as a solid; solutions are more sensitive. Compound **1** is soluble in CH_2Cl_2 and THF but insoluble in MeOH, EtOH, Et_2O, and hexanes. The complex is paramagnetic with $\mu_{eff} = 4.2$, in line with expectation for a high spin d^7 cobalt(II) complex. Complex **1** was oxidized using one equivalent of $AgPF_6$ in THF to give [**1**](PF_6) in a high yield (95%) (Scheme 3.1). By using $AgBF_4$ as the oxidizing agent, [**1**](BF_4) was synthesized in high yield (92%), which permits an investigation of the effect of counter ions on structural and electronic properties.

The synthesis of $[Rh(Me,Me)_2](PF_6)$, [**2**](PF_6), was started with the previously-reported $(NEt_4)[Rh(Me,Me)Cl_3]\cdot H_2O$ precursor.[12] An acetonitrile solution of $(NEt_4)[Rh(Me,Me)Cl_3]\cdot H_2O$ was refluxed for 15 hours with equimolars of H(Me,Me), $(NEt_4)(OH)$, and 3 equivalents of $TlPF_6$ to yield a desired red product [**2**](PF_6), which was purified by chromatography using a neutral alumina column (Scheme 3.2). The yield of this reaction was moderate (65%) compared to the overall yield of the cobalt reaction (78%). The one-pot reaction of commercially available $RhCl_3\cdot H_2O$ with 2 mol

equivalents of H(Me,Me), 2 mol equivalents of $(NEt_4)(OH)$, and 3 mol equivalents of $TlPF_6$ in acetonitrile gave the same product, but the yield was lower (42%) than the two-step synthesis.

[**3**](PF_6) was obtained in poor yields after longer reaction times. The long reaction time is reasonable because 3rd row transition metal ions are more kinetically inert than their 1st row counterparts. Thus as shown in Scheme 3.3, the desired yellow-green complex $[Ir(Me,Me)_2](PF_6)$, [**3**](PF_6), was synthesized by the reaction between $IrCl_3 \cdot 3H_2O$, H(Me,Me), $(NEt_4)(OH)$, and $TlPF_6$ by refluxing in EtOH for four days. The product was isolated with a low yield (18 %) after collecting the third band of the neutral alumina column. The unreacted ligand (42%) was collected as the first fraction. The low yield is due to a number of competing side products formed. The identity of side products could not be established owing to the complicated NMR spectra. Attempts were carried out to synthesize this complex following a similar two-step procedure used for [**2**](PF_6), but a lower overall yield (6%) was obtained versus the one-pot method.

By using the strong oxidant, $(NO)BF_4$, partially and fully oxidized derivatives were prepared. Thus, equimolar mixtures of $[M(Me,Me)_2]^+(X^-)$ (X = BF_4, or PF_6) with $(NO)BF_4$ in CH_3CN gave the respective [**1**]$(BF_4)_2$, [**2**]$(PF_6)(BF_4)$ and [**3**]$(PF_6)(BF_4)$. The reaction of $[M(Me,Me)_2]^+(X^-)$ with two equivalent $(NO)BF_4$ in CH_3CN gave [**1**]$(BF_4)_3$, [**2**]$(PF_6)(BF_4)_2$ and [**3**]$(PF_6)(BF_4)_2$. These oxidized complexes were stored in an argon filled dry-box as they were air and moisture sensitive.

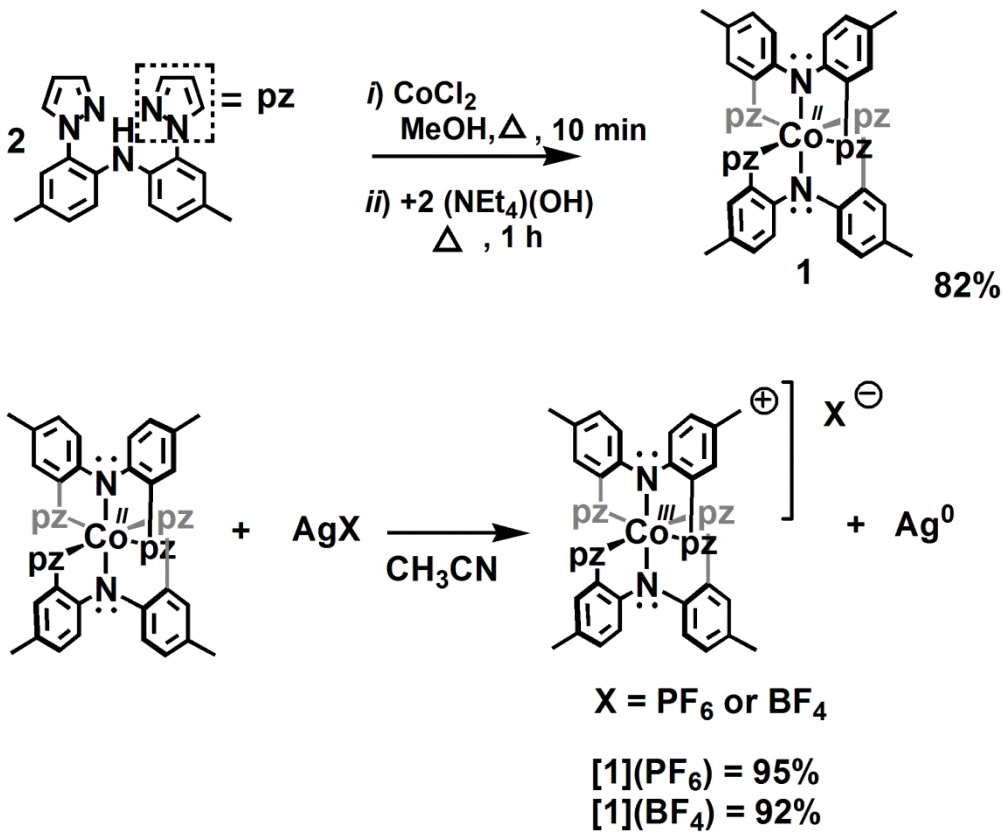

Scheme 3.1. Preparation of [Co(Me,Me)$_2$]X, [**1**]X complexes. (X = null or PF_6 and BF_4).

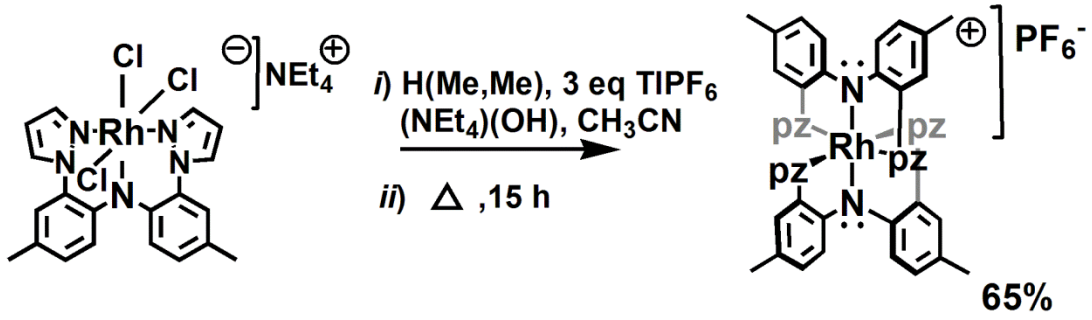

Scheme 3.2. Preparation of Rh(Me,Me)$_2$$PF_6$, [**2**]($PF_6$) complex.

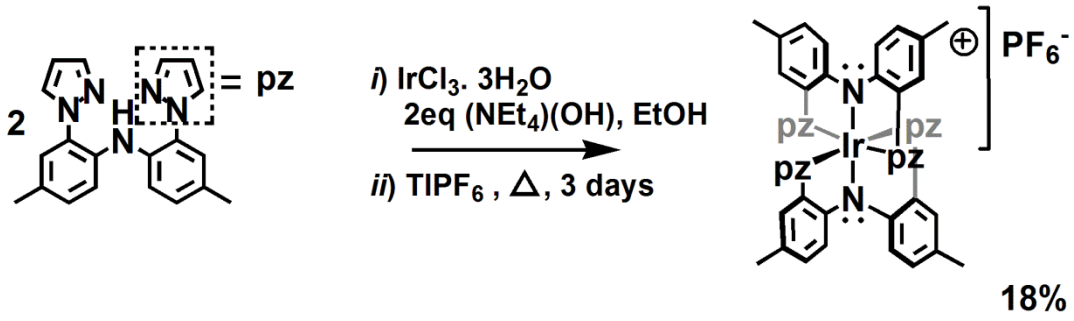

Scheme 3.3. Preparation of Ir(Me,Me)$_2$PF$_6$, [**3**](PF$_6$) complex.

3.2.2. Structures.

The solid state structures of **1**, [**1**](BF$_4$), [**1**](PF$_6$), [**2**](PF$_6$), [**3**](PF$_6$), and [**1**](BF$_4$)$_2$ have been determined by single-crystal X-ray diffraction. Single crystals of **1**, suitable for X-ray diffraction, were grown by layering hexanes on top of a CH_2Cl_2 solution in an argon-filled dry-box and allowing solvents to diffuse. The compound crystallizes in the triclinic crystal system with *P*-1 space group. The structure is shown in Figure 3.2, while X-ray crystallographic parameters and further details of data collection are given in Table 3.1-3. The cobalt center resides in a compressed octahedral geometry with six nitrogen atoms. Two of these nitrogen atoms are from the central amido groups of the two ligands, and others are from pyrazolyl rings, which give two types of Co-N bonds. The bonds associated with the diarylamido portion of the ligand, Co−N_{Ar}, have an average bond length of 2.030(12) Å, which is shorter than the average length of Co−N_{pz} bonds, 2.140(13) Å. All bond distances are given in Table 3.3. The amido nitrogens are linear across the cobalt center, separated by 4.060(12) Å. These nitrogen atoms have planar geometry with a 360° sum of angles about each atom. Diarylamido NC_2 moieties are

nearly coplanar across the cobalt atom, this geometry allows *p*-orbitals, containing the lone pair of electrons, of amido nitrogens to be roughly parallel to each other.

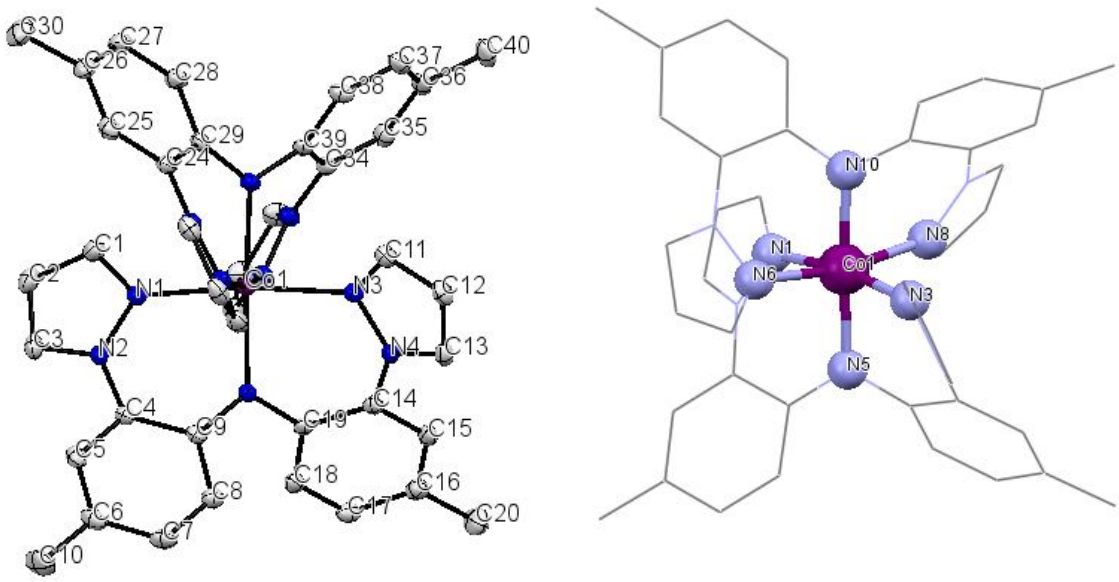

Figure 3.2. Solid state structure of **1**, Hydrogen atoms have been omitted for clarity.

The structures of [**1**](X = BF_4, PF_6) are similar to each other. Both crystallize in a monoclinic crystal system and the $P2_1/c$ space group. The only difference is the counter ion, indicated by formula [**1**](BF_4) and [**1**](PF_6). The PF_6^- of [**1**](PF_6) is completely disordered, while BF_4^- ion of [**1**](BF_4) is ordered. The structural geometry of the cation $[\mathbf{1}]^+$ in each is similar to **1**, but with differences in the bond lengths of the CoN_6 kernels. In $[1]^+$, the average Co-N_{Ar} bond lengths are slightly longer than the average Co-N_{pz} bond length, whereas the average Co-N_{Ar} bond length of **1** was shorter than that of Co-N_{pz} (Table 3.1). The comparison of these bond distances between **1** and $[\mathbf{1}]^+$ (Table 3.1, 3.3

and 3.4) show Co-N distances consistent with Co(III) and longer than in **1** with Co(II) as expected.

Table 3.1. Average M-N bond distances group 9 metal complexes.

	Bond Distance (Å)					
Complex	**1**	[**1**](BF_4)	[**1**](PF_6)	[**1**](BF_4)$_2$	[**2**](PF_6)	[**3**](PF_6)
M-N_{Ar} (avg)	2.030(12)	1.936(14)	1.944(7)	1.922(4)	2.041(3)	2.025(8)
M-N_{pz} (avg)	2.140(13)	1.925(14)	1.922(6)	1.917(4)	2.025(3)	2.020(8)

The single crystals of Rh(Me,Me)$_2PF_6$· CH_2Cl_2, [**2**](PF_6)·CH_2Cl_2 were grown by layering hexanes on a CH_2Cl_2 solution of the complex and allowing solvents to diffuse. It also shows similar structural features to the cobalt complexes of this ligand. The central rhodium atom has an RhN_6 octahedral geometry, which is composed of two types of Rh−N bonds from two central amido nitrogen atoms of two ligands and four pyrazolyl nitrogen atoms. The difference of these two bond lengths is negligible since average bond length of Rh−N_{Ar} is 2.041(3) Å, while the average bond length of Rh−N_{pz} is 2.025(3) Å. But there is a significant increase in these two bond lengths compared to analogue cobalt complexes. All bond distances are shown in Table 3.4., while the comparison of Rh-N bonds is given in Table 3.1.

The iridium complex, [**3**](PF_6), was crystallized in a $P2_1/c$ space group with a toluene-solvent molecule, [**3**](PF_6)·C_7H_8, after diffusion of toluene into a solution of the compound in CH_2Cl_2. The structure of the metal complex is similar to the other structures described above, where the average Ir−N_{Ar} and Ir−N_{pz} bond lengths are comparable to those of [**2**](PF_6) (Table 3.1).

Table 3.2. Crystallographic data collection and structure refinement of **1** and [**1**]$(BF_4)\cdot CH_2Cl_2$.

Compound	**1**	[**1**]$(BF_4)\cdot CH_2Cl_2$
Empirical formula	$C_{40}H_{36}CoN_{10}$	$C_{41}H_{38}BN_{10}F_4Cl_2Co$
Formula weight	715.72	887.45
Temperature/K	100.00(10)	100.00(10)
Crystal system	triclinic	monoclinic
Space group	P-1	$P2_1/c$
a/Å	8.8487(2)	11.83315(15)
b/Å	12.8919(4)	17.2910(3)
c/Å	15.9144(5)	19.1406(2)
α/°	79.470(3)	90
β/°	83.986(2)	90.7655(10)
γ/°	75.165(3)	90
Volume/$Å^3$	1722.17(9)	3915.94(9)
Z	2	4
$\rho_{calc}g/cm^3$	1.38	1.505
μ/mm^{-1}	0.544	0.64
F(000)	746	1824
Crystal size/mm^3	0.3607 × 0.1264 × 0.0934	0.5531 × 0.4175 × 0.0774
Radiation	MoKα (λ = 0.71073)	MoKα (λ = 0.71073)
2Θ range for data collection/°	5.7 to 59.16	5.44 to 58.94°
Reflections collected	27156	
Independent reflections	8473 (R_{int} = 0.0277)	9908 (R_{int} = 0.0380)
Data/restraints/parameters	8473/0/464	9908/0/536
Goodness-of-fit on F^2	1.038	1.042
Final R indexes [I>=2σ (I)]	R_1 = 0.0343, wR_2 = 0.0792	R_1 = 0.0400, wR_2 = 0.0953
Final R indexes [all data]	R_1 = 0.0423, wR_2 = 0.0839	R_1 = 0.0534, wR_2 = 0.1039
Largest diff. peak/hole / e $Å^{-3}$	0.33/-0.41	0.67/-0.79

Table 3.3. Selected bond lengths of **1**, and [**1**]$(BF_4)\cdot CH_2Cl_2$ and [**1**]$(BF_4)_2\cdot 3CH_2Cl_2$.

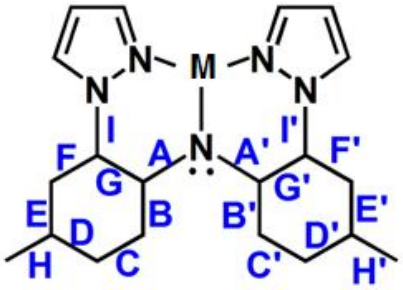

L1 : C1-C20, L2: C21-C40

	1 (Å)		[**1**]$(BF_4)\cdot CH_2Cl_2$ (Å)		[**1**]$(BF_4)_2\cdot 3CH_2Cl_2$ (Å)	
Bond	L1	L2	L1	L2	L1	L2
A	1.386(18)	1.383(19)	1.392(2)	1.392(2)	1.403(6)	1.376(6)
A'	1.398(19)	1.390(18)	1.390(2)	1.398(2)	1.378(6)	1.395(6)
B	1.413(2)	1.410(2)	1.409(3)	1.407(3)	1.415(7)	1.425(7)
B'	1.412(2)	1.409(2)	1.412(2)	1.411(2)	1.414(7)	1.417(7)
C	1.380(2)	1.379(2)	1.383(3)	1.385(2)	1.383(7)	1.377(8)
C'	1.380(2)	1.384(2)	1.379(2)	1.379(3)	1.377(7)	1.374(7)
D	1.394(2)	1.399(2)	1.393(3)	1.401(3)	1.392(8)	1.408(8)
D'	1.395(2)	1.393(2)	1.401(3)	1.398(3)	1.389(7)	1.398(7)
E	1.383(2)	1.385(2)	1.386(3)	1.385(3)	1.380(7)	1.399(7)
E'	1.389(2)	1.390(2)	1.386(3)	1.390(3)	1.383(7)	1.396(7)
F	1.401(2)	1.395(2)	1.391(2)	1.393(3)	1.397(6)	1.377(7)
F'	1.394(2)	1.393(2)	1.397(2)	1.401(2)	1.396(7)	1.384(7)
G	1.414(2)	1.416(2)	1.405(2)	1.412(2)	1.391(7)	1.421(6)
G'	1.411(2)	1.410(2)	1.404(2)	1.400(2)	1.399(6)	1.405(7)
H	1.509(2)	1.509(2)	1.512(3)	1.509(2)	1.520(7)	1.485(8)
H'	1.509(2)	1.510(2)	1.505(2)	1.512(3)	1.507(7)	1.499(7)
I	1.430(19)	1.433(19)	1.422(2)	1.421(2)	1.430(6)	1.411(6)
I'	1.428(18)	1.429(19)	1.423(2)	1.430(2)	1.423(6)	1.420(6)
$M\text{-}N_{amido}$	2.036(12)	2.024(12)	1.937(15)	1.936(14)	1.917(4)	1.926(4)
$M\text{-}N_{pz(avg)}$	2.136(13)	2.144(12)	1.929(15)	1.920(14)	1.921(4)	1.913(4)

Table 3.4. Selected bond lengths of [**1**](PF_6)·ace, [**2**](PF_6)·CH_2Cl_2,and [**3**](PF_6)·C_7H_8 complexes.

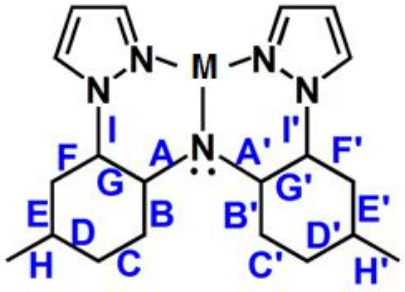

L1 : C1-C20, L2: C21-C40

	[**1**](PF_6)·ace (Å)		[**2**](PF_6)·CH_2Cl_2 (Å)		[**3**](PF_6)·C_7H_8 (Å)	
Bond	L1	L2	L1	L2	L1	L2
A	1.398(14)	1.390(10)	1.376(5)	1.394(5)	1.406(13)	1.384(12)
A'	1.390(10)	1.341(10)	1.404(5)	1.382(5)	1.391(12)	1.399(12)
B	1.405(10)	1.404(10)	1.417(6)	1.403(6)	1.421(15)	1.412(13)
B'	1.415(9)	1.428(10)	1.399(6)	1.409(6)	1.416(14)	1.430(13)
C	1.412(12)	1.376(11)	1.372(6)	1.380(6)	1.351(17)	1.394(14)
C'	1.370(11)	1.355(11)	1.378(6)	1.378(6)	1.390(13)	1.394(14)
D	1.362(12)	1.386(11)	1.400(6)	1.386(8)	1.410(2)	1.385(14)
D'	1.396(12)	1.406(11)	1.396(7)	1.403(6)	1.405(14)	1.418(14)
E	1.393(12)	1.399(10)	1.390(6)	1.378(7)	1.390(2)	1.407(13)
E'	1.390(9)	1.396(10)	1.385(7)	1.383(6)	1.398(13)	1.390(14)
F	1.440(15)	1.389(10)	1.392(5)	1.396(6)	1.380(15)	1.407(12)
F'	1.397(11)	1.395(12)	1.4.4(6)	1.402(6)	1.376(13)	1.392(14)
G	1.357(14)	1.405(10)	1.409(5)	1.396(6)	1.377(14)	1.402(12)
G'	1.410(11)	1.426(12)	1.396(6)	1.411(5)	1.402(13)	1.411(13)
H	1.532(14)	1.509(11)	1.505(6)	1.509(7)	1.530(2)	1.501(14)
H'	1.500(11)	1.490(12)	1.510(6)	1.508(6)	1.487(13)	1.509(14)
I	1.434(11)	1.421(8)	1.433(5)	1.428(6)	1.413(13)	1.406(12)
I'	1.428(8)	1.429(9)	1.431(5)	1.427(5)	1.438(12)	1.422(12)
M-N_{amido}	1.948(9)	1.941(5)	2.046(3)	2.036(3)	2.025(8)	2.047(8)
M-$N_{pz(avg)}$	1.907(6)	1.936(5)	2.022(3)	2.027(3)	2.088(8)	2.019(8)

It was possible to obtain X-ray quality crystals of [**1**]$(BF_4)_2 \cdot 3CH_2Cl_2$ after diffusing hexanes into the CH_2Cl_2 solution of the complex. Bond distances of this complex are listed in Table 3.3. Both [**1**](BF_4) and [**1**]$(BF_4)_2$ reside with similar structural parameters except the torsion angles of pyrazolyl groups. The torsion angle of pyrazolyl NC bonds of the [**1**]$(BF_4)_2$ is higher (67.21°) than that of the [**1**](BF_4) (36.35°).

3.2.3. Cyclic Voltammetry.

The electrochemical properties of [**1**](BF_4), [**2**](PF_6), and [**3**](PF_6) were studied by cyclic voltammetry. Voltammetric measurements were obtained in dichloromethane using $[N(Bu)_4]PF_6$ as the supporting electrolyte and potentials were measured against Ag/AgCl reference electrode. The cyclic voltammograms of each of these compounds shows two reversible one-electron oxidation waves; the cobalt and rhodium derivatives also show a single one-electron reduction wave.

Figure 3.3 shows a portion of the overlaid cyclic voltammogram (CV) obtained at a scan rate of 100 mV/s for a dichloromethane solution of each [**1**](BF_4), [**2**](PF_6), and [**3**](PF_6). While the potential of the first oxidation wave decreases from [**1**](BF_4) to [**3**](PF_6), the second potential is almost constant around 1 V vs Ag/AgCl. Thus, the difference between two oxidation potentials (ΔE) increases down group 9 (Figure 3.3). The potential differences ($\Delta E = E_2 - E_1$) (Table 3.5) between the two waves are 283, 402, and 557 mV for complexes $[\mathbf{1}]^+$, $[\mathbf{2}]^+$, and $[\mathbf{3}]^+$ gives rise to K_{com} values 6.84×10^4, 7.38×10^6, 3.28×10^9, respectively. Thus, according to electrochemistry, $[\mathbf{1}]^{2+}$ would be a class II Robin-Day mixed valence species, similar to $[Ni(Me,Me)_2]^+$ (Table 3.5). The rhodium complex, $[\mathbf{2}]^{2+}$can be classified as being at the Robin-Day class II/III borderline.

Interestingly, $[\mathbf{3}]^{2+}$ would be Robin-Day class III mixed valence species by the accepted conventions.

$$M(Me,Me)_2 + [M(Me,Me)_2]^{2+} \rightleftharpoons 2[M(Me,Me)_2]^{+}$$

$$K_{com} = [[M(Me,Me)_2]^{+}]^2 / [M(Me,Me)_2][[M(Me,Me)_2]^{2+}] \quad (1)$$

Table 3.5. Electrochemical data from cyclic voltammetry experiments of compound **1-3** and reference compounds in CH_2Cl_2.

	E^0, V vs Ag/AgCl[a]			
Compound	E^0_{ox1}(E_{pa} - E_{pc}, mV)	E^0_{ox2}(E_{pa} - E_{pc}, mV)	ΔE (mV)	K_{com}[b]
$[Ga(Me,Me)_2^{+}]$[27]	0.977(223)	1.165(207)	188	1.62×10^3
$Ni(Me,Me)_2$[28]	0.146(188)	0.428(187)	282	6.57×10^4
$Co(Me,Me)_2^{+}$, $[\mathbf{1}]^{+}$	0.716(070)	0.999(142)	283	6.84×10^4
$Rh(Me,Me)_2^{+}$, $[\mathbf{2}]^{+}$	0.620(140)	1.022(151)	402	7.38×10^6
$Ir(Me,Me)_2^{+}$, $[\mathbf{3}]^{+}$	0.390(204)	0.947(204)	557	3.28×10^9

[a]Average values obtained for scan rates of 50, 100, 200, 300, 400, and 500 mV/s with 0.1 *M* NBu_4PF_6 as supporting electrolyte. [b]$K_{com} = e^{(\Delta E \cdot F/RT)}$, T = 295 K.

The separation of oxidation waves alone is not sufficient to quantify the electronic communication of these types of systems because for weakly coupled systems the separation of waves may be due to simple Coulombic effects rather than, or in addition to, electronic communication. The resolution of waves in CV measurements is poor. For strongly coupled systems solvent effects are important for distinguishing between class II

and class III. Therefore, further evaluation of Robin-Day classification by spectroscopic methods is preferred as outlined earlier.

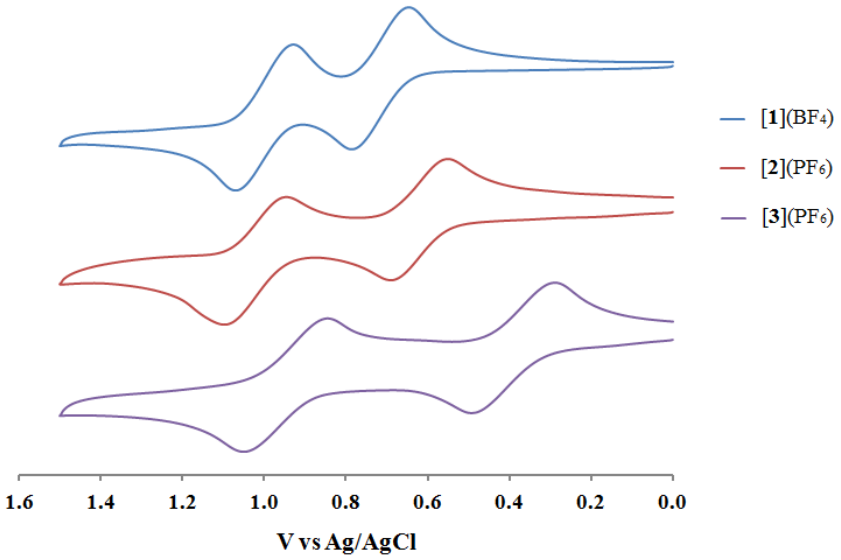

Figure 3.3. Overlay of cyclic voltammograms (CVs) of dichloromethane solutions of each metal complexes, [**1**](BF_4), [**2**](PF_6), and [**3**](PF_6) at a scan rate of 100 mV/s. [$N(Bu)_4$](PF_6) was used as the supporting electrolyte.

3.2.4. Spectroscopic Analysis.

The UV/visible spectra of **1** and [**1**](BF_4) are shown in Figure 3.4. Both show two strong absorbance bands centered at 337 nm and 391 nm, which would be assigned to ligand centered charge transfer transitions. In addition to that, complex **1** in CH_2Cl_2 shows a moderately weak intensity band ($\varepsilon = 4182\ M^{-1}cm^{-1}$) at 462 nm, and the complex $[\mathbf{1}]^+$ shows a more red-shifted band at 712 nm ($\varepsilon = 1384\ M^{-1}cm^{-1}$) which gives it its green color. The visible range of these two spectra is shown if Figure 3.4.b. Complex **1** shows a weak intensity band at 722 nm ($\varepsilon = 108\ M^{-1}cm^{-1}$), which can be assigned to the d-d

transitions. The bands for d-d transition of [**1**](BF_4) are likely obscured by other more intense bands.

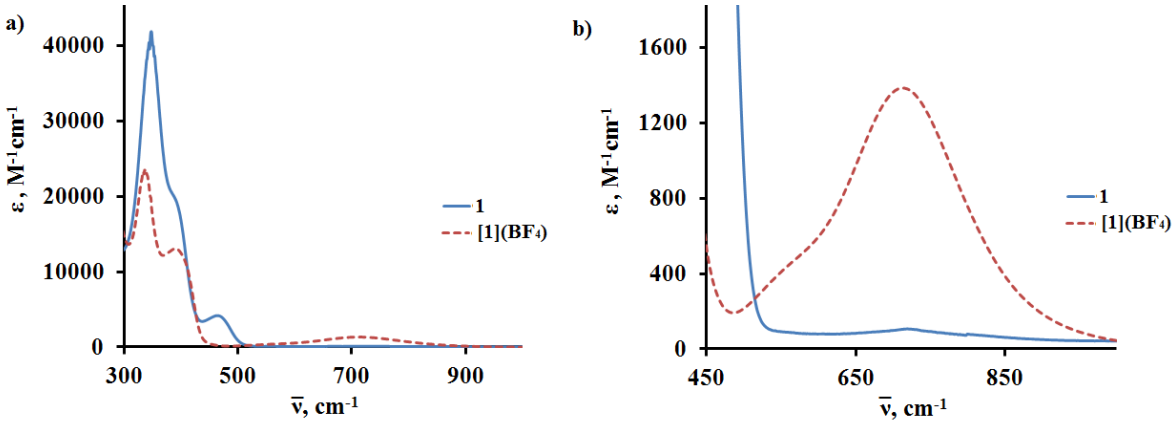

Figure 3.4. a) UV-Visible spectra of **1** and [**1**](BF_4) in CH_2Cl_2. b) Visible region of **1** and [**1**](BF_4) in CH_2Cl_2.

An overlay of UV-Visible spectra of $[M(Me,Me)]^+$ in CH_2Cl_2 is shown in Figure 3.5 and absorbance data is given in Table 3.6. The spectra show high intensity bands below 350 nm that are likely π-π^* transitions on the basis of energy and intensity considerations. Each complex shows medium intensity bands (ε = 5000 -15,000 $M^{-1}cm^{-1}$) in the 350 – 500 nm range. These transitions would be assigned to a LMCT or MLCT transitions by comparing the data gathered from spectroscopy and DFT calculations for the previously-reported Ni(II) complexes of the same ligand[9].

UV-Visible spectra of **1**, [**1**](BF_4), [**1**](BF_4)$_2$, and [**1**](BF_4)$_3$ in CH_2Cl_2 are shown in Figure 3.6 and peak data are found in Table 3.6. [**1**](BF_4)$_2$ and [**1**](BF_4)$_3$ shows medium intensity bands in the visible region for π-radical transitions. The mixed-valence

derivative, [**1**]$(BF_4)_2$, shows a weaker intensity broad band in the near- to mid-IR region which was assigned to the IVCT transition.

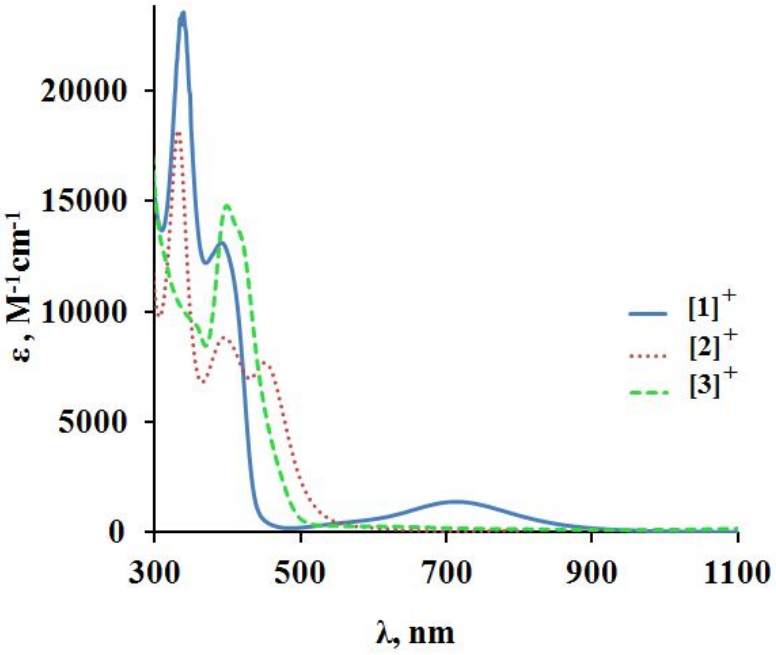

Figure 3.5. UV-vis-near IR spectrum of [**1**](BF_4) (blue), [**2**](PF_6) (red-dotted), and, [**3**](PF_6) (green-dashed) in CH_2Cl_2.

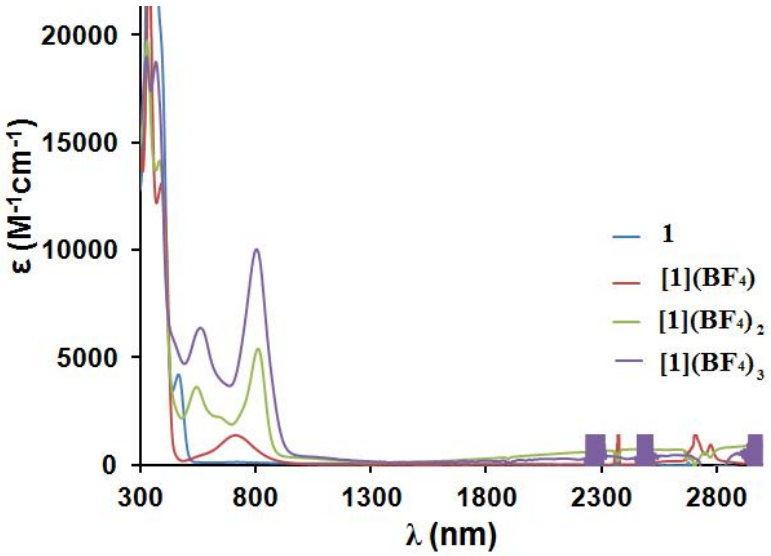

Figure 3.6. UV-Visible spectra of cobalt complexes in CH_2Cl_2.

UV-Visible spectra of rhodium complexes in CH_2Cl_2 are shown in Figure 3.7 and absorbance data of these spectra are found in Table 3.6. Similar to the cobalt complexes, oxidized derivatives show π radical transitions in the visible region. The IVCT band of [**2**]$(PF_6)(BF_4)$ is appeared at 2572 nm.

Figure 3.8 is shown the UV-Visible spectra of iridium complexes. Characteristic π radical transitions of oxidized derivatives are appeared at visible range. The IVCT band of [**3**]$(PF_6)(BF_4)$ is appeared at 1686 nm.

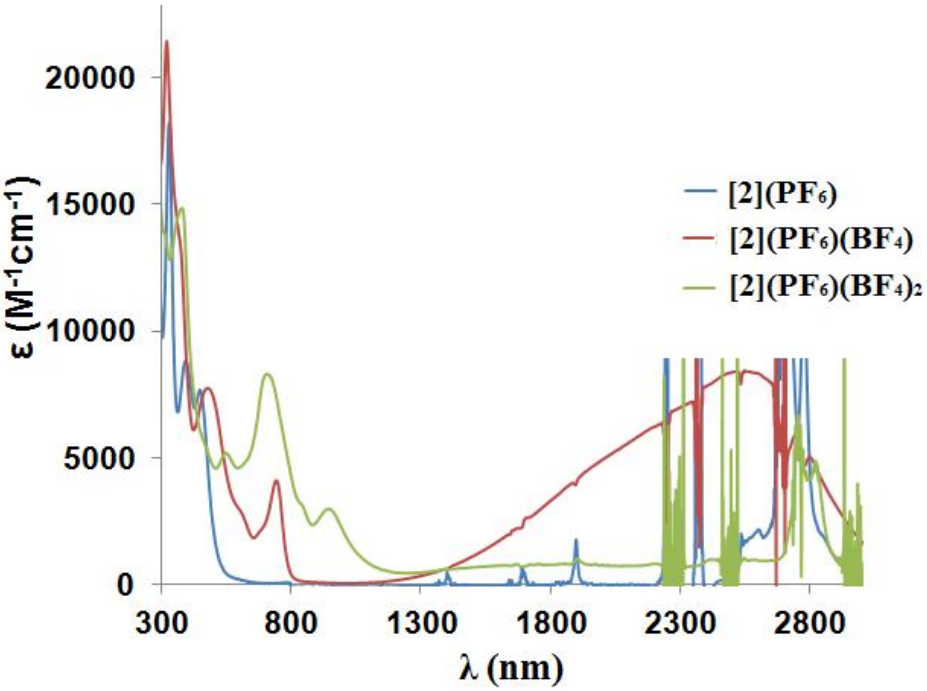

Figure 3.7. UV-Visible spectra of rhodium complexes in CH_2Cl_2.

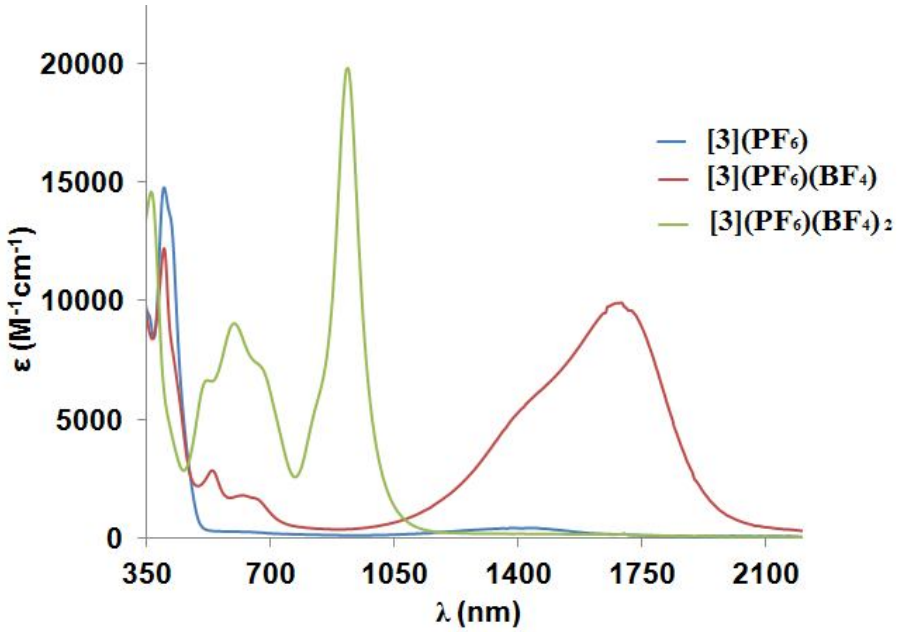

Figure 3.8. UV-Visible spectra of iridium complexes in CH_2Cl_2.

Table 3.6. UV-Visible absorbance data of various group 9 complexes from this study in CH_2Cl_2.

Complex	λ_{max}, nm (ε, $M^{-1}cm^{-1}$)
1	722 (108), 466 (4180), 388 (19945), 346 (41055)
[**1**](BF_4)	714 (1384), 392 (13109), 337 (23385)
[**1**](BF_4)$_2$	812 (4506), 544 (3105), 387 (14225), 331 (20357)
[**1**](BF_4)$_3$	804 (10021), 559 (6369), 367 (18755), 326 (18988)
[**2**](PF_6)	453 (7651), 392 8826), 332 (18212)
[**2**](PF_6)(BF_4)	744 (4000), 482 (7918), 376 (13479), 323 (21555)
[**2**](PF_6)(BF_4)$_2$	2572 (3246), 953 (1796), 737 (5885), 697 (5606), 544 (4569), 469 (5872), 368 (13336)
[**3**](PF_6)	1405 (414), 613 (266), 417 (13492), 399 (14774)
[**3**](PF_6)(BF_4)	1686 (9733), 654 (2176), 539 (3549), 400 (13969)
[**3**](PF_6)(BF_4)$_2$	914 (16764), 680 (6140), 600 (7938), 517 (6227), 367 (14170), 235 (74601)

The low energy bands of the dichloromethane solution of each singly oxidized complex, which could be assigned to the IVCT transitions, are shown in Figure 3.9. These bands were deconvoluted to find a Gaussian shaped, lowest energy peak to assign IVCT transitions. The deconvoluted spectra are shown in Figure 3.11, while data gathered after deconvolution of each spectrum is given in the Table 3.7. Moreover, non-oxidized or doubly oxidized complexes do not show any absorption peaks from the mid-IR to near-IR region, and therefore these peaks could be unambiguously assigned for the IVCT transitions. Typically, band shape analysis of the IVCT band is used to obtain information regarding the strength of electronic communication of mixed-valence complexes. In the case of complex [**1**]$(BF_4)_2$, the limited spectral range of the absorption spectrometer (Figure 3.6) and the difficulties inherent in obtaining molar absorptivity data from IR spectra hinder highly accurate band shape analysis, therefore an estimate was made by the partial band found in the IR region (Figure 3.10 and 3.11.a). The IVCT bands of both of the other complexes, [**2**]$(PF_6)(BF_4)$ and [**3**]$(PF_6)(BF_4)$ were found in the mid to near IR region, therefore complete Gaussian fits were made to find the IVCT band (Figure 3.11).

The Gaussian shape of the IVCT band and the indication of a Robin-Day Class II/III species from the analysis of K_{com} suggest that the Hush relations[20] (equation 2) can be used to estimate the strength of electronic communication of cobalt and rhodium complexes. The description of the Hush relations is found in chapter 1.

$$H_{ab}\ (cm^{-1}) = [(4.2 \times 10^{-4})\varepsilon_{max}\Delta\bar{\nu}_{1/2}E_{OP}]^{1/2}/d \qquad (2)$$

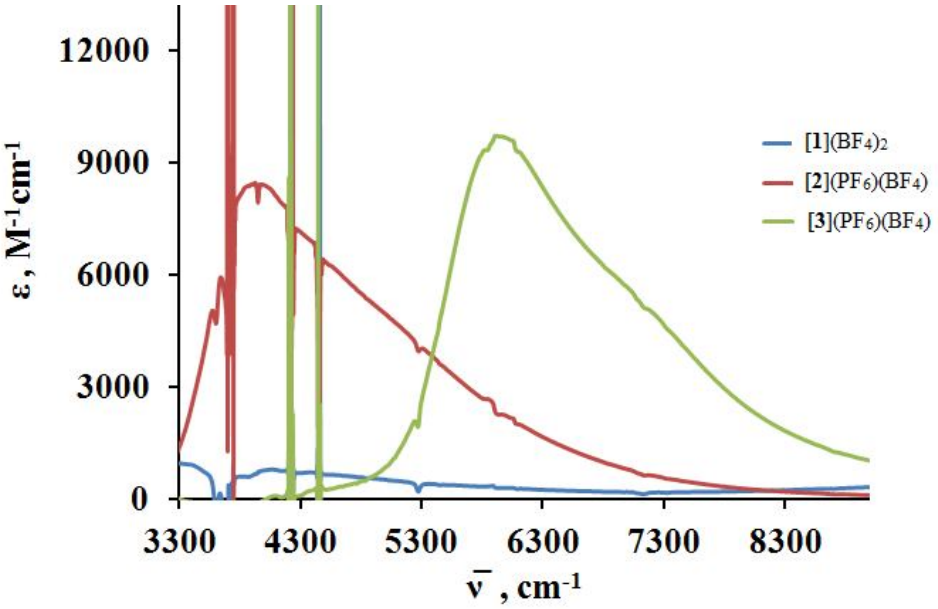

Figure 3.9. IVCT band of [**1**](BF$_4$)$_2$, [**2**](PF$_6$)(BF$_4$) and [**3**](PF$_6$)(BF$_4$) in CH_2Cl_2.

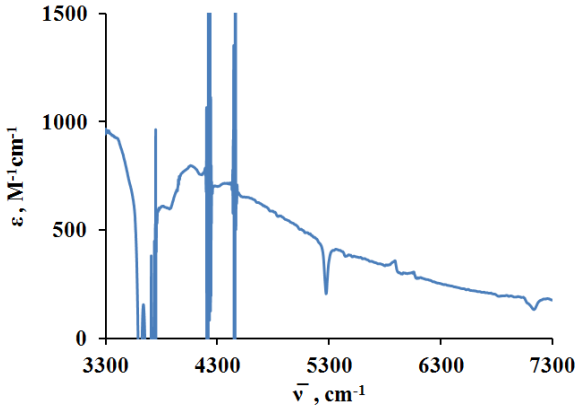

Figure 3.10. Close-up view of NIR region (in cm^{-1} units) of [**1**](BF$_4$)$_2$ in CH_2Cl_2.

For the consistency among various compounds the adjusted N-N distance of [**M**]$^+$ was used as the distance of two redox centers (d, eqn 2) of mixed-valence complexes. The inter-amido nitrogen distance of mixed-valence complex of **1,** [**1**](BF$_4$)$_2$, is 3.843(4) Å. The H_{ab} for [**1**](BF$_4$)$_2$ is 301 cm^{-1}. Examination of bond distances of cobalt complexes

shows that N-N distance decreases by 4.6% on going from **1** (HS d^7) to $\mathbf{1}^+$(LS d^6) and only by 0.8% further on continuing to $\mathbf{1}^{2+}$. It is noted that if one were to use N-N distance for $[\mathbf{1}]^+$ of 3.873(14) Å then H_{ab} would be 298 cm^{-1}, not significantly different than that using the actual crystallographic distances in $[\mathbf{1}]^{2+}$ 3.843(4) Å. The solid state N-N distances of $[\mathbf{1}]^+$, $[\mathbf{2}]^+$, and $[\mathbf{3}]^+$ could be used to calculate H_{ab} values, respectively (Table 3.7). Alternatively, an estimation of the N-N distances in $[\mathbf{2}]^{2+}$ and $[\mathbf{3}]^{2+}$ could be made in accord with the observations in distances for $[\mathbf{1}]^+$ and $[\mathbf{1}]^{2+}$, by applying a 1% contraction. Then d_{adj} for $[\mathbf{M}]^{2+}$ would be 0.99 x N-N distance of $[\mathbf{M}]^+$. The H_{ab} calculated using this approximation is not greatly different from the uncorrected one. For consistency the adjusted distance is used. Furthermore, electrochemical data revealed that the mixed

Table 3.7. Adjusted d (Å) and H_{ab} (cm^{-1}) in CH_2Cl_2.

Complex	**d[a] (Å)**	$\boldsymbol{H_{ab}}$ **(cm^{-1})**	$\mathbf{d_{adj}}$**[b] (Å)**	$\boldsymbol{H_{ab(adj)}}$ **(cm^{-1})**
$[\mathbf{1}]^+$	3.873(14)	298(1)	3.834(14)	301(1)
$[\mathbf{1}]^{2+}$	3.843(4)	301(1)		
$[\mathbf{2}]^+$	4.082(3)	457(1)	4.041(3)	461(1)
$[\mathbf{3}]^+$	4.072(8)	2918(6)[c]	4.072(8)	2918(1)[c]

[a] Measured N-N distance from solid state structure. [b] d_{adj} = d x 0.99. [c] $[\mathbf{3}]^{2+}$ is Robin-Day class III MV compound. Hence $2H_{ab} = \lambda$.

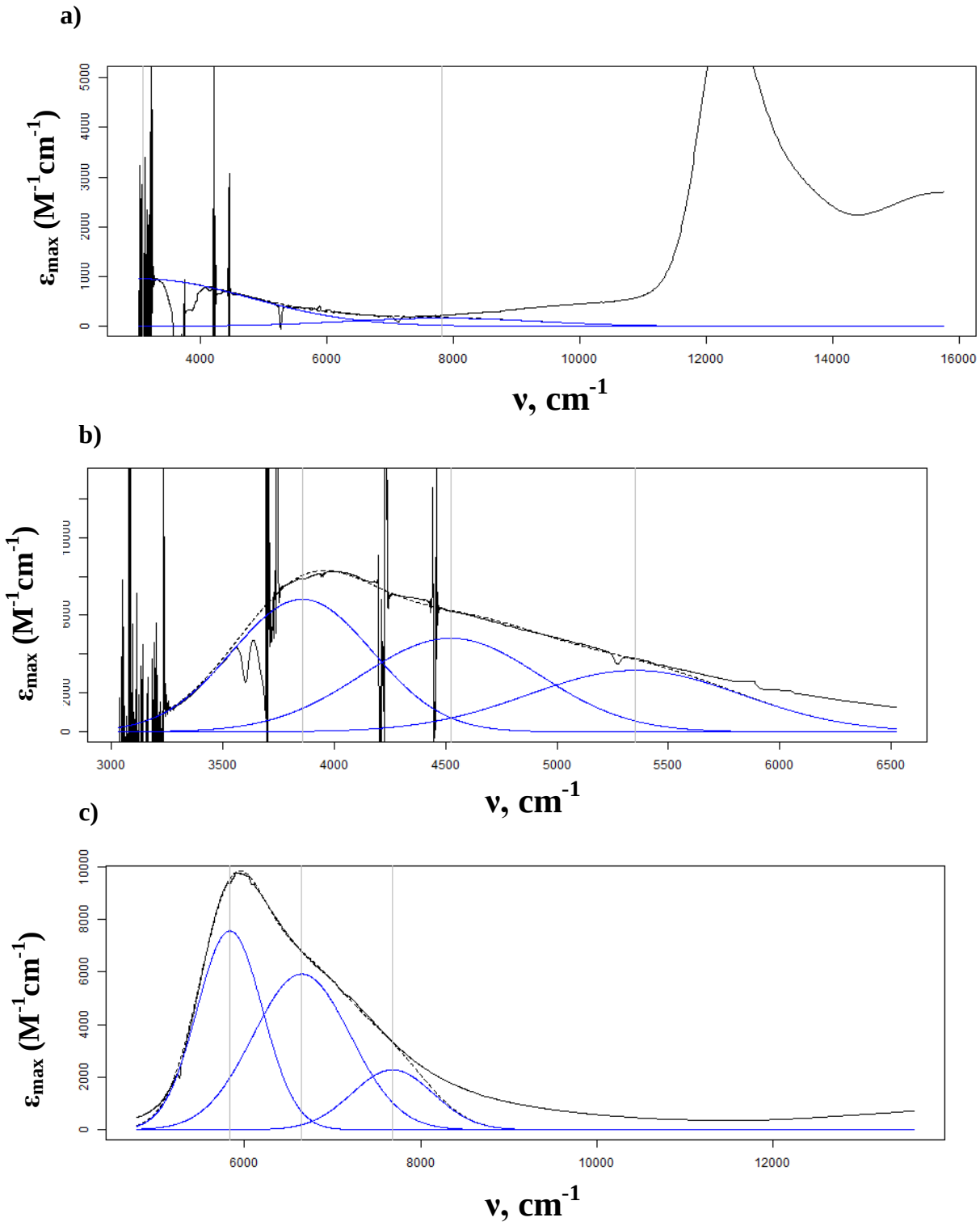

Figure 3.11. IVCT band shape fitting: **a)** [**1**]$(BF_3)_2$. **b)** [**2**]$(PF_6)(BF_4)$, **c)** [**3**]$(PF_6)(BF_4)$.

Table 3.8. Summary of IVCT band shape fitting and ET parameters of [**1**]$(BF_4)_2$, [**2**]$(PF_6)(BF_4)$ and [**3**]$(PF_6)(BF_4)$ in CH_2Cl_2 and CH_3CN.

	[1]$(BF_4)_2$		**[2]$(PF_6)(BF_4)$**		**[3]$(PF_6)(BF_4)$**	
	CH_2Cl_2	**CH_3CN**	**CH_2Cl_2**	**CH_3CN**	**CH_2Cl_2**	**CH_3CN**
$E_{op} = \lambda$ (cm^{-1})	3090(85)	2986(89)	3856(32)	3808(28)	5836(12)	5854(13)
ε_{max} ($M^{-1}cm^{-1}$)	951(6)	1097(7)	6822(7)	6169(12)	7550(9)	6268(8)
$\Delta\nu_{1/2}$ (cm^{-1})	1082(12)	1248(11)	315(4)	296(3)	372(3)	319(3)
d (Å)	3.834(14)	3.834(14)	4.041(3)	4.041(3)	4.072(8)	4.072(8)
H_{ab} (cm^{-1}), see ch 1	301(6)	340(7)	461(5)	423(4)	2918(6)	2927(6)
ΔG^* (cm^{-1}), see eq 3	501	445	558	576	0	0
k_{et} (s^{-1}), see eq 4	$3.3x10^{12}$	$5.6x10^{12}$	$5.2x10^{12}$	$4.1x10^{12}$	$2.6x10^{15}$	$2.6x10^{15}$

valence complex of iridium, [**3**]$(PF_6)(BF_4)$, is a Robin-Day class III system, and spectroscopic data further confirms it as the absorbance maxima of the low energy band is solvent independent or slightly dependent (Table 3.7). Therefore, Equation 2 cannot be used to calculate the electronic coupling element of this complex, and the relation $H_{ab} = \lambda/2$ has been used to calculate it.

The values of the electronic coupling element, H_{ab}, found for [**1**]$(BF_4)_2$ and [**2**]$(PF_6)(BF_4)$ in CH_2Cl_2 and CH_3CN reveal the solvent dependence of IVCT band, which is expected for Robin-Day Class II or II/III borderline mixed valence systems[21,22] (Table 3.8). The third row mixed valence complex of the series, [**1**]$(BF_4)_2$, has the lowest electronic coupling element of these group 9 complexes, and it is even lower than that of the previously reported $Ni(Me,Me)_2^+$.[9] The electronic coupling element of the cobalt complex is 301(6) cm^{-1}, while in the same row $Ni(Me,Me)_2^+$ had 466(26) cm^{-1}. The mixed-valence nickel complex has a divalent metal center, while the cobalt analogue is

trivalent. This low electron density of cobalt(III), compared to nickel(II) might be a reason for this difference in the electronic communication. Furthermore, the d-orbitals of Co(III) expected to be lower energy giving greater mismatch in energy with high energy p orbitals of nitrogens. However, this value (H_{ab} = 301(6) cm^{-1}) falls within the accepted limit of $0 < H_{ab} < \lambda/2$ for Robin-day class II species. The mixed valence rhodium complex has a higher electronic coupling element, H_{ab} = 461 (5) cm^{-1}, which is similar to the $[Ni(Me,Me)_2]^+$ and could be assigned to the Robin-Day Class II/III borderline. The iridium complex, [**3**]$(PF_6)(BF_4)$ has fully delocalized electronic status, hence it is a Robin-Day class III species.

The thermal energy barriers to electron transfer, ΔG*, calculated from Classical Marcus theory[23] (eq 3), are also found in Table 3.8. The corresponding rate constants for electron transfer k_{et} are found to be on the order of 10^{12} s^{-1} for the cobalt and rhodium complexes and 10^{15} s^{-1} for the iridium complex from equation 4, where temperature, T = 295 K, Planck's constant, h = 3.336 x 10^{-11} $cm^{-1}s$, and the Boltzmann's constant k_B = 0.695 $cm^{-1}K^{-1}$. These k_{et} values of [**1**]$(BF_4)_2$ and [**2**]$(PF_6)(BF_4)$ are about 2 order of magnitudes greater than that of the corresponding Ga(III) complex and 1 order of magnitude lower than that of the Ni(II) complex.[8,9]

$$\Delta G^* = (\lambda - 2H_{ab})^2 / 4\lambda \ \ cm^{-1} \qquad (3)$$

$$k_{et} = (2H_{ab}^2/h)[\pi^3 / \lambda k_B T]^{1/2} \exp-(\Delta G^*/k_B T) \qquad (4)$$

3.2.5. EPR Spectroscopy.

The EPR spectra of **1,** [**1**]$(BF_4)_2$, [**2**]$(PF_6)(BF_4)$, and [**3**]$(PF_6)(BF_4)$ in frozen CH_2Cl_2 are given in Figures 3.12 – 3.15, respectively. The complexes, [**1**]$(BF_4)_3$,

[**2**]$(PF_6)(BF_4)_2$, and [**3**]$(PF_6)(BF_4)_2$ were EPR silent. The EPR spectrum of **1** displays an intense peak at g = 6.0, as well as some weak features at high field (Figure 3.12). The former signal is indicative of a high spin S = 3/2 system expected for high spin d^7 cobalt(II). EPR spectra of [**1**]$(BF_4)_2$, [**2**]$(PF_6)(BF_4)$, and [**3**]$(PF_6)(BF_4)$ were simulated and shown in Figures 3.13-15.

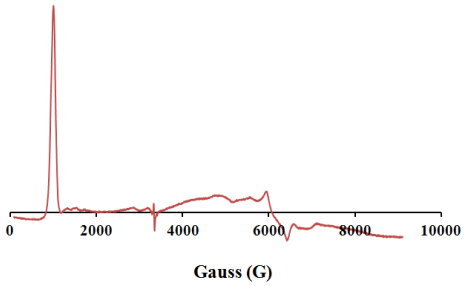

Figure 3.12. X-band (9.424 GHz) EPR spectrum of **1** in CH_2Cl_2 at 30 K.

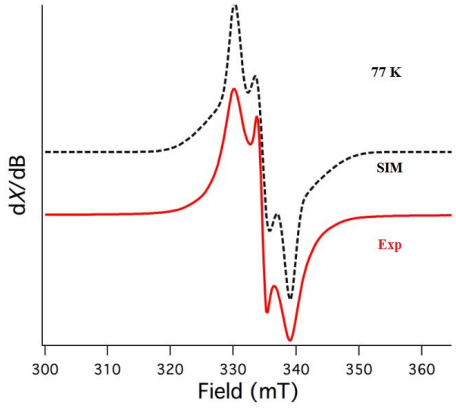

Figure 3.13. X-band (9.39 GHz) EPR spectrum of [**1**]$(BF_4)_2$ in CH_2Cl_2 at 77 K.

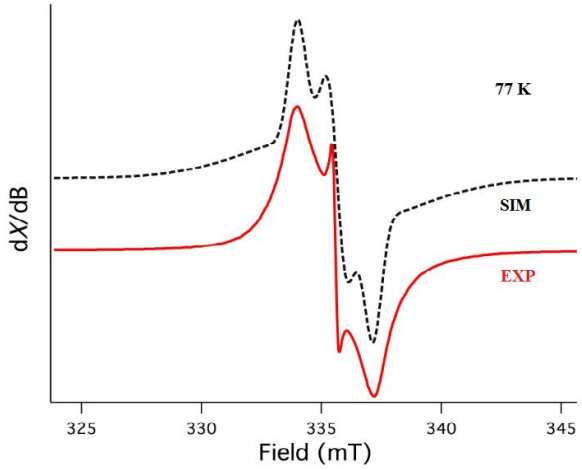

Figure 3.14. X-band (9.42 GHz) EPR spectrum of [**2**]$(PF_6)(BF_4)$ in CH_2Cl_2 at 77 K.

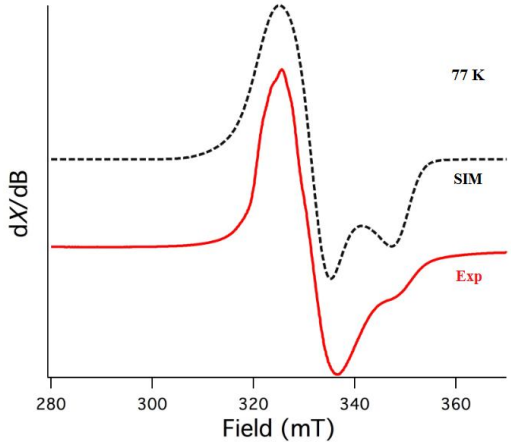

Figure 3.15. X-band (9.42 GHz) EPR spectrum of [**3**]$(PF_6)(BF_4)$ in CH_2Cl_2 at 77 K.

EPR spectrum of [**1**]$(BF_4)_2$ shows a rhombic spectrum at g = 2.012 indicative of S = ½ species. It was simulated with $g_{x,y,z}$ = 2.031, 2.004, 1.978; A = 103.92, 73.12, 110 (mT) and A_{strain} = 230, 110, 230. Similarly, the spectrum for $[\mathbf{2}]^{2+}$ gave a rhombic spectrum near g = 2.006 (S = ½) and was simulated with $g_{x,y,z}$ = 2.016, 2.006, 1.997; A = 35.035,

35, 38.75 (mT) and A_{strain} = 190, 40, 190. The spectrum of [**3**](PF_6)(BF_4) at 77 K was simulated with $g_{x,y,z}$ = 2.092, 2.031, 1.94; A = 80, 56.78, 80 (mT) ; g_{strain} = 0.03, 0, 0.03 and A_{strain} = 222.71, 0, 200.

3.3. CONCLUSION

As illustrated in this and previous chapters, the concept of assembling organic redox centers using transition metal ions as a bridge is very important for the development of molecular wires or conducting materials for the future design of efficient electronic materials. The quantification of the electronic communication of such redox centers over a metal ion and the investigation of the effect of the metal ion on the electronic communication would be crucial to design such materials with predicted properties. In order to address the role of the metal ion in the electronic communication, isostructural Co(III), Rh(III), and Ir(III) complexes of the NNN pincer-type ligand have been synthesized using three different synthetic techniques. The single crystal X-ray diffraction experiments reveal that these three complexes have similar structural geometries. As expected cobalt derivatives have shorter M-N bonds than either Rh or Ir. The distances of rhodium and iridium derivatives are nearly identical owing to lanthanide and relativistic contraction for iridium.

The electronic communication of two redox centers over the metal bridge was investigated using cyclic voltametry and spectroscopy. Dichloromethane solutions of complexes [**1**](BF_4), [**2**](PF_6), and [**3**](PF_6) showed two reversible one electron oxidations. These findings show that the electronic communication of redox active pincer-type ligands over the metal bridge of homoleptic complexes can be coarse tuned

without greatly changing spacer size (compared to organic systems). The delocalization of the unpaired electron is determined by the spatial overlap of the ligand and metal frontier orbitals, and, hence the relative energies of these orbitals. The iridium complex shows the highest value of electronic communication of this group, and it is a Robin-Day class III mixed-valence compound the first of this kind (LML). This high electron delocalization is likely due to the enhanced metal-ligand orbital overlap caused by the radial expansion of the 5d orbitals in iridium arising as a secondary consequence of relativistic core orbital contraction.

3.5 EXPERIMENTAL

General Considerations.

The compounds $CoCl_2$, $IrCl_3 \cdot 3H_2O$, $AgPF_6$, $AgBF_4$, Cs_2CO_3, $TlPF_6$, $N(Bu_4)PF_6$ and $NOBF_4$ were purchased commercially and used as received. The compounds H(Me,Me)[10,11] and $(NEt_4)[Rh(Me,Me)Cl_3] \cdot H_2O$[12] were prepared according to literature procedures. Solvents were dried by conventional means and distilled under nitrogen prior to use.

Physical Measurements.

Midwest MicroLab, LLC, Indianapolis, Indiana 45250, performed all elemental analyses. Melting point determinations were made on samples contained in glass capillaries using an Electrothermal 9100 apparatus and are uncorrected. ^{1}H,^{13}C, ^{19}F, and ^{31}P NMR spectra were recorded on a Varian 400 MHz spectrometer. Chemical shifts were referenced to solvent resonances at δ_H 7.27, δ_C 77.23 for $CDCl_3$, δ_H 5.33, δ_C 53.84 for CD_2Cl_2 or δ_H1.94, δ_C118.9 for CD_3CN and δ_H 2.05, δ_C 29.84 for acetone-d_6, while

those for ^{19}F and ^{31}P NMR spectra were referenced against external standards of $CFCl_3$(δ_F 0.00 ppm) and 85% H_3PO_4(aq) (δ_P 0.00 ppm), respectively. Abbreviations for NMR and UV−Vis data: br (broad), sh (shoulder), m (multiplet), ps (pseudo-), s (singlet), d (doublet), t (triplet), q (quartet), p (pentet), sept (septet). Electrochemical measurements were collected under a nitrogen atmosphere for samples as 0.1 mM solutions in CH_3CN and in CH_2Cl_2, each with 0.1 M NBu_4PF_6 as the supporting electrolyte. A three-electrode cell comprised of an Ag/AgCl electrode (separated from the reaction medium with a semipermeable polymer membrane filter), a platinum working electrode, and a glassy carbon counter electrode were used for the voltammetric measurements. Data were collected at scan rates of 50, 100, 200, 300, 400, and 500 mV/s. With this set up, the ferrocene/ferrocenium couple had an $E_{1/2}$ value of +0.53 V in CH_3CN and +0.41 V in CH_2Cl_2 at a scan rate of 200 mV/s, consistent with the literature values.[39] Solid state magnetic susceptibility measurements were performed using a Johnson-Matthey MSB-MK1 instrument. Electronic absorption (UV−Vis/NIR) measurements were made on a Cary 5000 instrument. Emission spectra were recorded on a JASCO FP-6500 spectrofluorometer. EPR spectra were obtained on both solid powder samples and as solutions ~0.2 mM in 1:1 CH_2Cl_2/toluene mixtures using a Bruker ELEXYS E600 equipped with an ER4116DM cavity resonating at 9.63 GHz, an Oxford instruments ITC503 temperature controller and a ESR-900 helium flow cryostat. The spectra were recorded using 100 kHz field modulation unless otherwise specified.

Co(Me,Me)$_2$, 1.

A solution of 1.062 g (3.43 mmol) of H(Me,Me) and 0.223 g (1.715 mmol) of $CoCl_2$ in 15 mL of degassed MeOH was heated at reflux under argon atmosphere for 10 mins. Next, 2.4mL of a 1.47 *M* (3.43 mmol) solution of $(NEt_4)(OH)$ in MeOH was injected into the hot reaction mixture by syringe. A yellow solid precipitated immediately and the mixture was heated at reflux for 1 hour for the completion of the reaction. The mixture was allowed to cool room temperature and insoluble portion was collected by vacuum filtration, was washed with 5 mL of MeOH and two portions of Et_2O, and was dried under vacuum to leave 1.015 g (82 % yield) of **1** as a yellow solid. Mp > 300 ^{0}C (decomposed). μ_B = 4.2. UV-Vis (CH_2Cl_2): nm (ε, $cm^{-1}M^{-1}$) 466 (4180), 388 (19945), 346 (41055). Crystals suitable for single-crystal X-ray diffraction were grown by layering a CH_2Cl_2 solution with hexanes and allowing solvents to diffuse.

[Co(Me,Me)$_2$](PF$_6$), [1](PF$_6$).

The green solution of 0.172 g (0.241 mmol) of **1** and 0.061 g (0.241 mmol) of $AgPF_6$ in 20 mL THF was stirred for 2h. THF was evaporated by vacuum distillation and the remaining green solid was extracted with 15mL (x 2) CH_2Cl_2 and filtered through a small pad of Celite. The volatile components were removed by vacuum distillation to leave 0.198 g (95 % yield) [**1**](PF_6) as a green solid. Mp = 143-145 ^{0}C (decomposed). ^{1}H NMR: (acetone , 293K) δ_H: 8.35 (d, 4H, *J* = 3 Hz, 3pz), 7.66 (d, 4H, *J* = 8 Hz, 6 Ar), 7.18 (s, 4H, 3Ar), 7.02 (d, 4H, *J* = 2Hz, 5pz), 7.01 (d, *J* = 2Hz, H, Ar), 6.34 (dd, *J* = 3, 2 Hz, 4pz), 2.23(s, 12H, *p*-Me) ppm. ^{13}C NMR: (acetone, 293K) δ_C: 145.2, 144.9, 132.4, 130.1, 129.1, 128.5, 127.4, 120.3, 109.5, 19.6 ppm. ^{19}F NMR: (acetone, 293K) δ_F -151.6

ppm. UV-Vis (CH_2Cl_2): nm (ε, $cm^{-1}M^{-1}$) 712 (790), 388 (8400), 340(15000). Crystals suitable for single-crystal X-ray diffraction were grown by layering an acetone solution with hexanes and allowing solvents to diffuse for 12h.

[Co(Me,Me)$_2$](BF$_4$), [1](BF$_4$).

The green solution of 0.208 g (0.291 mmol) of **1** and 0.057 g (0.291 mmol) of $AgBF_4$ in 20 mL THF was stirred for 12h. THF was evaporated by vacuum distillation and the remaining green solid was extracted with 15mL (x 2) CH_2Cl_2 and it was filtered through a small pad of Celite. The solvents were removed by rotary evaporation and dried under vacuum to leave 0.214 g (92 % yield) [**1**](BF_4) as a green solid. Mp = 212-215 ^{0}C (decomposed). ^{1}H NMR: (acetone , 293K) δ_H 8.36 (dd, *J* = 2.80, 0.93 Hz, 4H), 7.66 (d, *J* = 7.65 Hz, 4H), 7.19 (d, *J* = 1.28 Hz), 7.03 (dd, *J* = 2.54 , 0.94 Hz, 4H), 7.02 (dd, *J* = 7.65, 1.56 Hz), 6.34 (t, *J* = 2.69 Hz), 2.23 (s, 12H) ppm. ^{13}C NMR: (acetone, 293K) δ_C 146.1, 142.9, 133.3, 131.0, 130.1, 129.5, 128.4, 121.2, 110.4, 20.51 ppm. ^{19}F NMR: (acetone, 293K) δ_F 156.63 ppm. UV-Vis (CH_2Cl_2): nm (ε, $cm^{-1}M^{-1}$) 714 (1384), 392 (13109), 337 (23385). Crystals suitable for single-crystal X-ray diffraction were grown by layering a CH_2Cl_2 solution with hexanes and allowing solvents to diffuse for 12h.

[Rh(Me,Me)$_2$](PF$_6$), [2](PF$_6$).

A solution of 0.502 g (0.731 mmol) of (NEt_4)[Rh(Me,Me)Cl_3]·H_2O, 0.241 g (0.731 mmol) of H(Me,Me), 0.766 g (2.194 mmol) of $TlPF_6$ and 0.50 mL of a 1.4685 *M* (0.734 mmol) methanolic solution of (NEt_4)(OH) in 15 mL CH_3CN was heated at reflux for 15 hours. Then the mixture was allowed to cool to the room temperature and filtered through a short pad of Celite. The organic fractions were evaporated and 0.429 g (65% yield) the

desired product as a red brown solid was isolated by a column chromatography in alumina (R_f = 0.4) by eluting with 40:1 dichloromethane/methanol as a red band and removing solvents. Mp = 225 - 227 ^{0}C (decomposed). ^{1}H NMR: (acetone, 293K) δ_H : 8.44 (dd, *J* = 2.84, 0.79 Hz, 4H), 7.54 (d, *J* = 8.38 Hz, 4H), 7.21 (dd, *J* = 2.44, 0.68 Hz, 4H), 7.17 (d , *J* = 1.2 Hz, 4H), 7.04 (dd, *J* = 8.43, 1.19 Hz, 4H), 6.42 (t, *J* = 2.67 Hz, 4H), 2.22 (s, 12H) ppm. ^{13}C NMR: (acetone, 293K) δ_C 143.6, 142.9, 132.6, 131.5, 129.7, 128.5, 125.1, 123.0, 108.9, 19.5 ppm. ^{19}F NMR: (acetone, 293K) δ_F -78.8 ppm. ^{31}P NMR: (acetone, 293K) δ_P -144.26 (sept, *J* = 112.0 Hz) ppm. UV-Vis (CH_2Cl_2): nm (ε, $cm^{-1}M^{-1}$) 453 (7651), 392 (8826), 332 (18212). Crystals suitable for single-crystal X-ray diffraction were grown by layering a CH_2Cl_2 solution with hexanes and allowing solvents to diffuse for 12h.

[Ir(Me,Me)$_2$](PF$_6$), [3](PF$_6$).

A solution of 0.358 g (1.015 mmol) $IrCl_3 \cdot 3H_2O$, 0.668 g (2.030 mmol) of H(Me,Me) and 1.40 mL of 1.4685 *M* (2.056 mmol) methanolic solution of $(NEt_4)(OH)$ in 30 mL of ethanol was heated at reflux for 12 hours and then was allowed to cool to room temperature. After cooling 1.0690 g (3.120 mmol) of $TlPF_6$ was added and the mixture was heated at reflux for three days. Then it was allowed to cool to room temperature and was filtered through a short pad of celite. The filtrate was concentrated onto a small pad of alumina and was packed onto a fresh alumina column. Organic impurities were removed by elution with Et_2O and 0.180 g (18% yield) of the desired product as a yellow solid was isolated by eluting with ethyl acetate: methanol 10: 1 and removing solvents from the yellow band (R_f = 0.42). Single crystals were grown by slow diffusion of toluene into a concentrated dichloromethane solution. Mp = 210-213 ^{0}C (decomposed).

^{1}H NMR: (acetone, 293K) δ_H 8.44(d, *J* = 3 Hz, 4H, 3pz), 7.52 (d, *J* = 8 Hz, 4H), 7.25 (d, *J* = 2 Hz, 4H), 7.16 (s, 4H, Ar), 7.00 (d, *J* = 8 Hz, 4H), 6.43 (dd, *J* = 3, 2 Hz, 4H), 2.22 (s, 12H) ppm. ^{13}C NMR: (acetone, 293K) δ_C 142.7, 142.3, 131.5, 129.8, 129.5, 128.5, 125.8, 123.3, 108.3, 19.2 ppm. UV-Vis (CH_2Cl_2): nm (ε, $cm^{-1}M^{-1}$) 1405 (414), 613 (266), 417 (13492), 399 (14774). Crystals suitable for single-crystal X-ray diffraction were grown by layering a toluene solution with hexanes and allowing solvents to diffuse.

[Co(Me,Me)$_2$](BF$_4$)$_2$, [1](BF$_4$)$_2$.

A mixture of 0.0554 g (0.069 mmol) of [**1**](BF$_4$) and 0.0081 g (0.069 mmol) of (NO)BF$_4$ in 20 mL of degassed CH_3CN was stirred under argon which was immediately turned to the red/purple. After the purple solution had been stirred for 1 hour, solvents were removed under vacuum. The resulting black/brown residue was washed with two 5 mL portions of degassed Et_2O and was dried under a vacuum for several hours to leave 0.0505 g (83% yield) of [**1**](BF$_4$)$_2$. μ_B = 2.09, UV-Vis (CH_2Cl_2): nm (ε, $cm^{-1}M^{-1}$) 812 (4506), 544 (3105), 387 (14225), 331 (20357).

[Rh(Me,Me)$_2$](PF$_6$)(BF$_4$), [2](PF$_6$)(BF$_4$).

A mixture of 0.0509 g (0.056 mmol) of [**2**](PF$_6$) and 0.0066 g (0.056 mmol) of (NO)BF$_4$ in 20 mL of degassed CH_3CN was stirred under argon which was immediately turned to the red/brown. After the solution had been stirred for 1 hour, solvents were removed under vacuum. The resulting black/blue residue was washed with two 5 mL portions of degassed Et_2O and was dried under a vacuum for several hours to leave 0.049 g (92% yield) of [**2**](PF$_6$)(BF$_4$). μ_B = 2.05, UV-Vis (CH_2Cl_2): nm (ε, $cm^{-1}M^{-1}$) 744 (4000), 482 (7918), 376 (13479), 323 (21555).

[Ir(Me,Me)$_2$](PF$_6$)(BF$_4$), [3](PF$_6$)(BF$_4$).

A mixture of 0.0547 g (0.055 mmol) of [**3**](PF$_6$) and 0.0064 g (0.055 mmol) of (NO)BF$_4$ in 20 mL of degassed CH_3CN was stirred under argon which was immediately turned to the red/brown. After the solution had been stirred for 1 hour, solvents were removed under vacuum. The resulting black/blue residue was washed with two 5 mL portions of degassed Et_2O and was dried under a vacuum for several hours to leave 0.0446 g (75% yield) of [**3**](PF$_6$)(BF$_4$). μ_B = 1.93, UV-Vis (CH_2Cl_2): nm (ε, $cm^{-1}M^{-1}$) 1686 (9733), 654 (2176), 539 (3549), 400 (13969).

[Co(Me,Me)$_2$](BF$_4$)$_3$, [1](BF$_4$)$_3$.

A mixture of 0.061 g (0.076 mmol) of [**1**](BF$_4$) and 0.0178 g (0.152 mmol) of (NO)BF$_4$ in 20 mL of degassed CH_3CN was stirred under argon which was immediately turned to the purple. After the purple solution had been stirred for 1 hour, solvents were removed under vacuum. The resulting black/brown residue was washed with two 5 mL portions of degassed Et_2O and was dried under vacuum for several hours to leave 0.0696 g (94% yield) of [**1**](BF$_4$)$_3$. μ_B = 2.88, UV-Vis (CH_2Cl_2): nm (ε, $cm^{-1}M^{-1}$) 804 (10021), 559 (6369), 367 (18755), 326 (18988).

The following two compounds were prepared similarly.

[Rh(Me,Me)$_2$](PF$_6$)(BF$_4$)$_2$, [2](PF$_6$)(BF$_4$)$_2$.

A mixture of 0.055 g (0.061 mmol) of [**2**](PF$_6$) and 0.0142 g (0.122 mmol) of (NO)BF$_4$ in 20 mL of degassed CH_3CN was stirred under argon which was immediately turned to the blue color. After the blue solution had been stirred for 1 hour, solvents were removed

under vacuum. The resulting black/blue residue was washed with two 5 mL portions of degassed Et_2O and was dried under a vacuum for several hours to leave 0.0527 g (80% yield) of [**2**]$(PF_6)(BF_4)_2$. μ_B = 2.67, UV-Vis (CH_2Cl_2): nm (ε, $cm^{-1}M^{-1}$) 2572 (3246), 953 (1796), 737 (5885), 697 (5606), 544 (4569), 469 (5872), 368 (13336).

[Ir(Me, Me)$_2$](PF$_6$)(BF$_4$)$_2$, [3](PF$_6$)(BF$_4$)$_2$.

A mixture of 0.0691 g (0.0695 mmol) of [**3**](PF_6) and 0.0162 g (0.139 mmol) of $(NO)BF_4$ in 20 mL of degassed CH_3CN was stirred under argon which was immediately turned to the blue color. After the blue solution had been stirred for 1 hour, solvents were removed under vacuum. The resulting black/blue residue was washed with two 5 mL portions of degassed Et_2O and was dried under vacuum for several hours to leave 0.0702 g (86% yield) of [**3**]$(PF_6)(BF_4)_2$. μ_B = 2.87, UV-Vis (CH_2Cl_2): nm (ε, $cm^{-1}M^{-1}$) 914 (16764), 680 (6140), 600 (7938), 517 (6227), 367 (14170), 235 (74601).

CHAPTER 4

INTRAMOLECULAR ELECTRONIC COMMUNICATION OF RHENIUM OLIGOMERIC PINCER-TYPE COMPLEXES

4.1. INTRODUCTION

Organic mixed-valence compounds have been studied extensively for the potential applications of electronic and optical materials or for model to study fundamental intramolecular electron transfer processes.[1-5] The redox centers in many of organic mixed-valence compounds are comprised of organoamines.[6-11] Although other functional groups such as imides,[12] quinones,[13] nitro[14,15] and hydrazines[16,17] have also been extensively studied. The popularity of triarylamine based radicals is due in part to facile synthesis and to the stability of the radical cations.

Lambert et al. has synthesized and studied the electronic properties of a series of compounds where two triarylamine groups are linked by various organic bridges.[7] Two bis(triarylamine) complexes linked by different phenylenes are shown in Figure 4.1. The mono-oxidized bis(triarylamine) is a mixed valence compound since it has a neutral redox center and a oxidized redox center. Therefore, the electronic communication of these two centers could be occurred through the bridge. After the investigation of electron communication of two redox centers by the means of electrochemistry and spectro-electrochemistry, the bis(triarylamine) compound, which has a phenyl spacer, has been assigned to the Robin-Day class III mixed valence system. The bridge of two phenyl groups has not allowed delocalizing of the charge over two redox centers that much like the one phenyl group spacer and it has been assigned to the Robin-Day class II mixed

valence system. In this way, they have studied the mixed-valence properties of bis(triarylamines) as the function of the bridge and have shown that the nature of the bridge plays very important role in the electronic communication of two redox centers.

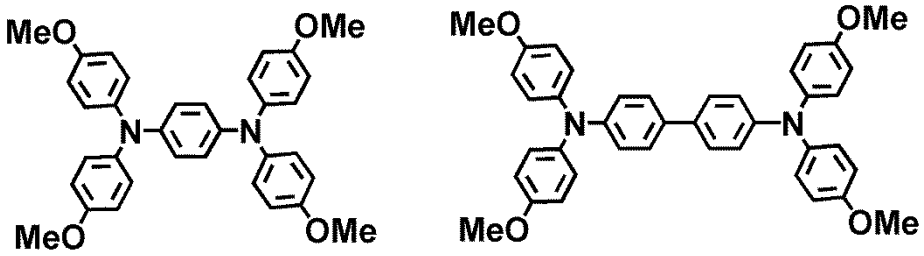

Figure 4.1. Two bis(triarylamine) complexes studied by Lambert et al.[7]

Mixed-valence properties of bis(diaryl)amines are not studied that much compared to the bis(triarylamine) derivatives. It might be due to the irreversible oxidation of diarylamines. Binding of metal ions to the diarylamine positions may stabilize the radicals and would permit a reversible oxidation. The redox active di(2-pyrazolyl-p-tolyl)amine ligand, H(Me,Me), which we have described in previous chapters, is a diaryl amine based pincer-type ligand. It have the ability to bind with metal ions in tridentate manner and redox properties of the ligand were investigated. Therefore, we were set to synthesize ditopic pincer ligands by connecting two mono-topic pincer ligands over phenylene bridges. This would results in dinucleating pincer ligands, which have two diarylamines linked over the phenylene bridges. Metal complexes of these ligands would provide reversible ligand centered oxidations and the stability to the mixed-valence complexes.

This chapter outlines the synthesis of three ditopic pincer ligands H_2(L1), H_2(L2), and H_2(L3) with one, two, and three phenylene rings between amido nitrogens. We also detail the bimetallic tricarbonyl derivatives and oxidized derivatives of these rhenium complexes to probe electronic properties.

4.2. RESULTS AND DISCUSSION

The three dinucleating pincer-type ligands were prepared by the pathways summarized in Schemes 4.1-4.3. The ligand H_2(L1), was synthesized by coupling two equivalents of pyrazole to 1,4-dibromo-2,5-difluorobenzene followed by $Pd_2(dba)_3$ catalyzed coupling of two equivalents of H(pzAn^{CH3}),[18] Scheme 4.1. This reaction only gave low yield (19%) of the product, but was the best among the other alternations (solvent, catalyst, reaction time, temperature) that were explored. A different procedure was followed to synthesize H_2(L2), Scheme 4.2. The $Pd_2(dba)_3$ catalyzed coupling reaction between *p*-toluidine and 4,4'-Diiodobiphenyl yielded 98% of the diarylamine intermediate, I2A, which was then subjected bromination using four molar equivalents bromine liquid in DMF to yield 92% of the desired tetra-brominated compound, I2B. The target H_2(L2) was obtained a moderate yield by CuI catalyzed amination reaction of I2B with pyrazole. The final ligand, H_2(L3) was synthesized in a high yield by the Suzuki coupling reaction between H(Me,Br)[19] and 1,4-phenylenediboronic acid (Scheme 4.3). Finally the model mono-nucleating ligand, H(L4), with CH_3 and Phenyl groups in the *para*-aryl positions, was synthesized by the Suzuki coupling of H(Me,Br) with phenyl boronic acid.

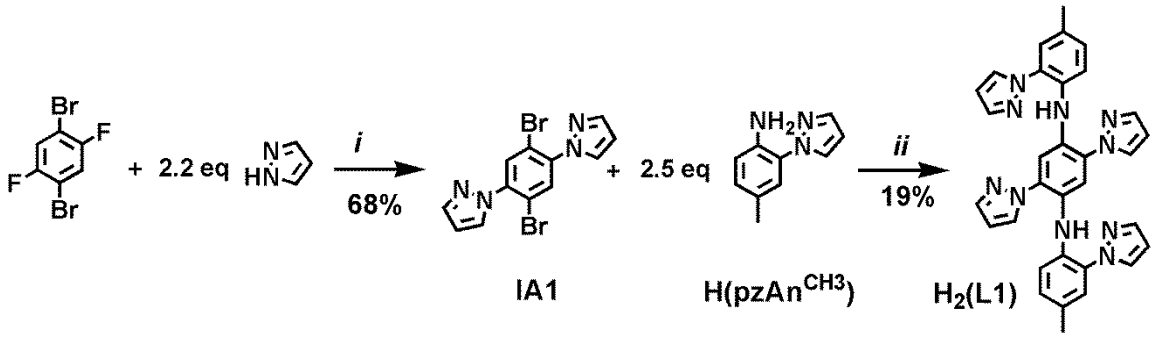

Scheme 4.1. Synthesis of H_2(L1). (i) 2.2 eq NaH, Δ, DMF; (ii) 2.5 eq ^{t}BuONa, 8 mol% DPPF, 4 mol% $Pd_2(dba)_3$, toluene, Δ.

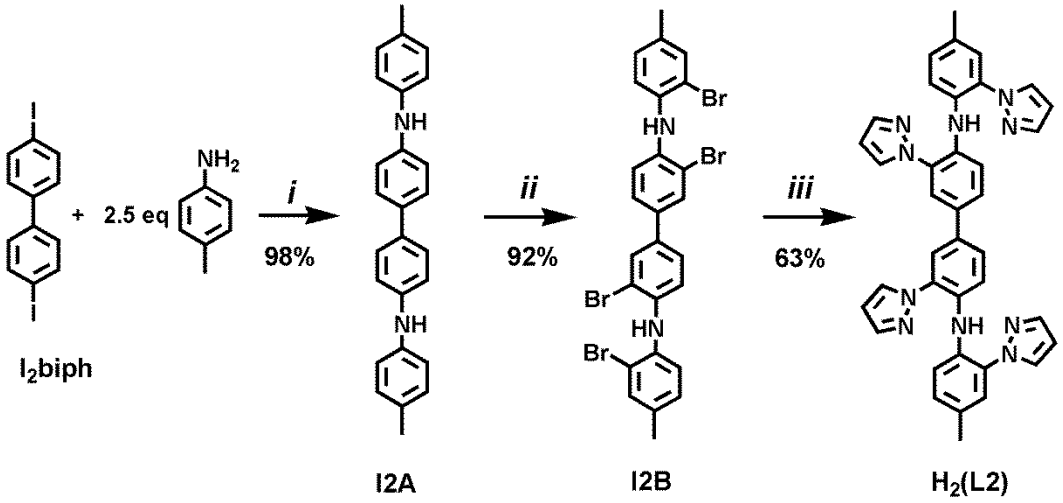

Scheme 4.2. Synthesis of H_2(L2). (i) 3 eq. ^{t}BuONa, 2 mol% P(^{t}Bu)$_3$, 2 mol% $Pd_2(dba)_3$, toluene, Δ; (ii) Br_2(*l*), DMF; (iii) 7 eq Hpz, 7 eq. K_2CO_3, 35 mol% DMED, CuI, xylene, Δ.

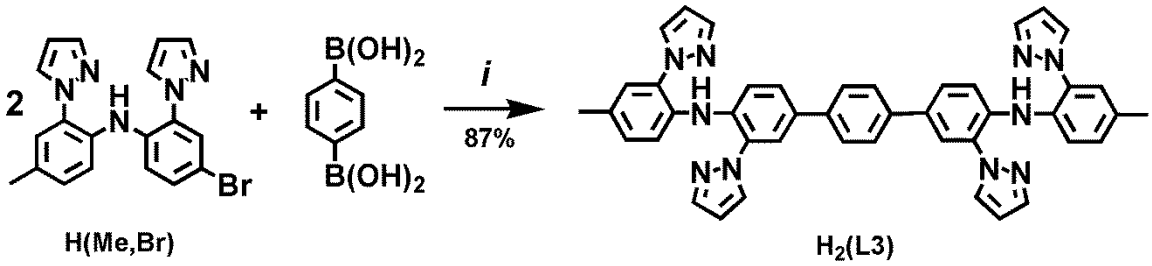

Scheme 4.3. Synthesis of H_2(L3). (i) 20 mol% $Pd(PPh_3)_4$, Na_2CO_3.

Schemes 4.4 - 4.6 shows the preparative routes to bis-tricarbonylrhenium(I) complexes of these ditopic pincer ligands. The complex $[Re(CO)_3]_2$(μ-L1)), **1** was synthesized by the reaction of H_2(L1) with 2 equivalents of each $Re(CO)_5Br$ and NEt_4OH in refluxing toluene as represented in Scheme 4.4. The desired product, **1**, was obtained by filtration as a yellow insoluble solid. Following a similar procedure, the other two rhenium complexes, $[Re(CO)_3]_2$(μ-L2), **2** and $[Re(CO)_3]_2$(μ-L3), **3** were prepared. The model compound $Re(CO)_3$(Me,Ph), **4** was synthesized by using a 1:1:1 ratio of H(L4): $Re(CO)_5Br$: NEt_4OH . As **4** is slightly soluble in toluene, toluene was evaporated by vacuum distillation and the product was purified by washing with MeOH. The complexes **1**-**3** are soluble in DMF, DMSO, and slightly soluble in CH_2Cl_2 but insoluble in most other organic solvents. The complex **4** is soluble in CH_2Cl_2, acetone, and acetonitrile.

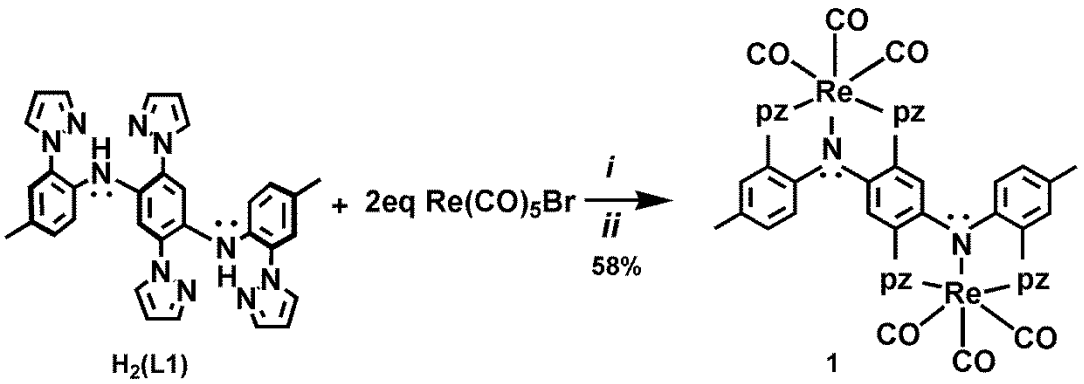

Scheme 4.4. Synthesis of $[Re(CO)_3]_2(\mu\text{-L1})$, **1**. *i*) toluene, Δ, 10 mins. *ii*) 2 eq NEt_4OH, Δ, 12 h.

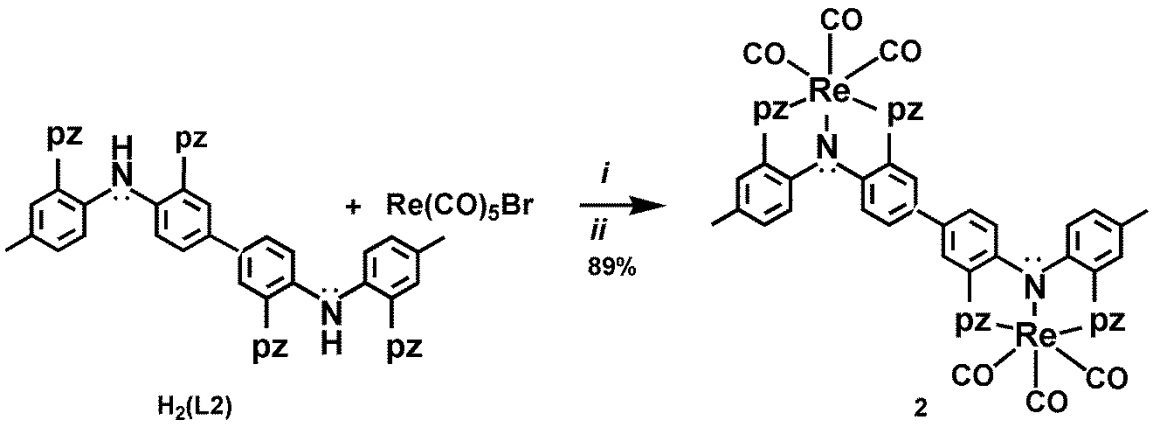

Scheme 4.5. Synthesis of $[Re(CO)_3]_2(\mu\text{-L2})$, **2**. *i*) toluene, Δ, 10 mins. *ii*) 2 eq NEt_4OH, Δ, 12 h.

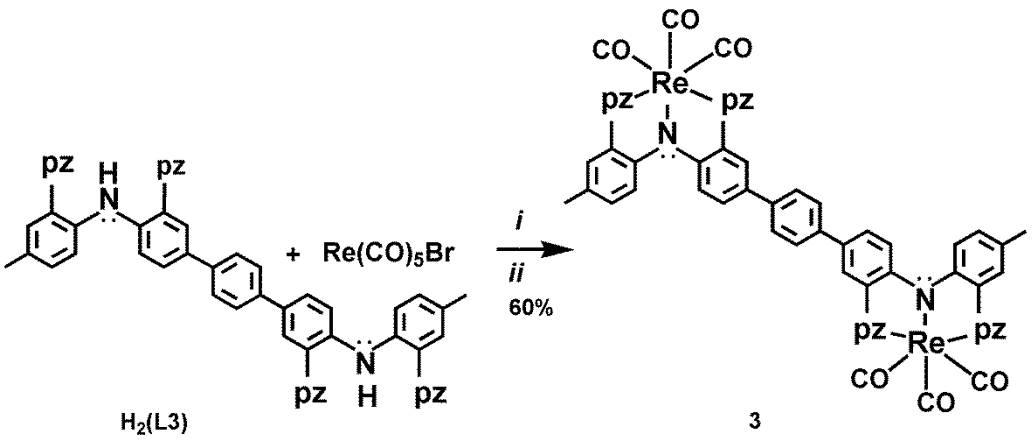

Scheme 4.6. Synthesis of $[Re(CO)_3]_2(\mu\text{-L3})$, **3**. *i*) toluene, Δ, 10 mins. *ii*) 2 eq NEt_4OH, Δ, 12 h.

The solid state structure of **2** and **4** were determined. The single crystals of model compound, **4**, were grown layering hexanes on top of CH_2Cl_2 solution of the complex (Figure 4.2). It has a distorted octahedral metal center with the ligand binding in a *fac*-κ^3 manner. This binding mode as well as Re-N bond distances and angles are similar to those reported for $(CO)_3$Re(Me,Me), **5** (Table 4.1).[20-21] The X-ray quality single crystals of **2**·1.6DMF·2Et_2O were grown by layering Et_2O on a DMF solution of the complex and allowing solvents to diffuse. The structure is shown in Figure 4.3, bond lengths and angles are are given in Table 4.1, while structure refinement data is listed in Table 4.2. The complex has approximate inversion symmetry. Each pincer part of the ligand is bound in the *fac*-κ^3 N-manner via the central amido nitrogen and two pyrazolyl nitrogens to each rhenium atom. The torsion angle of $Re1N_{Amido}$- $Re2N_{Amido}$ is 180 (2) ^{0} indicate that the rhenium atoms are on opposite sides of the mean plane of the bridging ligand. The bonding geometry of two rhenium centers is nearly the same; those are associated with two types of Re-N bonds, Re-N_{Ar} and Re-N_{pz}. The average bond distance of Re-N_{Ar}

(2.161(2) Å) is somewhat longer than the average bond length of Re-N_{pz} (2.157 (2) Å). The amido nitrogen is nearly planar and $\sum \angle$'s about N5 is 358 $(6)^0$. The rhenium-carbon bond lengths of carbonyls are not identical but are nearly the same with an 1.921(3) Å average bond length. Further, the two rings of the central biphenyl moiety are twisted from coplanarity with a 20^0 dihedral angle. It was not yet proven possible to grow suitable-sized X-ray quality crystals of either **1** or **3**; crystals formed from different solvent systems but were usually too small and those were seemingly large enough did not diffract at higher angles.

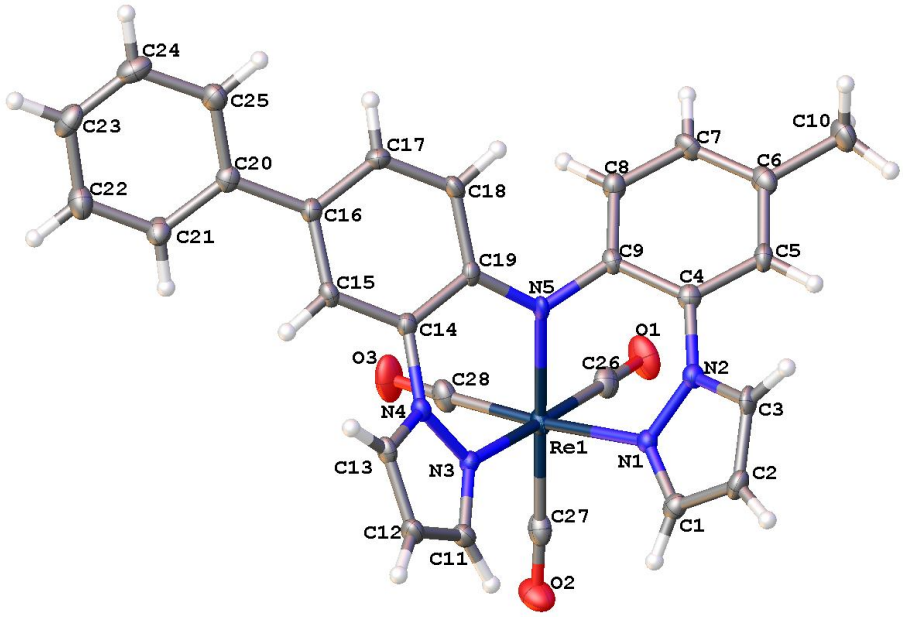

Figure 4.2. Molecular structure of **4** determined by X-ray crystallography.

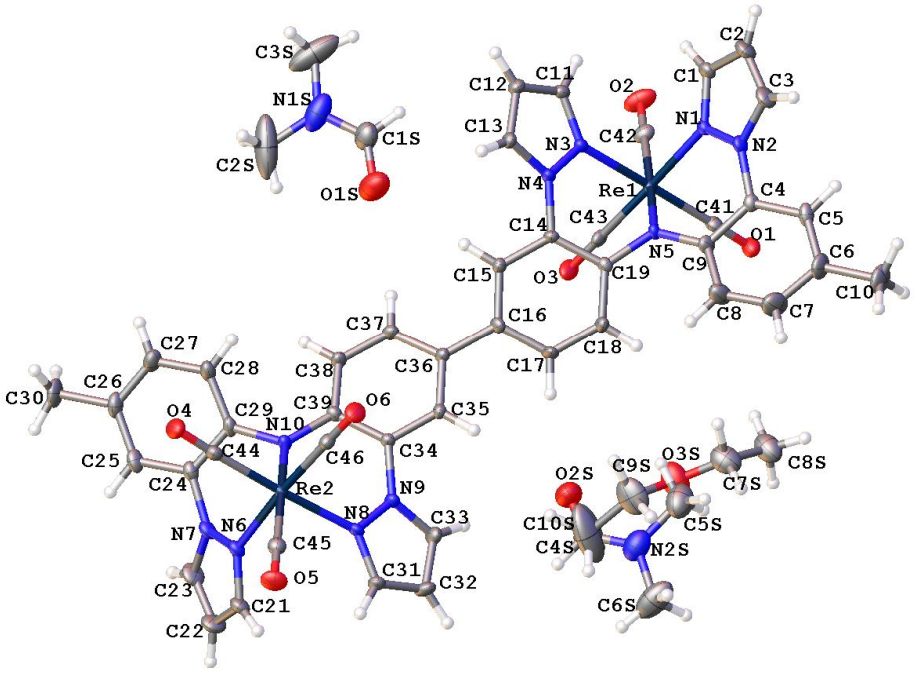

Figure 4.3. Structure of $[Re(CO)_3]_2(\mu\text{-L2})\cdot 1.6DMF\cdot 2Et_2O$ (**2**·1.6DMF· $2Et_2O$).

Table 4.1. Average bond distances and inter atomic angles of **2, 4,** and **5**.

	2·1.6DMF·2Et$_2$O	**4**	**5**
Re-N_{amido} (Avg),Å	2.160 (2)	2.157 (3)	2.163 (3)
Re-N_{pz} (Avg), Å	2.157 (2)	2.168 (3)	2.161 (3)
Re-C (avg), Å	1.962 (3)	1.917 (3)	1.928 (4)
Σ ∠N $_{Amido}$	356^0 (6) & 359^0 (6)	356^0 (6)	356^0 (6)
tol – tol	23.7^0 (3)& 25.2^0 (3)	24^0 (3)	

Table 4.2. Crystallographic data collection and structure refinement for **2·1.6DMF·2Et$_2$O** and **4**.

Compound	**2·1.6DMF·2Et$_2$O**	**4**
Empirical formula	$C_{50.40603}H_{45.21809}N_{11.59397}O_8Re_2$	$C_{28}H_{20}N_5O_3Re$
Formula weight	1313.79	660.69
Temperature/K	100.00(10)	100.00(10)
Crystal system	Triclinic	triclinic
Space group	P-1	P-1
a/Å	11.2495(2)	9.7304(2)
b/Å	14.7960(3)	11.5214(4)
c/Å	15.4484(3)	12.5751(4)
α/°	90.1200(15)	70.534(3)
β/°	94.8715(15)	72.056(3)
γ/°	106.7428(17)	67.271(3)
Volume/Å^3	2452.49(8)	1199.62(6)
Z	2	2
ρ_{calc}mg/mm^3	1.779	1.829
μ/mm^{-1}	4.999	5.107
F(000)	1286	644
Crystal size/mm^3	0.3044 × 0.088 × 0.0581	0.3796 × 0.1549 × 0.0218
Radiation MoKα,	(λ = 0.71073)	MoKα (λ = 0.71073)
2Θ range for data collection	5.76 to 59.04°	5.9 to 58.96
Index ranges	-15 ≤ h ≤ 15, -20 ≤ k ≤ 20, -21 ≤ l ≤ 20	-13 ≤ h ≤ 13, -15 ≤ k ≤ 15, -16 ≤ l ≤ 17
Reflections collected	46563	26564
Independent reflections	12205 [R_{int} = 0.0319, R_{sigma} = 0.0327]	6099 [R_{int} = 0.0523, R_{sigma} = 0.0510]
Data/restraints/parameters	12205/23/703	6099/0/335
Goodness-of-fit on F^2	1.059	1.043
Final R indexes [I>=2σ (I)]	R_1 = 0.0244, wR_2 = 0.0496	R_1 = 0.0304, wR_2 = 0.0550
Final R indexes [all data]	R_1 = 0.0319, wR_2 = 0.0532	R_1 = 0.0389, wR_2 = 0.0582
Largest diff. peak/hole / e Å^{-3}	1.45/-1.20	1.43/-1.08

[a] $R = \Sigma||F_o|-||F_c||/\Sigma|F_o|$. [d] $wR = [\Sigma w(|F_o^2|-|F_c^2|)^2/\Sigma w|F_o^2|^2]^{1/2}$

The IR spectra of each rhenium complex **1-4** measured in KBr pellets, are given in Figure 4.4 while data are presented in Table 4.3. All four spectra show the characteristic spectral pattern for three C-O stretching bands for *fac*-$Re(CO)_3$ units. Further, the data are all nearly identical and in very good agreement with *fac*-$Re(CO)_3(Me,Me)$, **5**.[20,21]Change in *para*-aryl substituents does not seem to impact the metal center CO stretch in contrast to Rh(I) derivatives.[22]

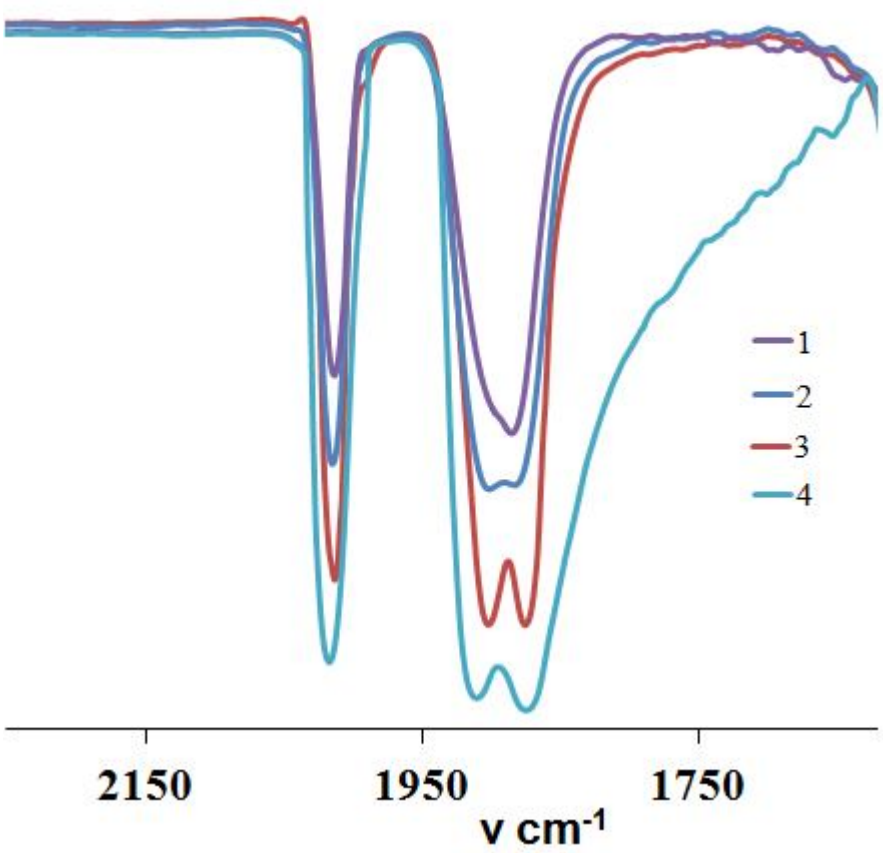

Figure 4.4. Solid state KBr pellet IR spectra of the new complexes, **1-4**.

Table 4.3. KBr pellet IR spectroscopic data for various $Re(CO)_3$ complexes.

Compound	ν_{C-O} cm^{-1}	Average ν_{C-O}, cm^{-1}
1	2013, 1900, 1884	1932
2	2015, 1901, 1882	1933
3	2013, 1901, 1876	1930
4	2017, 1911, 1874	1934
5	2013, 1901, 1876	1930

The electrochemical properties of four rhenium complexes were measured by cyclic voltammetry, and representative cyclic voltammograms are found in Figure 4.5, while data are summarized in Table 4.4. Compound **4** shows a quarsireversible one electron oxidations near +0.706 V versus Ag/AgCl (ΔE>>59 mV and $\Delta E = E_{pa}$-E_{pc} increases as a function of scan rate). The electrochemical behavior of **4** is similar to that reported for **5**, which has the oxidation at +0.651 V versus Ag/AgCl in DMF. The redox potentials of these two complexes increase with the average σ_p of the *para*-aryl substituents. The potentials at which this redox process occurs for both rhenium(I) complexes are conspicuously low for a heavily metal-centered oxidation. For instance, the anodic one-electron oxidation of $CpRe(CO)_3^{0/+}$ was identified at +1.16 V versus Ag/AgCl,[23,24] and this metal-centered oxidation of Cp ligand occurs at much higher potentials. Since the oxidation of H(L4) or H(L5) is irreversible but becomes reversible in **4** or **5**; the metals clearly are important to the redox behavior. Moreover, the one-electron oxidized **5**, $\mathbf{5}^+$, was demonstrated to contain a mainly ligand-centered radical, with significant metal character, by IR, EPR experiments, and a theoretical (DFT) study.[20,21]

Complex **1** and **2** show two one-electron oxidation waves assessed by comparison of current intensities with equimolar solutions of ferrocene. The third complex, **3**, exhibits a single two-electron oxidation wave, while the model compound **4** shows one one-electron oxidation. All of these oxidations were quasi-reversible because the ratios of current peak intensities were the same, but the separation between anodic and cathodic peaks were greater than 59 mV and increased with the scan rates (Table 4.4). Compound **1**, which has only one phenyl group spacer, in between two redox-active amide groups, shows two well separated oxidation waves, while **2** shows two oxidation waves, which overlap each other, but are clearly visible.

According to the data summarized in Table 4.4, the separation between the two oxidation potentials in **1** is 292 mV and in **2** is 119 mV; the separation between two oxidation waves decreases with increasing bridge length. Similarly, the first oxidation potentials of **1** and **2** increase with the length of spacer in between two redox centers. The appearance of a single two-electron oxidation in the compound **3**, indicates that a three-phenyl group spacer does not permit any electronic communication between two redox-active centers in the CV time scale. The redox potential of model compound, **4**, further shifts to a higher potential indicating the electron deficiency nature of redox center compared to other complexes.

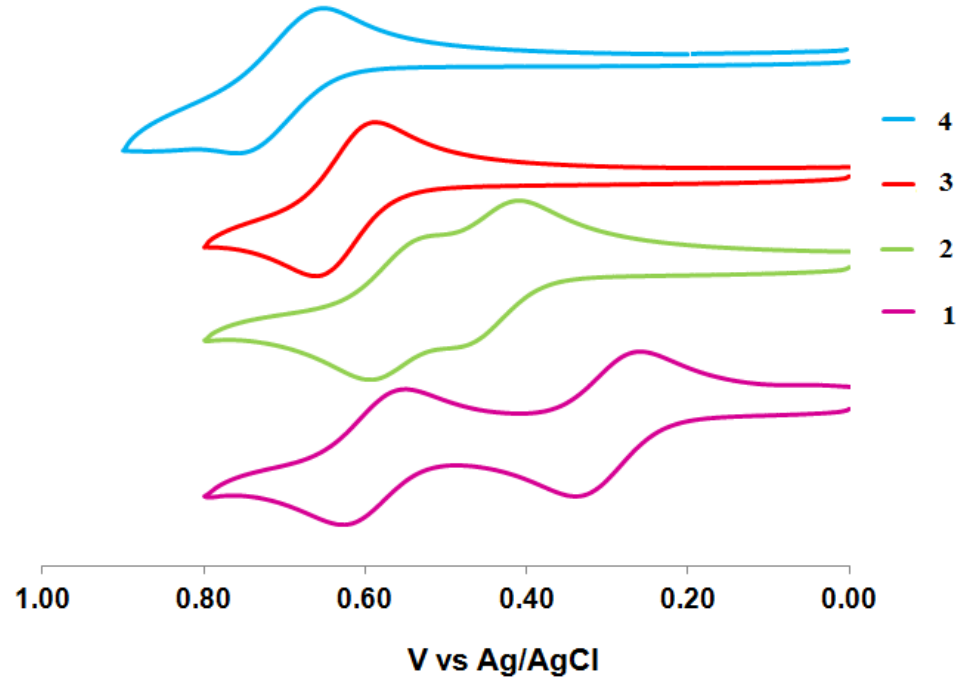

Figure 4.5. Cyclic voltammograms of **1, 2, 3,** and **4** in DMF obtained at a scan rate 100 mV/s. $N(Bu)_4PF_6$ was used as the supporting electrolyte and $Ag^+/AgCl$ as the reference electrode.

Table 4.4. Electrochemical data from cyclic voltammetry experiments of **1** - **5** in DMF.

Compound	E^0 , V vs Ag/AgCl[a]		
	E^0_{ox1} (E_{pa} – E_{pc} mV)	E^0_{ox2} (E_{pa} – E_{pc} mV)	K^b_{com}
1	0.300 (72)	0.592 (63)	9.55×10^5
2	0.443 (53)	0.562 (54)	1.10×10^2
3	0.626 (66)	-	-
4	0.706 (94)	-	-
5	0.651 (64)		

[a]Average values of $(E_{pa} + E_{pc})/2$ obtained for scan rates of 50, 100, 200, 300, 400, and 500 mV/s with 0.1 M NBu_4PF_6 as supporting electrolyte. [b] $K_{com} = e^{(\Delta E \cdot F/RT)}$, T = 295 K.

$$[Re(CO)_3]_2(\mu\text{-}L) + [Re(CO)_3]_2(\mu\text{-}L)]^{2+} \longleftrightarrow 2\,[[Re(CO)_3]_2(\mu\text{-}L)]^{+} \quad (1)$$

$$K_{com} = [[[Re(CO)_3]_2(\mu\text{-}L)]^{+}]^{2} / [[Re(CO)_3]_2(\mu\text{-}L)]\,[[Re(CO)_3]_2(\mu\text{-}L)]^{2+} \quad (2)$$

The comproportionation constants calculated from the electrochemical data are found in Table 4.4, reveals that the former complex, **1** (K_{com} = 9.6 x 10^5) is at the Robin-Day Class II/III borderline, **2** (K_{com} = 1.1 x 10^2) is Class I/II borderline, and **3** is Class I on the electrochemical time scale.[25] It is noted that a somewhat related, but purely organic, derivatives with two dianisylamine [(*p*-$MeOC_6H_4)_2N$] moieties connected by the *para*-phenyl, and *para*-biphenyl spacers are known, and their monooxidized derivative of one phenyl linked compound is a Robin-Day Class III and the other one is Class II species.[7] It is noted that the electrochemical properties of linked diarylamines, which are more closely related to **1**-**3**, are not known. The other physicochemical techniques with very different time scales can lead to quite different conclusions. Therefore the separation of oxidation waves alone is insufficient to establish the strength of the electronic communication, and further verification of Robin-Day class in $\mathbf{1}^{+}$-$\mathbf{3}^{+}$ was attempted by spectroscopic means.

In order to investigate IVCT band of mixed-valence derivatives, oxidized complexes were synthesized. Accordingly, doubly oxidized derivatives were prepared by chemical oxidation with $NOBF_4$ (Scheme 4.7). The oxidation potentials of all three rhenium complexes are low enough to permit two-electron oxidation with $NOBF_4$ (1.65 V vs Ag/AgCl) in CH_2Cl_2. The reaction of each complex with two equivalents of $NOBF_4$ in CH_2Cl_2 (as a suspension) gave solutions for the corresponding doubly oxidized **1**$(BF_4)_2$, **2**$(BF_4)_2$ and **3**$(BF_4)_2$. It is noted that each of the non-oxidized **1**, **2**, and **3** is

insoluble in CH_2Cl_2, but oxidized versions are soluble. These derivatives are paramagnetic and EPR silent in CH_2Cl_2 at 77 K. Also, for the comparison of spectral features **4** was oxidized to **4**(BF_4) with one equivalent of $NOBF_4$.Unfortunately it has not yet been possible to grow single crystals of these oxidized derivatives that on suitable for X-ray diffraction.

The IR spectra (KBr pellet) of **2** and $\mathbf{2}^{2+}$ are shown in Figure 4.6. On oxidation, there was a shift to higher frequency for the C-O stretching bands, reflecting lower capacity for metal-CO backbonding and increased strength of the CO bond. The change in average energy of the C-O stretching, $\Delta\nu_{CO}$(avg), increases by 14 cm^{-1} for **1** to $\mathbf{1}^{2+}$, 14 cm^{-1} for **2** to $\mathbf{2}^{2+}$, 21 cm^{-1} for **3** to $\mathbf{3}^{2+}$ and 24 cm^{-1} for **4** to $\mathbf{4}^{+}$**.** The IR streching frequency increase for the complex **5** upon oxidation was 41 cm^{-1} in KBr pellet. For comparison with a more heavily metal centered oxidation, rhenium-centered oxidation would be expected to have ν_{CO}(avg) increase on the order of $\Delta\nu_{CO}$(avg), for $CpRe(CO)_3$ to $CpRe(CO)_3^{+}$, about 100 cm^{-1}.[24]

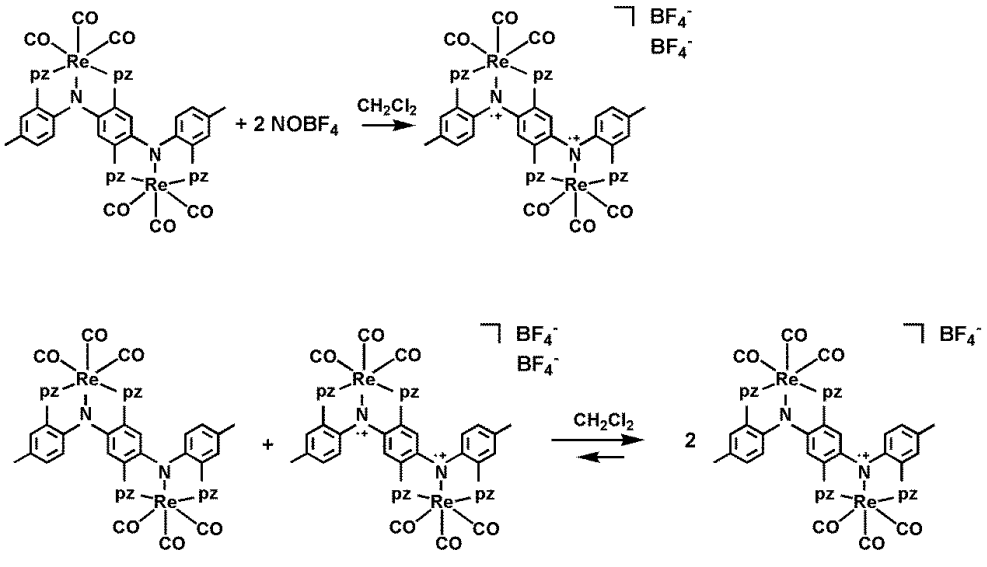

Scheme 4.7. Preparation of oxidized $\mathbf{1}^{n+}$, Top: n = 2, Bottom: n = 1.

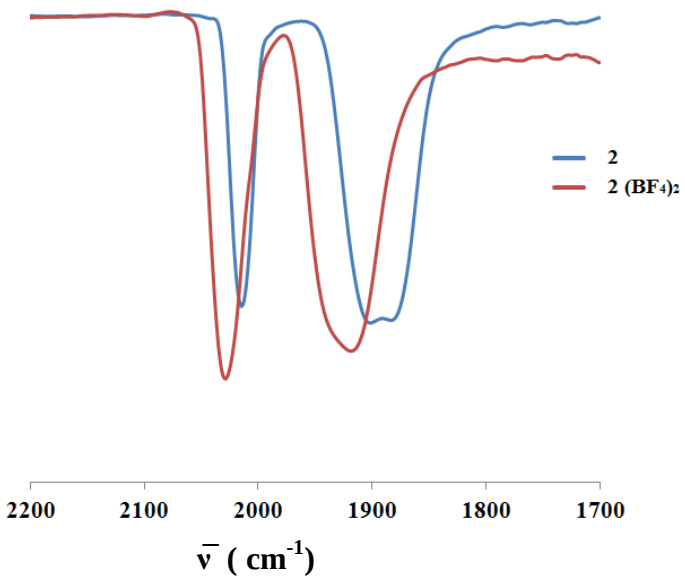

Figure 4.6. IR spectra of **2** and **2**$^{\cdot}$$(BF_4)_2$.

The electronic spectrum of each **1- 4** and **5** in CH_2Cl_2 shows single visible band near 380 nm, that gives rise to the yellow color of the complexes. The UV/visible/NIR spectra of **1**$(BF_4)_2$, **2**$(BF_4)_2$ and **3**$(BF_4)_2$ and **4**(BF_4) are shown in Figure 4.7. The spectra of doubly oxidized **2** and **3** complexes shows modestly intense ($2000 < \varepsilon < 18\ 000\ M^{-1}cm^{-1}$) lowest energy band in the region of 400-1000 nm that characteristic of π-radical transitions (π(HOMO-n) to π(SOMO)) similar to those found in the spectra of previously described mono- and di-oxidized $[Ga(Me,Me)_2]^+$ complexes.[26] The π-radical band in $\mathbf{1}^{2+}$ has a much lower intensity compared to $\mathbf{2}^{2+}$ or $\mathbf{3}^{2+}$ and shows a red shift along the series **1**$(BF_4)_2$ (λ_{max} = 524 nm) > **2**$(BF_4)_2$ (λ_{max} = 638 nm) > **3**$(BF_4)_2$ (λ_{max} = 793 nm). Dichloromethane solutions of these solutions have distinct colors, purple colored **1**$(BF_4)_2$, blue colored **2**$(BF_4)_2$, green colored **3**$(BF_4)_2$, and green/blue colored **4**(BF_4).

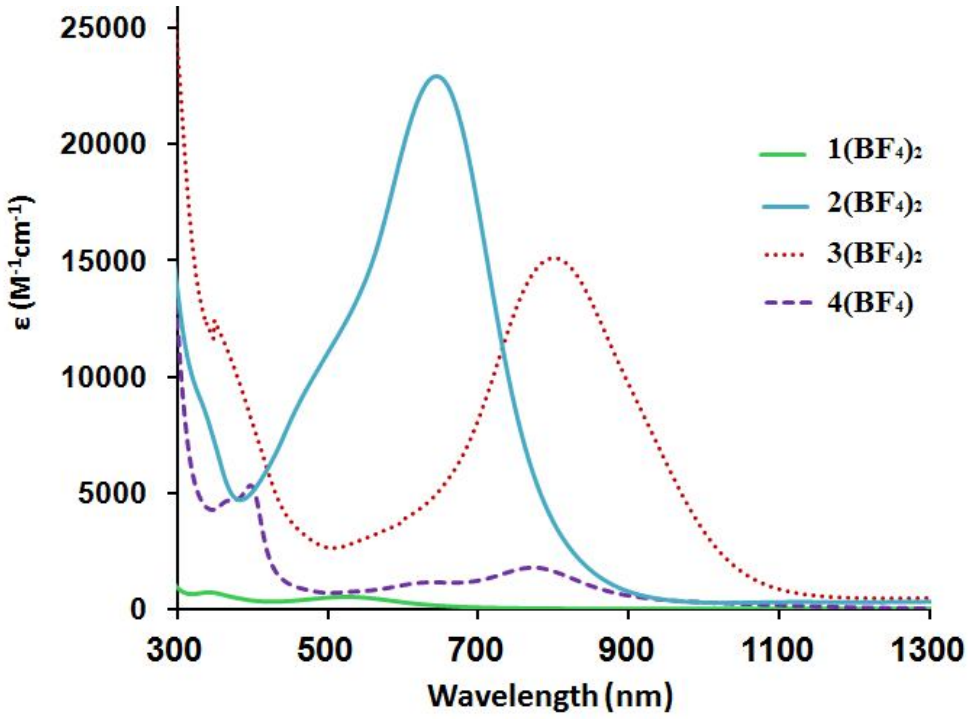

Figure. 4.7. UV-Visible spectra of doubly oxidized **1**, **2,** and **3,** and **4**(BF_4) in CH_2Cl_2.

The comproportionation reactions (eq 1 and Scheme 4.7) were used to prepare $\mathbf{1}^+$, $\mathbf{2}^+$, and $\mathbf{3}^+$. The X-band (9.65 GHz) EPR spectra of **1**$(BF_4)_2$, **2**$(BF_4)_2$, **3**$(BF_4)_2$, **1**(BF_4), **2**(BF_4), and **3**(BF_4) at 77 K and 293 K were recorded in CH_2Cl_2. The EPR spectra of **1**(BF_4) showed an isotopic signal at g = 2.00 , both at 293 K and 77 K. Rhenium has two EPR active isotopes, ^{185}Re (37.4 %) and ^{187}Re (62.6%) ; both have I = 5/2. EPR spectrum of $\mathbf{1}^+$ shows small hyperfine interaction between the electronic spin of the $^{185/187}$ Re nuclei. It might be due to the rapid interchange of the spin in-between two redox active centers, which would not detect any coupling with rhenium in the EPR time scale or the signal might be the averaged. In contrast to that, EPR spectra of **2**(BF_4) and **3**(BF_4) at room temperature show well-resolved signals due to the hyperfine interaction between the electron spin and two rhenium nucleic. On the other hand EPR spectra of these two

complexes at 77 K show broad peaks due to the quadrupolar interactions with rhenium nuclei.

Room temperature EPR spectra of **1**(BF_4), **2**(BF_4) and **3**(BF_4) were simulated successfully. The mono-oxidized **1** shows an isotropic EPR spectrum at room temperature that could be adequately simulated with g = 2.0052, a^{N1} = 0.71 mT, a^{N2} = 0.75 mT, a^{Re1} = 0.18 mT and a^{Re2} = 0.17 mT. The mono-oxidized complex **2** shows well resolved eleven lines spectra at g = 2.0027, which is close to the free electron value. The electron spin couples to two nitrogen atoms and two rhenium atoms, adequately simulated with a^{N1} = 3.21 mT, a^{N2} = 0.91 mT, a^{Re1} = 0.21mT and a^{Re2} = 1.52 mT.

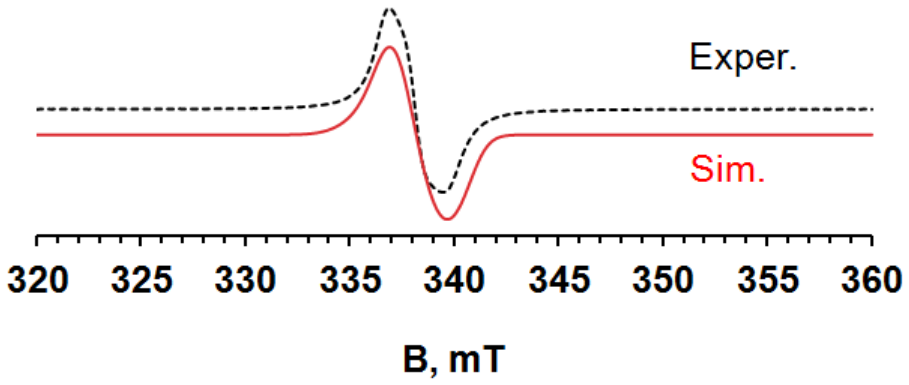

Figure 4.8. Experimental (top) and Simulated (bottom) X-band (9.49 GHz) EPR spectra of **1**(BF_4) in CH_2Cl_2 at 293 K.

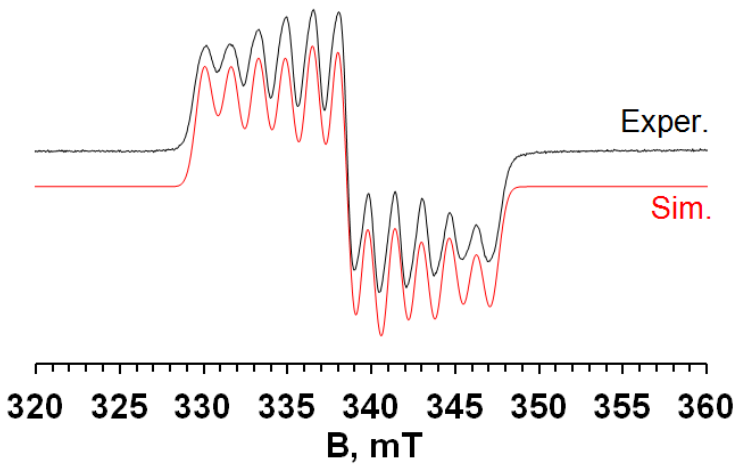

Figure 4.9. Experimental (top) and Simulated (bottom) X-band (9.49 GHz) EPR spectra of **2**(BF_4) in CH_2Cl_2 at 293 K.

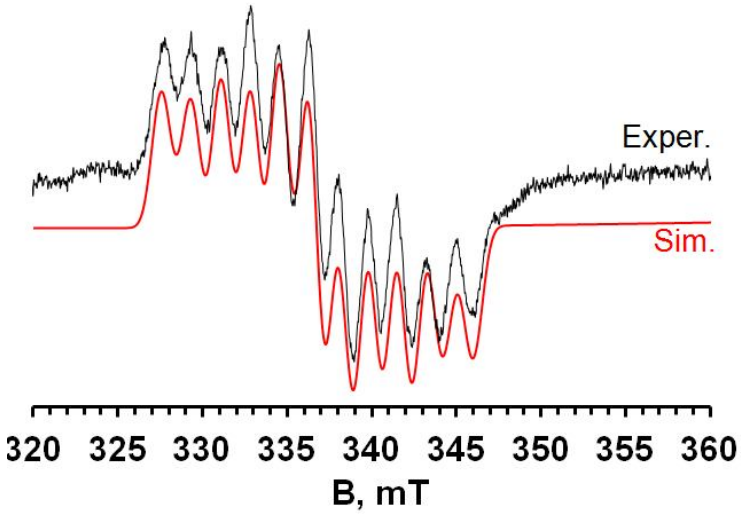

Figure 4.10. Experimental (top) and Simulated (bottom) X-band (9.46 GHz) EPR spectra of **3**(BF_4) in CH_2Cl_2 at 293 K.

The room temperature X-band EPR spectrum of **3**(BF_4) (Figure 4.10) is isotopic, centered at g = 2.0135. The hyperfine coupling was simulated using a^{N1} = 0.32 mT, a^{N2} = 3.24 mT, a^{Re1} = 0.5 mT and a^{Re2} = 1.77 mT. The uneven coupling constants are in line

with those of **2**(BF_4). As these radicals show hyperfine coupling with rhenium nuclei, a small amount of spin density is located unevenly on both metals. Hyperfine coupling was not observed in the EPR spectra of **1**(BF_4), perhaps due to the rapid exchange on the EPR time scale. Attempts to observe doubly oxidized derivatives by EPR spectroscopy were not fruitful.

The comproportionation reactions to form $\mathbf{1}^+$, $\mathbf{2}^+$, and $\mathbf{3}^+$ were probed by spectroscopic titrations of neutral rhenium complexes with doubly-oxidized derivatives. Upon the addition of sub-stoichiometric amounts of doubly oxidized $\mathbf{1}^{2+}$ into the yellow solution of **1** in CH_2Cl_2, new bands at 820 nm, 539 nm and 417 nm grew at the expense of the band at 386 nm for **1** until one equivalent was reached (Figure 4.8). The two higher energy bands are assigned to the π-radical transition, while the band at 820 nm is assigned as the valence charge transfer (IVCT) transition.

Similar spectral changes were observed for the titration of **2** with $\mathbf{2}^{2+}$ (Figure 4.12). However the disappearance of the band at 401 nm **2** was observed concomitantly with the growth of new bands near 1126 nm and 533 nm (π-radical) and 1335 nm (IVCT). Similarly, the IVCT band at 2204 nm and π-radical bands at 555 nm and 403 nm appeared at the expense of the broad spectrum of **3** during the course of titration (Figure 4.13). By the comparison of the data for three titrations, it is noted that the intensity of bands for $\mathbf{2}^+$ are much higher than for $\mathbf{1}^+$ or $\mathbf{3}^+$. The same observation was made

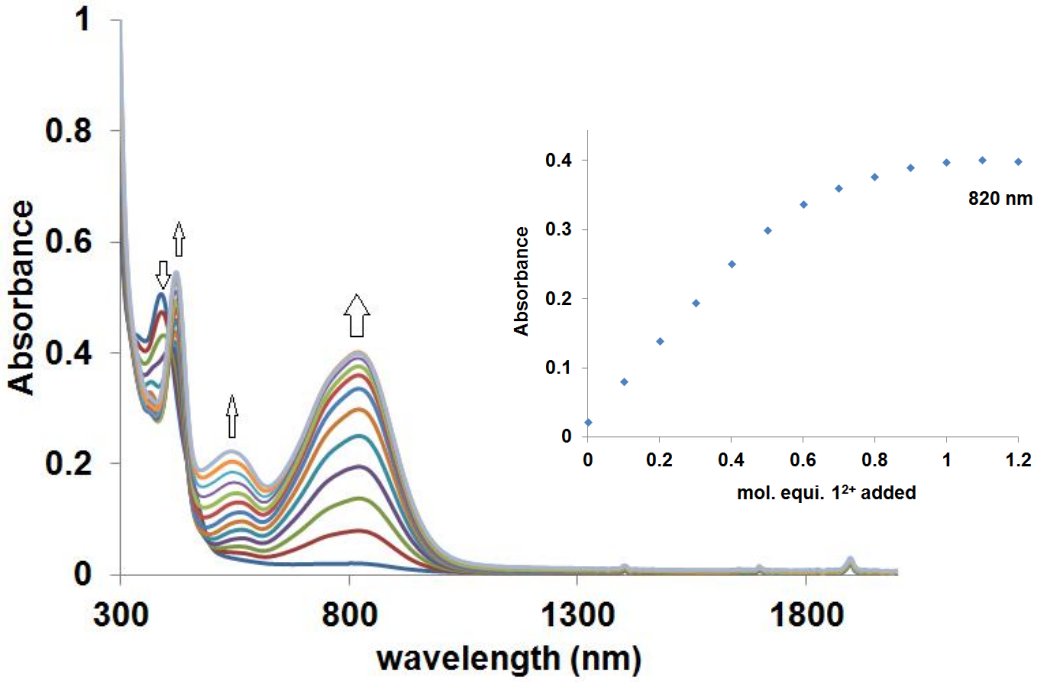

Figure 4.11. Spectrophotometric titration of **1** with $\mathbf{1}^{2+}$ in CH_2Cl_2. Inset: Absorbance vs mol. equi. of $\mathbf{1}^{2+}$ added at 820 nm.

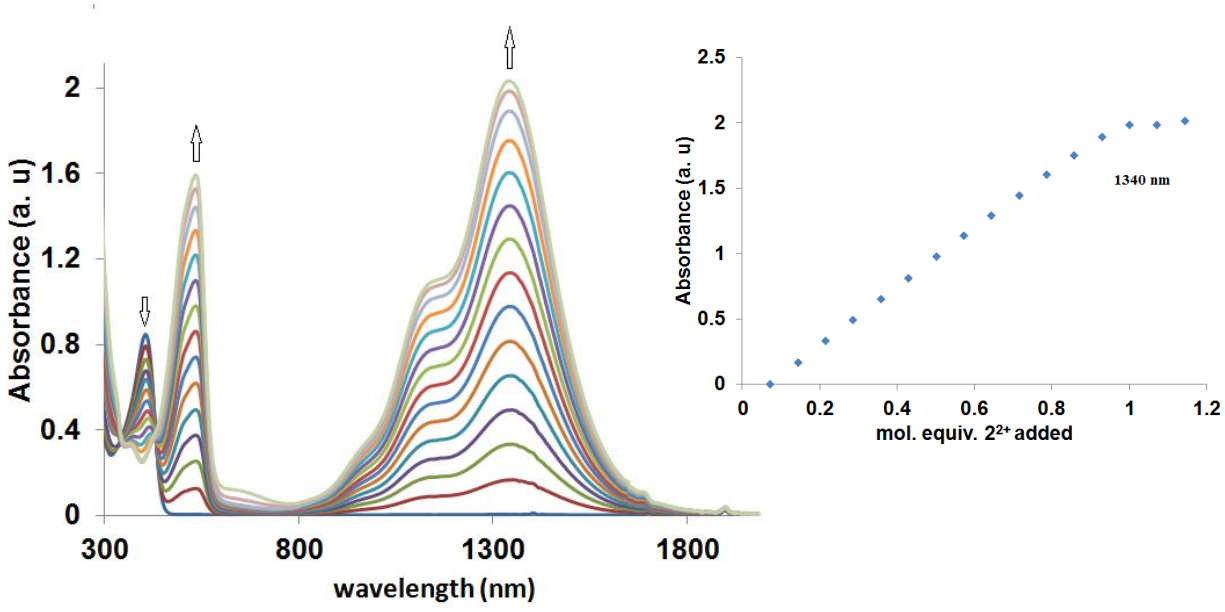

Figure 4.12. Spectrophotometric titration of **2** with $\mathbf{2}^{2+}$ in CH_2Cl_2. Inset: Absorbance vs mol. equi. of $\mathbf{2}^{2+}$ added at 1340 nm.

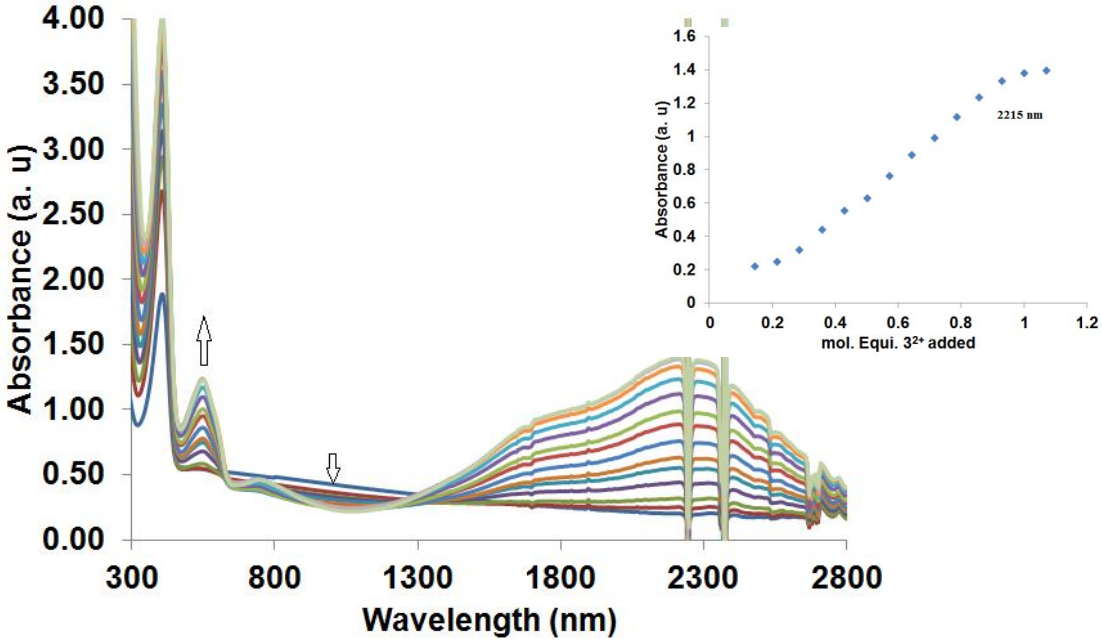

Figure 4.13. Spectrophotometric titration of **3** with $\mathbf{3}^{2+}$ in CH_2Cl_2. Inset: Absorbance vs mol. equi. Of $\mathbf{3}^{2+}$ added at 820 nm.

repeatedly on authentically pure samples and we currently have no satisfacting explanation as to the origin of the enhanced intensity.

The mono-oxidized complexes were also prepared on the synthetic scale by the comproportionation reaction in CH_2Cl_2 using 1:1 mixture of non-oxidized: doubly oxidized complex (Scheme 4.7). The same complexes were also prepared independently using 1:1 mixture of $NOBF_4$ and either **1**, **2**, or **3**. While there was no significant difference in products by two methods, the comproportionation reaction is more convenient because the required mass of $NOBF_4$ was very low for the other method as difference of molar masses between $NOBF_4$ and either **1-3** made it difficult to measure small masses of the former. Also $(\mathbf{1\text{-}3})^+$ have greater solubility than $NOBF_4$ in many solvents.

IVCT bands of $\mathbf{1}^+$, $\mathbf{2}^+$, and $\mathbf{3}^+$ are shown in Figure 4.14-4.17. The energy of IVCT bands increases with decreasing length of the spacer (Figure 4.14). Each IVCT band has a characteristic shape that can be fit as the sum of three increasing energy, decreasing intensity and overlapping Gaussian bands that are separated by ~500 cm^{-1} ($\mathbf{1}^+$); ~1400 cm^{-1} ($\mathbf{2}^+$); and ~1200 cm^{-1} ($\mathbf{3}^+$) that may be part of a vibrational progression. The lowest energy of the three bands was used in Hush relations to extract H_{ab} and other parameters in Table 4.5.[27,28] E_{OP} decreases with increasing length of spacer being 11,900(16) cm^{-1} for $\mathbf{1}^+$, 7442 (9) cm^{-1} for $\mathbf{2}^+$, and 4363(30) cm^{-1} for $\mathbf{3}^+$.

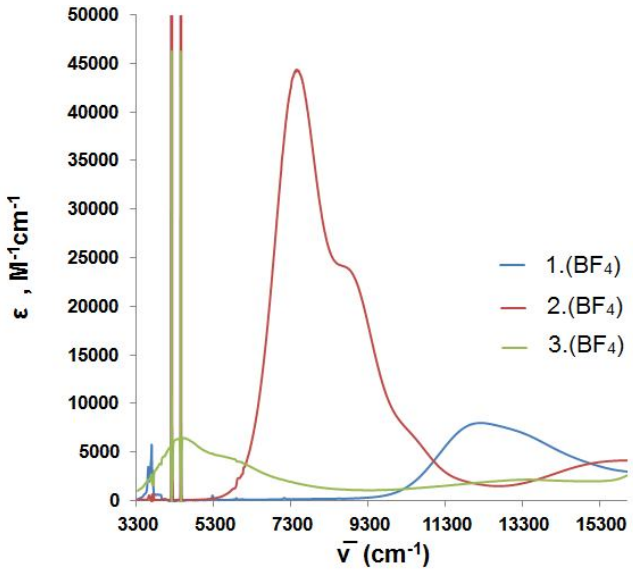

Figure 4.14. IVCT bands of singly oxidized rhenium complexes in CH_2Cl_2.

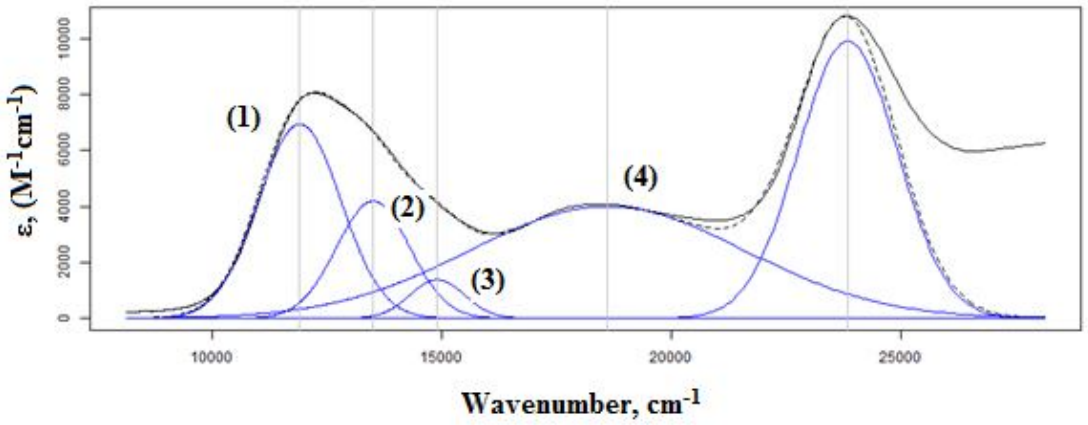

Figure 4.15. Deconvolution of IVCT band of **1**(BF_4). Parameters for curve fitting: (λ_{max} (cm^{-1}), $\Delta\nu_{1/2}$ (cm^{-1}), ε ($M^{-1}cm^{-1}$)): Curve 1 (11900, 900, 6938), Curve 2(13570, 882, 4180), Curve 3(15000, 600, 1000), Curve 4(18542, 2839, 3970).

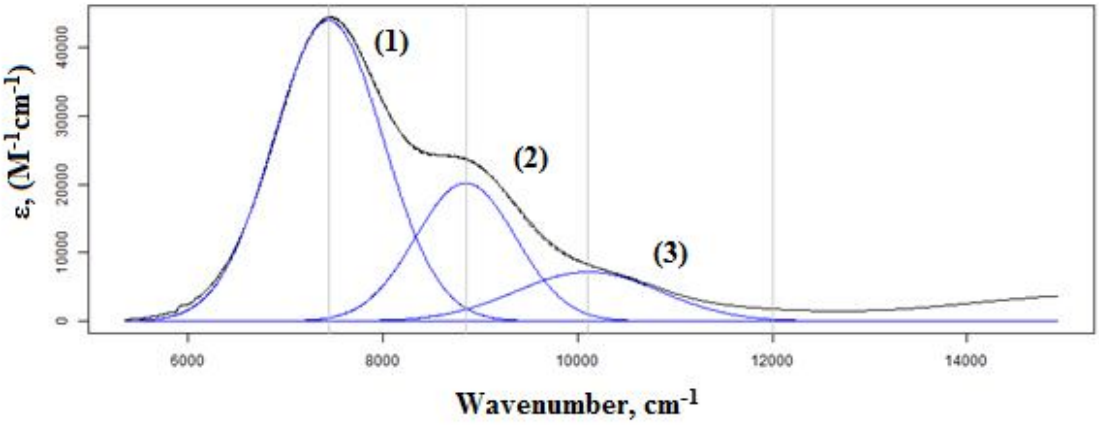

Figure 4.16. Deconvolution of IVCT band of **2**(BF_4). Parameters for curve fitting: (λ_{max} (cm^{-1}), $\Delta\nu_{1/2}$ (cm^{-1}), ε ($M^{-1}cm^{-1}$)): Curve 1 (7442, 563, 43904), Curve 2(8901, 560, 20735), Curve 3 (10290, 917, 5269).

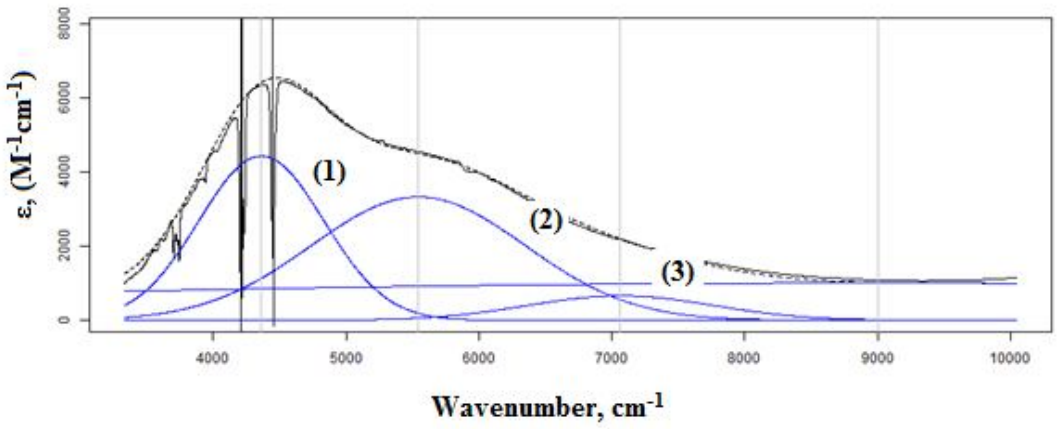

Figure 4.17. Deconvolution of IVCT band of **3**(BF_4). Parameters for curve fitting: (λ_{max} (cm^{-1}), $\Delta\nu_{1/2}$ (cm^{-1}), ε ($M^{-1}cm^{-1}$)): Curve 1 (4362, 482, 4580), Curve 2 (5567, 800, 3499), Curve 3 (7150, 500, 732), Curve 4 (9000, 1000, 5000).

The value of d for $\mathbf{2}^+$ was estimated from the crystallographic data of **2**. As the first approximation the value of d was selected as the intra ligand N_{Aryl}-N_{Aryl} distance. It was also assumed that the distance did not significantly contract on oxidation. The d values for the other two complexes were estimated using appropriate bond lengths measured by the crystal structure of **2** to save as a reasonable limit for maximum H_{ab}. Thus, for **3**, three C1···C4 distances of phenyl group (3 x 3.184 Å) plus two C-C bonds (2 x 1.483 Å) and two N-C bonds (2 x 1.394 Å) gives 17.20 Å N_{Aryl}-N_{Aryl} distance. Similarly, 6.60 Å N_{Aryl}-N_{Aryl} distance was obtained for **1**. IVCT band analysis data for these three complexes are given in Table 4.5.

Table 4.5. Summary of IVCT band shape fitting and ET parameters of **1**(BF_4), **2**(BF_4), **3**(BF_4).

	1(BF_4)	**2**(BF_4)	**3**(BF_4)
$E_{OP} = \lambda$ (cm^{-1}), Ch. 1	11900 (± 16)	7442 (± 9)	4363 (± 30)
ε_{max} ($M^{-1}cm^{-1}$)	6938 (± 4)	43904 (± 2)	4580 (± 6)
$\Delta\tilde{\nu}_{1/2}$ (cm^{-1})	900 (± 7)	563 (± 3)	482 (± 4)
d (Å)	6.60	11.90	17.20
H_{ab} (cm^{-1}), see Ch. 1	846 (± 5)	739 (± 4)	116 (± 4)
$\alpha = 2H_{ab}/\lambda$	0.14	0.20	0.05
ΔG^* (cm^{-1}), see Ch. 1	2189	1194	977
k_{et} (s^{-1}), see Ch. 1	3.53×10^9	4.35×10^{11}	4.03×10^{10}

The obtained H_{ab} values for these mono-oxidized complexes fall in a wide range from 116(4) cm^{-1} to 846(5) cm^{-1}. This increase in the series also was reflected by the oxidation potential splitting ΔE, as determined by the cyclic voltammetry. In the cyclic voltammetric time scale complex **3** showed zero splitting and it shows very low electronic coupling element, 116 cm^{-1} in the spectroscopic time scale. The mono-oxidized complex **2** shows H_{ab} = 739 cm^{-1} electronic coupling element. The mono-oxidized complex **1** has the highest value (H_{ab} = 846 cm^{-1}), which is consistent with the highest ΔE of cyclic voltammetry. These all three complexes are in the Robin Day Class II mixed valence complexes according to the Marcus-Hush model as their $2H_{ab}$ values are smaller than λ.[29] Proper assignments to the Robin-day classes cannot be made as the solvent dependency of this IVCT was not measured. The complexes (**1**-**3**)$^+$ decomposed in acetonitrile, DMF and THF preventing measurements. While the current complexes show lesser electronic communication with increasing of spacer as with other systems

(Organic).[7,30-32] The current ones fall off much more quickly. Future theoretical studies may provide better clues as to the origin of the increased damping effect in these areas of complexes.

4.3. CONCLUSIONS

Bimetallic tricarbonylrhenium(I) complexes of three dinucleating pincer-type ligands were successfully synthesized and characterized. The spacer-between the redox active ends of these oligomeric ligands ranged from one to three phenylenes. The electronic properties of these three complexes were probed by cyclic voltametric and spectroscopic studies. The electronic communication drastically diminished in strength with the size of the spacer.

The equilibrium constants for comproportionation (K_{com}) were calculated by using the oxidation potential splitting. Complex **1** has large K_{com} value, 9.55×10^5, which is the upper limit of Robin-Day class II (1×10^6) mixed valence compounds. Therefore, it can be assigned to the Robin-Day class II(A) mixed-valence compound. Complex **2** belong to the Robin Day Class II, while complex **3** does not show any electronic communication in the cyclic voltammetric time scale.

The electronic coupling element, H_{ab}, of mono-oxidized complexes was determined by analyzing their intervalence charge transfer (IVCT) bands. H_{ab} for $\mathbf{1}^+$, $\mathbf{2}^+$, and $\mathbf{3}^+$ are 846 cm^{-1}, 739 cm^{-1}, and 116 cm^{-1}, respectively. Those are within expected limit for the Robin-Day class II ($0 < Hab < \lambda$). The limited solubility and limited stability of mixed-valence $(\mathbf{1}\text{-}\mathbf{3})^+$ solvents other than CH_2Cl_2 prevented the investigation of solvent dependence to the NIR transition; giving uncertainty to $\mathbf{1}^+$. Of importance, it was found

that evaluation of strength of electronic communication needs to be probed by multiple methods since electrochemistry indicated compound **3** as class I, whereas class II behavior was observed by NIR spectral analysis.

These ligands should viable to support long range intramolecular charge transport in assemblies or polymeric chains. Future works of Dr. Gardinier's lab will focus on making discrete heterometallic derivatives by putting different metals in one at a time or on making metallo polymers.

4.4 EXPERIMENTAL

General Considerations. The compounds CuI, M_2CO_3 (M = Na, K, Cs), NaH, ^tBuONa, $MgSO_4$, $Na_2S_2O_3$, $NaHCO_3$, $NOBF_4$, *N*-Bromosuccinimide (NBS), Bromine liquid, $Pd_2(dba)_3$, 1,1'-Bis(diphenylphosphino)ferrocene (DPPF), 1,4-dibromo-2,5-difluorobenzene, pyrazole, N,N'-dimethylethylenediamine (DMED), 1,4-phenylenediboronic acid, 4,4'-Diiodobiphenyl, p-toluidine, tri-t-butylphosphine, bromine, anhydrous DMF and the 1.47 *M* [25% (w/w)] solution of $(NEt_4)(OH)$ in CH_3OH were purchased commercially and used as received. The compounds $H(pzAn^{CH3})$[18] $H(Me,Br)$[19], $Re(CO)_5Br$[33] and $Pd(PPh_3)_4$[34] were prepared according to literature procedures. Diethyl Ether (Et_2O) was dried over sodium/benzophenone ketyl. toluene, *p*-xylene and CH_2Cl_2 were dried over CaH_2. Solvents used in reactions were distilled under argon prior to use.

Physical Measurements. Midwest MicroLab, LLC, Indianapolis, Indiana 45250, performed all elemental analyses. Melting point determinations were made on samples contained in glass capillaries using an Electrothermal 9100 apparatus and are

uncorrected. ^{1}H and ^{13}C NMR spectra were recorded on a Varian 400 MHz spectrometer. Chemical shifts were referenced to solvent resonances at δ_H 7.27, δ_C 77.23 for $CDCl_3$ and δ_H 8.05 (s), 2.95(q) and 2.75(q) for DMF. Abbreviations for NMR and UV-Vis br (broad), sh (shoulder), m (multiplet), ps (pseudo-), s (singlet), d (doublet), t (triplet), q (quartet), p (pentet), sept (septet). Electrochemical measurements were collected under a nitrogen atmosphere for samples as 0.1 m*M* solutions in DMF with 0.1 M NBu_4PF_6 as the supporting electrolyte. A three-electrode cell comprised of an Ag/AgCl electrode (separated from the reaction medium with a semipermeable polymer membrane filter), a platinum working electrode, and a glassy carbon counter electrode was used for the voltammetric measurements. Data were collected at scan rates of 50, 100, 200, 300, 400, and 500 mV/s. With this set up, the ferrocene/ferrocenium couple had an $E_{1/2}$ value of +0.55 V in DMF at a scan rate of 200 mV/s, consistent with the literature values.[18] Electronic absorption (UV-Vis/NIR) measurements were made on a Cary 5000 instrument. Infrared spectra were recorded on samples as KBr pellet using Magna-IR 560 spectrometer. EPR spectra were obtained as solutions ~0.2 m*M* in CH_2Cl_2 using a Bruker ELEXYS E600 equipped with an ER4116DM cavity resonating at 9.63 GHz, an Oxford instruments ITC503 temperature controller and a ESR-900 helium flow cryostat. The spectra were recorded using 100 kHz field modulation unless otherwise specified.

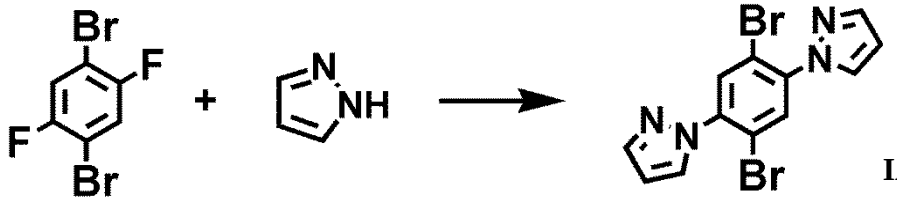

IA1

IA1.

A solution of 5.000g(18.39 mmol) 1,4-Dibromo-2,5-difluorobenzene 2.759g (40.45 molo, 2.2 eq) H-pyrazole and 0.971g (40.45 mmol, 2.2 eq) NaH on 60 mL of DMF were heated at reflux for 40 mins. The mixture was then poured into 100 mL DI water and the resulting white precipitate was filtered under vacuum and washed with 3 x 50 mL DI water. The product was dried under vacuum to yield 4.589 g (68% yield) IA1. Mp, 176-178 ^{0}C. ^{1}H NMR ($CDCl_3$): δ_H 7.96 (dd, J = 2.5, 0.5 Hz, 2H, H_5pz), 7.94 (s, 2H, Ar), 7.79 (dd, J = 1.8, 0.5 Hz, 2H, H_3pz), 6.52 (dd, J = 2.5, 1.8 Hz, 2H, H_4pz) ppm. ^{13}C NMR ($CDCl_3$): δ_C 141.89, 139.93, 132.77, 131.54, 116.79, 107.51, 29.91ppm.

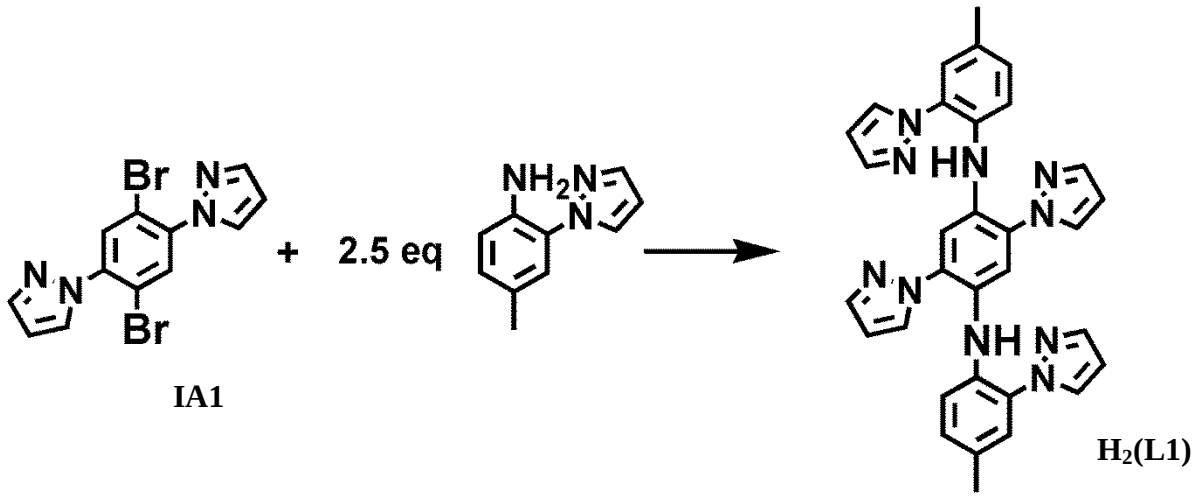

IA1 **H_2(L1)**

H_2(Me, μ-Ph, Me), H_2(L1).

In an argon-filled drybox, a Schlenk flask was charged with 1.005 g (2.73 mmol) IA1, 1.184 g (6.8 mmol, 2.5 eq) H($pzAn^{CH3}$), 0.787 g (8.19 mmol, 3 eq) ^{t}BuONa, 0.121 g (0.22 mmol, 8 mol%) DPPF, and 0.100 g (0.11mmol, 4 mol%) $Pd_2(dba)_3$. The flask was removed from the drybox and was attached to a Schlenk line. Then, 20 mL of toluene that was previously purged with argon 20 min, was transferred via cannula into the reaction flask. After the reaction mixture had been heated at 80 ^{0}C 4 days, toluene was removed

by vacuum distillation. The residue was dissolved in a biphasic mixture of 50 mL distilled water and 50 mL ethyl acetate. The organic and aqueous phases were separated. The aqueous phase was extracted with two 50 mL portions ethyl acetate. The combined organic layers were dried over $MgSO_4$, filtered, and solvent was removed by rotary evaporation to leave an oily residue. The residue was subjected to column chromatography on silica gel using 6:1 hexanes:ethyl acetate as the eluent. The desired product 0.199 g (19%) was obtained as a white solid after removing solvent from the fourth band (R_f = 0.26). Mp, 193-194 ^{0}C. ^{1}H NMR (acetone): δ_H 8.95 (s, 2 H, NH), 8.03 (d, *J* = 2.4 Hz, 2 H, H_5pz), 7.99 (d, *J* = 2.4 Hz, 2 H, H_5pz), 7.74 (br s, 4 H, pz), 7.39 (s, 2H, Ar),7.30 (d, *J* = 8.3 Hz, 2 H, Ar), 7.25 (d, *J* = 1.6 Hz, 2 H, Ar), 7.08 (dd, *J* = 8.3, 1.8 , 2H, Ar), 6.47 (t, *J* = 2.0 Hz, 2 H, H_3pz), 6.46 (t, *J* = 2.0 Hz, 2 H, H_3pz), 2.30 (s, 6 H, Ar-CH_3). ^{13}C NMR (acetone): δ_C 141.42, 141.17, 135.47, 131.40, 131.36, 131.18, 131.11, 131.07, 130.89, 129.72, 126.31, 119.61, 116.61, 107.63, 107.40, 20.51.

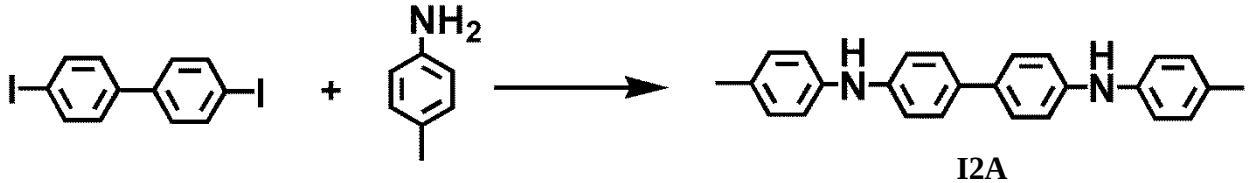

I2A

I2A.

In an argon filled drybox, a schlenk flask was charged with 4.004 g (9.84 mmol) 4,4'-Diiodobiphenyl, 2.644 g (24.68 mmol, 2.5 eq) p-toluidine, 2.844 g (29.6 mmol, 3 eq) NaO^tBu, 0.6 mL (2mol%) tri-t-butylphosphine and 0.181 g (0.20mmol, 2 mol%) $Pd_2(dba)_3$. The schlenk flask was removed from the drybox and 40 mL of deoxygenated toluene was added via cannula transfer. After the reaction mixture had been heated at reflux 15h under argon, solvents were removed by vacuum distillation. The resulting

solid was washed with 150 mL DI water and three 50 mL portions Et_2O and was vacuum dried to afford 3.529 g (98% yield) of desired product. Mp, 238-239 ^{0}C. ^{1}H NMR (DMSO-d_6): δ_H 8.09 (s, 2H, NH), 7.45 (d, *J* = 8.6 Hz, 4H), 7.06 (broad s, 8H), 7.00 (d, *J* = 8.4 Hz, 4H), 2.23 (6H, s) ppm. ^{13}C NMR (DMSO-d_6): δ_C 142.6, 140.7, 131.0, 129.6, 128.6, 126.4, 117.5, 116.3, 20.3 ppm.

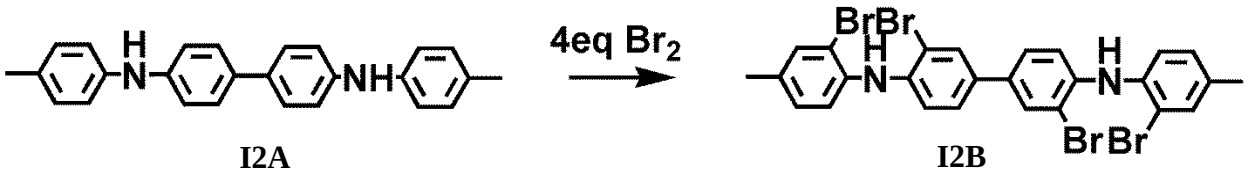

I2A **I2B**

I2B.

A solution of 0.25 mL (4.85 mmol, 4 eq) Br_2 in 10 mL DMF was added drop wise to a cold (0 ^{o}C) solution of 0.4384 g (1.21 mmol) I2A in 10 mL DMF. After complete addition, the mixture was stirred at 0 ^{o}C for 1 h and then was allowed reach room temperature and stirred total 4 hrs. Then, 10 mL of a saturated aqueous $Na_2S_2O_3$ solution was added. The biphasic mixture was poured into 100 mL dilute $NaHCO_3$ and the solid formed was separated by gravity filtration. The pale brown solid was further washed with 100mL DI water and vacuum dried to afford 0.755g (92% yields) of desired product. Mp, 198-199 ^{o}C. ^{1}H NMR ($CDCl_3$): δ_H 7.74 (d, *J* = 2.1 Hz, 2H), 7.44 (br s, 2H), 7.35 (dd, *J* = 8.5, 2.1 Hz, 2H), 7.25 (d, *J* = 8.5 Hz, 2H), 7.20 (d, *J* = 8.5 Hz, 2H), 7.07 (dd, *J* = 8.1, 1.5 Hz, 2H), 6.36(s, 2H, NH), 2.32 (s, 6H, CH_3)ppm. ^{13}C NMR ($CDCl_3$): δ_C 139.96, 137.21, 133.79, 133.59, 133.28, 131.00, 129.03, 126.29, 119.87, 116.75, 115.49, 113.70, 20.65 ppm.

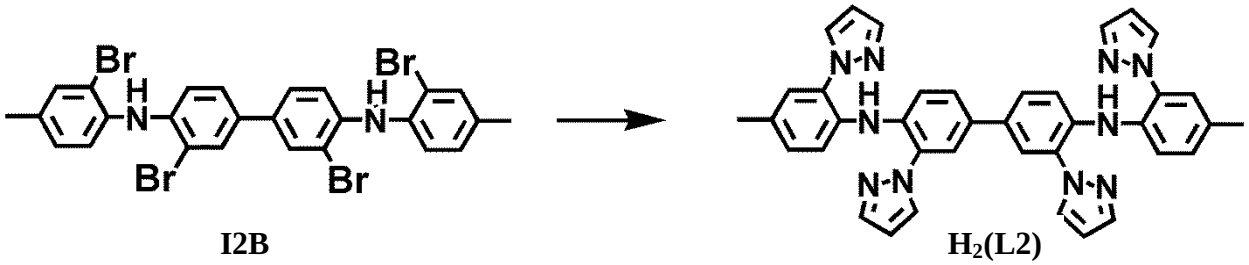

I2B **H_2(L2)**

H_2(L2).

A Schlenk flask charged with 1.504 g (2.21 mmol) I2B, 1.055 g (15.50 mmol, 7eq) pyrazole, 2.140 g (15.50 mmol) K_2CO_3 and 0.50 mL (0.4g, 4.58 mmol) DMED was deoxygenated by three evacuation and argon back-fill cycles. A 20 mL aliquot of dry, distilled, and argon-purged *p*-xylenes was added by syringe. Then, 0.200 g (1.05 mmol) CuI was added under an argon blanket. After the resulting mixture had been heated at reflux 2 d under argon, the mixture was cooled to room temperature. Then the solvent was evaporated by vacuum distillation and resulted solid was dissolved in a biphasic mixture of 50 mL ethyl acetate and 50 mL H_2O. The aqueous and organic layers were separated. The aqueous layer was extracted with three 25 mL portions ethyl acetate. The combined organic layers were dried over $MgSO_4$ and filtered. Volatiles were removed under vacuum to give a dark oil. The oil was subjected to flash chromatography on silica gel. First, elution with hexanes removed residual xylene. Then, 3:1 hexane:ethyl acetate was used to remove unreacted and partially reacted starting materials and finally 0.830 g (63.4 %) of H_2(L2) as a pale brown solid was collected after eluting with 1:1 hexanes : ethyl acetate (R_f = 0.53). Mp, 85-86^{o}C. ^{1}H NMR ($CDCl_3$): δ_H 7.74 (m, 8H), 7.50 (s, 2H), 7.40 (s, 4H), 7.39 (d, *J* = 6.6Hz, 2H), 7.20 (s, 2H), 7.09 (d, *J* = 8.1 Hz, 2H), 6.47, (t, *J* = 1.9 Hz, 2H, pz), 6.42 (t, *J* = 1.9 Hz, 2H, pz), 2.35 (s, 6H, CH_3) ppm. ^{1}H NMR (acetone): δ_H 9.27 (s, 2H, NH), 8.14 (dd, *J* = 2.5, 0.4 Hz, 2H, pz), 7.99 (dd, *J* = 2.4, 0.4 Hz, 2H, pz),

7.79 (d, *J* = 1.9 Hz, Ar), 7.75 (d, *J* = 1.8 Hz, Ar), 7.73 (d, *J* = 2.3 Hz, pz), 7.59 (dd, *J* = 8.6, 2.3 Hz, 2H, Ar), 7.43 (d, *J* = 8.6 Hz, 2H, Ar), 7.41 (dd, *J* = 8.3, 1.9Hz, 2H, Ar), 6.51 (t, *J* = 2.1Hz, 2H, pz), 6.47 (t, *J* = 2.1Hz, 2H, pz), 2.33 (s, 6H, CH_3) ppm. ^{13}C NMR ($CDCl_3$): δ_c 140.85, 140.66, 136.77, 133.70, 132.08, 131.64, 131.06, 130.22, 130.00, 128.95, 127.38, 126.27, 125.87, 123.19, 120.18, 117.88, 106.89, 106.80, 20.75 ppm.

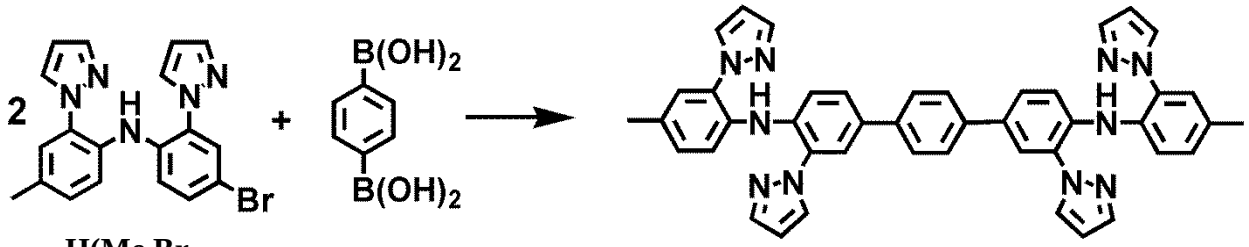

H(Me,Br **H$_2$(L3)**

H$_2$(L3).

A degassed mixture of 35 mL benzene and 11 mL of ethanol was added into a Schlenk flask containing 1.217 g (3.09 mmom, 2.5 eq) H(Me,Br), 0.205g (1.23 mmol) 1,4-phenylenediboronic acid and 0.028 g (0.25 mmol, 20 mol%) $Pd(PPh_3)_4$. Then 15 mL of degassed aqueous 2M Na_2CO_3 solution was added by cannula and the mixture was heated at 80 ^{0}C for 15h. Then the organic layer was separated and the aqueous layer was washed with two 20 mL aliquots ethyl acetate. The combined organic fractions were dried with anhydrous $MgSO_4$ filtered, and evaporated to leave a brown solid. The solid was washed with two 20 mL portions of ethanol, 20 mL of Et_2O and was dried under vacuum to yield 0.757g (87%) H_2(L3) as a pale yellow. Mp, 235-236 ^{0}C. ^{1}H NMR ($CDCl_3$): δ_H 8.26 (s, 2H, NH), 7.78 (d, *J* = 2.4 Hz, 2H), 7.76 (d, *J* = 1.85 Hz, 2H), 7.73 (d, *J* = 2.4 Hz, 2H), 7.70 (d, *J* = 1.8 Hz, 2H), 7.60 (s, 4H, Ar), 7.59 (d, *J* = 2.1 Hz, 2H), 7.48 (dd, *J* = 8.6, 2.1 Hz, 2H), 7.42 (dd, *J* = 8.6, 1.9 Hz, 4H), 7.20 (d, *J* = 1.8 Hz, 2H), 7.10 (dd, *J* = 8.2, 1.7 Hz, 2H), 6.48 (t, *J* = 2.4Hz, 2H), 6.42 (t, *J* = 2.3 Hz, 2H), 2.35 (s, 6H) ppm. ^{13}C NMR

($CDCl_3$): δ_C 140.9, 140.7, 138.6, 137.3, 133.6, 132.6, 131.8, 131.3, 130.3, 130.1, 129.9, 129.0, 127.0, 126.8, 126.0, 123.7, 120.5, 117.7, 107.0, 106.9, 20.8 ppm.

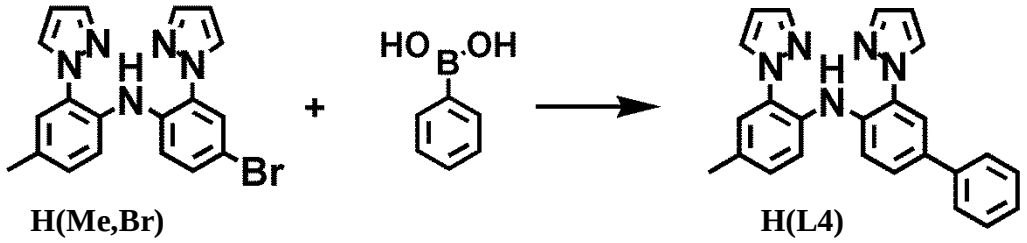

H(Me,Br) **H(L4)**

H(Me,Ph), H(L4).

In an argon-filled dry box, a Schlenk flask was charged with 0.797 g (2.022 mmol) H(Me,Br), 0.370 g (3.034 mmol) phenyl boronic acid, and 0.2336 g (0.202 mmol) $Pd(PPh_3)_4$. The flask was removed from the drybox and attached to a Schlenk line. A solution of 30 mL C_6H_6 and 10 mL absolute ethanol was purged with argon 15 min and was transferred to the reaction flask under argon via cannula. Next, 10 mL of an argon-purged 2 *M* aqueous Na_2CO_3 solution was transferred via cannula to the reaction flask. After the magnetically-stirred biphasic mixture had been heated at 80 ^{0}C for 16 h with the aid of an external oil bath, the mixture was cooled to room temperature and poured into 100 mL H_2O. The aqueous and organic fractions were separated. The aqueous layer was extracted with two 50 mL portions ethyl acetate. The combined organic layers were dried over $MgSO_4$ and filtered. The oily residue that was obtained after removing solvents under vacuum was subjected to column chromatography on silica gel using 4 :1 ethyl acetate : hexanes as an eluent to obtain desired product (0.6298g , 80%) H(Me, Ph) as a colorless solid after removing solvents and drying under vacuum 1 h. Mp, 81-82 ^{0}C. ^{1}H NMR ($CDCl_3$): δ_H 7.77 (dd, *J* = 2.4, .05 Hz, 1H, pz), 7.75 (dd, *J* = 1.8, 0.5 Hz, 1H, pz), 7.73 (dd, *J* = 2.4, 0.5 Hz, 1H, pz), 7.70 (dd, *J* = 1.8, 0.5 Hz, 1H, pz), 7.58-7.53 (m, 3H,

Ar), 7.47-7.39 (m, 6H, Ar and NH), 7.31 (tt, *J* = 7.3, 1.9 Hz, 1H, Ar), 7.20 (d, *J* = 1.5 Hz, 1H, Ar), 7.09 (dd, *J* = 8.3, 1.9 Hz, 1H, Ar), 6.48 (t, *J* = 2.1 Hz, 1H, pz), 6.42 (t, *J* = 2.1 Hz, 1H, pz), 2.35 (s, 3H, CH_3) ppm. ^{13}C NMR ($CDCl_3$): δ_C 140.8, 140.6, 137.1, 133.6, 133.2, 131.7, 131.1, 130.2, 130.0, 129.7, 128.9, 127.1, 126.9, 126.6, 125.9, 123.8, 120.3, 120.4, 117.6, 106.84, 106.77, 20.7 ppm.

Synthesis of Rhenium complexes

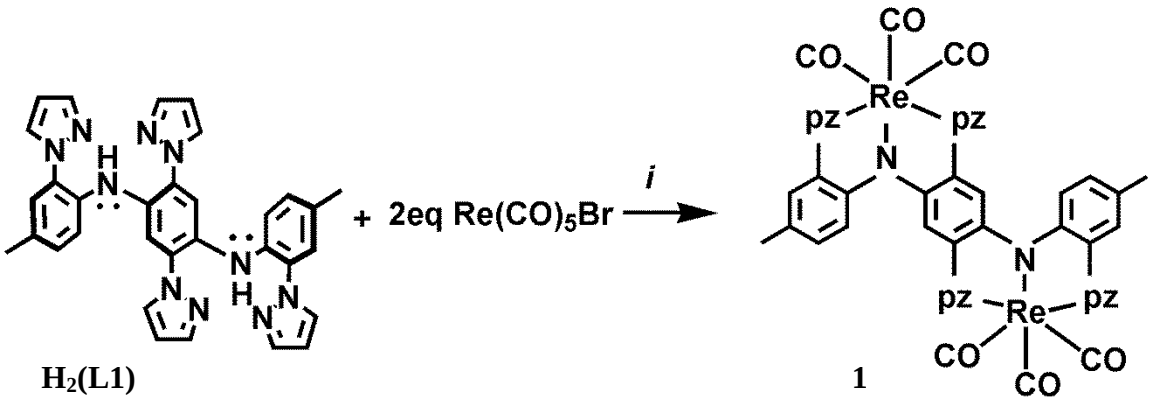

H_2(L1) **1**

[Re(CO)$_3$]$_2$(μ-L1), 1.

A solution of 0.184 g (0.33 mmol) H_2(L1) and 0.270 g (0.66 mmol, 2 eq) $Re(CO)_5Br$ in 25 mL of toluene was heated at reflux 10 min. Then 0.46 mL of 1.47 *M* (0.66 mmol) NEt_4OH in methanol was injected to the hot reaction mixture by syringe. The solution became yellow immediately upon mixing and a yellow solid soon precipitated. The mixture was heated at reflux for 12 h, then was allowed to cool room temperature. The insoluble portion was collected by filtration, was washed with 2 x 15mL MeOH, 15 mL Et_2O and was dried under vacuum to leave 0.211g (58%) of desired product as yellow powder. Mp, >350 ^{0}C. Anal. Calcd. (Found) for $Re_2C_{38}N_{10}H_{26}O_6$: C, 41.83 (41.81); H, 2.40 (2.60); N, 12.84 (12.46). IR(KBr) ν_{CO} 1886, 1897, 2013 cm^{-1}.^{1}H NMR (DMF-d_7): δ_H

8.82 (dd, *J* = 2.8, 0.7 Hz, 2H, pz), 8.65 (dd, *J* = 2.4, 0.8 Hz, 2H, pz), 8.62 (dd, *J* = 2.4, 0.7 Hz, 2H, pz), 8.55 (dd, *J* = 2.8, 0.7 Hz, 2H, pz), 8.07(s, 2H), 8.02 (d, *J* = 8.8 Hz, 2H), 7.42 (d, *J* = 1.4Hz, 2H), 7.15 (dd, *J* = 8.8, 1.8 Hz, 2H), 6.81(t, *J* = 2.5 Hz, 2H, pz), 6.77 (t, *J* = 2.5 Hz, 2H, pz), 2.32 (s, 6H) ppm. UV-Vis λ_{max}, nm (ε, $M^{-1}cm^{-1}$), CH_2Cl_2: 813 (776), 387 (18118), 227 (55308).

Except where noted, the following compounds were prepared in a similar manner where the heating time and subsequent work-up procedure were identical to that described for the above complex. The amounts of ligand, rhenium salt, base and solvent were used varied in the preparation of each complex and given below along with the yield and characterization data.

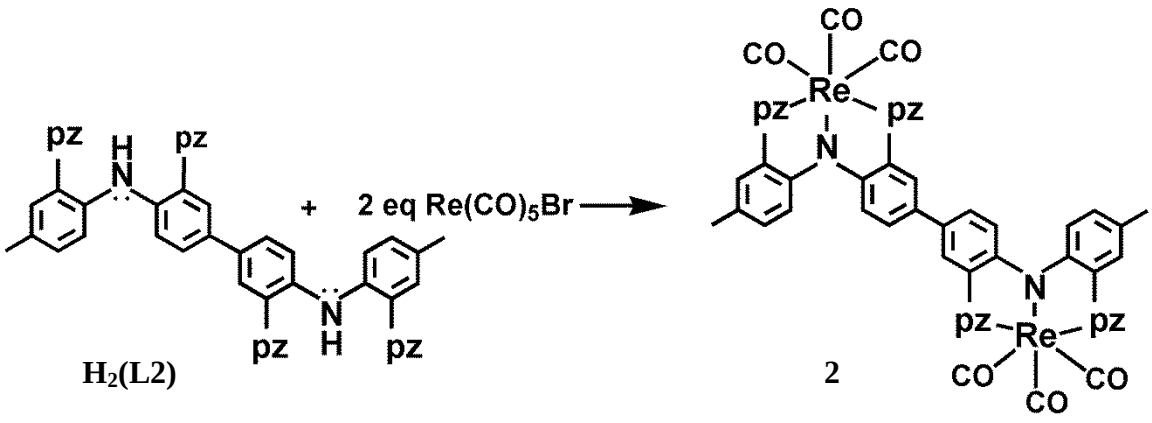

H_2(L2) **2**

$[Re(CO)_3]_2$(μ-L2), 2.

A mixture of 0.127g (0.20 mmol) H_2(L2), 0.164g (0.40 mmol) $Re(CO)_5Br$ and 0.28 mL 1.47 *M* (0.40 mmol) NEt_4OH in 10 mL toluene gave 0.211g (89%) **2** as a yellow powder. Mp, 260-261 ^{0}C (Decomposed). Anal. Calcd. (Found) for $Re_2C_{44}N_{10}H_{30}O_6$: C, 45.28 (45.54); H, 2.59 (2.78); N, 12.00 (11.84). IR(KBr) ν_{CO} 1882, 1905, 2013 cm^{-1}. ^{1}H NMR (DMF-d_7): δ_H 8.74 (d, *J* = 2.7Hz, 2H,pz), 8.64 (d, *J* = 2.4Hz, 2H,pz), 8.62 (d, *J* = 2.26 Hz,

2H, pz), 8.61 (d, *J* = 2.6 Hz, 2H,pz), 7.98 (d, *J* = 8.3Hz, 2H, Ar), 7.96 (d, *J* = 8.8 Hz), 2H, Ar), 7.74 (dd, *J* = 8.8, 2.1 Hz, 2H, Ar), 7.45 (s, 2H, Ar), 7.28 (dd, *J* = 8.3, 1.7 Hz, 2H, Ar), 7.21 (s, 2H, Ar), 6.82 (t, *J* = 2.5Hz, pz), 6.77 (t, *J* = 2.4Hz, 2H, pz), 2.37 (6H, CH_3) ppm. UV-Vis λ_{max}, nm (ε, $M^{-1}cm^{-1}$), CH_2Cl_2: 402 (22433), 238 (36349).

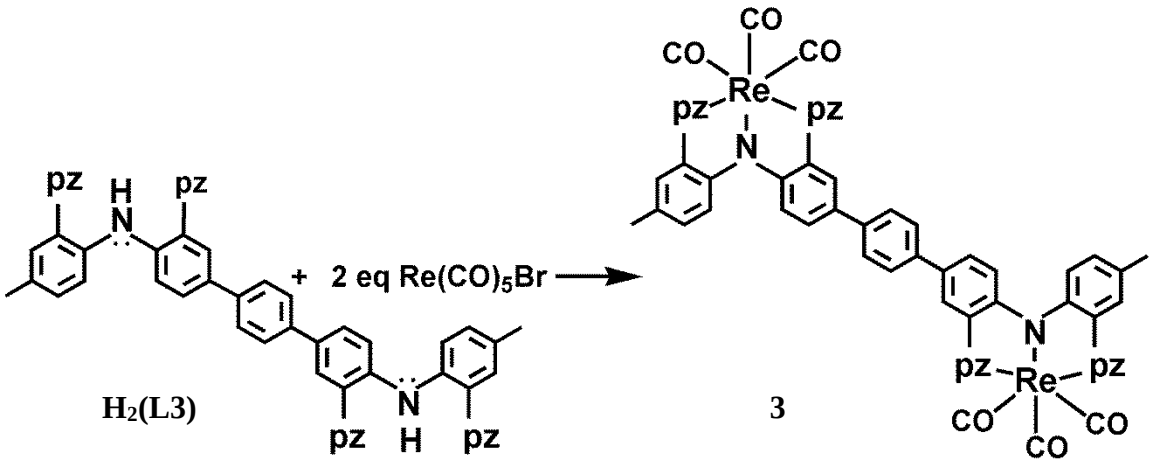

H_2(L3) **3**

$[Re(CO)_3]_2$(μ-L3), 3.

A mixture of 0.115 g (0.163 mmol) H_2(L3), 0.132 g (0.33 mmol, 2eq) $Re(CO)_5Br$ and 0.22 mL 1.47*M* (0.33 mmol) NEt_4OH in 10 mL toluene gave 0.121 g (60%) compound as a yellow powder. Mp, 330 ^{0}C (Decomposed). Anal. Calcd. (Found) for $Re_2C_{50}N_{10}H_{34}O_6$: C, 48.30 (48.66); H, 2.76 (2.95); N, 11.27 (11.10). IR(KBr) ν_{CO} 1876, 1901, 2013 cm^{-1}. ^{1}H NMR (DMF-d_7): δ_H 8.94 (dd, *J* = 2.7, 0.7 Hz, 2H, pz), 8.82 (dd, *J* = 2.4, 0.7 Hz, 2H, pz), 8.79 (br d, *J* = 2.6 Hz, 4H, pz), 8.16 (d, *J* = 6.2 Hz, 2H, Ar), 8.15 (s, 2H, Ar), 8.14 (d, *J* = 5.5 Hz, 2H, Ar), 8.04 (s, 4H, Ar), 7.87 (dd, *J* = 8.9, 2.2 Hz, 2H, Ar), 7.62 (d, *J* = 1.9 Hz, 2H, Ar), 7.48 (dd, *J* = 8.5, 1.8 Hz, 2H, Ar), 6.99 (t, *J* = 2.5Hz, 2H, pz), 6.92 (t, *J* = 2.5Hz, 2H,pz), 2.55 (s, 6H) ppm. UV-Vis λ_{max}, nm (ε, $M^{-1}cm^{-1}$), CH_2Cl_2: 403 (3737), 227 (5684).

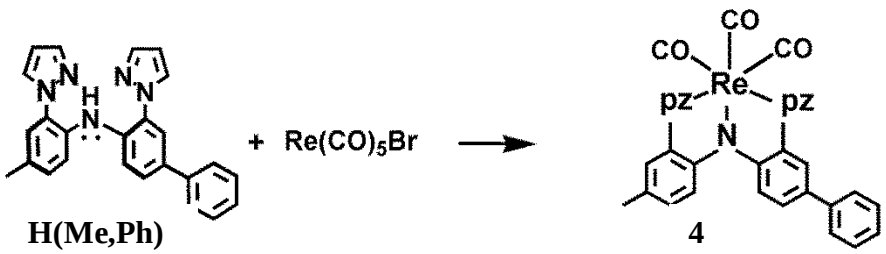

H(Me,Ph) **4**

[Re(CO)$_3$](L4), 4.

A mixture of 0.201 g (0.514 mmol) H(Me,Ph), 0.2087 g (0.514 mmol) $Re(CO)_5Br$ and 0.35 mL 1.47 *M* (0.514 mmol) NEt_4OH in 15 mL toluene was heated at reflux 12h. Toluene was evaporated in vacuum and the residue was washed with two 10 mL portions of methanol. The product was dried under vacuum to yield 0.252 g (74%) **4** as a yellow powder. Mp, 251-252 ^{0}C (Decomposed). Anal. Calcd. (Found) for $Re_2C_{50}N_{10}H_{34}O_6$: C, 50.90 (51.26); H, 3.05 (3.11); N, 10.60 (10.87). IR (KBr) ν_{CO} 1874, 1911, 2017. ^{1}H NMR (DMF-d_7): δ_H: 8.77 (d, *J* = 2.3 Hz, 1H, pz), 8.65 (d, *J* = 1.9 Hz, 1H, pz), 8.64-6.6 (m, 2H, pz), 8.00 (d, *J* = 6.7 Hz, 1H, Ar), 7.98 (d, *J* = 6.9 Hz, 1H, Ar), 7.94 (d, *J* = 2.0 Hz, 1H, Ar), 7.8 (d, *J* = 7.5 Hz, 2H, Ar), 7.65 (dd, *J* = 8.9, 2.0 Hz, 2H, Ar), 7.49-7.42 (m, 3H, Ar), 7.30 (t, *J* = 7.3 Hz, 2H, Ar), 6.82 (t, *J* = 2.4 Hz, 1H, pz), 6.76 (t, *J* = 2.4 Hz, 1H, pz), 2.38 (s, 3H) ppm. ^{1}H NMR (acetone-d_6): δ_H: 8.50 (d, *J* = 2.7 Hz, 1H, pz), 8.42 (d, *J* = 2.2 Hz, 1H, pz), 8.37(d, *J* = 2.5 Hz, 2H, pz), 7.96 (d, *J* = 4.8 Hz, 1H, Ar), 7.94 (d, *J* = 5.3 Hz, 1H, Ar), 7.78 (d, *J* = 2.2 Hz, 1H, Ar), 7.71 (br d, *J* = 7.4 Hz, 2H), 7.57 (dd, *J* = 8.8, 2.3 Hz, 1H, Ar), 7.44-7.38 (br t, 2H), 7.35 (d, *J* = 1.4 Hz, 1H, Ar), 7.29-7.24 (m, 2H, Ar), 6.72 (t, *J* = 2.5 Hz, 1H, pz), 6.52 (t, *J* = 2.5 Hz, 1H, pz), 2.37 (s, 3H) ppm. ^{13}C NMR (DMF-d_7): δ_C: 197.3, 195.9, 195.8, 147.8, 146.2, 144.6, 144.1, 139.9, 132.8, 132.2, 132.1, 129.8, 129.2, 129.1, 128.9, 128.7, 126.7, 126.1, 125.9, 124.8, 121.5, 121.3, 116.6, 108.43, 108.42, 20.0 ppm. ^{13}C NMR (acetone-d_6): δ_C: 197.5, 196.4, 196.1, 148.4, 147.0, 144.6,

144.1, 140.7, 132.8, 132.7, 132.2, 130.3, 129.8, 129.6, 129.5, 129.4, 127.1, 126.7, 126.5, 125.1, 122.3, 121.8, 117.2, 108.8, 108.7, 20.5 ppm.

Oxidation of Rhenium complexes

$[Re(CO)_3]_2(\mu$-L1$)(BF_4)_2$, 1$(BF_4)_2$.

In an argon filled drybox, a Schlenk flask was charged with 0.0298g (0.027 mmol) **1** and 0.0064 g (0.055 mmol, 2eq) $NOBF_4$. The flask with starting materials was taken out and attached to vacuum/Argon line. A 20 mL aliquot of argon-purged CH_2Cl_2 was added to reaction mixture, immediately giving a green color solution that turned to purple within 30 min stirring. The purple solution was stirred for two hours and solvent was evaporated by vacuum distillation. The residue was washed with two 10 mL portions of dry distilled Et_2O and dried to give 0.0297 g (86%) **1**$(BF_4)_2$ as a black/purple. Mp, > 350 ^{0}C dec. μ_{eff} (solid, 295 K) = 2.95 μ_B, IR (KBr) ν_{CO} 1897, 1920, 1955 cm^{-1}. UV-Vis (CH_2Cl_2): cm^{-1} (ε, M^{-1} cm^{-1}) 18749 (517), 29126 (713), 44334 (3014).

Except where noted, the following oxidized complexes were prepared in a similar manner where the stirring time, the amount of solvent and subsequent work-up procedure were identical to that described for the above complex. The amounts of non-oxidized rhenium complex and $NOBF_4$ varied in the preparation of each complex and given below along with the yield.

$[Re(CO)_3]_2(\mu$-L2$)(BF_4)_2$, 2$(BF_4)_2$.

A mixture of 0.0353g (0.030 mmol) **2** and 0.0071g (0.061 mmol) $NOBF_4$ yielded 0.0341g (84%) of **2**$(BF_4)_2$ as a blue/black solid. Mp, > 350 ^{0}C dec. μ_{eff} (solid, 295 K) =

2.86μ_B, IR (KBr) 1914, 1936, 2028 cm^{-1}. UV-Vis (CH_2Cl_2): cm^{-1} (ε, M^{-1} cm^{-1}) 15280 (45600), 18108 (31000), 44117 (230675).

$[Re(CO)_3]_2(\mu\text{-}L3)(BF_4)_2$, $3(BF_4)_2$.

A mixture of 0.0345g (0.0.028 mmol) **3** and 0.0065g (0.056 mmol) $NOBF_4$ yielded 0.0329g (84%) of **3**$(BF_4)_2$ as black solid. Mp, > 350 ^{0}C dec. μ_{eff} (solid, 295 K) = 2.68μ_B, IR (KBr) 1914, 1938, 2034 cm^{-1}. UV-Vis (CH_2Cl_2): cm^{-1} (ε, M^{-1} cm^{-1}) 12245 (149000), 44117 (54700).

$[Re(CO)_3](L4)(BF_4)$, $4(BF_4)$.

A mixture of 0.0343g (0.0.052 mmol) **4** and 0.0061g (0.052 mmol) $NOBF_4$ yielded 0.030g (77%) of **4**(BF_4) as a purple solid. Mp, > 350 ^{0}C dec. IR (KBr) 1906, 2033 cm^{-1}. UV-vis (CH_2Cl_2): nm (ε, M^{-1} cm^{-1}) 773 (1812), 627 (1165), 395 (5339).

$[Re(CO)_3]_2(\mu\text{-}L1)(BF_4)$, $1(BF_4)$.

Under an argon atmosphere, a green/brown solution of 0.0173 g (0.0159 mmol) of **1** and 0.0201 g (0.0159 mmol) of **1**$(BF_4)_2$ in 20 mL of CH_2Cl_2 was stirred for 2 h. Solvent was removed under vacuum and then was dried at room temperature under vacuum for 12h to leave 0.0312 g (83 %) of **1**$(BF_4)_2$ as a brown solid. Mp, > 350 ^{0}C, IR (KBr) ν_{CO} 1910 (br), 2021. UV-Vis (CH_2Cl_2): cm^{-1} (ε, M^{-1} cm^{-1}) 12026 (8010), 18255 (4080), 23746 (55022).

$[Re(CO)_3]_2(\mu\text{-}L2)(BF_4)$, $2(BF_4)$.

Under an argon atmosphere, green/brown solution of 0.0232 g (mmol) of **2** and 0.0266 g (mmol) of **2**$^{\cdot}(BF_4)_2$ in 20 mL of CH_2Cl_2 was stirred for 2 h. Solvent was removed under vacuum and then was dried further at room temperature under vacuum for 12h to leave

0.0361 g (72 %) of **2**$(BF_4)_2$ as a brown solid. Mp, > 350 ^{0}C, μ_{eff} (solid, 295 K) = 1.55μ_B, IR (KBr) ν_{CO} 1901 (broad), 2012. UV-Vis (CH_2Cl_2): cm^{-1} (ε, M^{-1} cm^{-1}) 7420 (44300), 8746 (24000), 14778 (3550), 18710 (35600), 27108 (7700).

$[Re(CO)_3]_2$(μ-L3)(BF_4), 3(BF_4).

Under an argon atmosphere, green/brown solution of o.0238 g (mmol) of **3** and 0.0271 g (mmol) of **3**$(BF_4)_2$ in 20 mL of CH_2Cl_2 was stirred for 2 h. Solvent was removed under vacuum and then was dried at room temperature under vacuum for 12h to leave 0.0401g (79 %) of **3**$(BF_4)_2$ as a brown solid. Mp, > 350 ^{0}C, μ_{eff} (solid, 295 K) = 1.49μ_B, IR (KBr) ν_{CO} 1892, 1920, 1940, 2021. UV-vis (CH_2Cl_2): cm^{-1} (ε, M^{-1} cm^{-1}) 4529(6440), 13025 (2110), 18255 (5720), 24590 (1870).

CHAPTER 5

COORDINATION POLYMERS AND METAL-ORGANIC FRAMEWORKS BASED ON REDOX-ACTIVE PINCER COMPLEXES

5.1. INTRODUCTION

Coordination polymers and 3D coordination polymers or metal-organic frameworks (MOFs) are currently attracting considerable attention because they are promising materials for many potential applications such as hydrogen storage, carbon capture, separation, and catalysts.[1-23] Mixed metal-organic frameworks (MMOFs) or mixed metal coordination polymers (MMCPs) are an interesting sub class of these materials, having two types of metal ions that may have both structural and functional roles in the network structure.[20,21] A useful strategy to MMOFs is self assembly of metalloligands (metal containing building blocks with divergent lewis donors) that can bind to a second metal (Figure 5.1).

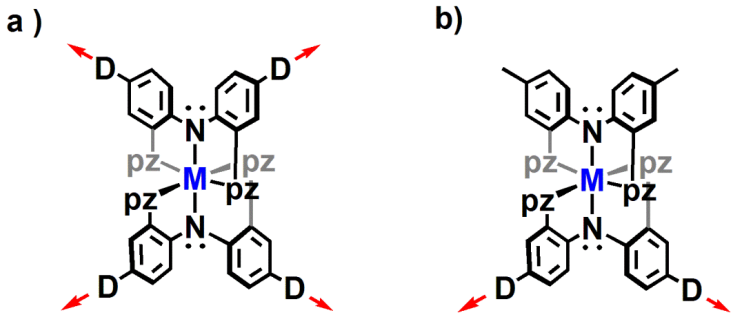

Figure 5.1. Metal containing building blocks with divergent lewis donors.

In this chapter, initial exploration to form coordination networks using either heteroleptic or homoleptic pincer complexes(Figure 5.1.a and b, respectively) is

described. The preparation of new ligands with carboxylate ester and pyridyl groups along with their discrete nickel(II) and rhodium(III) complexes is reported first. The successful approach along with challenges encountered. The use of these metallo ligands to prepare mixed metal polymers and networks is described.

5.2. RESULTS AND DISCUSSION

Four different pyrazolyl-containing pincer-type ligands with Lewis donors at the *para*- aryl positions were prepared since these 'bifunctional' derivatives can be envisioned to give high dimensional materials. The H(CN,CN) ligand was synthesized by the amination reaction between H(pzAn^{CN}) and Br-CNPhPz using CuI as the catalyst as described in a previous chapter. Similarly, the diester ligand, H(CO_2Et,CO_2Et), was prepared from the corresponding diarylamine as in the top of Scheme 5.1. The pyridine containing, H(4py,4py) and H(3py,3py) were synthesized by the Suzuki coupling reactions of H(Br,Br) ligand with 3- or 4-pyridine boronic acid respectively (the synthesis of H(py,py) is shown in the bottom of Scheme 5.1).

The self-assembly of the organic ligand H(CN,CN) with $AgPF_6$ was first explored. After a solution of H(CN,CN) in acetone was carefully layered with an acetone solution of $AgPF_6$ and solvents were allowed to diffuse, X-ray quality colorless needles formed within 1d. The single crystal X-ray structure (Figure 5.3) revealed that the crystals had a composition {Ag[H(CN,CN)]}(PF_6). The asymmetric unit contains two ligands, two silvers, one well-ordered and one disordered PF_6^- anion (top of Fig. 5.2).

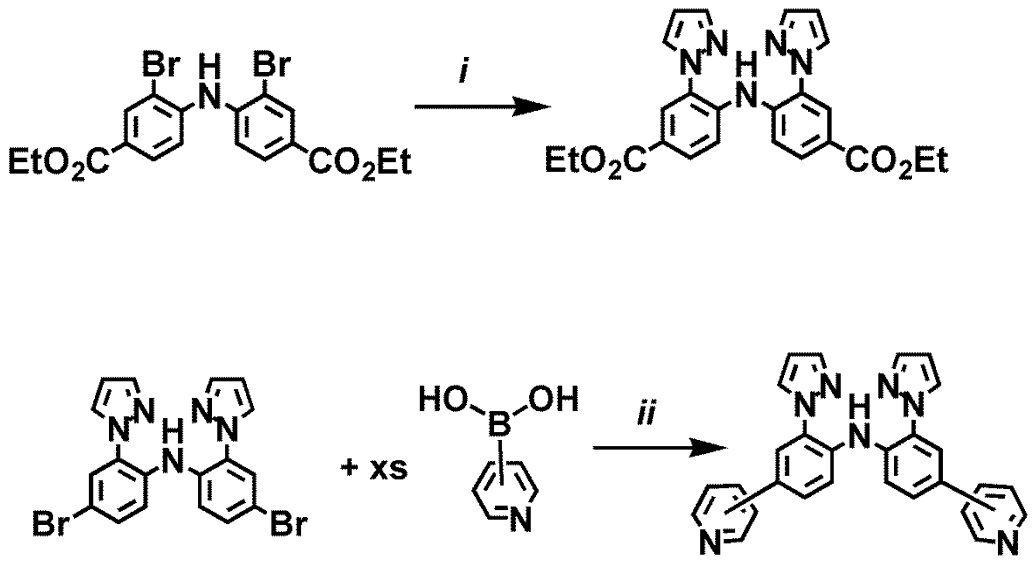

Scheme 5.1. Synthesis of $HN(CO_2Et,CO_2Et)_2$, HN(3py,3py) and HN(4py,4py). Key: ***i***) 3.5 eq K_2CO_2, 3.5 eq 1-H-Pyrazole, 10 mol% CuI, 40 mol% DMED ; *ii*) 20 mol% $Pd(PPh_3)_4$, 2 *M* Na_2CO_3, 30 mL C_6H_6, 10 mL EtOH, Δ 80^0C, 12H.

The coordination geometry about each silver is a distorted AgN_4 tetrahedron where the nitrogen atoms come from four different ligands. Two of these nitrogen atoms (N1 and N11) are from pyrazolyl groups while the other two (N3, N6) are from cyanophenyl groups (Middle left of Fig 5.2). Two Ag-Npz bonds are nearly same with average bond distance 2.342 Å (Ag-N1 and Ag-N11) other Ag-N(CN) bonds differ by 0.129 Å from each other (Ag-N3 = 2.223 Å and Ag-N6 = 2.352 Å). Each ligand binds four different silver centers in a unidentate manner, using two pyrazolyl nitrogen donors and the two nitrogens from the cyano groups to form a very distorted (μ_4-L)Ag_4

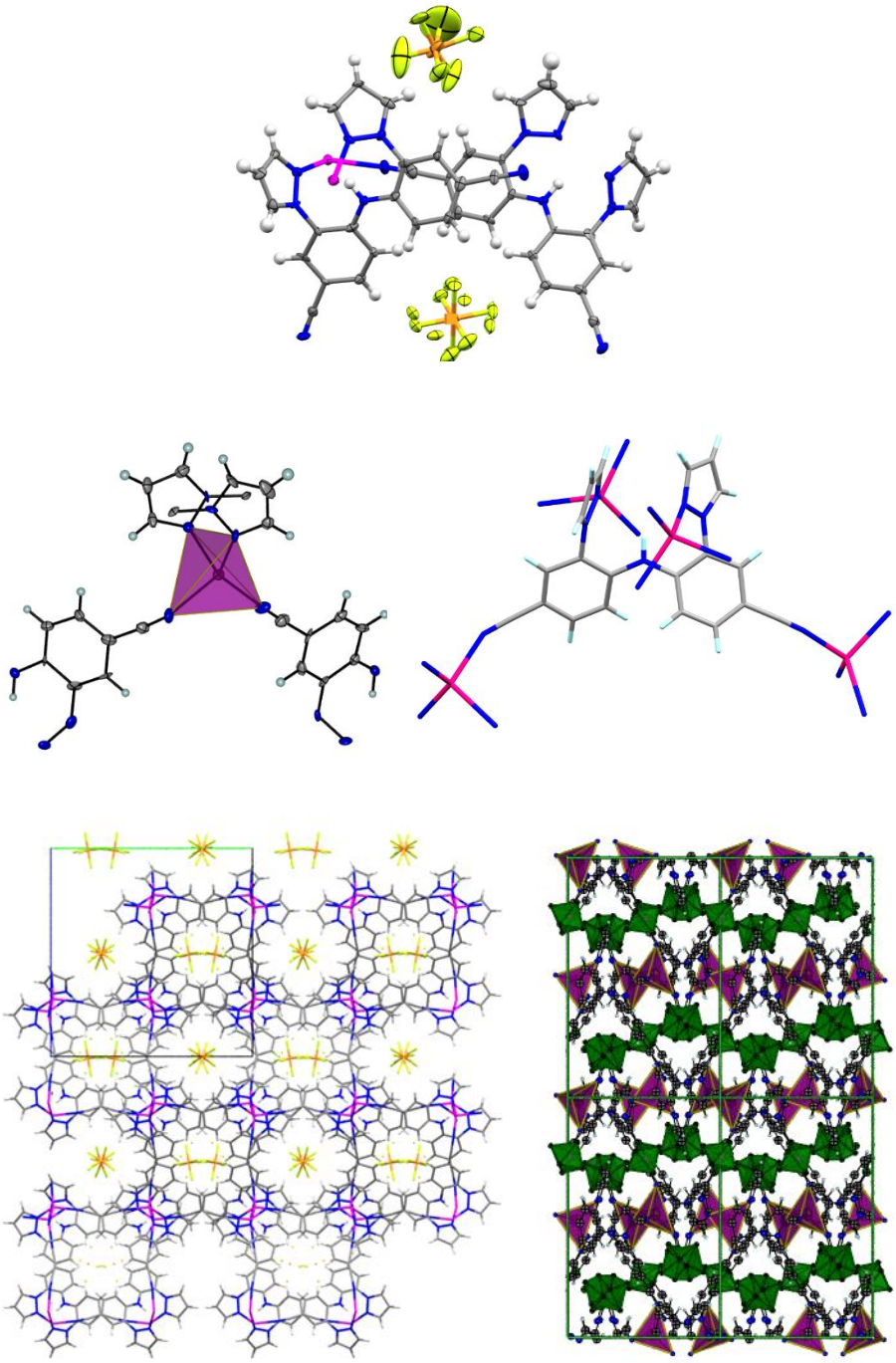

Figure 5.2. Top**:** Asymmetric unit of {Ag[H(CN,CN)]}(PF_6); Middle Left: View of coordination environment about silver. Middle Right: View of ligand environment. Bottom Left: View of 2x2x2 supercell with some PF_6 anions removed to show channels along *a*- direction. Bottom Right: View of 2x2x2 supercell down the *b*- axis where AgN_4 tetrahedra are shown in pink and PF_6 anions are shown as green octahedra.

tetrahedron (middle right of Fig. 5.2). As a result, a three-dimensional network is formed that has large channels along the *a*- direction that are filled with PF_6^- anions (Bottom left of Fig. 5.2).

The self-assembly of H(4py,4py) with $Zn(NO_3)_2$ was also studied. X-ray diffraction quality single crystals of $\{Zn[H(4py,4py)](NO_3)_2(DMSO)\}\cdot DMSO$ as yellow needles were obtained after a DMSO solution of H(4py,4py) ligand was layered with 1 equivalent of $Zn(NO_3)_2$ in ethanol and solvents were allowed diffuse slowly at room temperature over the course of 1 day. The asymmetric unit contains one zinc, one H(4py,4py) ligand, two nitrates and two DMSO molecules (Figure 5.3a). One of the nitrates is bound to zinc in a bidentate fashion (Zn-O4 2.254 Å, Zn-O5 2.267 Å) whereas the second nitrate is bound to zinc in a monodentate fashion (Zn-O1 2.107 Å). Also, one of the DMSO molecules is disordered over two nearby positions where each disorder component is bound to zinc(II) through the oxygen atom (Zn-O1 2.042 Å, Zn-O1a 2.334 Å). The second DMSO molecule is well-ordered but is a solvate molecule that is not bound to zinc. The coordination sphere of zinc is completed by binding to two pyridyl groups of two different ligands (Zn-N7 2.046 Å, Zn-N6 2.077 Å) thereby giving rise to a distorted ZnO_4N_2 octahedron (Figure 5.3b). Thus, the ligand bridges zinc centers binding the metals in a unidentate fashion through pyridyl groups (Figure 5.3c). As a result, a 1D coordination polymer is formed that propagates along the [101] direction. Two chains related by a 2_1 screw axis are stacked along the *b*- direction via a combination of π-π (Ct(Aryl)-Ct(aryl) 3.529 Å), CH···N, and CH···O interactions, as in Figure 5.3e. The polymers are connected in the third dimension by a longer and presumably weak CH···O interaction between a pyridyl hydrogen (*meta*- to the nitrogen) and an oxygen atom of the

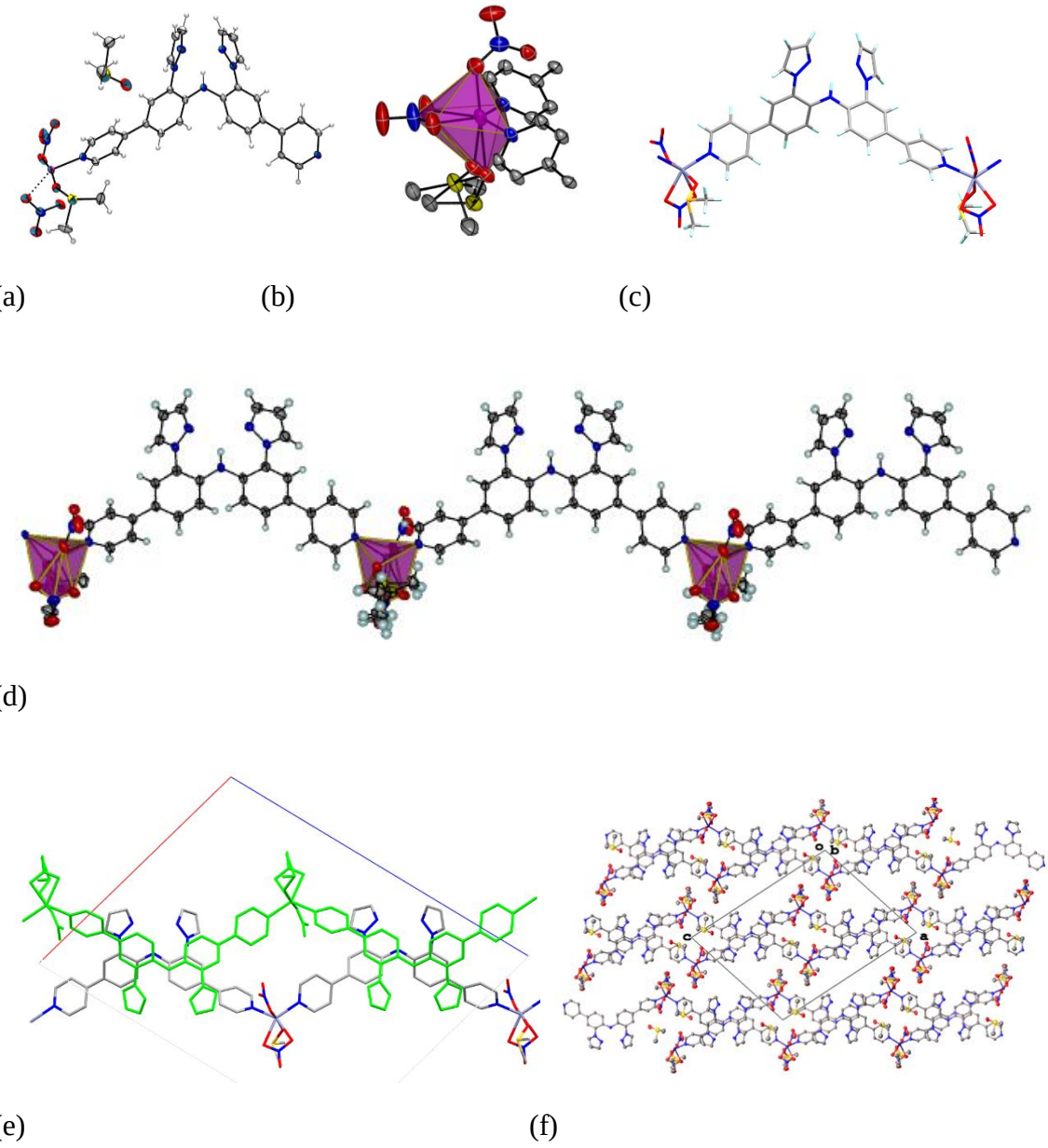

Figure 5.3 (a) Asymmetric unit of {Zn[H(4py,4py)]$(NO_3)_2$(DMSO)}·DMSO with one of the disordered Zn-bound DMSO molecules removed for clarity. (b) View of coordination sphere around zinc, with hydrogens removed. (c) View of local environment around ligand. (d) View down *b*-axis of one chain. (e) View down b-axis of two chains (f)View of molecular packing diagram down *b*-axis showing six neighboring chains.

nitrate that is bound in a bidentate manner to Zn (C11H11···O6, 2.558 Å, 125°). The result is a porous structure with channels along the *b*-direction that are filled with disordered and partially populated solvent molecules. These were excluded from the structure solution by using the SQUEEZE program. Attempts will be made by our group to determine the quantity of solvent by other means (elemental analyses, TGA, NMR) and to complete the characterization of the above two compounds during future (repeated) preparations of the compounds in our lab.

In an effort to determine whether a metalloligand approach is viable for the newly prepared bifunctional pincer ligands, attempts were made to first prepare homoleptic $Ni(X,X)_2$ complexes. At the outset, was not known if the strong donor properties of pyridyl groups, for instance, would interfere with our previously described synthetic route to the nickel derivatives. Gratifyingly, the one-pot reaction between $NiCl_2 \cdot 6H_2O$ and two mol equivalents of each of four H(X,X) ligands and $(NEt_4)(OH)$ in MeOH afforded high yields of the desired nickel complexes (Scheme 5.2). The structures of $Ni(3py,3py)_2$ and $Ni(CO_2Et,CO_2Et)_2$ were determined by single crystal X-ray diffraction and views of the complexes are given in Figure 5.4. As with the previous $Ni(X,Y)_2$ complexes, the metal center resides in a compressed NiN_6 octahedron where the average Ni-N_{Ar} distance (2.052 Å in $Ni(3py,3py)_2$ and 2.054 Å in $Ni(CO_2Et,CO_2Et)_2$) is shorter than the average Ni-Npz distance (2.089 Å in $Ni(3py,3py)_2$ and 2.064 Å in $Ni(CO_2Et,CO_2Et)_2$). The physical, electrochemical, and spectroscopic properties of these derivatives are in accord with other complexes of this type (Table 5.1 and 5.2). It is noted that the compound $Ni(CO_2Et,CO_2Et)_2$ was prepared because this species is anticipated to be a useful precursor to the carboxylic acid $Ni(CO_2H,CO_2H)_2$ or the tetracarboxylate

tetraanion. These latter species may either be obtained directly by hydrolysis or could be formed in-situ via solvothermal reactions during the preparation of MOFs. A preliminary reaction (Scheme 5.3) of $Ni(CO_2Et,CO_2Et)_2$ with excess KOH in a THF:MeOH mixture resulted in the precipitation of an orange solid that was insoluble in all organic solvents but was soluble in water.

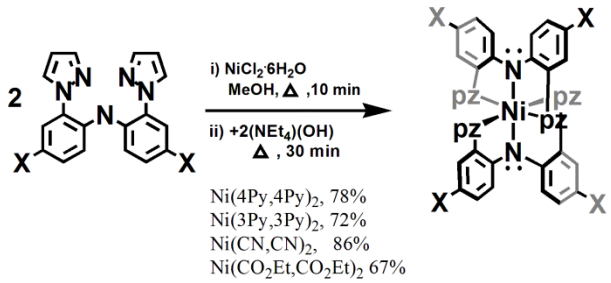

Scheme 5.2. Preparation of $Ni(X,X)_2$ complexes.

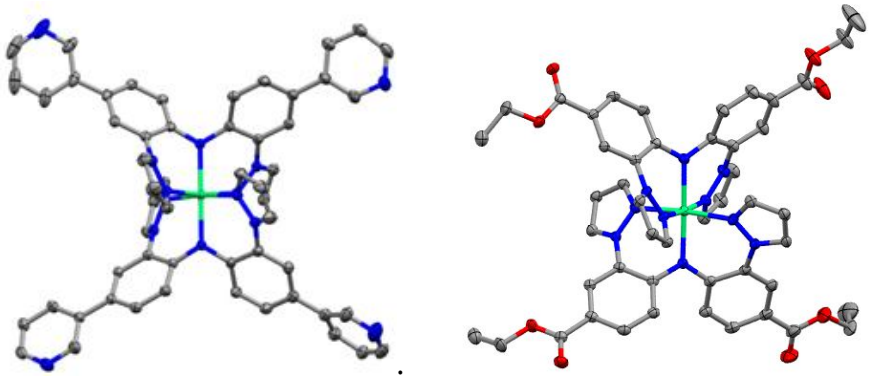

Figure 5.4. X-ray structures of $Ni(3py,3py)_2$ (Left) and $Ni(CO_2Et,CO_2Et)_2$ (Right).

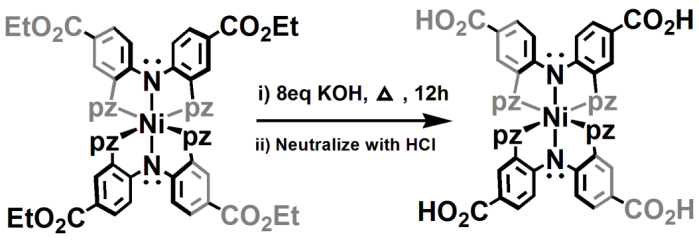

Scheme 5.3. Preparation of carboxylate derivative from $Ni(CO_2Et,CO_2Et)_2$.

Table 5.1. Electrochemical data from cyclic voltammetry experiments of $Ni(3py,3py)_2$, $Ni(4py,4py)_2$ and $Ni(CO_2Et,CO_2Et)_2$ with other Ni complexes of Chapter 2.

	$E^{o'}$, V vs Ag/AgCl[a]	
Compound	$E_{1/2,ox1}$/ V	$E_{1/2,ox2}$ / mV
$Ni(Me,Me)_2$	0.146 (188)	0.428 (187)
$Ni(Me,H)_2$,	0.257 (154)	0.536 (156)
$Ni(H,H)_2$,	0.311 (187)	0.604 (192)
$Ni(Me,Br)_2$,	0.318 (163)	0.582 (165)
$Ni(Me,CO_2Et)_2$	0.409 (230)	0.656 (208)
$Ni(Me,CF_3)_2$	0.464 (174)	0.724 (173)
$Ni(Br,Br)_2$	0.500 (161)	0.751 (153)
$Ni(Me,CN)_2$	0.584 (175)	0.810 (176)
$Ni(CF_3,CF_3)_2$	0.763 (170)	1.019 (168)
$Ni(CN,CN)_2$	0.882 (232)	1.085 (208)
$Ni(^{tBu}Ph,^{tBu}Ph)$	0.274 (136)	0.524 (138)
$Ni(^{CN}Ph,^{CN}Ph)_2$,	0.455 (153)	0.657 (151)
$Ni(3py,3py)_2$	**0.354 (129)**	**0.569 (133)**
$Ni(4py,4py)_2$	**0.502 (213)**	**0.701(215)**
$Ni(CO_2Et,CO_2Et)_2$	**0.695 (226)**	**0.927 (145)**
Ferrocene	0.522 (180)	---

[a]Average values obtained for scan rates of 50, 100, 200, 300, 400, and 500 mV/s with 0.1 *M* NBu_4PF_6 as supporting electrolyte in CH_2Cl_2.

Table 5.2. Elecronic absorption data of lowest energy d-d spectra of $Ni(X,Y)_2$ complexes in CH_2Cl_2.

Compound	$\bar{\upsilon}$, cm^{-1} (ε, $M^{-1}cm^{-1}$)
	$^3A_{2g} \rightarrow {}^3T_{2g}$
$Ni(Me,Me)_2$	11,470 (120)
$Ni(Me, H)_2$	11,520 (110)
$Ni(H, H)_2$	11,510 (110)
$Ni(Me, Br)_2$	11,490 (120)
$Ni(Me,CO_2Et)_2$	11,640 (150)
$Ni(Me,CF_3)_2$	11,500 (120)
$Ni(Br,Br)_2$	11,480 (140)
$Ni(Me,CN)_2$	11,590 (195)
$Ni(CF_3,CF_3)_2$	11,640 (120)
$Ni(CN,CN)_2$	**11,600 (170)**
$Ni(3py,3py)_2$	**11,862 (310)**
$Ni(4py,4py)_2$	**11,890 (159)**
$Ni(CO_2Et,CO_2Et)_2$	**11,919 (272)**

An inspection of experimental and calculated structures of various $Ni(X,Y)_2$ derivatives reveals that these compounds may provide ideal platforms for the construction of three-dimensional solids. For instance, if donor groups are attached to para-aryl positions (Figure 5.5) they would be essentially aligned in one plane and could afford connectivity in two dimensions. The addition of donor groups at the 4-pyrazolyl positions would afford connectivity in the third dimension (right of Fig. 5.5). Greater structural diversity may be expected if donor groups are located at other positions such as shown in Figure 5.6 for Ni(3py,3py).

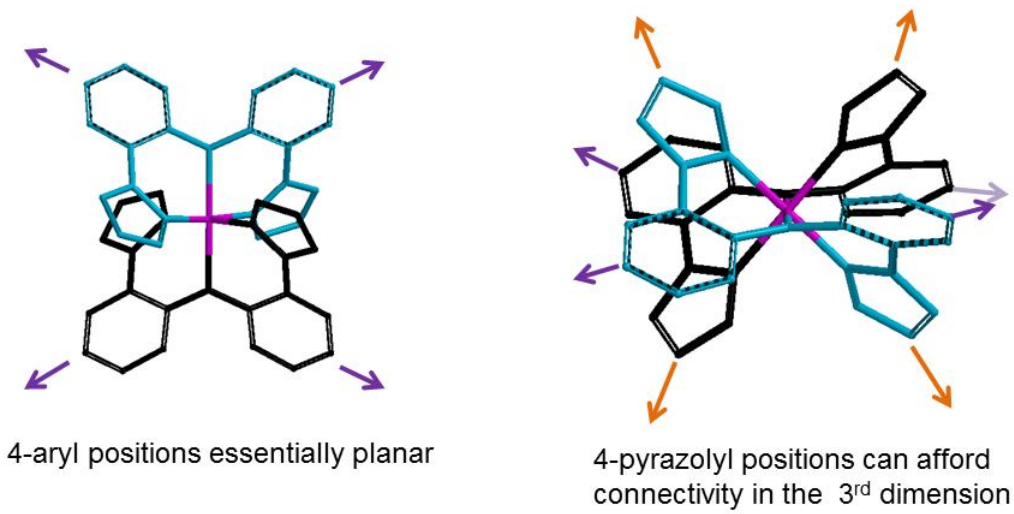

Figure 5.5. View of a model $Ni(X,Y)_2$ complex showing relative disposition of para-aryl and 4-pyrazolyl groups.

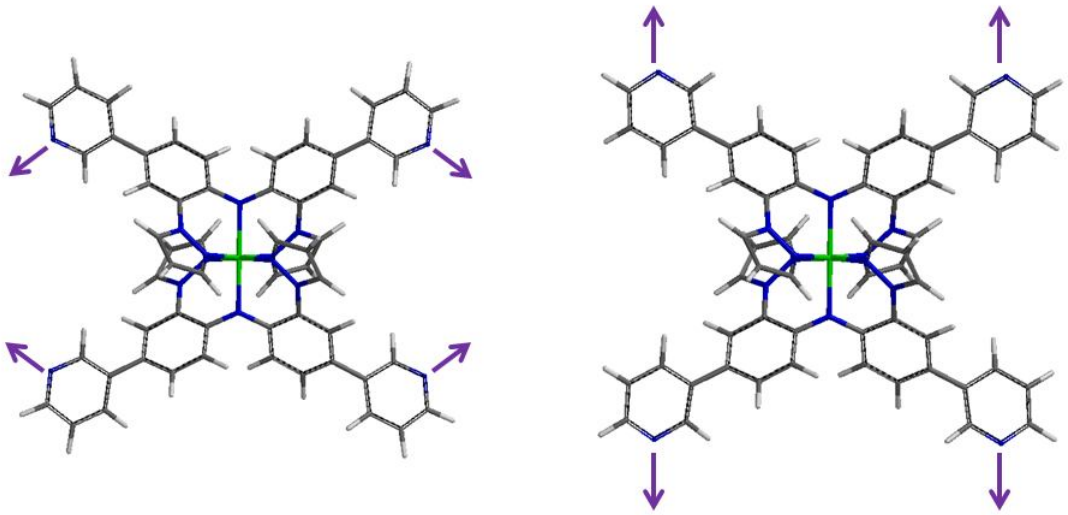

Figure 5.6. Two possible conformers of $Ni(3py,3py)_2$ illustrating potential connectivity patterns.

Based on this idea, initial attempts were made to prepare MMCPs and MMOFs by layering solutions of the $Ni(CN,CN)_2$ metalloligand with solutions of silver(I) salts. In each of the cases described below, large crystals (minimum dimension 0.5 mm per side)

were obtained in numerous attempts under different crystallization conditions (solvents, anions, temperature, stoichiometry, concentration) but none of the crystals diffracted at high angles and all also exhibited twinning and disorder. Thus, the diffraction data were only of sufficient quality to establish connectivity but not metrical parameters. Future efforts will be directed at growing well-behaved (nicely diffracting) crystals by changing donor groups, metals, trying new solvent combinations, and adding substituents to the pyrazolyl to promote better packing. Regardless, a description of findings for the current system is given below. The structure of the crystals obtained by layering THF solutions of $Ni(CN,CN)_2$ and $AgBF_4$ and allowing solvents to diffuse shows layers of 4,4-connected nets (Figure 5.7).

The cationic sheets of $(\{Ag[Ni(CN,CN)_2]\}^+)_n$ are stacked on top of each other, presumably by van der Waals interactions, and give channels along the *b*- direction that are filled with anions as well as disordered (partially populated) solvent. On the other hand, the structure determined from crystals obtained after layering equimolar solutions of $Ni(CN,CN)_2$ and AgOTf (and allowing solvents to diffuse) showed two identical interpenetrating three-dimensional 4,4-networks where bridging triflate aions afforded connectivity in the third dimension of each network. A view of one of the two interpenetrating networks of $\{Ag(OTf)[Ni(CN,CN)_2]\}$ is given on the left of in Figure 5.8. The second similar network fills the void-space of the first network.

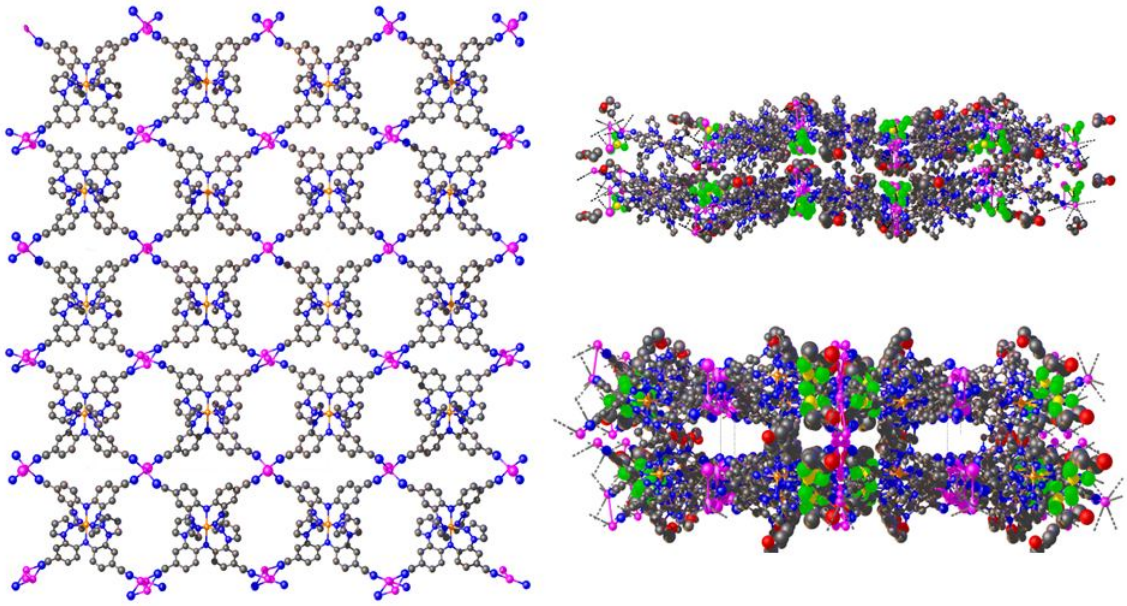

Figure 5.7. Views of the sheet structure in $[Ni(CN,CN)_2](AgBF_4)\cdot xTHF$.

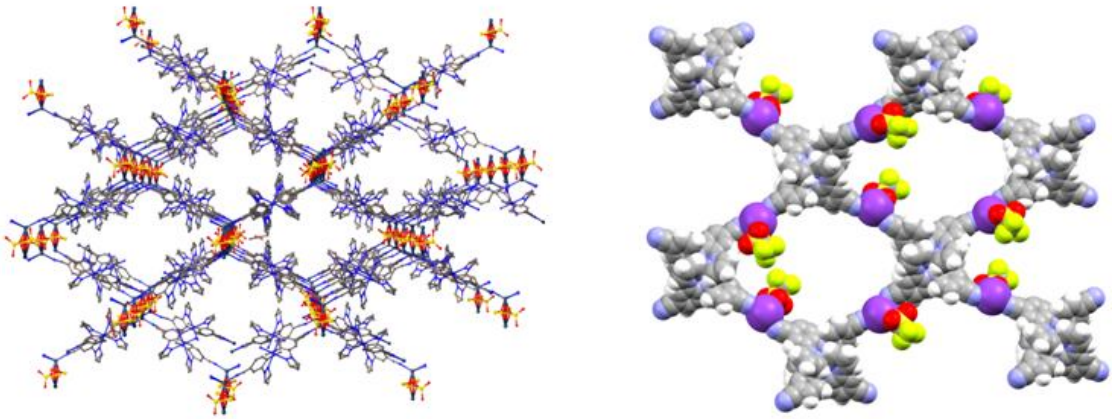

Figure 5.8. View of one part of the interpenetrating 3D network in $Ag(OTf)[Ni(CN,CN)_2]$.

Although we obtained large crystals in each case, we could not get the complete X-ray diffraction data to establish the structure. It suffered either disordered structure or did not diffract at higher angles. These homoleptic metal complexes have D_2 symmetry

and hence are chiral (Figure 5.9). Unsuccessful X-ray crystallographic refinements indicated that both isomers are superimposed at the same site. This disorder combined with disorder in solvents and anions positions lead to the difficulties in structural solutions. Attempts were made to obtain coordination polymer of silver with nickel complexes of 4-pyridyl and 3-pyridyl derivatives. DMF solution of nickel complexes were layered on top of the DMF solution of silver salts in order to get crystals. But it resulted in silver metal instead of coordination polymers. The electron rich nickel complex has reduced silver(I) to silver metal. Therefore, charge neutral nickel pyridyl complexes are not good precursors to prepare MMOFs with silver salts. Differences in solubility of charge neutral $Ni(X,Y)_2$ complexes and metal salts also provides difficulties in obtaining MMOFs. Metal salts tend to be are insoluble in solvents for $Ni(X,Y)_2$ and vice versa. There were very limited choice for solvents, and often solvates of starting materials rather than desired products were obtained.

Good success has been achieved using heteroleptic rhodium(III) pincers. The $[Rh(Me,Me)(4py,4py)(PF_6)$ was synthesized according to Scheme 5.4. The H(4py,4py) ligand was reacted with equal molar amount of previously reported $(NEt_4)[Rh(Me,Me)Cl_3]\cdot H_2O$ [25] in acetonitrile, followed by three equivalents of $TlPF_6$ and one equivalent of base, NEt_4OH.

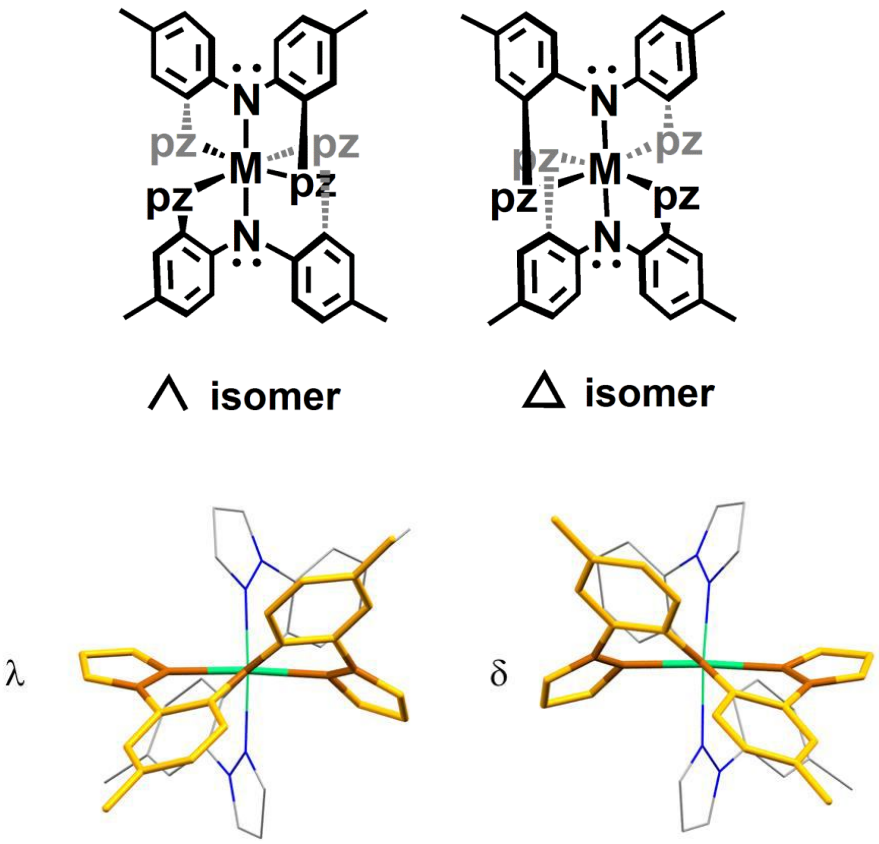

Figure 5.9. Stereo isomers of $M(MeMe)_2$ complex.

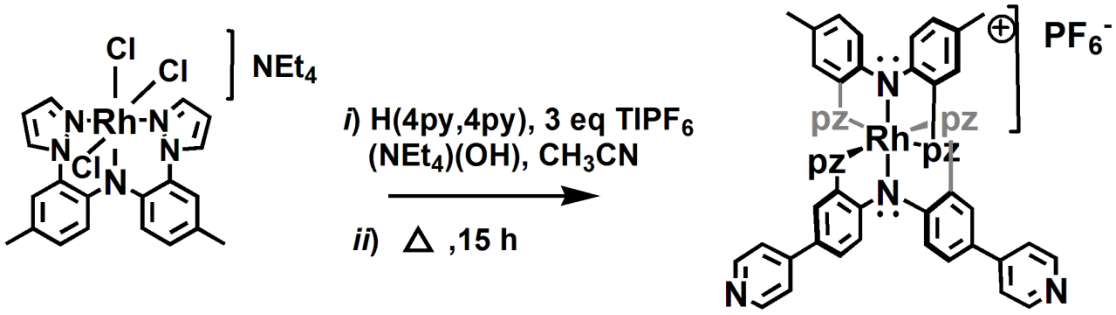

Scheme 5.4. Synthesis of $Rh(Me,Me)(4py,4py)(PF_6)$

The X-ray quality crystals of $[Rh(Me,Me)(4py,4py)][Zn(DMSO)_4](NO_3)_2$ as orange needles were obtained after a DMSO solution of $[Rh(Me,Me)(4py,4py)](PF_6)$

complex was layered with one molar equivalent of $Zn(NO_3)_2$ in ethanol and solvents were allowed diffuse slowly at room temperature for 7 days. This complex is a heterometallic coordination polymer. The asymmetric unit contains one rhodium complex, one zinc, four DMSO, and two nitrate ions (Figure 5.10). Rhodium has an octahedral RhN_6 geometry with nearly identical two Rh-N_{Ar} bonds and four Rh-N_{pz} bonds (avg. 2.032 (4) Å) and four Rh-N_{pz} bonds (avg. 2.016 (3) Å). The N_{Ar}-Rh-N_{Ar} bond is linear and two C-N_{Ar}-C planes are parallel to each other. The zinc center has an octahedral geometry, being bound to two 4-pyridyl nitrogens (from two rhodium complexes) and to four oxygen atoms from DMSO molecules. The *trans*-Zn-N bond distances (2.109(4)) Å are identical.

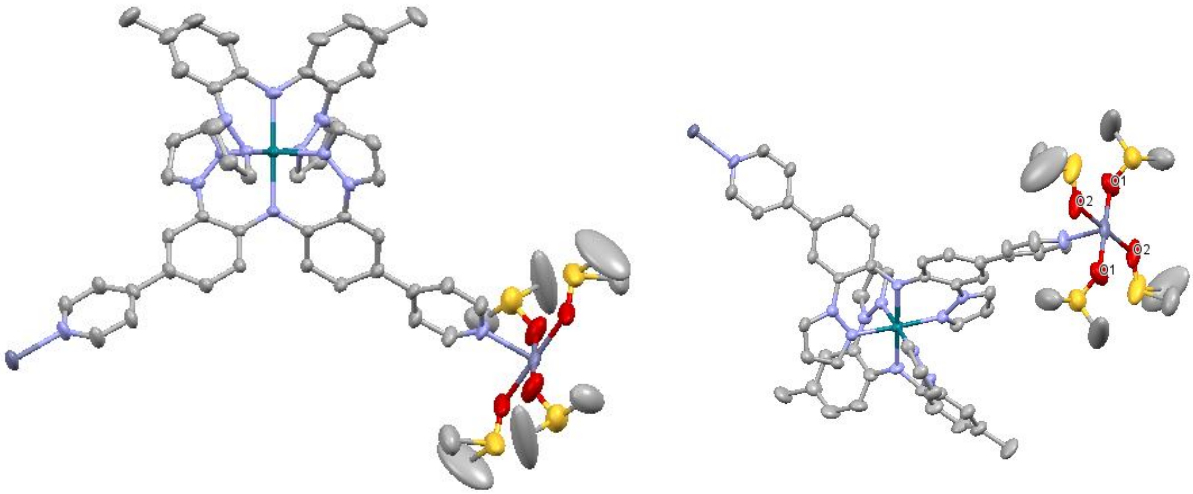

Figure 5.10. Asymmetric unit of [Rh(Me,Me)(4py,4py)][Zn(DMSO)$_4$](NO_3)$_2$.

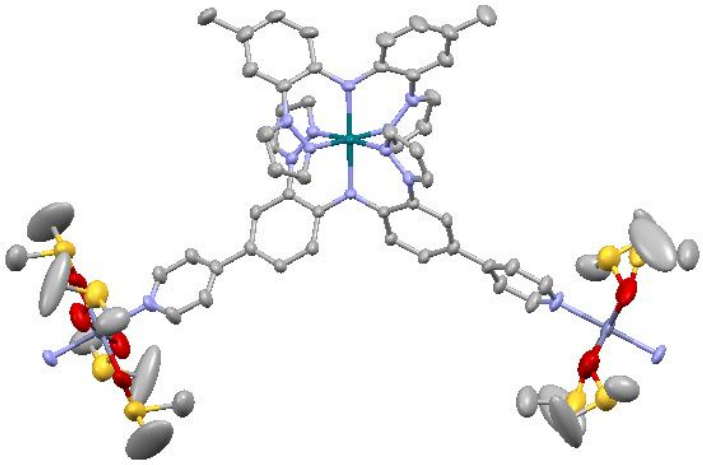

Figure 5.11. View of the local environment around the rhodium complex.

(a)

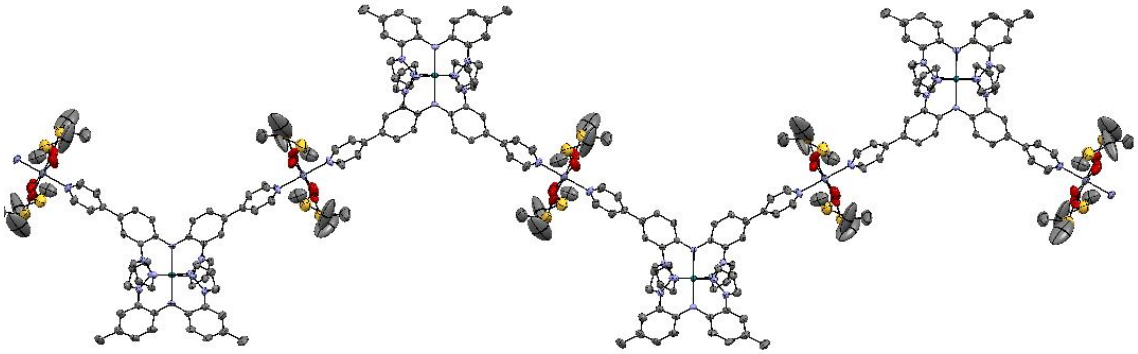

(b)

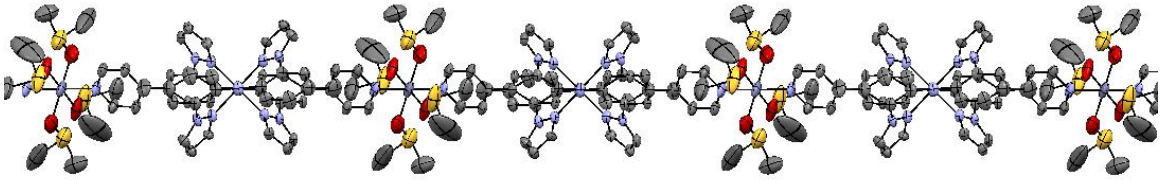

Figure 5.12. Views of the propagation of the coordination chain along b-direction.

Trans Zn-O bonds of four Zn-O bonds are similar to each other. Zn-O1 bonds (Zn-O1, Figure 5.10) bonds have 2.190(8) Å bond distances, while Zn-O2 bonds have 2.103(5) Å. Thus, the rhodium complexes bridge zinc centers to give a zigzag chain, which propagates along the *b*-axis (Figure 5.12). The crystal packing of this coordination polymer is shown in Figure 5.13. The hydrogen atoms of exo-methyl groups of rhodium complex have weak interactions with both oxygens of DMSO and π-cloud of pyridine rings. These CH···π and CH···O weak interactions help assemble neighbor chains in to a sheet structure Figure 5.13.

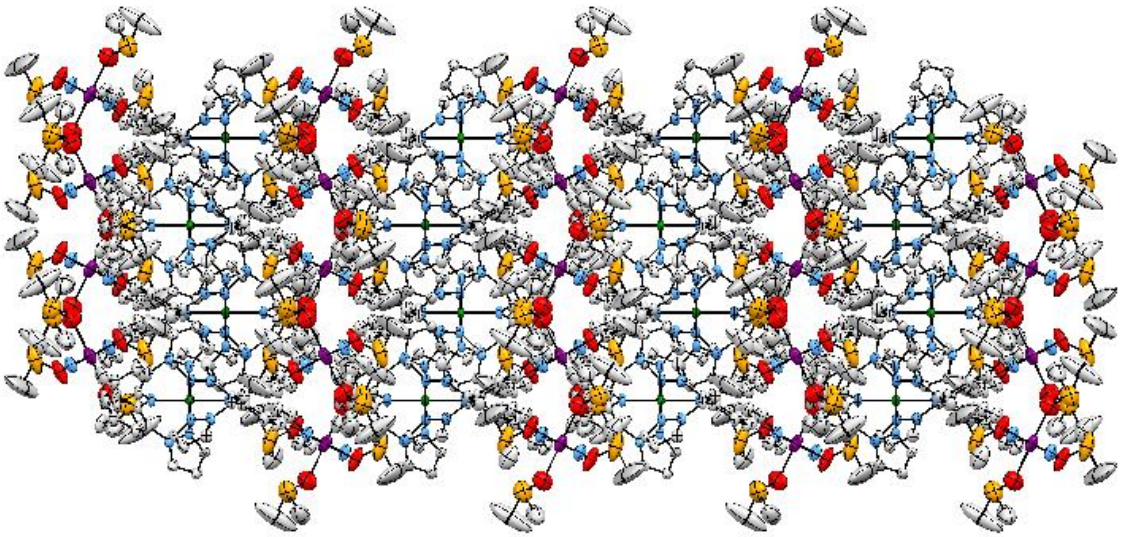

Figure 5.13. Crystal packing of [Rh(Me,Me)(4py,4py)][Zn(DMSO)$_4$](NO$_3$)$_2$.

5.3. FUTURE DIRECTIONS

Initial attempts to make MMOFs and MMCPs posed unexpected challenges, but these also lead to promising results. Although layering of solution of $Ni(X,X)_2$ (X is a lewis donor) and some metal salts produce large crystals (~ 1 mm) that appeared single to the naked eye, attempts of diffraction revealed that they were poorly diffracting, twinning, disordered, or all of above. If one can make coordination polymers by separating the enantiomers, it may solve one source of disorder.

The charge neutral nickel(II) complexes are insoluble in most of the polar solvents, but most of the metal salts are soluble in polar solvents. If one can make ionic metallo-ligands instead of charge neutral nickel complexes, it would answer the solubility issue. Furthermore, silver(I) salts might not be a good choice to make MMOF with this electron-rich complexes, because the DMF solution of $Ni(4py,4py)_2$ resulted in Ag metal instead of a silver bound coordination polymer. Mono-cationic $[Rh(Me,Me)(4py,4py)](PF_6)$ made successful 1D coordination polymer with redox silent Zn^{2+}. Therefore zinc salt might be a good source to make 2D or 3D coordination polymers with electron rich-metalloligands.

Furthermore, if one modifies these ligands by substituting other donor groups in 4-pyrazolyl positions, donor capability of these ligands would be extended. Instead of sticking on central metal, nickel, further approaches of various metals for these metalloligands could be investigated. It would resolve the solubility issue and reduce the power of this electron-rich nature of charge neutral nickel complexes. One can expand this scope further designing of new ligands with different donors. It is possible to make

fixed donor groups on *para*-aryl positions as shown in Figure 5.14.b-c. It will shorten the contacts of metal centers, resulting in MMOFs with higher conductivity compared to longer contacts. Proposed pincer ligands are shown is Figure 5.14.

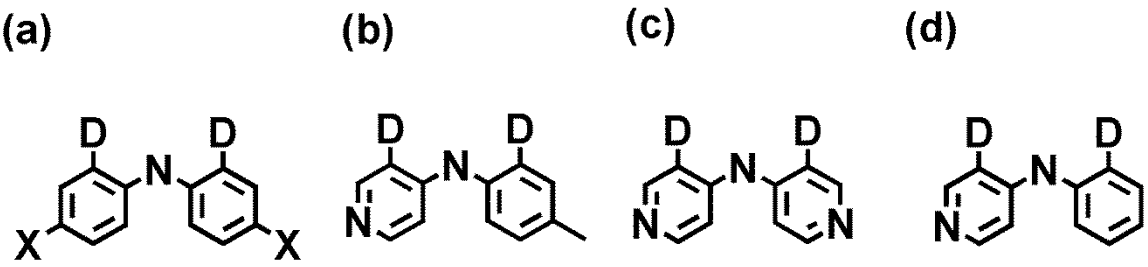

Figure 5.14. Proposed pincer type ligands for future MOFs. D is a donor group (pz, PPh_2, SCH_3,O^-, OCH_3…etc).

The ultimate goal of this project is to make conductive MMOFs or MMCPs. Therefore conductivity measurements of synthesized polymers should be measured. It can be achieved by growing these CPs on indium tin oxide (ITO) or fluorine doped tin oxide (FTO) plates. The bulk conductivity of powder can be measured using the four probe method.

5.4. EXPERIMENTAL

Materials. CuI, anhydrous Na_2CO_3, Cs_2CO_3, $Zn(NO_3)_2$, 3-pyridine boronic acid, 4-pyridine boronic acid, Ethyl 4-iodobenzoate, Ethyl 4-aminobenzoate were purchased from commercial sources and used without further purification. The compounds $Pd(PPh_3)_4$,[24] $HN(CO_2Et)_2$, $(NEt_4)[Rh(Me,Me)Cl_3]\cdot H_2O$[25] were prepared by literature methods. Solvents used in the preparations were dried by conventional methods and were distilled under nitrogen prior to use.

Physical measurements. ^{1}H, ^{13}C and ^{31}P NMR spectra were recorded on a Varian 400 MHz spectrometer. Chemical shifts were referenced to solvent resonances at δ_H 7.26 and δ_C 77.16 for $CDCl_3$, δ_H 5.32 and δ_C 53.84 for CD_2Cl_2, δ_H 2.05 and δ_C 29.84 for acetone-d_6. Melting point determinations were made on samples contained in glass capillaries using an Electrothermal 9100 apparatus and are uncorrected.

Ligand Precursor Synthes

HN(2-Br-4 –$C_6H_4CO_2Et)_2$

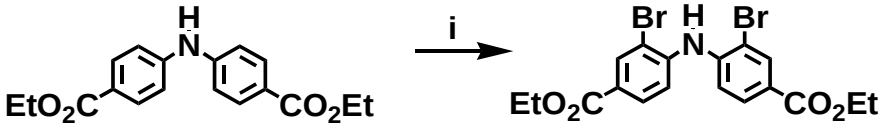

i) 2 eq N-Bromosuccinimide, CH_3CN, 0^oC

A solution of 0.575g (3.23 mmol, 2 eq) N-Bromosuccinimide dissolved in 30 mL of CH_3CN was added dropwise (1 mL/min) to a cold (0 ^{0}C), magnetically stirred solution of 0.5058g (1.61 mmol) Benzoic acid, 4,4'-iminobis-, diethyl ester in 20 mL CH_3CN. After complete addition, the white precipitate was isolated by filtration to give 0.646g (85%) of the desired product. Mp: 158-159 ^{0}C. ^{1}H NMR ($CDCl_3$): δ_H 8.29 (s, 2H, Ar), 7.94 (d, *J* = 8.4Hz, 2H, Ar), 7.40 (d, *J* = 8.5 Hz, 2H, Ar), 7.05 (s, 1H, NH), 4.37 (q, *J* = 7.1 Hz, 4H, CH_2), 1.40 (t, *J* = 7.0 Hz, 6H, CH_3). ^{13}C NMR ($CDCl_3$): δ_C 165.2, 142.7, 134.9, 130.1, 125.1, 116.4, 113.6, 61.3, 14.4.

Ligand Synthesis

H(CN,CN)

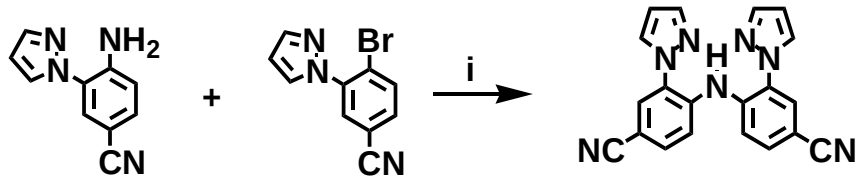

i)1.2 eq Cs_2CO_3, 20 mol% CuI, Dioxane, Δ 15h

A Schlenk flask charged with 0.755 g (4.10 mmol) H(pzAn^{CN}), 1.017 g (4.10 mmol) Br-CNPhPz, 1.603 g (4.92 mmol) Cs_2CO_3 was deoxygenated by three evacuation and argon back-fill cycles. Next, 15 mL of argon-purged, dry dioxane was added by syringe and then 0.156 g (0.820 mmol) CuI was added under an argon blanket. After the reaction mixture had been heated at reflux 15 h under argon, it was cooled to room temperature and dioxane was removed by vacuum distillation. The resulting solid was dissolved in a biphasic mixture of 50 mL H_2O and 50 mL ethyl acetate. The aqueous and organic fractions were separated. The aqueous fraction was extracted with three 30 mL portions ethyl acetate. The combined organic fractions were dried over $MgSO_4$, filtered and volatiles were removed under vacuum with the aid of a rotary evaporator. The resulting brown oil was subjected to column chromatography on silica gel using 1:1 ethyl acetate:hexanes as the eluent. The desired product was obtained as a yellowish solid after removing solvent from the second band (R_f = 0.37). Recrystallization by cooling a boiling absolute ethanol solution to room temperature over the course of hours and then to -30 ^{o}C overnight afforded 0.72 g (50%) of H(CN,CN) as pale yellow crystals. Mp: 178-180 ^{o}C. ^{1}H NMR ($CDCl_3$): δ_H 10.32 (s, 1 H, NH), 7.79 (d, J = 1.9 Hz, 2 H, H_3pz),

7.77 (d, *J* = 2.5 Hz, H_5pz), 7.64 (d, *J* = 1.6 Hz, 2 H, Ar), 7.56 (s, 2 H, Ar), 7.55 (d, *J* = 1.6 Hz, Ar), 6.55 (dd, *J* = 2.5, 1.9 Hz, 2 H, H_4pz). ^{13}C NMR ($CDCl_3$): δ_C 141.8, 139.5, 132.2, 130.5, 130.1, 128.8, 118.9, 118.3, 108.1, 104.9. IR (KBr) ν_{CN} 2226 cm^{-1}.

H(3py,3py)

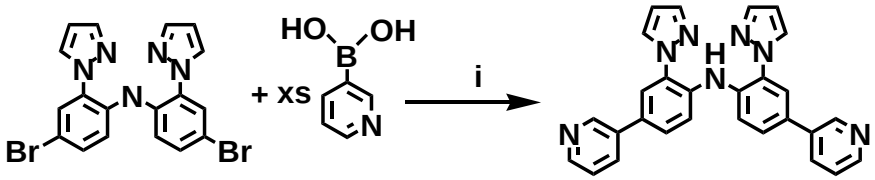

i) 20 mol% $Pd(PPh_3)_4$, 2 *M* Na_2CO_3, 30 mL C_6H_6, 10 mL EtOH, Δ 80^{0}C, 12H

In an argon-filled dry box, a Schlenk flask was charged with 0.707g (1.54 mmol) H(Br,Br), 0.568g (4.62 mmol) pyridine 3-boronic acid, and 0.356g (0.308 mmol) $Pd(PPh_3)_4$. The flask was removed from the drybox and attached to a Schlenk line. A solution of 30 mL C_6H_6 and 10 mL absolute ethanol was purged with argon 15 min and was transferred to the reaction flask under argon via cannula. Next, 10 mL of an argon-purged 2 *M* aqueous Na_2CO_3 solution was transferred via cannula to the reaction flask. After the magnetically-stirred biphasic mixture had been heated at 80 ^{0}C for 16 h with the aid of an external oil bath, the mixture was cooled to room temperature and poured into 100 mL H_2O. The aqueous and organic fractions were separated. The aqueous layer was extracted with two 50 mL portions ethyl acetate. The combined organic layers were dried over $MgSO_4$ and filtered. The oily residue that was obtained after removing solvents under vacuum was subjected to column chromatography on silica gel using 2 :1 ethyl acetate : hexanes to remove first two spots and then used 10:1 ethyl acetate : methanol as an eluent to obtain desired product (0.589 g , 84%) H(3py,3py) as a colorless solid after

removing solvents and drying under vacuum 1 h. Mp: 59-60 ^{0}C. ^{1}H NMR ($CDCl_3$): δ_H 9.12 (s, 1H, NH), 8.86 (d, *J* = 1.8Hz, 2H, H_5pz), 8.58 (dd, *J* = 4.8, 1.4 Hz, 2H, Ar), 7.87 (dt, *J* = 7.9 , 2.3 Hz, 2H, Ar), 7.82 (dd, *J* = 2.4, 0.5 Hz, 2H, Ar), 7.78 (dd, *J* = 1.9, 0.5 Hz, 2H, Ar), 7.63 (d, *J* = 8.5Hz, 2H, Ar), 7.59 (d, *J* = 2.1 Hz, 2H, H_3pz), 7.51 (dd, *J* = 8.4, 2.2 Hz, 2H, Ar), 7.37 (dd, *J* = 8.2, 5.0 Hz, 2H, Ar), 6.51 (t, *J* = 2.4 Hz, 2H, H_4pz). ^{13}C NMR ($CDCl_3$): δ_C 148.5, 147.9, 141.2, 136.6, 135.5, 134.0, 132.3, 130.9, 130.2, 128.7, 127.0, 123.9, 119.3, 107.3.

H(4py,4py).

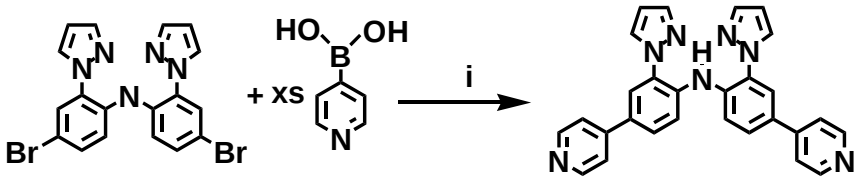

i) 20 mol% $Pd(PPh_3)_4$, 2 *M* Na_2CO_3, 30 mL C_6H_6, 10 mL EtOH, Δ 80^{0}C, 12H

In an argon-filled dry box, a Schlenk flask was charged with 0.707g (1.54 mmol) H(Br,Br), 0.568g (4.62 mmol) pyridine 4-boronic acid, and 0.356g (0.308 mmol) $Pd(PPh_3)_4$. The flask was removed from the drybox and attached to a Schlenk line. A solution of 30 mL C_6H_6 and 10 mL absolute ethanol was purged with argon 15 min and was transferred to the reaction flask under argon via cannula. Next, 10 mL of an argon-purged 2 *M* aqueous Na_2CO_3 solution was transferred via cannula to the reaction flask. After the magnetically-stirred biphasic mixture had been heated at 80 ^{0}C for 16 h with the aid of an external oil bath, the mixture was cooled to room temperature and poured into 100 mL H_2O. The aqueous and organic fractions were separated. The aqueous layer was extracted with two 50 mL portions ethyl acetate. The combined organic layers were dried

over $MgSO_4$ and filtered. The oily residue that was obtained after removing solvents under vacuum was subjected to column chromatography on silica gel using 2 :1 ethyl acetate : hexanes to remove first two spots and then used pure methanol as an eluent to obtain desired product H(4py,4py) as a colorless solid after removing solvents and drying under vacuum 1 h. (0.3019g , 43%) .Mp, 102-103 ^{0}C. ^{1}H NMR ($CDCl_3$): δ_H 9.34 (s, 1H, NH), 8.65 (br s, *J* = 4.8 Hz, 4H), 7.81 (br s, *J* = 12.2 Hz, 4H), 7.62 (m, 6H), 7.50 (br s , *J* = 4.8 Hz, 4H), 6.50(br s, 2H, pz). ^{13}C NMR ($CDCl_3$): δ_C 150.4, 146.7, 141.2, 137.2, 132.1, 130.9, 130.8, 130.1, 128.7, 126.7, 123.8, 120.9, 119.1, 107.3.

H(CO_2Et, CO_2Et)$_2$

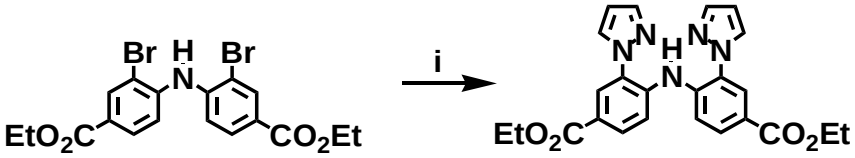

i) 3.5 eq K_2CO_3, 3.5 eq 1-H-Pyrazole, 10 mol% CuI, 40 mol% DMED

A mixture of 0.6463 g (1.37 mmol) HN(2-Br-4-$C_6H_4CO_2$Et)$_2$, 0.3269 g (4.80 mmol, 3.5 equiv) pyrazole, 0.6635 g (4.80 mmol, 3.5 equiv) K_2CO_3, 0.1 mL (0.548 mol, 40 mol %) DMED, and 10 mL of distilled xylenes was purged with argon 15 min. Then, 0.026 g (0.137 mmol, 10 mol %) CuI was added as a solid under argon and the mixture was heated at reflux for 36 h under nitrogen. After cooling to room temperature, 100 mL of H_2O was added and the mixture was extracted with three 50 mL portions of ethyl acetate. The combined organic layers were dried over $MgSO_4$, filtered, and solvent was removed by rotary evaporation to give an oily residue that was purified by column

chromatography on silica gel. Elution using 8:1 hexanes:ethyl acetate (R_f = 0.4) afforded 0.276 g (45 %) of H(CO_2Et, CO_2Et)$_2$ as sticky glue , after removing solvent and drying under vacuum. ^{1}H NMR($CDCl_3$): δ_H 9.96 (s, 1H, NH), 8.01 (d, *J* = 1.7Hz, 2H, H_5pz), 7.94 (d, *J* = 9.6 Hz, 2H, Ar), 7.79 (d, *J* = 2.1 Hz, 2H, pz), 7.76 (s, 2H, Ar), 7.57 (d, *J* = 8.8 Hz, 2H, Ar), 6.49 (br s, 2H, pz), 4.36 (q, *J* = 7.2 Hz, 4H, CH_2), 1.36 (t, *J* = 7.3 Hz, 6H, CH_3), ^{13}C NMR ($CDCl_3$): δ_C 165.7, 141.2, 140.0, 131.5, 130.2, 129.8, 126.7, 123.5, 117.8, 107.3, 61.2, 14.4.

Metal Complex Synthesis

Ni(3py,3py)$_2$, 1.

The solution of 0.449 g (0.987 mmol) H(3py,3py) and 0.117 g (0.493 mmol) $NiCl_2 \cdot 6H_2O$ in 15 mL MeOH was heated at reflux 10 min and it formed orange solution immediately. Then, 0.70 mL of a 1.47 *M* (0.99 mmol) solution of (NEt_4)(OH) in MeOH was injected to the hot reaction mixture by syringe. The solution became dark brown and an orange-brown solid precipitated. After the orange-brown suspension had been heated at reflux 30 min, the mixture was allowed to cool to room temperature. The insoluble portion was collected by filtration, was washed with 5 mL MeOH, then 5 mL of Et_2O, and was dried under vacuum to leave 0.526 g (72% yield) of Ni(3py,3py)$_2$ as a red-brown solid. Mp, >350^{0}C. Anal. Calcd. (found) for $C_{56}H_{40}N_{14}Ni$: C, 69.50 (63.70); H, 4.17 (4.31); N, 20.26 (17.42). μ_{eff} (solid, 295 K) = 3.3 μ_B. UV-Vis (CH_2Cl_2) λ_{max}, nm (ε, $M^{-1}cm^{-1}$): 248 (71,670), 418 (78,587), 528 (1272), 844 (389).

The following compound was prepared in a similar manner where the heating time, amount of solvent, and subsequent work-up procedure were identical to that described for $Ni(3py,3py)_2$.

$Ni(4py,4py)_2$, 2.

A mixture of 0.220 g (0.484 mmol) H(4py,4py), 0.058 g (0.24 mmol) $NiCl_2 \cdot 6H_2O$, and 0.49 mmol $(NEt_4)(OH)$ (0.33 mL of a 1.47 *M* solution in MeOH) gave 0.183 g (78%) $Ni(4py,4py)_2$ as a red-brown solid. Mp: $>350^0$C. Anal. Calcd. (found) for $C_{56}H_{40}N_{14}Ni$: C, 69.50 (68.42); H, 4.17 (4.23); N, 20.26 (19.62).μ_{eff} (solid, 295 K) = 3.0 μ_B. UV-Vis (CH_2Cl_2) λ_{max}, nm (ε, $M^{-1}cm^{-1}$): 534 (1730), 843 (310).

$Ni(CN,CN)_2$, 3.

Owing the relatively lower solubility of the ligand in MeOH versus other ligands, the mixture of 0.240 g (0.682 mmol) H(CN,CN), 0.0810 g (0.341 mmol) $NiCl_2 \cdot 6H_2O$, and 0.68 mmol $(NEt_4)(OH)$ (0.46 mL of a 1.47 *M* solution in MeOH) was heated at reflux 6h and was filtered hot. After washing with Et_2O and drying under vacuum 0.222 g (86%) **3** was obtained as an orange-brown solid. Mp: $>350^o$C. Anal. Calcd. (found) for $C_{40}H_{24}N_{14}Ni$: C, 63.26 (59.56); H, 3.19 (3.23); N, 25.82 (24.28).μ_{eff} (solid, 295 K) = 3.2 μ_B. IR (KBr) ν_{CN} 2214 cm^{-1}. λ_{max}, nm (ε, $M^{-1}cm^{-1}$): 242 (99,200), 303 (22,300), 346 (27,300), 407 (118,000), 491 (930), 512 (982), 792 sh (81), 841 (159) , 893 (160).

$Ni(CO_2Et, CO_2Et)_2$, 4.

A mixture of 0.276 g (0.612 mmol) $H(CO_2Et, CO_2Et)_2$, 0.074 g (0.306 mmol) $NiCl_2.6H_2O$, and 0.612 mmol $(NEt_4)(OH)$ (0.42 mL of a 1.47 *M* solution in MeOH) gave

0.236 g (67%) Ni(CO_2Et, CO_2Et)$_2$ as a red-brown solid. Mp: >350^{0}C. Anal. Calcd. (found) for $C_{48}H_{44}N_{10}O_8Ni$: C, 60.84 (58.43); H, 4.68 (4.43); N, 14.78 (14.09). μ_{eff} (solid, 295 K) = 2.9 μ_B. IR (KBr) ν_{CO} 1699 cm^{-1}. UV-Vis (CH_2Cl_2) λ_{max}, nm (ε, $M^{-1}cm^{-1}$): 244 (62,714), 316 (15,793), 344 (21881), 417 (79413), 515 (1180), 839 (272), 887 (271).

Rh(Me,Me)(4py, 4py)(PF_6), 5.

A solution of 0.157 g (0.229 mmol) of(NEt_4)[Rh(Me,Me)Cl_3]·H_2O, 0.241 g (0.229 mmol) of H(4pr,4py), 0.240 g (0.687 mmol) of $TlPF_6$ and 0.16 mL of 1.4685 *M* (0.0.229 mmol) of methanolic solution of NEt_4OH in 15 mL CH_3CN was heated in refluxing for 15 h. Then it was allowed to cool to room temperature and filtered through a short pad of celite. The organic fractions were evaporated and 0.140 g (59% yield) of the desired product as a red/brown solid was isolated after column chromatography on neutral alumina by eluting with 10:1 dichloromethane/methanol collecting the red band (R_f = 0.6). Mp: 236 - 238 ^{0}C (decomposed). . ^{1}H NMR($CDCl_3$): δ_H 8.7(d, *J* = 2.7 Hz, 2H, pz), 8.56 (br d, *J* = 5.4 Hz,, 4H, pz), 8.47 (d, *J* = 2.8 Hz, 2H, pz), 7.90 (d, *J* = 9.0 Hz, 2H), 7.88 (s, 2H), 7.77 (dd, *J* = 8.7, 2.1 Hz, 2H), 7.68 (br d, *J* = 6.0 Hz, 4H), 7.58 (d, *J* = 8.2 Hz, 2H), 7.32 (dd, *J* = 11.5, 2.4 Hz, 4H), 7.20 (s, 2H), 7.06 (d, *J* = 8.3 Hz, 2H), 6.51 (t, *J* = 2.8 Hz, pz, 2H), 6.51 (t, *J* = 2.8 Hz, 2H, pz), 6.44 (t, *J* = 2.8 Hz, 2H, pz), 2.23 (s, 6H).

Attempts to prepare coordination polymers (CPs) and mixed metal organic frameworks (MMOFs).

H(CN,CN)$_2$•AgPF_6. A solution of 0.010 g (0.013 mol) H(CN,CN) in 2 mL of acetone was layered with a solution of 0.007 g (0.026 mmol) $AgPF_6$ in 4 mL THF and solvents were allowed to diffuse over 3d, to give $AgPF_6$H(CN,CN) yellow needles.

H(4py,4py)• $Zn(NO_3)_2$. A solution of 0.010 g (0.021 mmol) H(4py,4py) in 2mL DMSO was layered with 0.065 g (0.021 mmol) $Zn(NO_3)_2 \cdot 6H_2O$ in 4 mL EtOH and solvents were allowed to diffuse over 1day to give $Zn(NO_3)_2$[H(4py,4py)] pale yellow needles.

$Ni(CN,CN)_2$•$AgBF_4$. A solution of 0.020 g (0.026 mmol) Ni(CN,CN) in 2 mL of acetone was layered with a solution of 0.010 g (0.052 mmol) $AgBF_4$ in 4 mL THF and solvents were allowed to diffuse over 3d, to give $Ni(CN,CN)_2$:$AgBF_4$ yellow needles.

$Ni(CN,CN)_2$ •AgOTf. A solution of 0.020 g (0.026 mmol) $Ni(CN,CN)_2$ in 2 mL of THF was layered with a solution of 0.014 g (0.054mmol) AgOTf in 4 mL THF and solvents were allowed to diffuse over 1d to give $Ni(CN,CN)_2$:AgOTf red brown blocks.

Rh(Me,Me)(4py,4py)(PF_6)•$Zn(NO_3)_2$. A solution of 0.0098 g (0.0095 mmol) [Rh(Me,Me)(4py,4py)](PF_6) in 2 mL of DMSO was layered with a solution of 0.0031 g (0.010 mmol) $Zn(NO_3)_2$ in 4 mL of EtOH and solvents were allowed to diffuse over 7d to give Rh(Me,Me)(4py,4py)·$Zn(DMSO)_4(NO_3)_2$ orange needles.

5.5 CRYSTALLOGRAPHY.

X-ray intensity data from a long brown prism of Ni(3py,3py)·1.5 CH_2Cl_2, a yellow needle of $Ni(CO_2Et,CO_2Et)_2 \cdot 0.5CH_2Cl_2$ were collected at 100.0(1) K with an Oxford Diffraction Ltd. Supernova diffractometer equipped with a 135 mm Atlas CCD detector using Mo(Kα) radiation. Raw data frame integration and Lp corrections were performed with either CrysAlis Pro (Oxford Diffraction, Ltd.)[20] or SAINT+ (Bruker).[21] Analysis of the data showed negligible crystal decay during collection in each case. Direct methods structure solutions, difference Fourier calculations and full-matrix least-squares refinements against F^2 were performed with SHELXTL.[22] Hydrogen atoms were placed

in geometrically idealized positions and included as riding atoms. The X-ray crystallographic parameters and further details of data collection and structure refinements are given in Table 5.3.

Table 5.3.Crystallographic Data Collection and Structure Refinement for Ni(3py,3py)$_2$, **1**·1.5 CH_2Cl_2, Ni(CN.CN)$_2$·acetone, **3**·acetone, Ni(CO_2Et,CO_2Et)$_2$, **4**·0.5 CH_2Cl_2**.**

Compound	**1**·1.5 CH_2Cl_2	**3**·acetone	**4**·0.5 CH_2Cl_2
Formula	$C_{57}H_{41}Cl_3N_{14}Ni$	$C_{43}H_{30}N_{14}NiO$	$C_{48}H_{44}Cl_{0.5}N_{10}NiO_8$
Formula weight	1043.11	817.52	960.61
Crystal system	triclinic	monoclinic	monoclinic
Space group	P-1	P 2_1/n	C2/c
Temperature [K]	99.95(10)	100.0(1)	100.00(10)
a [Å]	9.7474(3)	14.21320(17)	50.0642(8)
b [Å]	14.7610(5)	15.60318(16)	11.16515(14)
c [Å]	18.6394(6)	17.3945(2)	16.41104(19)
α[°]	95.027(3)	90.00	90.00
β[°]	103.898(3)	103.6602(13)	96.1625(12)
γ [°]	104.064(3)	90.00	90.00
V [Å^3]	2494.77(14)	3748.49(8)	9120.3(2)
Z	2	4	8
$D_{calcd.}$ [gcm^{-3}]	1.389	1.449	1.399
λ[Å] (Cu or Mo	0.7107	0.7107	0.7107
μ [mm^{-1}]	1.888	0.575	1.332
Abs. Correction	numerical	numerical	numerical
F(000)	1078.0	1688	4003.0
θ range [°]	6.24 to 147.74°	2.88 to 29.20	7.1 to 147.76°
Reflections	24773	42291	44705
Independent Rflns	9791[R_{int} =	9159	9119[Rint = 0.0263]
T_min/max		0.922/0.958	0.834/0.941
Data/restr./param.	9791/3/680	9159/0/534	9119/6/650
Goodness-of-fit	1.067	1.047	1.031
$R1^a$ /$wR2^b$	0.0611/ 0.1827	0.0476/0.1128	0.0340/ 0.0913
*R*1/*wR*2 (all data)	0.0658/ 0.1880	0.0592/0.1201	0.0376/ 0.0946
peak/hole / e Å^{-3}	1.52/-0.73	0.747/-0.792	0.72/-0.41

[a] $R1 = \Sigma||F_o| - |F_c||/\Sigma|F_o|$ [b] $wR2 = [\Sigma w(|F_o| - |F_c|)^2/\Sigma w|F_o|^2]^{1/2}$.

CHAPTER 6

SYNTHESIS AND CHARACTERIZATION OF COINAGE METAL COMPLEXES OF FUNCTIONALIZED N,N'-DIARYLFORMAMIDINATES

6.1. INTRODUCTION

The study of multi-nuclear, coinage metal complexes has gained considerable attention because the properties of group 11 metals are quite different compared to the other metals. The mono-cationic group 11 metals have closed-shell d^{10} electronic configuration. Sometimes these complexes associate to give interactions in which metal-metal distances are shorter than the sum of their van der Waals radii.[1-10] These metal-metal interactions often bestow in unusual luminescence properties and chemical reactivity to the complex.[5,23] There has been interest in developing ligands that can support or vary the proximity and hence the strength of the metallophilic interactions. In group 11 chemistry a given multinucleating ligand can promote molecules in a number of ways (many times unexpectedly); Figure 6.1.

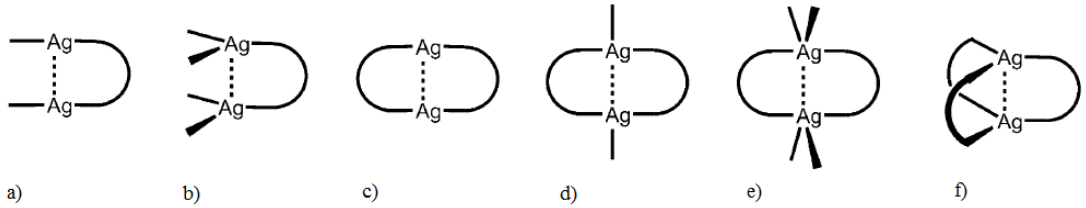

Figure 6.1. Ligand supported dinuclear silver complexes from reference 4.

The anionic amidinate ligands are known to support metal-metal interactions.[1-6] Further, amidinates have multiple coordination modes leading to various molecular arrangements (Figure 6.2). These amidinate ligands are isoelectronic with the well known

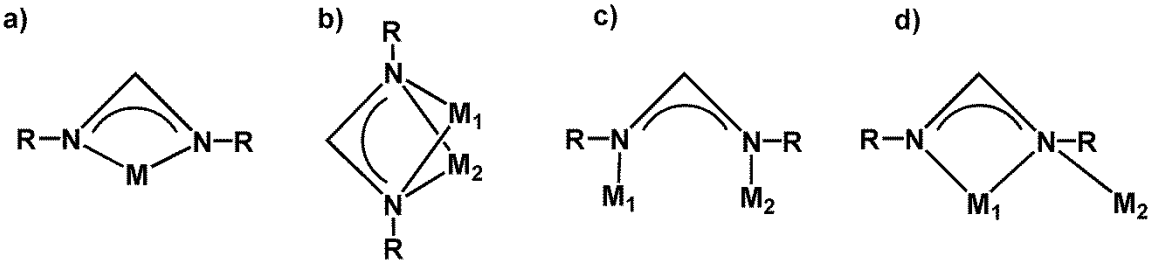

Figure 6.2. Metal binding coordination modes of amidinates. M: metal, R: organic group. a) Chelating, κ. b) Bridging-Chelating (symmetric), μ-κ. c) Bridging, μ. d) Bridging-Chelating (asymmetric).

carboxylate ligands, which also exhibit diverse binding modes. Cotton et al. first synthesized the N,N'-di-*p*-tolylformamidinato disilver(I) ($Ag_2(form)_2$) complex shown in Figure 6.3.a,[1] and thereafter numerous coinage metal amidinate complexes have been synthesized.[1-6] The $Ag_2(form)_2$ complex (Figure 6.3.a) has short Ag···Ag contacts, where inter atomic distance is 2.705(1) Å. Since diarylformamidinates are N,N' donors, introducing additional donor groups to the *ortho*-aryl positions provides possibilities for making extended pincer ligands, where the added donors can stabilize a central M_2 fragment anchored by NCN moiety. Such complexes with sulfur and oxygen donor flanking donor groups have reported by Archibald and co-workers (Figure 6.3.b-c).[2]

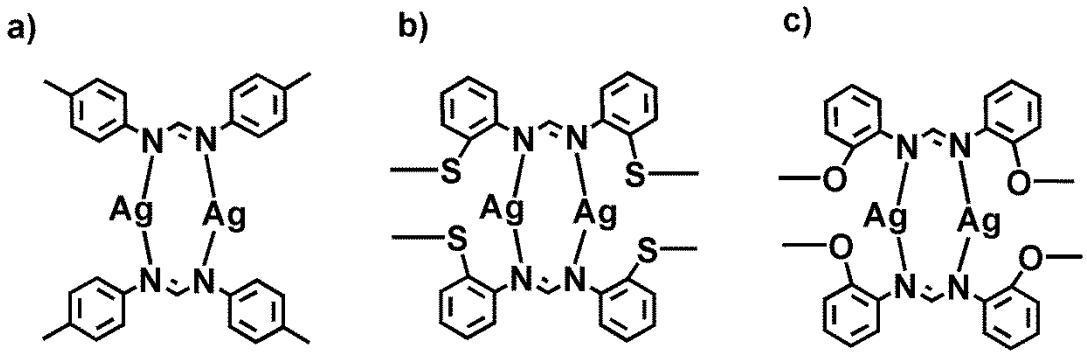

Figure 6.3. a) First disilver diformamidinate ($Ag_2(form)_2$) complex synthesized by Cotton et al. at 1988.[1] b) thioether and c) methylether functionalized N,N'-diphenylformamidinate silver(I) dimers.[2]

The silver complex, which has sulfur flanking donors has 2.801 Å silver-silver inter atomic distance while oxygen donor complex has 2.780 Å. Yamaguchi and co-workers have prepared a series of such extended pincer ligands with phosphorous flanking donors.[25] Their bimetallic palladium and platinum complexes, which have metal-metal interactions, were studied for potential metal-metal cooperativity in catalytic reactions.

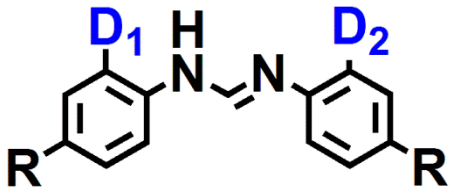

Figure 6.4. Diarylformamidinate ligand with ortho-aryl donor groups. R is an alkyl or hydrogen.

Previous studies by He and co-workers on various mono and dinuclear silver(I) complexes indicated that those with Ag···Ag interactions are active catalysts for olefin

aziridination reactions while others are not.[23] Perez and co-workers has shown that mononuclear silver(I) scorpionate complex can efficiently catalyze this reaction however.[29] In each cases, the potential of silver(I) formamidinate complexes to act as catalysts has not been explored. These types of ligands provide good platform to synthesize multi-nuclear metal complexes and here we document the synthesis of multi-nuclear silver complexes of three extended pincer ligands. Therefore potentials of silver(I) formamidinate complexes for the catalytic activity of this reaction will be described to determine whether or not such catalytic reactivity can be used to gauge of metallophilic interactions.

Further, substitution of phosphino donor groups into the *ortho*-aryl provides hard and soft binding sites to the ligand (Figure 6.5). Having different donor sites in a ligand may permit preferentially binding of metal ions based on Pearson's Hard-Soft acid/base preferences. Therefore, self sorting ability of the ligand toward different group 11 complexes was examined.

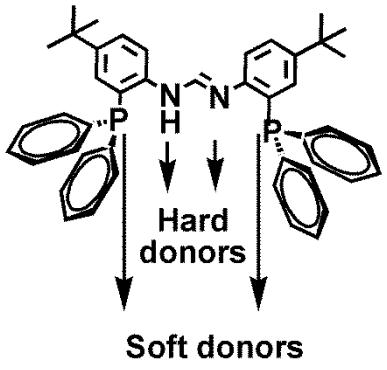

Figure 6.5. Hard and soft donor sites of PNNP ligand.

6.2. RESULTS AND DISCUSSION

6.2.1. Ligand Syntheses.

Three N,N'-diarylformamidinate ligands that have various donor groups at the *ortho* aryl positions were prepared. The protonated ligands are labeled according to their donor sets H(NNNN), H(PNNP), and H(PNNN). H(NNNN) has pyrazolyl flanking donors. When the flanking donors are diarylphosphines, the ligand is H(PNNP). Finally, the unsymmetrical species with a pyrazolyl and a diarylphosphine flanking donor set is H(PNNN). The ligand, H(NNNN) was synthesized by heating the mixture of two equivalents of H(pzAn^{Me})[13] with one equivalent of triethylorthoformate in the presence of a catalytic amount of acetic acid for 4 hours (Scheme 6.1). The ligand could be purified by washing with hexanes, because all impurities including starting materials are soluble in hexane; the ligand is insoluble. The synthesis of H(PNNP) was carried out similarly, but two equivalents of H(DPPAn^{tBu}) was used as a starting material (Scheme 6.2). The purification of this ligand was more complicated as it is soluble in the most of organic solvents and it decomposes on silica or alumina gels preventing purification by column chromatography. Therefore it was used "as formed" for the ensuing reactions; the resulted metal complexes can be purified easier. The asymmetric formamidinate H(PNNN) was prepared in two steps. In a manner similar to Eisen[30], the reaction between equimolar amounts of H(pzAn^{Me}) and triethylorthoformate gave hexane soluble an intermediate IA (Scheme 6.3). This intermediate was then reacted with H(DPPAn^{Me}) to give the desired H(PNNN) (Scheme 6.4).

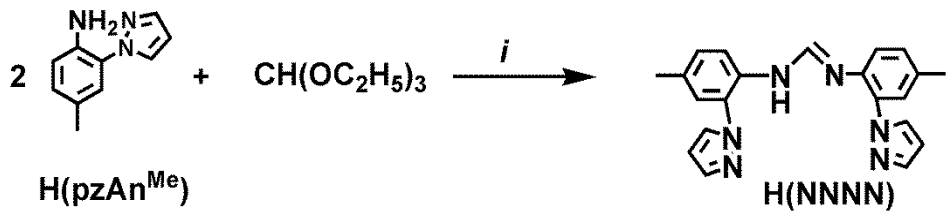

Scheme 6.1. Preparation of H(NNNN). *i*) catalytic amount of acetic acid, Δ , 4 hours.

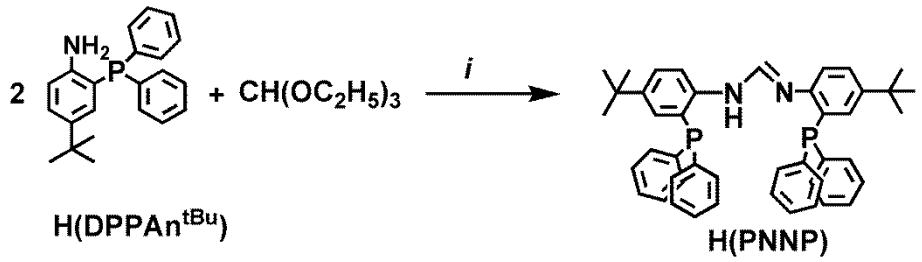

Scheme 6.2. Preparation of H(PNNP). *i*) catalytic amount of acetic acid, Δ , 4 hours.

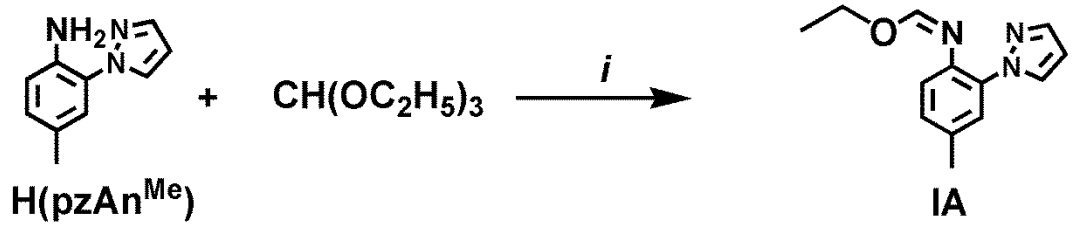

Scheme 6.3. Preparation of IA. *i*) catalytic amount of acetic acid, Δ , 3 hours.

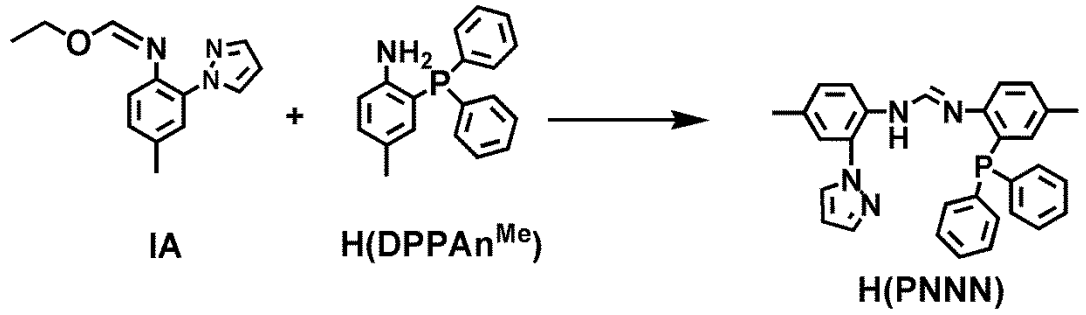

Scheme 6.4. Preparation of H(PNNN). *i*) catalytic amount of acetic acid, Δ , 4 hours.

6.2.2. Alkali Metal Complexes.

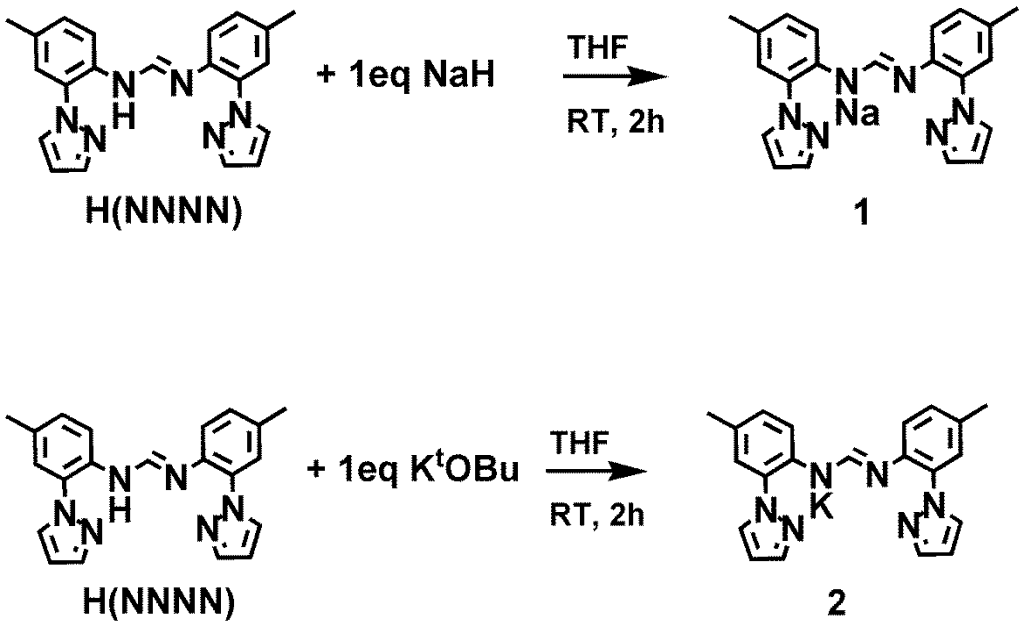

Scheme 6.5. Preparation of alkali metal complexes, **1** and **2**.

Alkali metal complexes were prepared and characterized since they can be starting materials to other complexes. The complexes M(NNNN) M = Na^+, K^+ were prepared by the reaction between H(NNNN) and either NaH or KO^{t}Bu, as appropriate, Scheme 6.5. The complexes M(PNNP) and M(PNNN) were prepared in-situ by similar methods but were not isolated because they were used successfully in preparation and purification of silver complexes, vide infra.

The yellow plates of THF solvated **1** were grown by layering hexanes on top of the THF solution of **1** and allowing solvents to diffuse for 24 h. The asymmetric unit is shown in Figure 6.6 and consists of two ligands, two Na, and two THF molecules. One sodium is bound two chelating ligands with four nearly identical Na-N bonds that average 2.427(3) Å. The two ligands are nearly perpendicular having an 85^0 angle

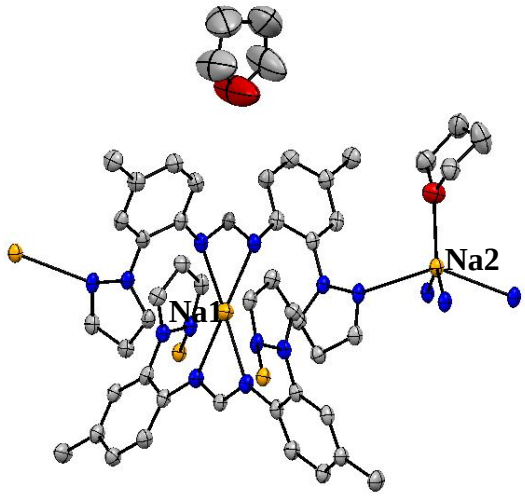

Figure 6.6. Asymmetric unit of the structure of **1**.

between NCN planes. The two N-C bonds of each ligand are also identical with average bond length of 1.327(3) Å. The second sodium is coordinated to four different pyrazole nitrogen atoms from four ligands (avg. 2.548(3) Å) and with one solvent molecule to give a 2D sheet structure, as shown in Figure 6.7. The second THF solvate molecule is located between stacked sheets.

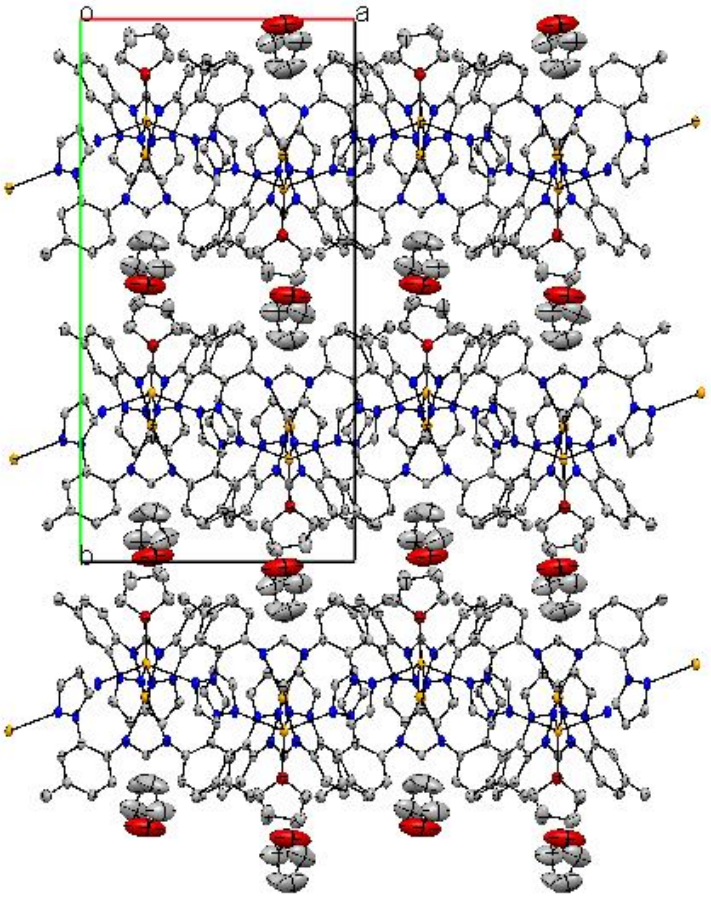

Figure 6.7. Crystal packing of **1.**

The structure of the pale yellow needles of **2**, which were grown by layering hexanes on top the THF solution of complex and allowing solvents to diffuse for 24h, was determined crystallographically. Complex **2** has a complicated polymeric structure as a result of association of different dimeric κ(NNN) units and a portion of polymeric structure is shown in Figure 6.8. The formamidinate group has a semi-bridging role in forming centrosymmetric dimers in crystals and each amidinato nitrogen interact with potassium atoms (Figure 6.8). The interatomic distance of two potassium atoms is 3.599(1) Å. The average bond length of K-N_{Am} is 2.984(3) Å, which is longer than the average K-N_{pz} bond legth (2.843(3) Å). This pyrazole comes from a neighboring dimer.

Two C-N_{Am} bonds of each ligand is similar with 1.318(3) Å. The dimers, in turn, are connected in chains along the x-axis via coordination through pyrazole side groups (Figure 6.8 and Figure 6.10). The crystal packing is depicted in the Figure 6.9. The chains propagate along the direction of the x-axis leaving spacious channels between them. The channels are filled by partially populated THF molecules.

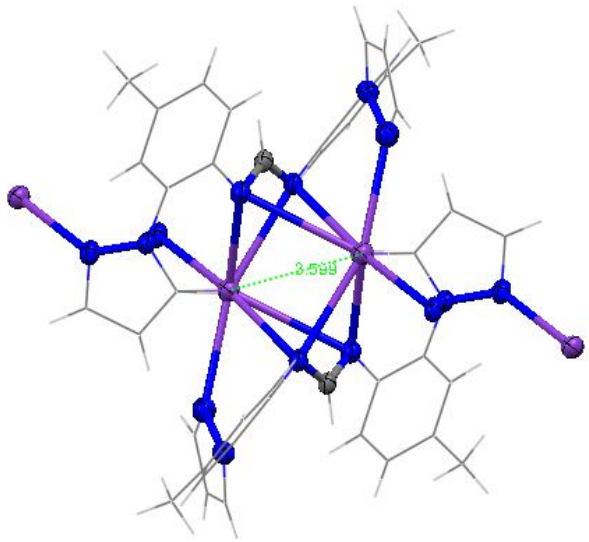

Figure 6.8. Dimeric structure of **2**·THF. Inter atomic distance of potassium is 3.599 Å.

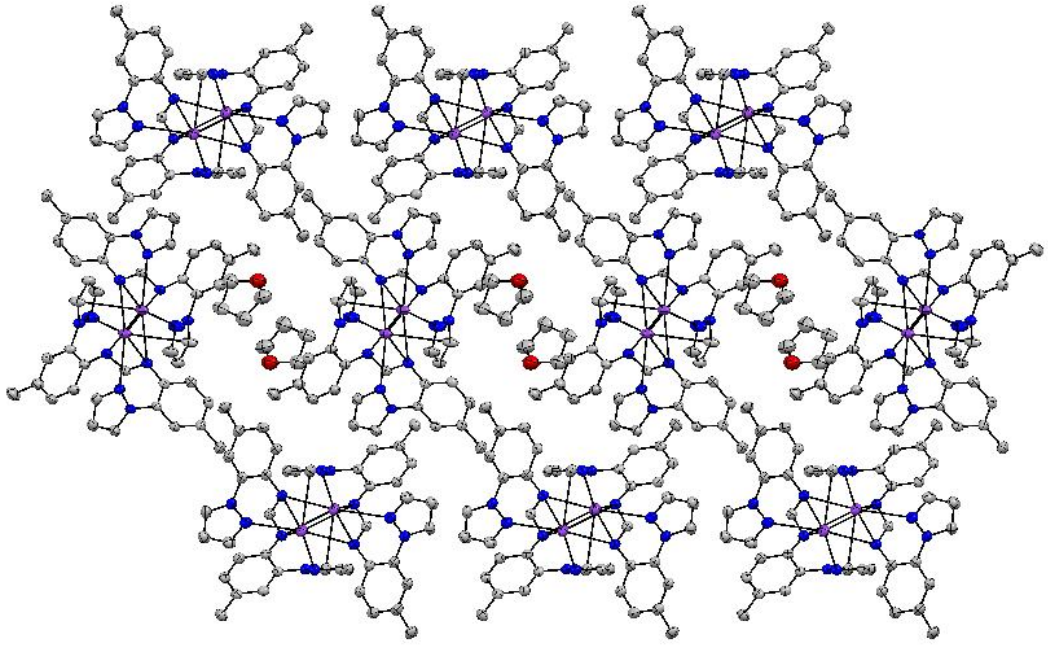

Figure 6.9. Crystal packing of **2**·THF**.**

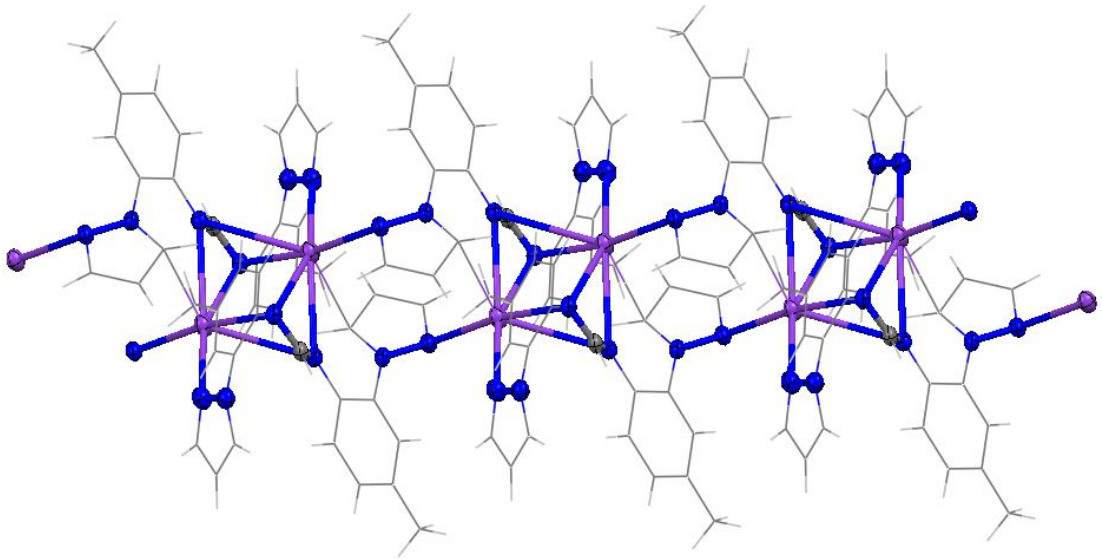

Figure 6.10. The chain of **2**·THF is propagated through the interaction of each potassiums with neighboring pyrazole groups.

6.2.3. Silver Complexes.

6.2.3.1. Ag(NNNN), 3

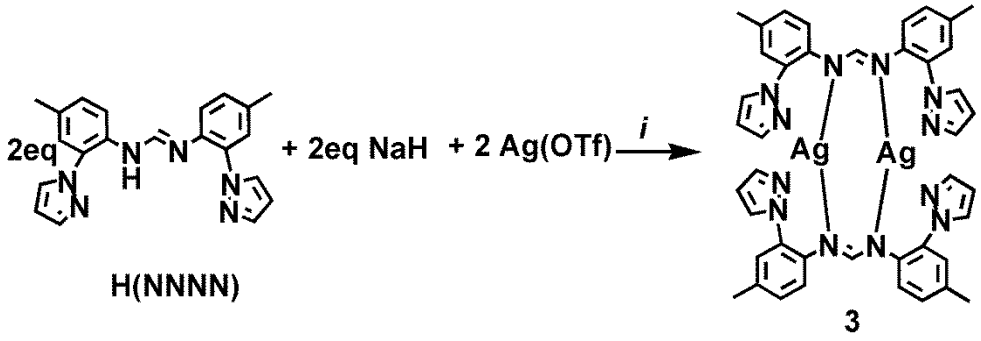

Scheme 6.6. Synthesis of Ag(NNNN), **3**. *i*) THF, stir room temperature, 12 h.

The complex Ag(NNNN), **3**, was prepared by the reaction of AgOTf and Na(NNNN) in THF. Complex **3** is soluble in chlorinated solvents and THF but is insoluble in hexanes, pentane, and diethyl ether. Crystals suitable for single crystal X-ray diffraction were grown by layering hexanes on top of CH_2Cl_2 solution of **3** and allowing solvents to diffuse for 12 h.

The solid state structure of **3** shows a dimeric motif (Figure 6.11).[2,17,18] The eight-membered $Ag_2(NCN)_2$ ring of this dimer is essentially planar. It has an inversion center through the midpoint of the Ag···Ag interaction. Each silver atom is coordinated with two amidinate nitrogen donors, one from each ligand. In addition to these Ag-N_{Am} bonds there is a weak Ag···N_{pz} interaction with a pyrazolyl nitrogen of one ligand. The other pyrazole is not interacting with silver (Figure 6.11). Both silver atoms are identical by symmetry. The Ag1-N6 bond distance is 0.014(2) Å shorter than that of the Ag1-N5 bond (2.164(2) Å). The Ag-N_{pz} distance (2.496(2) Å) is longer than the Ag-N_{Am} bond. This

distance is much more shorter than the average Ag··S interaction (2.865(2) Å) of Figure 6.3.b and Ag··O interaction (2.757 (5) Å) of Figure 6.3.c. Two silver atoms have a short inter-atomic distance of 2.782 (4) Å. The silver-silver interatomic distance (2.872 (5) Å) is 0.658 Å shorter than the sum of the van der Waals radii of silver (3.440 Å) that is 0.262 Å longer than the sum of ionic radii (2.520 Å).[19] This Ag···Ag short interaction is

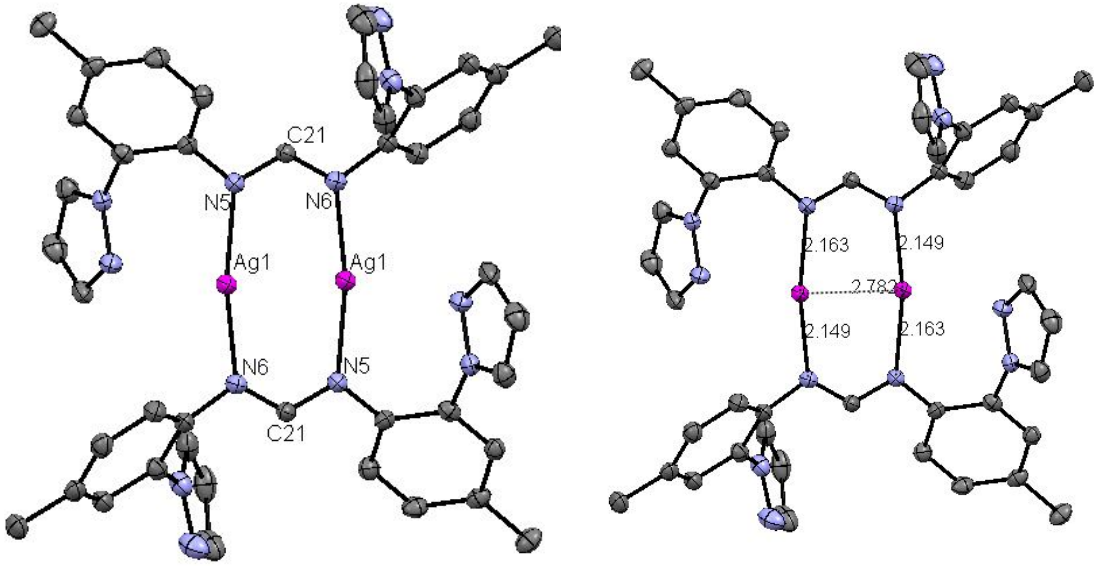

Figure 6.11. Thermal ellipsoid plot of **3**. Hydrogen atoms have been omitted for clarity.

shorter than most of the other dimetallic silver complexes reported, but it is 0.077 Å longer than that of $Ag_2(form)_2$ 2.705 (1) Å (Figure 6.3.a).[1] The weak interactions between the pyrazolyl nitrogen atoms and silver in **3** might be the reason for the longer Ag··Ag separation in **3** versus $Ag_2(form)_2$. The similar types of dinuclear silver complexes, which have sulfur and oxygen donors on *ortho*-aryl positions respectively (Figure 6.3), also show the elongated Ag···Ag interactions compared to the analogue complex, which does

not have a donor group at *ortho*-aryl positions.[2] This asymmetric ligand environment (two pyrazole flanking donors are not symmetric in the solid structure) does not exist in the solution. The ^{1}H NMR spectrum of **3** in $CDCl_3$ shows symmetric ligand environment and does not show two sets of peaks for pyrazole protons. Other characterization will be described later.

6.2.3.2. Ag(PNNP), 4.

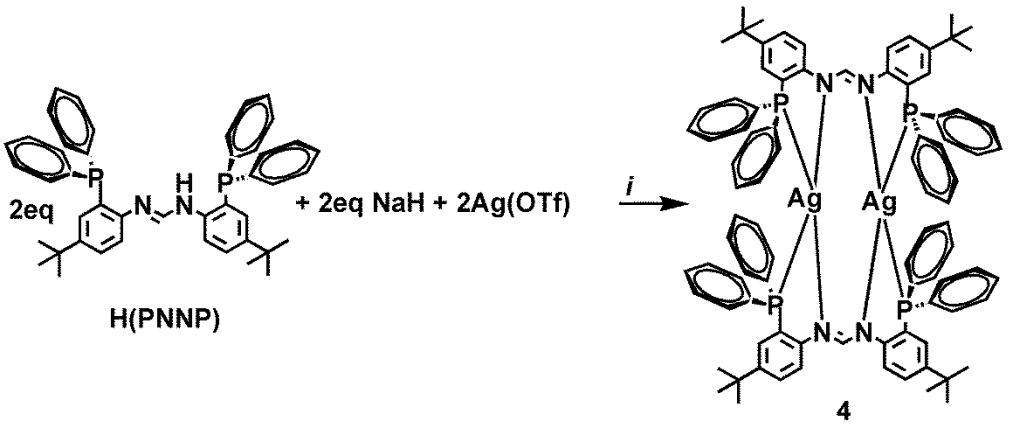

Scheme 6.7. Synthesis of Ag(PNNP), **4**. *i*) THF, stir at room temperature, 12 h.

Complex **4** was prepared following a similar procedure described for **3** (Scheme 6.7). The analytically pure yellow complex can be isolated by washing the crude mixture with diethyl ether. All impurities, including the unreacted ligand, could be removed from the product at this stage. Therefore this complex could be used as a pure reagent for future reaction chemistry. Single crystals suitable for X-ray diffraction were grown by layering pentane on top of the CH_2Cl_2 solution of **4**.

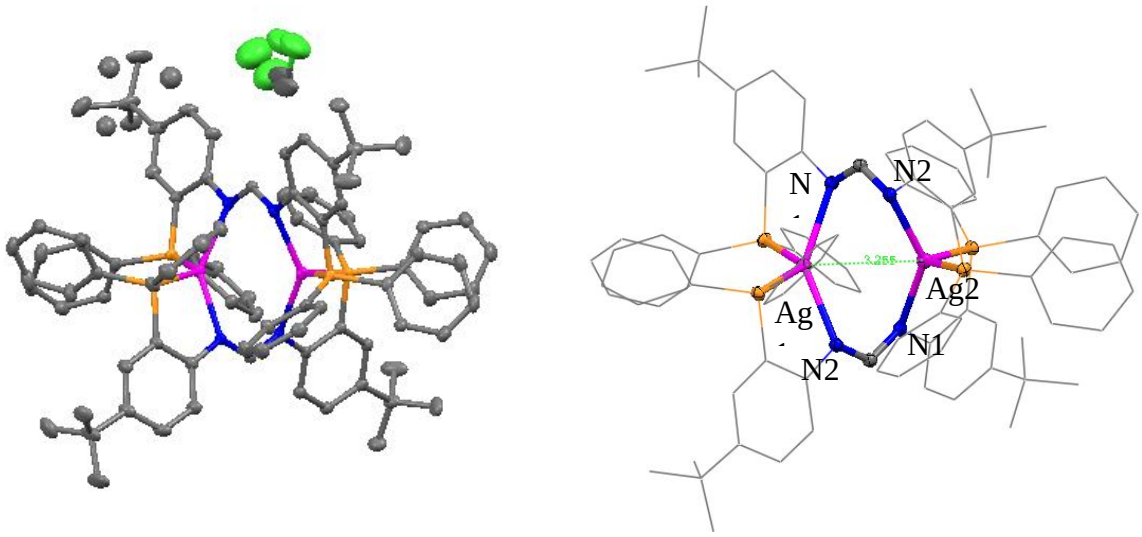

Figure 6.12. X-ray crystallographic structure of **4**. Ag···Ag inter-atomic distance is 3.254(3) Å.

The structure of **4** shows it to be a dimer in the solid state (Figure 6.12). Unlike **3**, eight membered $Ag_2(NCN)_2$ ring in **4** is not planar. Two ligands are nearly perpendicular to each other with a 92° angle between mean NCN planes. The structure has a 2-fold symmetry axis along the Ag···Ag vector. Each silver atom is four coordinate (μ-κN;κP), with a distorted tetrahedral AgN_2P_2 coordination environment, with one nitrogen and phosphorous from each ligand. The silver-silver interatomic distance of 3.254(3) Å is longer than that in complex **3** (2.782(4) Å). The two Ag-N_{Am} bonds distances are different (Ag1-N1 = 2.321(2) Å and Ag1 -N2 = 2.355(2) Å). Both Ag-P bond distances are identical at 2.465(6) Å.

If this structure persist in the solution, ^{1}H NMR and ^{31}P NMR should show symmetric resonance pattern for the ligands. The characteristic ^{31}P NMR pattern of this type of

complex is two doublets (coupling with ^{109}Ag and ^{107}Ag) with coupling constants in range of 400 – 550 Hz. The ^{31}P NMR of **4** shows two types of phosphorus resonances at room temperature, as shown Figure 6.13. There are two ligands and two silver atoms in the dimeric form and therefore it has four phosphorus atoms, two from each ligand. The middle resonance of ^{31}P NMR spectrum at room temperature integrates into one, while the summation of the outer two resonances integrates to one. It indicates that there are two types of phosphorus atoms present in the solution in equal amounts. If two out of four phosphorous atoms, likely one from each ligand, are bound to silver atoms, the NMR peak for those phosphorous atoms would be appeared as the two outer signals and it appears as a triplet in the room temperature NMR. The other two phosphorus atoms are exchanging very fast and the time-averaged signal appears as the middle signal (Figure 6.13). This rapid exchange is lowered when the sample temperature is decreased. Then the ^{31}P NMR shows the characteristic set of doublet resonances, which is expected for chemically equivalent phosphorous bound to a silver atom (Figure 6.13). Silver has two naturally occurring NMR active (I= ½) isotopes. One of these two is ^{107}Ag, and its natural abundance is 52%, while the rest is ^{109}Ag. These two isotopes give two doublets in 52:48 ratio, and we can see that pattern in the low temperature ^{31}P NMR of **4** (Figure 6.13 : Left-top). The low temperature NMR has 370 Hz ($^1J_{109Ag\text{-}P}$) and 327 Hz ($^1J_{107Ag\text{-}P}$) coupling constants, those are much lower than the other silver complexes with two phosphorous atoms bound to the silver such as 473 Hz for [Ag(PL)(PPh_3)][OTf],[14]

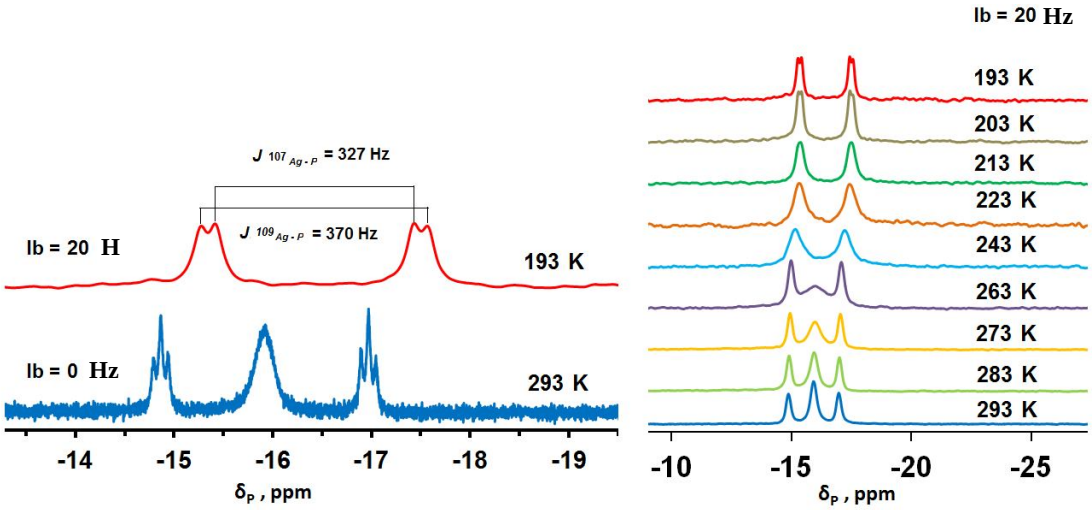

Figure 6.13. Left: ^{31}P NMR of **4** at 293 K and 193 K, Right: Overlay of spectra ^{31}P NMR of **4** in CD_2Cl_2 acquired at different temperatures. lb = line broadening.

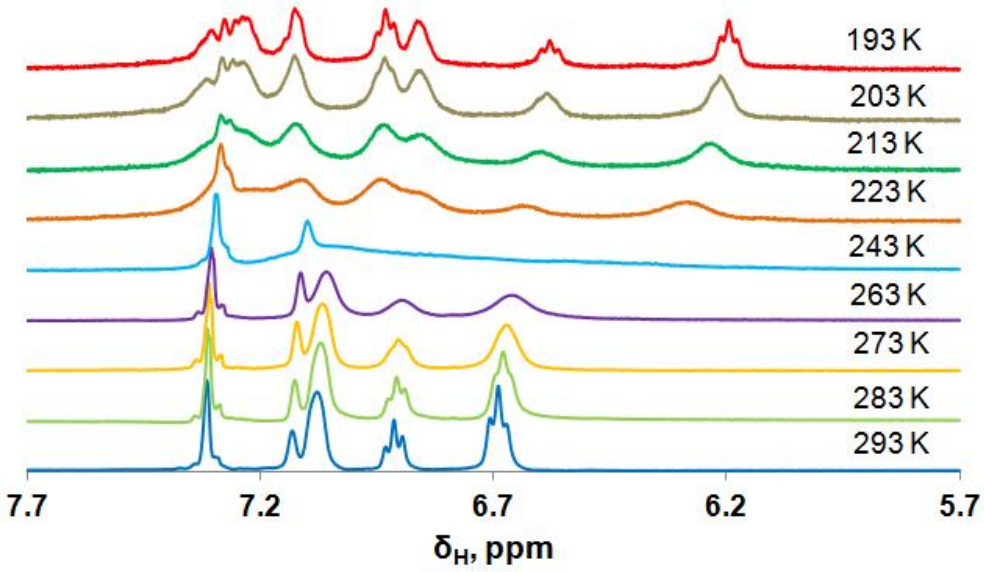

Figure 6.14. Overlay of spectra ^{1}H NMR of **4** in CD_2Cl_2 acquired at different temperatures.

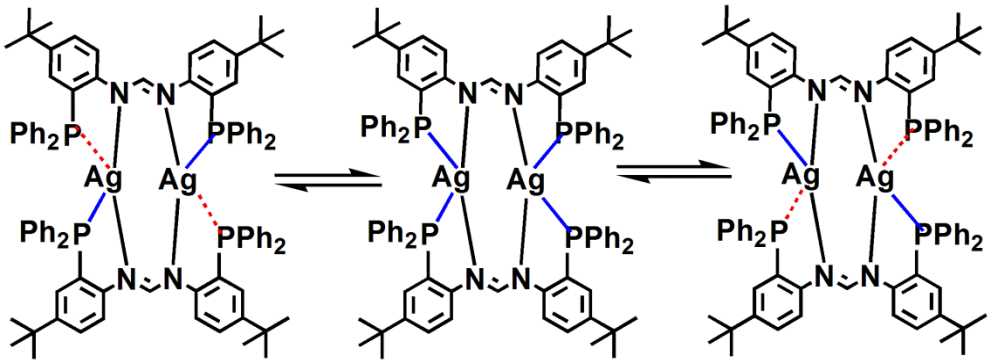

Figure 6.15. Rapid exchange of two phosphorous atoms.

496 Hz for $[(p\text{-tolyl}_3P)_2Ag]PF_6$,[15] 507 Hz for $[(Ph_3P)_2Ag](PF_6)$, and 432 Hz for $[(tBu_3P)_2Ag](NO_3)$.[16] This is one possibility to explain the structure of **4** in solution, further experiments need to be done to establish the structure with solid evidences. High temperature NMR and 2D NMR experiments would permit to identify the structure and it will be done by the group near the future.

6.2.3.3. Ag(PNNN), 5.

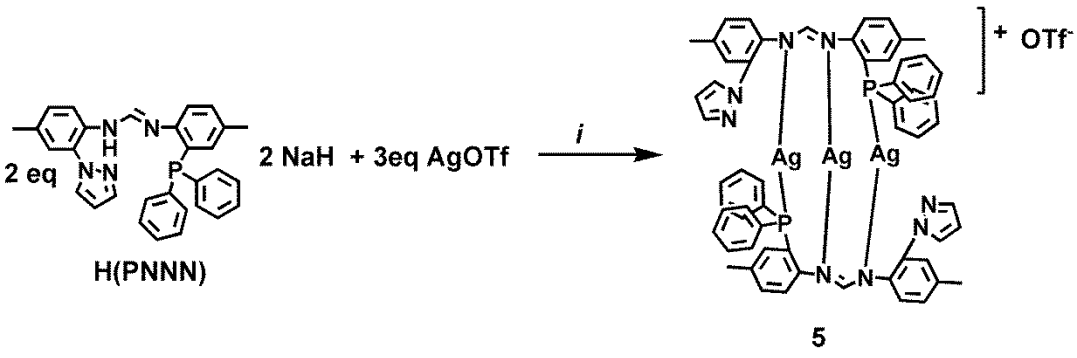

Scheme 6.8. Synthesis of Ag(PNNN) ligand, **5.** ***i)***. THF, stir at room temperature.

Complex **5** was prepared by stirring Na(PNNN) with 3 equivalents AgOTf in THF, shown in Scheme 6.8. Attempts to prepare a dinuclear complex were unsuccessful, **5** was obtained in all cases. Compound **5** is soluble in chlorinated solvents and THF, but insoluble in Et_2O and hexanes. Crystals of **5** for X-ray diffraction were grown by layering hexanes on top of a CH_2Cl_2 solution and the structure is shown in Figure 6.16. Two ligands are oriented in head-to-tail arrangement and those are bound through three silver atoms. Silver atoms have distorted tetrahedral coordination geometry. The inter silver distances are disperate with Ag1···Ag2 2.906 (8) Å and Ag2-Ag3 is 2.871(8) Å. Both are longer than that in **3**. The Ag-N_{Am} bonds are similar to each other and average 2.147(8) Å. Ag-P bond length is 2.358(7) Å, that is shorter than the Ag-P bond length of **4** (2.465(6) Å). ^{31}P NMR of **5** in CD_2Cl_2 shows characteristic doublet resonance for silver bound phosphorus, which appears at 0.47 ppm with J = 551 ($J_{109Ag\text{-}P}$) Hz.

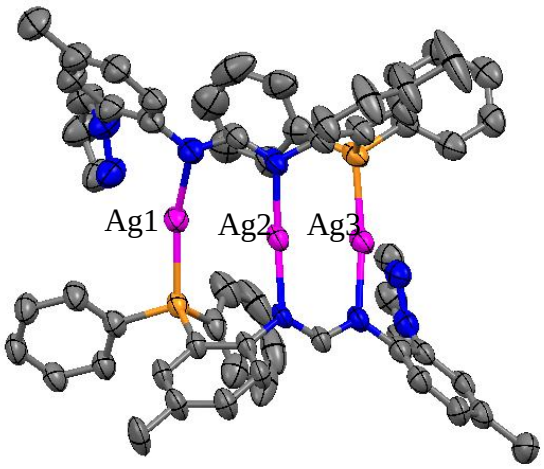

Figure 6.16. Views of the molecular structure of **5**. Hydrogen atoms have been omitted for clarity.

6.2.4. Preparation of tetra nuclear complexes.

Syntheses of tetrametallic complexes are shown in Scheme 6.9. Analytically pure **4** was used as the starting material in the syntheses of $[M_2Ag_2(PNNP)_2](X_2)$ (M = Ag, X = OTf for **6** and M = Cu, X = PF_6 for **7**). Compounds **6** and **7** were prepared by mixing **4** with an equivalent of AgOTf or $[Cu(CH_3CN)_4](PF_6)$, respectively. The solid state structure of **6** consists of a dicationic tetranuclear silver(I) complex (Figure 6.17). Four donor positions of each ligand are bound with silver atoms. There are two types of silver atoms, those that are bound with nitrogen atoms and those that are bound with phosphorous atoms. Each of the two middle silver atom is bound with two amidinate nitrogens, one from each ligand, and the outer two silver atoms each is bound with two phosphorus donor groups, one from each ligand. The Ag-N_{Am} bond lengths are similar to each other with average distance 2.169(4) Å, which is shorter than the average Ag-N_{Am} of **4** (2.338(17) Å). Average Ag-P bond distance is (2.421(11) Å) also shorter than **4** (2.465(6) Å). Triflate ions are bridging with two silver atoms via oxygen atoms and Ag-O average bond distance is 3.002(4) Å. Two outer silver atoms are located on the either side of the mean plane of two central silver atoms, forming a zigzag chain. Two ligands are nearly perpendicular to each other forming 105° angle between NCN planes of each ligand. The outer two Ag-Ag bond distances are identical and longer than the middle Ag-Ag bond. The inter atomic Ag1-Ag2 distance of the outer bond is 3.002(4) Å, while the inner Ag1-Ag1 bond distance is 2.850(6) Å. The inner Ag1-Ag1 bond length is 0.068 Å longer than the Ag-Ag bond found in **3** and 0.404 Å longer than **4**.

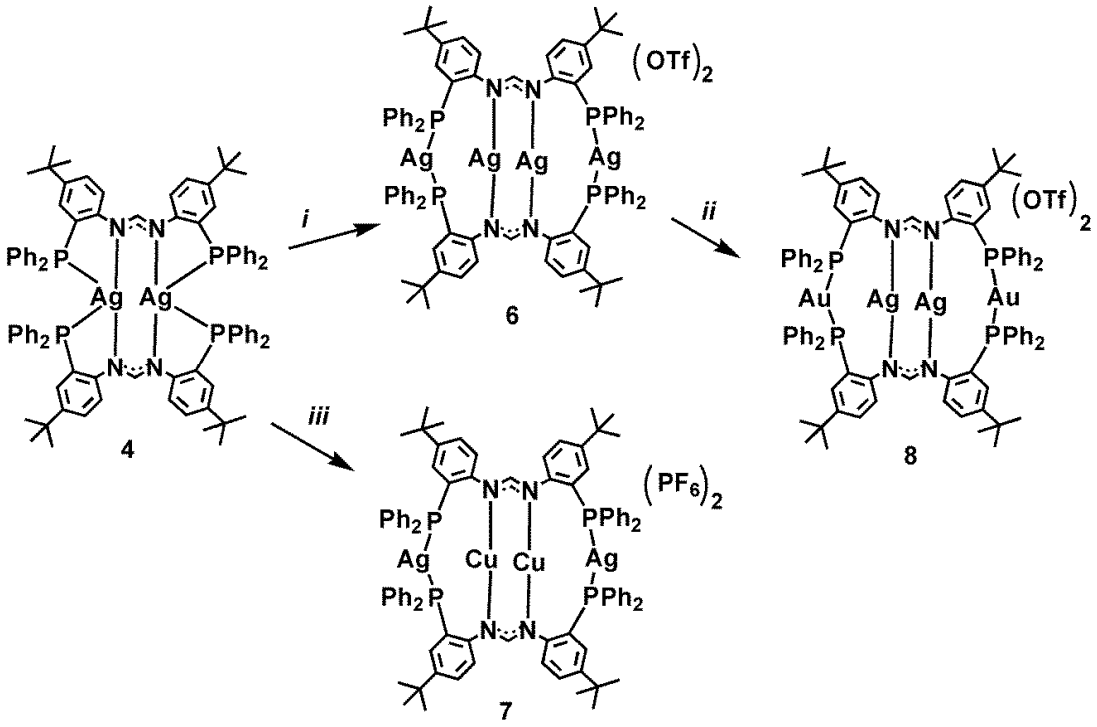

Scheme 6.9. Syntheses of tetra nuclear complexes, **6**, **7**, **8**.. i) AgOTf, THF. ii) $AuCl(SC_4H_8)$,THF. iii) $[Cu(CH_3CN)_4](PF_6)$, THF/ACN.

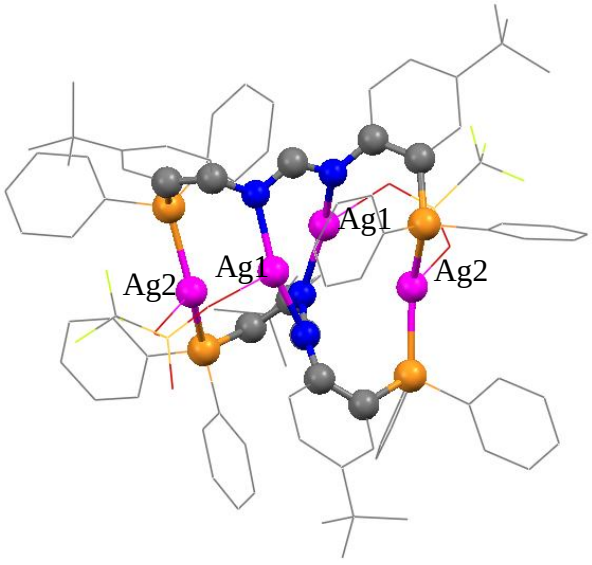

Figure 6.17. Structure of **6**. Hydrogen atoms and counter ions have been omitted for clarity.

The ^{31}P NMR spectrum of **6** in CD_2Cl_2 at 253 K shows characteristic doublet due to one bond coupling with Ag-107/109 nuclei (Figure 6.18). The coupling constant $^1J_{109AgP}$ = 551 Hz (253 K) is in line with other complexes with two phosphorus bound to silver such as [(p-tolyl$_3$P)$_2$Ag](PF$_6$) ($^1J_{109AgP}$ 507 Hz).[15]

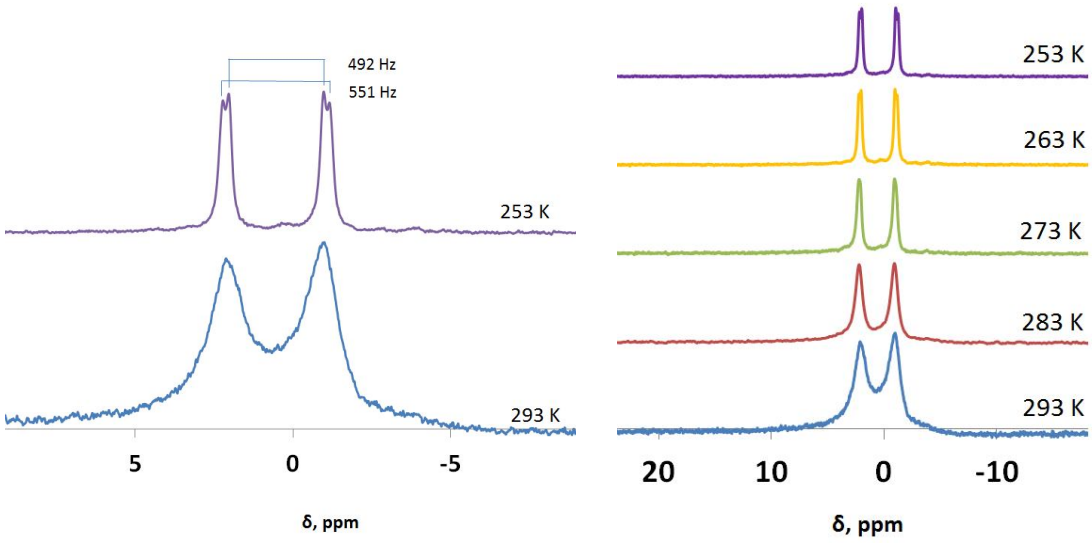

Figure 6.18. Overlay of ^{31}P NMR of **6** in CD_2Cl_2 acquired at different temperatures.

The solid state structure of the copper silver mixed metallic complex [AgCu(PNNP)](PF$_6$), **7** is shown in Figure 6.19. Single crystals were grown by layering hexanes on CH_2Cl_2 solution of complex **7**. Two ligands are parallel to each other and bound by two silver atoms and two copper atoms. Two copper atoms have taken the place of silver atoms and silver is bound with phosphorous donors. It is in line with the expected properties of this PNNP ligand, which were that harder copper should bind with hard nitrogen donor, while the softer metal silver should bind with soft donor, phosphorous. Four metals are in a zigzag pattern and it does not have a Ag···Ag

interaction and the interatomic distance of Cu···Cu is 2.582(6) Å. Two Ag-P bond lengths are similar to each other with 2.430(2) Å and Cu-N bond distances are slightly different to each other (Cu1-N1 = 1.894(1) Å and Cu1-N2 = 1.920(1) Å). The ^{31}P NMR spectrum of **7** in CD_2Cl_2 at 293 K shows characteristic doublet due to one bond coupling with Ag-107/109 nuclei ($^1J_{109AgP}$ = 563 Hz K).

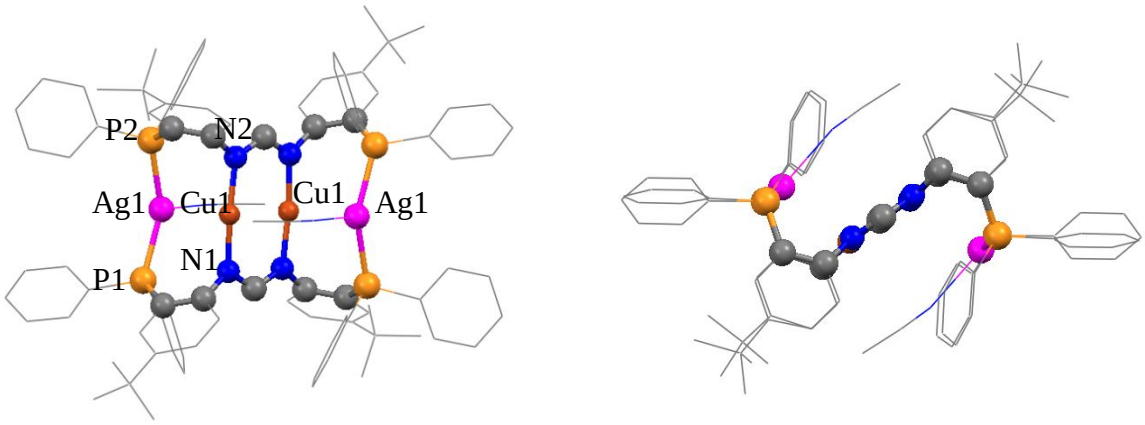

Figure 6.19. Views of the structure **7**. H atoms have been omitted for clarity.

Equivalent molar amounts of complex **6** and $AuCl(SC_4H_8)$ were stirred in THF for 12 h to prepare **8** (Scheme 6.9). Crystals suitable for single crystal X-ray diffraction were grown by layering pentane on top of the CH_2Cl_2 solution of **8** and structure is shown in Figure 6.20. Complex **8** is a dinuclear tetrameric complex which has two ligands, two silver(I), two gold(I), and two counter ions triflate. As we expected more harder silver is bound with amidinato nitrogen while soft metal gold is bound with phosphorous atom. Four metal atoms are not in a linear arrangement but in a zigzag arrangement like complex **6**. Despite the complex **6**, two ligands are parallel each other and eight membered $Ag_2(NCN)_2$ ring is planer. The Ag···Ag interatomic distance of this complex is 2.569 (4) Å, the shortest Ag···Ag interaction that we found in this study. The average

Ag···Au distance is 2.912 (10) Å. The ^{31}P NMR shows a doublet (J = 6.3 Hz) at 35.2 ppm. This small coupling constant is due to the long range coupling with a silver atom.

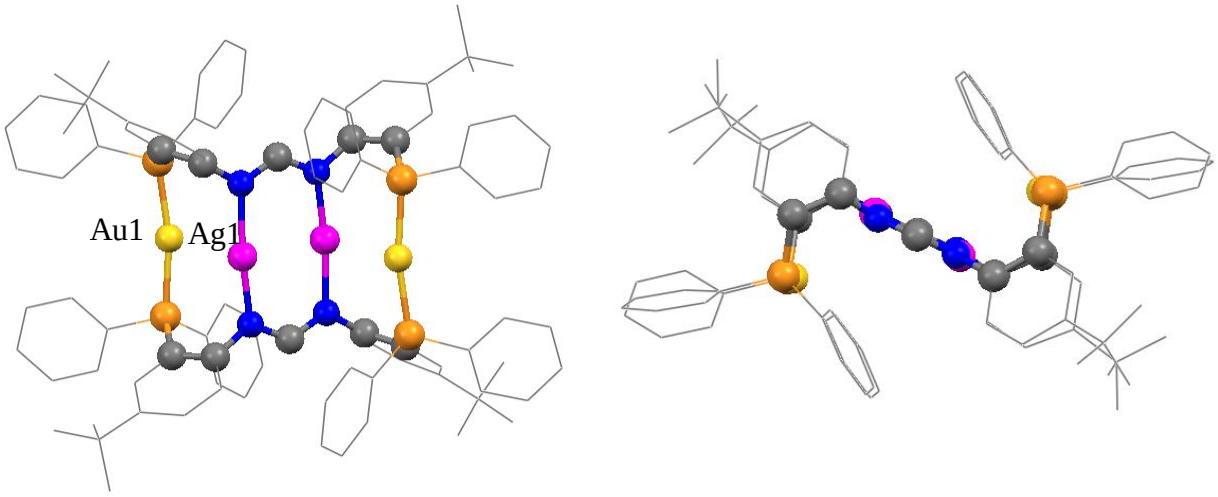

Figure 6.20. Views of the structure **8**. H atoms have been omitted for clarity.

6.2.5. Spectroscopy.

Dichloromethane solutions of these silver complexes are luminescent in room temperature. Absorbance and emission spectra of these complexes were measured and representative absorbance and emission spectra of **4** and **6** in CH_2Cl_2 are shown in Figure 6.21 where data are given in Table 6.1. Complex **4** shows strong emission at 460 nm when excited 394 nm in CH_2Cl_2 at ambient temperature. Similarly, complex **6** was

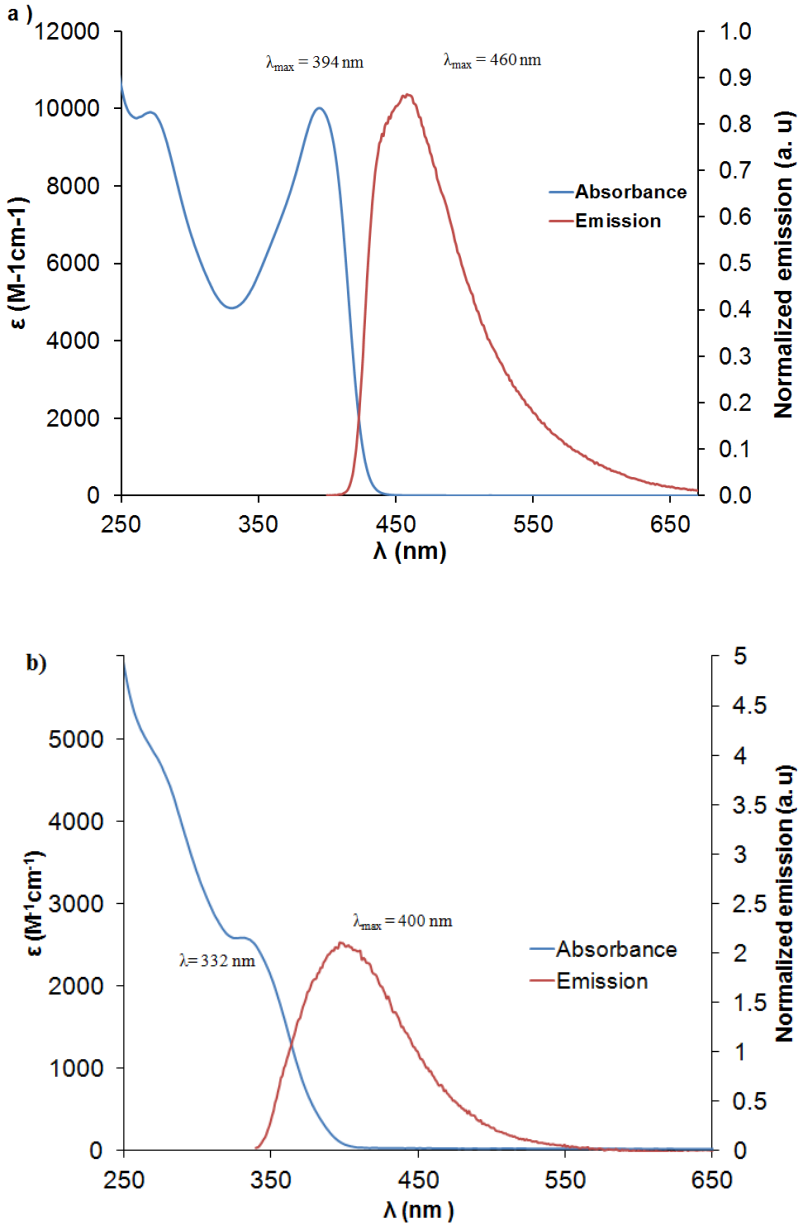

Figure 6.21. a) UV-Visible (blue) and emission (red) spectra of **4** in CH_2Cl_2. b) UV-visible (blue) and emission (red) spectra of **6** in CH_2Cl_2.

Table 6.1. Excitation and emission wave lengths of silver complexes.

Compound	$\lambda_{Excitation}$ (nm)	$\lambda_{Emission}$ (nm)	Absorbance λ_{max}^{nm} (ε, $M^{-1}cm^{-1}$)
3	300	413	310 (49524)
4	394	460	394 (10013), 276 (9745)
5	328	396	328 (37506), 268 (72450)
6	332	400	332 (2564)
8	310	439	310 (19883)

excited at 332 nm and it gave its emission peak at 400 nm. Excitation and emission wave lengths of remaining complexes are given in Table 6.1. The small stokes shift between excitation and emission seem to indicate fluorescence emission. The photo physical properties will need to be investigated more fully in the future.

Silver(I) complexes have been traditionally used in the stoichiometric oxidation of organic and inorganic substrates. However, silver metal nano particles are now being used as efficient catalysts for alkene epoxidations in industry.[21,22] Recently, He et al. showed that bimetallic silver(I) complexes, that have strong silver-silver interactions can be used as catalysts for olefin aziridination (Scheme 6.10).[23] Therefore, we investigated the potential of the current complexes (**3**, **4**, and **6**) to act as catalysts for aziridination of styrene with PhI=NTs (Scheme 6.10). A reaction was observed when **3** was used as a catalyst but not in other cases. While TLC monitoring indicated reaction had occurred, only very low yield (3.4 %) of product was isolated, therefore the reaction is not catalytic.

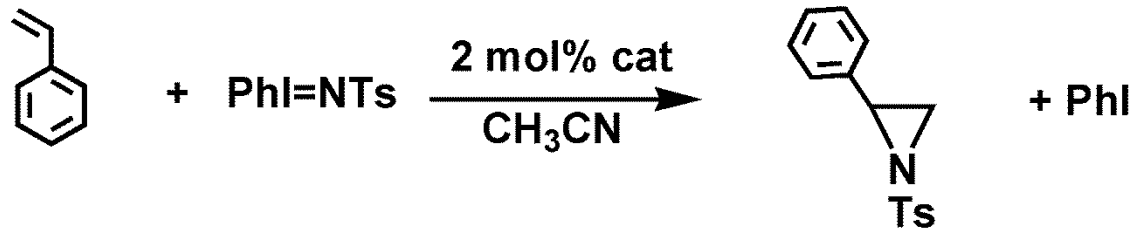

Scheme 6.10. Silver(I) promoted olefin aziridination.

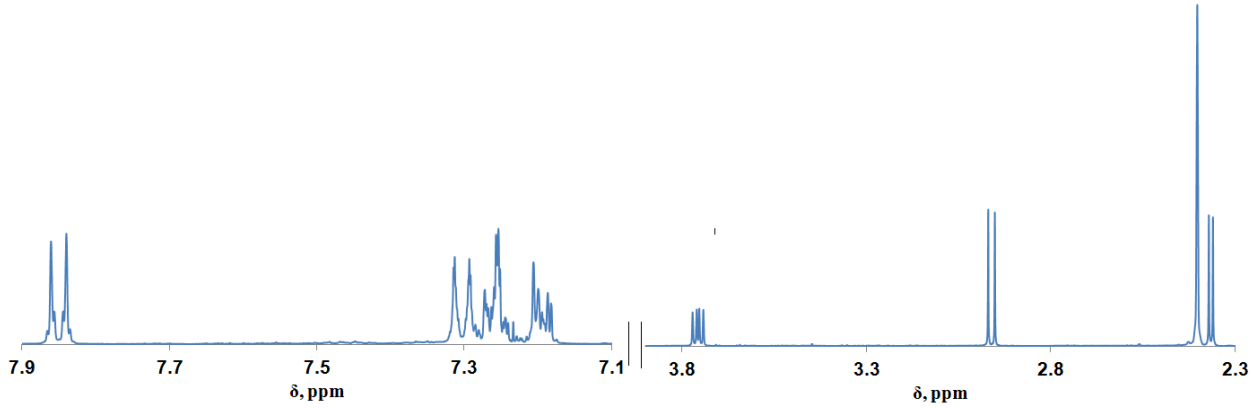

Figure 6.22. ^{1}H NMR of isolated product, 2-Phenyl-1-(toluene-4-sulfonyl)-aziridine in $CDCl_3$.

A portion of ^{1}H NMR spectrum of the isolated product is shown in Figure 6.22 for convenience in the future investigation of the catalytic activity of these complexes. The observation of a reaction for **3** but not other potential catalysts (**4** and **6**) may be related to the fact that **3** has the shortest Ag···Ag distance and that the pyrazolyl franking donors have a greater propensity for dissociation versus phosphorous.[31] Future screenings will involve examining the catalytic activity of Ag(OTf), **5**, **8**, $Ag_2(form)_2$[1] and reported catalysts as controls.

6.3. CONCLUSIONS

Three new N,N'-Diaryllformamidinate ligands were synthesized that had either pyrazolyl or diphenylphosphino groups substituted at the *ortho* position of each aryl ring where the ligands exhibited diverse binding nodes. The M(NNNN) (M = Na, K) complexes neither shows metal-metal interactions. On the other hand, Ag(NNNN) had μ-κN, κN' (Figure 6.2.c) binding mode which also showed very short inter silver contacts. Ag(PNNP) gave μ-κP,κN binding mode and had a very large inter silver separation of 3.254(3) Å. Only Ag_3(PNNN) could be isolated from the reaction of Na(PNNN) and AgOTf. In this structure Ag-Ag distances are 2.871(8) Å and 2.906(8) Å.

The $(PNNP)^-$ ligand indeed has the ability to sort univalent group 11 metals on the basis of their Pearson's hardness with the softest metal binding to the softest phosphorous in tetrametallic complexes (μ_4-κP, κN, κN, κP).

Preliminary investigation of the catalytic activity of the silver only complexes (**3**, **4**, and **6**) for the aziridination of olefins showed that only **3** with the shortest Ag-Ag separation and weakest donor set gave any reaction (albeit in low yield). Future repeated investigations of these and other formamidinates will determine the utility of this class of compounds in similar reactions.

6.4. EXPERIMENTAL

General Considerations.

The compounds $CH(OC_2H_5)_3$, Cs_2CO_3, I_2, N,N'-DMED, CuI, Ag_2SO_4, KO^tBu, NaH, $HAuCl_4$, AgOTf, tetrahydrothiophene, $[Cu(CH_3CN)_4](PF_6)$, pyrazole, 4-tert-

butylaniline, glacial acetic acid, styrene and $HPPh_2$ were purchased commercially and used as received. The compounds $H(pzAn^{Me})$,[13] $Pd(PPh_3)_4$,[26] PhI=NTs[27] and $AuCl(SC_4H_8)$[28] were prepared according to a literature procedures. Solvents were dried by conventional means and distilled under nitrogen prior to use.

Physical Measurements.

Midwest MicroLab, LLC, Indianapolis, Indiana 45250, performed all elemental analyses. Melting point determinations were made on samples contained in glass capillaries using an Electrothermal 9100 apparatus and are uncorrected. ^{1}H, ^{13}C, ^{19}F, and ^{31}P NMR spectra were recorded on a Varian 400 MHz spectrometer. Chemical shifts were referenced to solvent resonances at δ_H 5.33, δ_C 53.84 for CD_2Cl_2, δ_H 7.26, δ_C 77.23 for $CDCl_3$, δ_H 1.94, δ_C118.9 for CD_3CN and δ_H 2.05, δ_C 29.84 for acetone-d_6, while those for ^{19}F and ^{31}P NMR spectra were referenced against external standards of $CFCl_3$(δ_F 0.00 ppm) and 85% H_3PO_4(aq) (δ_P 0.00 ppm), respectively. Abbreviations for NMR and UV−Vis br (broad), sh (shoulder), m (multiplet), ps (pseudo-), s (singlet), d (doublet), t (triplet), q (quartet), p (pentet), sept (septet). Electronic absorption (UV−Vis/NIR) measurements were made on a Cary 5000 instrument. Emission spectra were recorded on a JASCO FP-6500 spectrofluorometer.

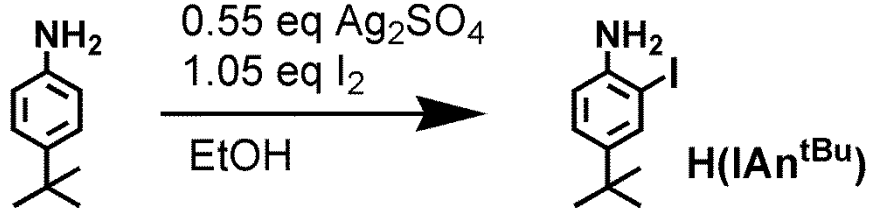

$H(IAn^{tBu})$.

To a 250 mL Schlenk flask charged with I_2 (8.367 g, 33.0 mmol), Ag_2SO_4 (5.38 g, 17.26 mmol), and 150 mL of ethanol, was added 4-tert-butylaniline (5.0 mL, 31.39 mmol) all in one portion. A yellow solid (AgI) began to precipitate out of solution almost immediately. The suspension was stirred at room temperature for 4 hours, then was filtered through Celite and ethanol was removed under reduced pressure. The remaining reddish oil was dissolved in 50 mL of CH_2Cl_2 and washed with 50 mL of DI water. After separation, the organic layer was dried over $MgSO_4$, filtered, and concentrated *in vacuo*. The remaining red oil was purified on a column of silica gel by eluting with hexane/dichoromethane (1:1). The second fraction contains the desired product, after concentration of eluent, as a red oil (R_f = 0.43, mass = 6.39 g, yield = 74%). ^{1}H NMR ($CDCl_3$) δ_H: 7.62 (d, *J* = 2.2 Hz, 1 H, aromatic H), 7.17 (dd, *J* = 2.3, 8.4 Hz, 1 H, aromatic H), 6.71 (d, *J* = 8.3 Hz, 1 H, aromatic H), 4.07 (br s, 2 H, amine-H's) 1.26 (s, 9 H, t-Bu H's) ppm. ^{13}C NMR ($CDCl_3$) δ_C: 144.25, 143.51, 135.80, 126.67, 114.74, 84.71, 33.97, 31.54 ppm.

H(IAn^{Me}).

A similar procedure to that above was followed but the following amounts of reagents were used. 3.000 g (27.998 mmol) of *p*-toluidine , 7.461 g (29.40 mmol) of I_2 yielded 3.499 g (54 %) of the desired product as a black liquid after purification by a silica gel column using 10:1 hexanes: ethyl acetate, as the eluent (R_f = 0.37). ^{1}H NMR ($CDCl_3$)

δ_H:7.48 (d, *J* = 1.2 Hz, 1 H), 6.95 (dd, *J* = 8.1, 2 Hz, 1 H), 6.70 (d, *J* = 8.1 Hz, 1 H), 3.91 (s, 2 H, NH_2), 2.21 (s, CH_3) ppm. ^{13}C NMR ($CDCl_3$) δ_C: 145.3, 140.7, 130.0, 128.7, 117.8, 83.8, 20.4 ppm.

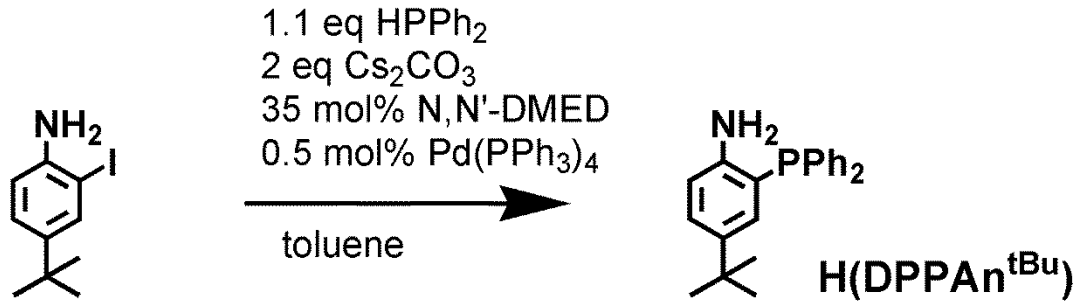

H(DPPAn^{tBu}).

A 100 mL Schlenk flask was charged with Cs_2CO_3 (15.602 g, 47.888 mmol) and a stir bar before being evacuated, backfilled with argon, and taken into the glove box. Diphenylphosphine (5.00 mL, 28.733 mmol) and $Pd(PPh_3)_4$ (0.1383 g, 0.5 mol%) were added, then the Schlenk flask was removed from the glove box. Meanwhile, argon gas was bubbled through another Schlenk flask containing 2-iodo-4-*tert*-butylaniline (6.588 g, 23.994 mmol), N,N'-dimethylethylenediamine (0.86 mL, 35 mmol%), and 50 mL toluene. The toluene solution was then cannula transferred into the Schenk flask containing the remaining reagents. Quantitative transfer was assured by rinsing with 5 mL of toluene. The reaction mixture was heated at reflux for 15 hours, during which time a white solid precipitated. The mixture was then brought to room temperature, filtered through Celite, and the solvent was removed under reduced pressure. The remaining brownish solid was dissolved in DI water (50 mL) in a separtory funnel and extracted using three 50 mL portions ethyl acetate. The organic fractions were combined, dried over $MgSO_4$, filtered, and solvents removed *in vacuo*. The remaining yellowish solid is purified on a column of silica gel eluting with hexane/dichloromethane (2:1) to remove

impurities with high R_f values before switching to pure CH_2Cl_2 to elute the desired product as a pale yellow solid after concentration (R_f = 0.26, mass = 6.52 g, yield = 82%). ^{1}H NMR ($CDCl_3$) δ_H: 7.34 (m, 10 H, phenyl H's), 7.20 (dd, *J* = 2.3, 8.3 Hz, 1 H, aromatic H), 6.79 (dd, *J* = 2.3, 6.5 Hz, 1 H, aromatic H), 6.67 (dd, *J* = 5.5, 8.3 Hz, 1 H, aromatic H), 3.25 (br s, 2 H, NH_2), 1.10 (s, 9 H, CH_3) ppm. ^{13}C NMR ($CDCl_3$) δ_C: 147.38 (d, *J* = 19.1 Hz), 141.37 (d, *J* = 2.4 Hz), 135.80 (d, *J* = 8.2 Hz), 133.75 (d, *J* = 18.7 Hz), 131.50 (d, *J* = 4.5 Hz), 128.87, 128.65 (d, *J* = 7.1 Hz), 127.50, 118.99 (d, *J* = 8.3 Hz), 115.35 (d, *J* = 3.0 Hz), 34.11, 31.42 ppm. ^{31}P NMR ($CDCl_3$) δ_P: -18.96 ppm.

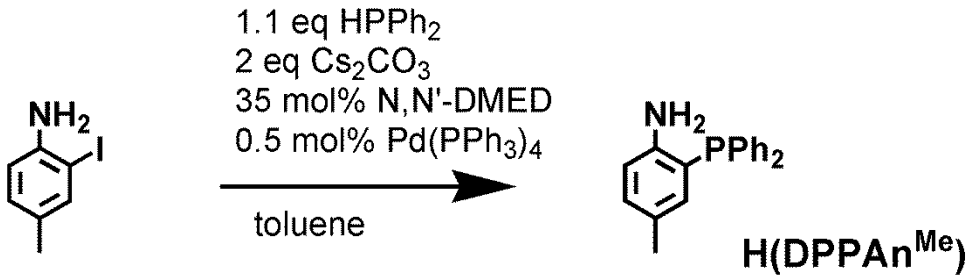

H(DPPAn^{Me}).

The above procedure was followed except 1.832 g (8.214 mmol) of 2-iodo-4-methylbenzenamine, 5.353 g (16.429 mmol) Cs_2CO_3, 1.72 mL (9.988 mmol) diphenylphosphine , 0.30 mL (35 mol%) N,N'-DMED, and 0.0475 g (0.5 mol%) $Pd(PPh_3)_4$ were used to give 1.603 g (70% yield) of desired product as colorless solid after purification by silica gel chromatography (10:1, hexanes:ethyl acetate as the eluent, R_f = 0.6). ^{1}H NMR ($CDCl_3$): δ_H (7.37-7.29) (m , 10 H, Ph), 7.00 (dd, *J* = 7.9, 1.9 Hz, 1 H), 6.67 (dd, *J* = 8.0, 5.5 Hz, 1 H), 6.59 (dd, *J* = 5.9, 1.8 Hz, 1 H), 3.58 (br s, NH_2), 2.11 (s, 3 H) ppm. ^{13}C NMR ($CDCl_3$): δ_C 135.6, 135.5, 134.6, 133.8 (d, *J* = 19 Hz), 131.4, 128.9, 128.7 (d, *J* = 6.7 Hz), 128.4, 116.1, 20.7 ppm. ^{31}P NMR ($CDCl_3$) δ_P -19.96 ppm.

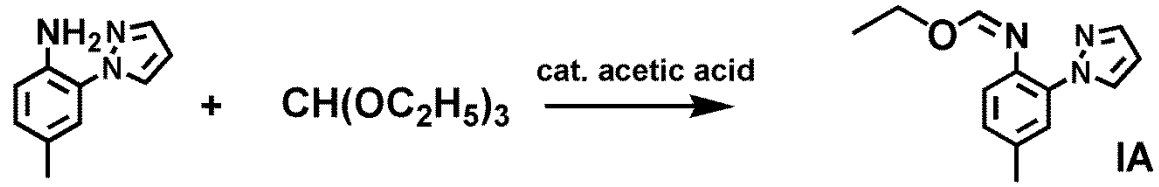

IA.

A mixture of 1.534 g (8.868 mmol) H(pzAn^{Me}), 1.47 mL (8.868 mmol) of $CH(OC_2H_5)_3$ and 30 μL of glacial acetic acid was heated at reflux for 1 hour. Then the condenser was removed and a distillation head was attached. Ethanol was removed by distillation (2 hrs). After cooling, the brown residue was extracted with 3 x 10 mL hexanes. Hexanes were removed with aid of a rotary evaporator to give 1.364 g (66 %) of desired product as a brown oil. ^{1}H NMR ($CDCl_3$): δ_H 8.03 (dd, *J* = 2.4, 0.6 Hz, 1 H), 7.67 (dd, *J* = 1.8, 0.5 Hz, 1 H), 7.66 (s, 1 H), 7.53 (d, *J* = 1.5 Hz, 1 H), 7.07 (dd, *J* = 8.2, 2.3 Hz, 1 H), 6.84 (d, *J* = 8.0 Hz, 1 H), 6.38 (dd, *J* = 2.4, 1.8 Hz, 1 H), 4.25 (quartet d, *J* = 7.1, 0.7 Hz, 2 H), 2.37 (s, CH_3), 1.31 (d, *J* = 7.1 Hz, 4 H) ppm. ^{13}C NMR ($CDCl_3$): δc 159.1, 140.6, 147.8, 133.4, 131.2, 129.9, 128.8, 124.8, 123.2, 106.4 42.3, 20.9, 20.7 ppm.

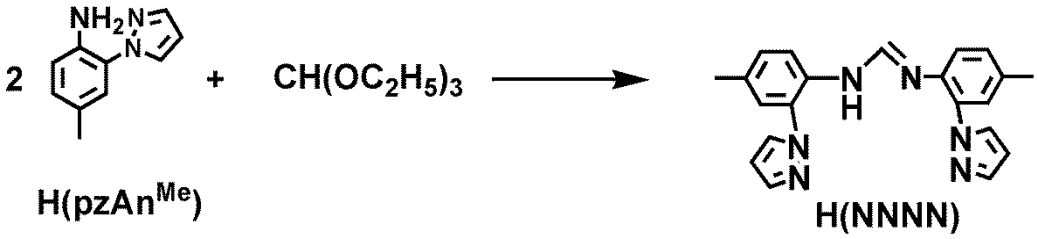

H(NNNN).

A mixture of 2.104 g (12.137 mmol) H(pzAn^{Me}), 1.01 mL (6.072 mmol) of $CH(OC_2H_5)_3$ and 35 μL of glacial acetic acid was heated at reflux for 2 hours. Then the condenser was

removed and a distillation head was attached. Then the mixture was heated for additional 2 hours during which time EtOH was completely removed by distillation. After cooling, the brown residue was washed with 3 x 10mL hexanes,10 mL diethyl ether, and then dried under vacuum to give 1.900 g (88%) of H(NNNN) as a off-white solid. M.p.: 110-111 ^{0}C. ^{1}H NMR ($CDCl_3$): δ_H 9.30 (br s, NH), 7.94 (s, 2 H), 7.90 (s, 1 H), 7.72 (s, 2 H), 7.34 (s, 2 H), 7.20 (br, 2 H), 7.07 (d, *J* = 7.9 Hz, 2 H), 6.42 (2 H), 2.36 (s, 6 H) ppm. ^{13}C NMR ($CDCl_3$): δ_C 147.6, 140.7, 133.6, 131.1 (br), 128.8, 124.7 (br), 120.0 (br), 106.8. 20.9 ppm.

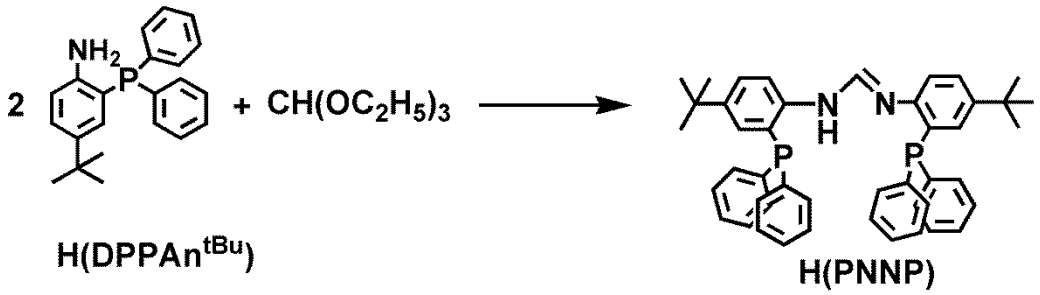

H(PNNP).

As above, a mixture of 1.167 g (3.500 mmol) H(DPPAn^{tBu}), 0.29 mL (1.75 mmol) of $CH(OC_2H_5)_3$ and 20 μL of glacial acetic acid was heated at reflux for 2 hours. Then the condenser was removed a distillation head was attached and the mixture was heated 2 hrs until EtOH has distilled. After cooling to room temperature, 1.114 g of product contaminated with trace of H(DPPAn^{tBu}) that could not be separated was collected as pale yellow solid. The H(PNNP) is soluble in all organic solvents including heptanes, hexanes, and Et_2O and was successfully used in the reactions to make alkali metal and silver salts. ^{31}P NMR ($CDCl_3$) (293 K): δ_P -17.5 (br, line width at half maximum = 324 Hz) ppm.

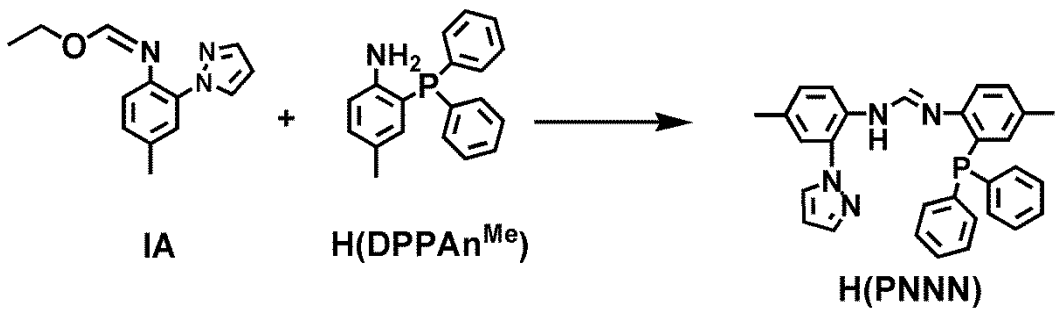

H(PNNN).

A mixture of 0.859 g (3.747 mmol) of IA, 1.092 mL (3.747 mmol) of 2-diphenylphosphino-4-methylaniline and 20 μL of glacial acetic acid was heated at reflux for 2 hours. Then the condenser was removed and a distillation head was attached. Then it was heated for additional 2 hours. After cooling to room temperature, 1.460 g of product contaminated with trace amount of H(DPPAn^{Me}) was collected as pale yellow solid. The mixture components were equally soluble in all organic solvents including heptanes, hexanes, and ether. Therefore, the mixture was used directly without further purification. ^{31}P NMR ($CDCl_3$): δ_P -14.9 (br, line width at half maximum = 230 Hz) ppm.

Na(NNNN), 1.

A solution of 0.168 g (0.415 mmol) H(NNNN) in 10 mL of THF was transferred into a suspension of 0.010 g (0.417 mmol) of NaH in 10 mL of THF. The flask originally contained ligand was washed with 5 mL of THF and the washing were transferred into the solution mixture to ensure the qualitative transfer of the ligand. The resulting yellow solution was stirred 2 hrs and THF was evaporated by vacuum distillation. The vacuum dried 0.131 g (84% yield) of **1** as a pale yellow solid was obtained. M.p.:103-104 ^{0}C. ^{1}H NMR (CD_3CN): δ_H 8.32 (s, 1 H), 7.97 (d, *J* = 2.3 Hz, 2 H, pz), 7.51 (d, *J* = 1.6 Hz, 2 H,

pz), 7.15 (s, 2 H), 6.98 (br s, 4 H), 6.29 (t, *J* = 2.2 Hz, 2 H, pz), 2.27 (s, 6 H) ppm. ^{13}C NMR (CD_3CN): δ_C 140.6, 137.4, 133.4, 133.1, 130.5, 129.6, 126.8, 121.1, 106.7, 20.7 ppm.

Crystals suitable for single crystal X-ray diffraction were grown by layering THF solution with pentane and allowing solvents to diffuse over 15 h.

K(NNNN), 2.

A solution of 0.167 g (0.467 mmol) H(NNNN) in 10 mL of THF was transferred into a solution of 0.052 g (0.467 mmol) of K^{t}OBu in 10 mL of THF. The flask originally containing H(NNNN) was washed with 5 mL of THF and it was transferred into the reaction mixture to ensure the qualitative transfer of the ligand. After stirring 2 hrs, THF was evaporated by vacuum distillation to give 0.152 g (83% yield) of **2** as a pale yellow solid. M.p.: 98-99 ^{0}C. ^{1}H NMR (CD_3CN): δ_H 8.23 (s, 1 H), 8.04 (d, *J* = 2.4 Hz, 2 H, pz), 7.60 (d, *J* = 1.7 Hz, 2 H, pz), 7.22 (s, 2 H), 7.0-7.17 (br m, 4 H), 6.37 (t, *J* = 2.0 Hz, 2 H, pz), 2.29 (s,6 H) ppm. ^{13}C NMR (CD_3CN): δ_C 141.4, 140.7, 133.2, 130.3, 130.0, 126.5, 125.7, 120.9(br), 106.8, 20.9 ppm.

Crystals suitable for single crystal X-ray diffraction were grown by layering THF solution with pentane and allowing solvents to diffuse over 15 h.

Ag(NNNN), 3.

A solution of 0.307 g (0.859 mmol) H(NNNN) in 10 mL of THF was transferred into a suspension of 0.021 g (0.859 mmol) of NaH in 10 mL of THF. The flask that originally contained H(NNNN) was washed with 5 mL of THF and the washing was transferred

into the reaction mixture. The solution of Na(NNNN) was stirred for 30 mins and then was cannula transferred into the solution of 0.221 g (0.859 mmol) of AgOTf in 10 mL THF. To ensure quantitative transfer of reagents, an additional 5 mL portion of THF was added to the "Na(NNNN)" flask and the washing was added to the reaction mixture. After the suspension had stirred 1 hour a turbid mixture formed which was stirred 12 h to ensure the completion of the reaction. Then, THF was evaporated by vacuum distillation, and the remaining solid was extracted with 2 x 20 mL dichloromethane. Dichloromethane was removed by vacuum distillation to give 0.364 g (92 % yield) of **3** as a colorless solid. M.p: 232-233 ^{0}C. Anal. Calcd for $C_{22}H_{21}AgClN_6$: C 51.06, H 3.99, N 16.62. Found: C 51.53, H 4.01, N 16.74. ^{1}H NMR ($CDCl_3$): δ_H 7.66 (s, 1 H), 7.61 (d, *J* = 2.1 Hz, 2 H, pz), 7.12 (s, 2 H), 7.07 (br, 4 H), 6.86 (d, *J* = 8.1 Hz, 2 H), 6.22 (t, *J* = 1.0 Hz, 2 H, pz), 2.30 (s, 6 H) ppm. ^{13}C NMR ($CDCl_3$): δ_C 163.4, 144.2, 140.5, 133.0, 132.8, 131.8, 129.7, 127.1, 124.3, 106.3, 20.7 ppm.

Crystals suitable for single crystal X-ray diffraction were grown by layering dichloromethane solution with hexanes and allowing solvents to diffuse over 15 h.

Ag(PNNP), 4.

A solution of 2.014 g (2.976 mmol) H(PNNP) in 20 mL of THF was transferred into the suspension of 0.072 g (2.976 mmol) NaH in 20 mL of THF. The flask originally containing H(PNNP) was washed with 10 mL of THF and the washing was transferred into the solution mixture. After strring for 30 mins, a clear solution formed that was cannula transferred into a solution of 0.765 g (2.976 mmol) AgOTf in 20 mL THF. To ensure quantitative transfer of reagents, an additional 10 mL portion of THF was added to

the flask and the washing was added to the reaction mixture. After the mixture had been stirred for 12 h, THF was evaporated by vacuum distillation, and the remaining solid was extracted with 2 x 20 mL dichloromethane. Dichloromethane was evaporated in the rotary evaporator and the remained solid was washed with 20 mL of Et_2O. The yellow Et_2O insoluble solid was vacuum dried to give 1.756 g (75 % yield) of **4**. M.p: 282- 283 ^{0}C (Decomposed). Anal. Calcd for $C_{45}H_{45}AgN_2P_2$: C 68.97, H 5.79, N 3.57. Found: C 69.26, H 6.00, N 3.74. ^{1}H NMR (CD_2Cl_2): δ_H 9.50 (s, 1 H), 7.32 (s, br, 4 H), 7.22-7.02 (m, 10 H), 6.92 (t, J = 7.1 Hz, 4 H), 6.70 (m, 8 H), 1.17 (s, 18 H) ppm. ^{13}C NMR (CD_2Cl_2): δ_C 159.7, 154.8, 142.4, 136.4, 134.4, 133.8, 132.2, 128.5, 128.4, 124.4, 116.1, 34.5, 31.6 ppm. ^{31}P NMR (CD_2Cl_2) (193 K): δ_P -16.42 (d, J_{109AgP} = 370 Hz; J_{107AgP} = 327 Hz). Crystals suitable for single crystal X-ray diffraction were grown by layering dichloromethane solution with pentane and allowing solvents to diffuse over 15 h.

Ag(PNNN), 5.

A solution of 0.8837 g (1.862 mmol) H(PNNN) in 20 mL of THF was transferred into the suspension of 0.0447 g (1.863 mmol) NaH in 20 mL of THF. The flask originally containing H(PNNN) was washed with 10 mL of THF and the washing was transferred into the solution mixture. After stirring for 30 mins, a clear solution formed that was cannula transferred into a solution of 1.4385 g (5.599 mmol) AgOTf in 20 mL THF. To ensure quantitative transfer of reagents, an additional 10 mL portion of THF was added to the flask and the washing was added to the reaction mixture. After the mixture had been stirred for 12h, THF was evaporated by vacuum distillation, and the remaining solid was extracted with 2 x 20 mL dichloromethane. Dichloromethane was evaporated in the rotary evaporator and the remained solid was washed with 20 mL of Et_2O. The white

Et_2O insoluble solid was vacuum dried to give 1.0989 g (54% yield) of **5** as a colorless solid. M.p: 238-239 ^{0}C (Decomposed). ^{1}H NMR (CD_2Cl_2): δ_H 7.86 (d, J = 2.4 Hz, 1 H), 7.68-7.56 (br s, 4 H), 7.50 (dd, J = 16.32, 12.2 Hz, 1 H), 7.40-7.28 (br s, 7 H), 7.26 (d, J = 8.1 Hz, 1 H), 7.13 (d, J = 8.1 Hz, 1 H), 7.03 (s, 1 H), 6.94 (dd, J = 7.8, 5.4 Hz, 1 H), 6.77 (d, J = 8.1 Hz, 1 H), 6.60-6.54 (m, 2 H), 2.36 (s, 3 H), 2.17 (s, 3 H) ppm. ^{13}C NMR (CD_2Cl_2): δ_C 194.4, 152.1 (d, J = 8 Hz), 143.4, 141.9, 134.8 (br), 134.5 (d, J = 7.9 Hz), 134.1, 133.1, 132.8 (d, J = 6.7 Hz), 132.5, 132.1, 131.8, 130.3, 129.5 (d, J = 11.1 Hz), 127.0, 125.6 (d, J = 4.5 Hz), 125.4, 124.7, 124.3, 107.6, 21.1, 20.7 ppm. ^{31}P NMR (CD_2Cl_2) (293 K): δ_P 0.47 (d, J_{109AgP} = 551 Hz; J_{107AgP} = 492 Hz) ppm.

Crystals suitable for single crystal X-ray diffraction were grown by layering dichloromethane solution with hexanes and allowing solvents to diffuse over 15 h.

[Ag_2(PNNP)](OTf), 6.

A mixture of 0.276 g (0.352 mmol) Ag(PNNP), **4**, and 0.091g (0.352 mmol) AgOTf was dissolved in 20 mL of THF and stirred 2 h at room temperature. THF was then removed by vacuum distillation. The white solid residue was washed with 10 mL Et_2O and vacuum dried to give 0.293 g (80% yield) of **6** as a white solid. M.p.: 220 ^{0}C (Decomposed). Anal. Calcd for $C_{51}H_{57}Ag_2F_3N_2O_3P_2S$: C 55.05, H 5.16, N 2.52. Found: C 54.16, H 4.92, N 2.66. ^{1}H NMR (CD_2Cl_2): δ_H 7.5-7.35 (m, 20 H), 7.32 (dd, J = 8.1, 2.0 Hz, 2 H), 6.87 (s, 1 H), 6.78 (m, 2 H), 6.11 (s, 2 H), 1.1 (s, 18 H) ppm. ^{13}C NMR (CD_2Cl_2): δ_C 167.0, 151.5, 148.2, 134.7 (br), 131.9, 130.8, 129.9 (br), 126.1, 123.2, 37.9, 31.3 ppm. ^{31}P NMR (CD_2Cl_2) (293 K): δ_P 0.6 (d, J = 498 Hz) , (253 K) 0.6 (dd, J = 551, 492 Hz) ppm.

Crystals suitable for single crystal X-ray diffraction were grown by layering dichloromethane solution with hexanes and allowing solvents to diffuse over 15 h.

[AgCu(PNNP)](PF$_6$), 7.

A solution of 0.1208 g (0.154 mmol) of **4** in 10 mL of THF was cannula transferred into the solution of 0.0336g (0.105 mmol) Cu(CH_3CN)$_4$(PF_6) in 10 mL of acetonitrile. The resulting solution was stirred for 15 h, then solvent was evaporated to yield 0.0705 g of **7** contaminated with starting material **4**. Crystals of **7** suitable for single crystal X-ray diffraction were grown by layering dichloromethane solution with hexanes and allowing solvents to diffuse over 15 h. ^{1}H NMR (CD_2Cl_2): δ_H 7.75 (t, J = 7.1 Hz, 2 H), 7.68-7.56 (m, 6 H), 7.55-7.45 (m, 8 H), 7.38-7.3 (m, 4 H), 7.28 (dd, J = 8.5, 2.3 Hz, 2 H), 6.7 (t, J = 4Hz, 2 H), 6.21 (s, 1 H), 5.7 (dt, J = 8.1, 3.0 Hz, 2 H), 1.1 (s, 18 H) ppm. ^{31}P NMR (CD_2Cl_2) (293 K): δ_P 2.33 (d, J_{109AgP} = 563 Hz; J_{107AgP} = 490 Hz).

[AgAu(PNNP)](OTf), 8.

A mixture of 0.1089 g (0.105 mmol) of **6** and 0.0336g (0.105 mmol) AuCl(SC_4H_8) was stirred in 20 mL of CH_2Cl_2 for 15 h. The soluble part was separated from a white precipitate (AgCl) by filtration. Solvents were removed by vacuum distillation to give 0.0705 g of product contaminated with the starting material **6**. Compound **8** was crystallized by layering pentane on top of CH_2Cl_2 solution. ^{1}H NMR (CD_2Cl_2): δ_H 7.86 (t, J = 6.3 Hz, 2 H), 7.73 (t, J = 7.5 Hz, 4 H), 7.68-7.46 (m, 14 H), 7.33 (d, J = 8 Hz, 2 H), 6.71 (t, J = 6.8 Hz, 2 H), 5.57 (d, 7.6 Hz, 2 H), 1.1 (s, 18 H) ppm. ^{31}P NMR (CD_2Cl_2) (293 K): δ_P 35.2 (d, J = 6.3 Hz) ppm. ^{19}F (CD_2Cl_2): δ_F -79 ppm.

Crystals suitable for single crystal X-ray diffraction were grown by layering dichloromethane solution with pentane and allowing solvents to diffuse over 15 h.

Investigation of Catalytic Activity.

In a dry 100 mL Schlenk flask, a suspension of PhI=NTs (0.186 g, 0.5 mmol), metal complex (0.02 mmol), 4 Å activated molecular sieves (0.5 g), and styrene (2.5 mmol, 5 equiv.) in CH_3CN was stirred for 12 hrs at room temperature under argon. The reaction mixture was filtered through a short pad of Celite and the filter cake was washed with 25 mL CH_2Cl_2. The combined filtrates were concentrated under reduced pressure and aziridine was collected by a silica column using 4:1 hexane:EtOAc as the eluent (R_f = 0.52).

BIBLIOGRAPHY

CHAPTER 1

1) Li, J. R.; Kuppler, J.; Zhou, H.C. *Chem. Soc. Rev*. **2009**, *38*, 1477.

2) Cook, T. R.; Zheng, Y. R.; Stang, P. J. *Chem. Rev*. **2013**, *113*, 734.

3) Stock, N.; Biswas, S. *Chem. Rev*. **2012**, *112*, 933.

4) Shustova, N. B.; McCarthy, B. D.; Dinca, M. *J. Am. Chem. Soc.* **2011**, *133*, 20126.

5) Bradshaw, D.; Prior, T. J.; Cussen, E. J.; Claridge, J. B.; Rosseinsky, M. J. *J. Am. Chem. Soc*. **2004**, *126*, 6106.

6) Cui, J.; Wong, Y.; Zeller, M.; Hunter, A. D.; Xu, Z. *Angew. Chem. Int. Ed*. **2014**, *53*, 14438.

7) Sun, D.; Fu, Y.; Liu, W.; Ye, L.; Wang, D.; Yang, L.; Fu, X.; Li, Z. *Chem. Eur. J.* **2013**, *19*, 14279.

8) Narayan, T. C.; Miyaki, T.; Seki, S.; Dinca, M. *J. Am. Chem. Soc*. **2012**, *134*, 12932.

9) Alvaro, M.; Carbonell, E.; Ferrer, B.; Xamena, F. X. L.; Garcia, H.; *Chem. Eur. J.* **2007**, *13*, 5106.

10) Talin, A. A.; Centrone, A.; Ford, A. C.; Foster, M. E.; Stavila, V.; Haney, P.; Kinney, R. A.; Szalai, V.; Gabaly, F. E.; Yoon, H. D.; Leonard, F.; Allendorf, M. D. *Science* **2014**, *343*, 66.

11) Duhovic, S.; Dinca, M. *Chem. Mater*. **2015**, *27*, 5487.

12) Sun, L.; Hendon, C. H.; Minier, M. A.; Walsh, A.; Dinca, M. *J. Am. Chem. Soc.* **2015**, *137*, 6164.

13) Campbell, M. G.; Sheberla, D.; Liu, S. F.; Swager, T. M.; Dinca, M. *Angew. Chem. Int. Ed.* **2015**, *54*, 4349.

14) Park, S. S.; Hantz, E. R.; Sun, L.; Hendon, C. H.; Walsh, A.; Voorhis, T. V.; dinca, M. *J. Am. Chem. Soc*. **2015**, *137*, 1774.

15) Sheberla, D.; Sun, L.; Martin, A.; Forsythe, B.; Suleyman, E.; Wade, C. R.; Brozek, C. K.; Gazik, A. A.; Dinca, M. *J. Am. Chem. Soc*. **2014**, *136*, 8859.

16) Wade, C. R.; Li, M.; Dinca, M. *Angew, Chem. Int. Ed*. **2013**, *52*, 13377.

17) Alessandro, D. M.; Kanga, J. R. R.; Caddy, J. S. *Aust. J. Chem*. **2011**, *64*, 718.

18) Zhu, H.; Shan, R.; Wu, Y.; Lou, Y.; *Eur. J. Inorg. Chem*. **2014**, 1356.

19) Stavila, V.; Talin, A. A.; Allendorf, M. D. *Chem. Soc, Rev*. **2014**, *43*, 5994.

20) Solomon, E. I.; Xie, X.; Dey, A. *Chem. Soc. Rev*. **2008**, *37*, 613.

21) Schinzel, S.; Schraut, J.; Arbuznikov, A. V.; Siegbahn, P. E. M.; Kaupp, M. *Chem. Eur. J*. **2010**, *16*, 10424.

22) Siebahn, P. E. M. *Acc. Chem. Res*. **2009**, *42*, 1871.

23) Antholine, W. E.; Kastrau, D. H. W.; Steffens, G. C. M.; Buse, G.; Zumft, W. G.; Knoneck, P. M. H. *Eur. J. Biochem*. **1992**, *209*, 875.

24) Barbara, P. F.; Meyer, T. J.; Ratner, M. A. *J. Phys. Chem*. **1996**, *100*, 13148.

25) *Chem. Rev*. **1992**, *92*, 369. This issue is devoted to electron transfer processes in biological systems.

26) Wasielewski, M. R. *Chem. Rev*. **1992**, *92*, 435.

27) Low, P. J. *Dalton Trans*. **2005**, 2821.

28) Launay, J. P. *Chem. Soc. Rev*. **2001**, *30*, 386.

29) Coat, F.; Lapinte, C. *Organometallics* **1996**, *15*, 477.

30) Paul, F.; Lapinte, C. *Corrd. Chem. Rev*. **1998**, *178*, 431.

31) Venkasesan, K.; Blacque, O.; Berke, H. *Dalton Trans*. **2007**, 1091.

32) Kaim, W.; Lahiri, G. K. *Angew. Chem. Int. Ed*. **2007**, 1091.

33) Miller, J. S.; Epstein, A. J. *Angew. Chem. Int. Ed*. **1984**, *33*, 385.

34) Chisholm, M. H.; Patmore, N. J. *Acc. Chem. Res*. **2007**, *40*, 19.

35) Nast, R. *Coord. Chem. Rev*. **1982**, *47*, 89.

36) Petty, M. C.; Bryce, M. R.; Bloor, D. Introduction to molecular electronics, Oxford University press, New York, **1995**.

37) Carroll, R. L.; Gorman, C. B. *Angew. Chem. Int. Ed*. **2002**, *41*, 4378.

38) Torres, F. S.; Hutchison, G. R.; Stoltzberg, L. J.; Abruna, H. D. *J. Am. Chem. Soc*. **2006**, *128*, 1513.

39) Creutz, C.; Taube, H. *J. Am. Chem. Soc*. **1969**, *91*, 3988.

40) Creutz, C.; Taube, H. *J. Am. Chem. Soc*. **1973**, *95*, 1086.

41) Demadis, K. D.; Hartshorn, C. M.; Meyer, T. J. *Chem. Rev*. **2001**, *101*, 2655.

42) Reimers, J. R.; Hush, N. S. *Inorg. Chem*. **1990**, *29*, 3686.

43) Lambert, C.; Noll, G. *J. Am. Chem. Soc*. **1999**, *121*, 8434.

44) Heckmann, A.; Lambert, C. *Angew, Chem. Int. Ed*. **2012**, *51*, 326.

45) Yao, C.; Yao, J.; Zhong, Y. *Inorg. Chem*. **2011**, *50*, 6847.

46) Barlow, S.; Risko, C.; Chung, S. J.; Tucker, N. M.; Coropceanu, V.; Jones, S. C.; Levi, Z.; Bredas, J.; Marder, S. R. *J. Am. Chem. Soc*. **2005**, *127*, 16900.

47) Lambert, C.; Amthor, S.; Schelter, J. *J. Phys. Chem. A* **2004**, *108*, 6474.

48) Kaupp. M.; Renz, M.; Parthey, M.; Stolte, M.; Wurthner, F.; Lambert, C. *Phys. Chem. Chem. Phys.* **2011**, *13*, 16973.

49) Volker, S. F.; Renz, M.; Kaupp, M.; Lambert, C. *Chem. Eur. J*. **2011**, *17*, 14147.

50) Nelsen, S. F.; Ismagilov, R. F.; Powell, D. R. *J. Am. Chem. Soc.* **1996**, *118*, 6313.

51) Lambert, C.; Risko, C.; Coropceanu, V.; Schelter, J.; Amthor, S.; Gruhn, N. E.; Durivage, J. C.; Bredas, J. L. *J. Am. Chem. Soc*. **2005**, *127*, 8508.

52) Coropceanu, V.; Malagoli, M.; Andre, J. M.; Bredas, J. L. *J. Am. Chem. Soc*. **2002**, *124*, 10519.

53) Keniley, L. K.; Dupont, N.; Ray, L.; Ding, J.; Kovnir, K.; Hoyt, J. M.; Hauser, A.; Shatruk, M. *Inorg. Chem*. **2013**, *52*, 8040.

54) McClenaghan, N. D.; Passalacqua, R.; Loiseau, F.; Campagna, S.; Verheyde, B.; Hameurlaine, A.; Dehaen, W. *J. Am. Chem. Soc*. **2003**, *125*, 5356.

55) Nelsen, S. F.; Chang, H.; Wolff, J. J.; Adamus, J. *J. Am. Chem. Soc.* **1993**, *115*, 12276.

56) Nelsen, S. F.; Ismagilov, R. F.; Powell, D. R. *J. Am. Chem. Soc.* **1996**, *118*, 6313.

57) Jozefiak, T. H.; Miller, L. L. *J. Am. Chem. Soc.* **1987**, *109*, 6560.

58) Nelsen, S. F.; Weaver, M. N.; Zink, J. I. *J. Am. Chem. Soc.* **2005**, *127*, 10611.

59) Lu, J. M.; Rosokha, S. V.; Lindeman, S. V.; Neretin, I. S.; Kochi, J. K. *J. Am. Chem. Soc*. **2005**, *127*, 1797.

60) Robin, M.; Day, P. *Adv. Inorg. Radiochem*. **1967**, *10*, 247.

61) Demadis, K. D.; Hartshorn, C. M.; Meyer, T. J. *Chem Rev*. **2001**, *1001*, 2655.

62) Brunschwig, B. S.; Creutz, C.; Sutin, N. *Chem. Soc. Rev*. **2002**, *31*, 168.

63) Hush, N. S. *Prog. Inorg. Chem*. **1967**, *8*, 391.

64) Hush, N. S. *Coord. Chem. Rev*. **1985**, *64*, 135.

65) Marcus, R. A.; Sutin, N. *Biochim. Biophys. Acta* **1985**, *30*, 441.

66) Wanniarachchi, S.; Liddle, B. J.; Toussaint, J.; Lindeman, S. V.; Bennett, B.; Gardinier, J. R. *Dalton Trans*. **2010**, *39*, 3167.

67) Wanniarachchi, S.; Liddle, B. J.; Toussaint, J.; Lindeman, S. V.; Bennett, B.; Gardinier, J. R. *Dalton Trans*. **2011**, *40*, 8776.

68) Wanniarachchi, S.; Liddle, B. J.; Lindeman, S. V.; Gardinier, J. R. *J. Organomet. Chem*. **2011**, *696*, 3623.

69) Liddle, B. J.; Wanniarachchi, S.; Hewage, J. S.; Lindeman, S. V.; Bennett, B.; Gardinier, J. R. *Inorg. Chem*. **2012**, *51*, 12720.

70) Wanniarachchi, S.; Liddle, B. J.; Kizer, B.; Hewage, J. S.; Lindeman, S. V.; Gardinier, J. R. *Inorg. Chem*. **2012**, *51*, 10572.

71) Abbott, A. P.; Rusling, J. F. *J. Phys. Chem*. **1990**, *94*, 8910.

72) Deanna, M.; Alessandro, D.; Keene, F. R. *Chem. Soc. Rev*. **2006**, *35*, 424.

73) Bard, A. J.; Faulkner, L. R. *Electrochemical Methods, Fundaments and Applications; John Wiley and Sons*: New York, **1995**.

74) Dong, T. Y.; Lin, H. Y.; Lin, S. F.; Huang, C. C.; Wen, Y. S.; Lee, L. *Organometallics* **2008**, *27*, 555.

75) Dong, T. Y.; Lee, S. H.; Chang, C. K.; Lin, H. M.; Lin, K. J. *Organometallics* **1997**, *16*, 2773.

76) Ghosh, P.; Samanta, S.; Roy, S. K.; Demeshko, S.; Meyer, F.; Goswami, S. *Inorg. Chem.* **2014**, *53*, 4678.

CHAPTER 2

1) (a) Kaim, W. Eur. *J. Inorg. Chem*. **2012**, *3*, 343−348. (b) Caulton, K. G. *Eur. J. Inorg. Chem*. **2012**, *3*, 435−443. (c) Kaim, W. *Inorg. Chem*. **2011**, *50*, 9752−9765. (d) Forum on redox-active Ligands: Kaim, W. *Inorg. Chem*. **2011**, *50*, 9737−9914. (e) Kaim, W.; Schwederski, B. *Coord. Chem. Rev.* **2010**, *254*, 1580−1588.

2) (a) Ray, K.; Petrenko, T.; Wieghardt, K.; Neese, F. *Dalton Trans*. **2007**, 1552−1566. (b) Hirao, T. *Coord. Chem. Rev*. **2002**, *226*, 81−91.(c) Pierpont, C. G. *Coord. Chem. Rev*. **2001**, 216−217, 99−125.

3) (a) Munha, R. F.; Zarkesh, R. A.; Heyduk, A. F. Dalton Trans. 2013, 42, 3751−3766. (b) Luca, O. R.; Crabtree, R. H. Chem. Soc. Rev. 2013, 42, 1440−1459. (c) Praneeth, V. K. K.; Ringenberg, M. R.; Ward, T. R. Angew. Chem., Int. Ed. 2012, 51, 10228−10234. (d) Lyaskovskyy, V.; de Bruin, B. ACS Catal. 2012, 2, 270−279. (e) Pratt, R. C.; Lyons, C. T.; Wasinger, E. C.; Stack, T. D. P. J. Am. Chem. Soc. 2012, 134, 7367−7377.

4) (a) Paul, N. D.; Rana, U.; Goswami, S.; Mondal, T. K.; Goswami, S. *J. Am. Chem. Soc.* **2012**, *134*, 6520−6523. (b) Givaja, G.; AmoOchoa, P.; Gómez-García, C. J.; Zamora, F. *Chem. Soc. Rev*. **2012**, *41*, 115−147. (c) Hou, C.; Peng, J.; Xu, Q.; Ji, Z.; Hu, X. *RSC Adv*. **2012**, *2*, 12696−12698 and references. (d) Allendorf, M. D.; Schwartzberg, A.; Stavila, V.; Talin, A. A. *Chem.Eur. J*. **2011**, *17*, 11372−11388. (e) Evangelio, E.; Ruiz-Molina, D. *Eur. J. Inorg. Chem*. **2005**, *15*, 2957−2971.

5) For example: (a) Fortier, S.; Le Roy, J. J.; Chen, C.-H.; Vieru, V.; Murugesu, M.; Chibotaru, L. F.; Mindiola, D. J.; Caulton, K. G. *J. Am. Chem. Soc.* **2013**, *135*, 14670−14678. (b) Matson, E. M.; Opperwall, S. R.; Fanwick, P. E.; Bart, S. C. *Inorg. Chem*. **2013**, *52*, 7295−7304. (c) Matsumoto, T.; Chang, H.-C.; Wakizaka, M.; Ueno, S.; Kobayashi, A.; Nakayama, A.; Taketsugu, T.; Kato, M. *J. Am. Chem. Soc*. **2013**, *135*, 8646−8654. (d) Tsvetkov, N. P.; Chen, C.-H.; Andino, J. G.; Lord, R. L.; Pink, M.; Buell, R. W.; Caulton, K. G. *Inorg. Chem*. **2013**, *52*, 9511−9521. (e) Ghosh, P.; Samanta, S.; Roy, S. K.; Joy, S.; Krämer, T.; McGrady, J. E.; Goswami, S. *Inorg. Chem*. **2013**, *52*, 14040−14049 and references. (f) Lippert, C. A.; Riener, K.; Soper, J. D. *Eur. J. Inorg. Chem*. **2012**, *3*, 554−561. (g) Cates, C. D.; Myers, T. W.; Berben, L. A. *Inorg. Chem*. **2012**, *51*, 11891−11897. (h) Ouch, K.; Mashuta, M. S.; Grapperhaus, C. A. *Inorg. Chem*. **2011**, *50*, 9904−9914. (i) Ringenberg, M. R.; Kokatam, S. L.; Heiden, Z. M.; Rauchfuss, T. B. *J. Am. Chem. Soc*. **2008**, *130*, 788−789. (j) Chaudhuri, P.; Wagner, R.; Pieper, U.; Biswas, B.; Weyhermüller, T. *Dalton Trans*. **2008**, 1286−1288. (k) Verani, C. N.; Gallert, S.; Bill, E.; Weyhermüller, T.; Weighardt, K.; Chaudhuri, P. *Chem. Commun*. **1999**, 1747−1748.

6) (a) Ghosh, P.; Samanta, S.; Roy, S. K.; Demeshko, S.; Meyer, F.; Goswami, S. *Inorg. Chem*. **2014**, *53*, 4678−4686. (b) Fullmer, B. C.; Fan, H.; Pink, M.;

Huffman, J. C.; Tsvetkov, N. P.; Caulton, K. G. *J. Am. Chem. Soc*. **2011**, *133*, 2571−2582. (c) He, T.; Tsvetkov, N. P.; Andino, J. G.; Gao, X.; Fullmer, B. C.; Caulton, K. G. *J. Am. Chem. Soc*. **2010**, *132*, 910−911. (d) Rimmer, R. D.; Grills, D. C.; Fan, H.; Ford, P. C.; Caulton, K. G. *J. Am. Chem. Soc*. **2007**, *129*, 15430−15431.

7) (a) Hojilla Atienza, C. C.; Milsmann, C.; Semproni, S. P.; Turner, Z. R.; Chirik, P. J. *Inorg. Chem.* **2013**, *52*, 5403−5417. (b) Tondreau, A. M.; Stieber, S. C. E.; Milsmann, C.; Lobkovsky, E.; Weyhermuller, T.; Semproni, S. P.; Chirik, P. J. *Inorg. Chem*. **2013**, *52*, 635−646. (c) Darmon, J. M.; Stieber, S. C. E.; Sylvester, K. T.; Fernandez, I.; Lobkovsky, E.; Semproni, S. P.; Bill, E.; Wieghardt, K.; DeBeer, S.; Chirik, P. J. *J. Am. Chem. Soc*. **2012**, *134*, 17125−17137. (d) Russell, S. K.; Bowman, A. C.; Lobkovsky, E.; Wieghardt, K.; Chirik, P. J. *Eur. J. Inorg. Chem.* **2012**, 535−545. (e) Russell, S. K.; Milsmann, C.; Lobkovsky, E.; Weyhermuller, T.; Chirik, P. J. *Inorg. Chem*. **2011**, *50*, 3159−3169. (f) Bowman, A. C.; Milsmann, C.; Bill, E.; Lobkovsky, E.; Weyhermuller, T.; Wieghardt, K.; Chirik, P. J. *Inorg. Chem*. **2010,** *49*, 6110−6123. (g) Bowman, A. C.; Milsmann, C.; Hojilla Atienza, C. C.; Lobkovsky, E.; Wieghardt, K.; Chirik, P. J. *J. Am. Chem. Soc.* **2010**, *132*, 1676−1684.

8) (a) Mossin, S.; Tran, B. L.; Adhikari, D.; Pink, M.; Heinemann, F. W.; Sutter, J.; Szilagyi, R. K.; Meyer, K.; Mindiola, D. J. *J. Am. Chem. Soc*. **2012**, *134*, 13651−13661. (b) Kilgore, U. J.; Sengelaub, C. A.; Fan, H.; Tomaszewski, J.; Karty, J. A.; Baik, M.-H.; Mindiola, D. J. *Organometallics* **2009**, *28*, 843−852. (c) Adhikari, D.; Mossin, S.; Basuli, F.; Dible, B. R.; Chipara, M.; Fan, H.; Huffman, J. C.; Meyer, K.; Mindiola, D. J. *Inorg. Chem*. **2008**, *47*, 10479−10490. (d) Adhikari, D.; Mossin, S.; Basuli, F.; Huffman, J. C.; Szilagyi, R. K.; Meyer, K.; Mindiola, D. J. *J. Am. Chem. Soc*. **2008**, *130*, 3676−3682. (e) Fafard, C. M.; Adhikari, D.; Foxman, B. M.; Mindiola, D. J.; Ozerov, O. V. *J. Am. Chem. Soc*. **2007**, *129*, 10318−10319.

9) (a) Smith, D. A.; Herbert, D. E.; Walensky, J. R.; Ozerov, O. V. *Organometallics* 2013, 32, 2050−2058. (b) Bacciu, D.; Chen, C.-H.; Surawatanawong, P.; Foxman, B. M.; Ozerov, O. V. *Inorg. Chem*. **2010**, *49*, 5328−5334. (c) Radosevich, A. T.; Melnick, J. G.; Stoian, S. A.; Bacciu, D.; Chen, C.-H.; Foxman, B. M.; Ozerov, O. V.; Nocera, D. G. *Inorg. Chem*. **2009**, *48*, 9214−9221.

10) (a) Klein, A.; Vicic, D. A.; Biewer, C.; Kieltsch, I.; Stirnat, K.; Hamacher, C. *Organometallics* **2012**, *31*, 5334−5341. (b) Madhira, V. N.; Ren, P.; Vechorkin, O.; Hu, X.; Vicic, D. A. *Dalton Trans*. **2012**, *41*, 7915−7919. (c) Kieltsch, I.; Dubinina, G. G.; Hamacher, C.; Kaiser, A.; Torres-Nieto, J.; Hutchison, J. M.; Klein, A.; Budnikova, Y.; Vicic, D. A. *Organometallics* **2010**, *29*, 1451−1456.

11) (a) Munha, R. F.; Zarkesh, R. A.; Heyduk, A. F. *Inorg. Chem*. **2013**, *52*, 635−646. (b) Wong, J. L.; Sanchez, R. H.; Logan, J. G.; Zarkesh, R. A.; Ziller, J. W.; Heyduk, A. F. *Chem. Sci*. **2013**, *4*, 1906−1910. (c) Shaffer, D. W.; Szigethy,

G.; Ziller, J. W.; Heyduk, A. F. *Inorg. Chem*. **2013**, *52*, 2110−2118. (d) Szigethy, G.; Heyduk, A. F. *Dalton Trans*. **2012**, *41*, 8144−8152. (e) Szigethy, G.; Shaffer, D. W.; Heyduk, A. F. *Inorg. Chem*. **2012**, *51*, 12606−12618. (f) Lu, F.; Zarkesh, R. A.; Heyduk, A. F. Eur. J. *Inorg. Chem*. **2012**, 467−470. (g) Heyduk, A. F.; Zarkesh, R. A.; Nguyen, A. I. *Inorg. Chem*. **2011**, *50*, 9849−9863. (h) Nguyen, A. I.; Blackmore, K. J.; Carter, S. M.; Zarkesh, R. A.; Heyduk, A. F. *J. Am. Chem. Soc*. **2009**, *131*, 3307−3316.

12) (a) Breitenfeld, J.; Ruiz, J.; Wodrich, M. D.; Hu, X. *J. Am. Chem. Soc*. **2013**, *135*, 12004−12012. (b) Breitenfeld, J.; Scopelliti, R.; Hu, X. *Organometallics* **2012**, *31*, 2128−2136. (c) Breitenfeld, J.; Vechorkin, O.; Corminboeuf, C.; Scopelliti, R.; Hu, X. *Organometallics* **2010**, *29*, 3686−3689. (d) Vechorkin, O.; Csok, Z.; Scopelliti, R.; Hu, X. L. *Chem. Eur. J*. **2009**, *15*, 3889−3899. (e) Vechorkin, O.; Hu, X. L. Angew. *Chem., Int. Ed*. **2009**, *48*, 2937−2940. (f) Csok, Z.; Vechorkin, O.; Harkins, S. B.; Scopelliti, R.; Hu, X. *J. Am. Chem. Soc*. **2008**, *130*, 8156−8157.

13) Wright, D. D.; Brown, S. N. *Inorg. Chem*. **2013**, *52*, 7831−7833.

14) Myers, T. W.; Berben, L. A. *J. Am. Chem. Soc*. **2013**, *135*, 9988−9990.

15) (a) Frazier, B. A.; Williams, V. A.; Wolczanski, P. T.; Bart, S. C.; Meyer, K.; Cundari, T. R.; Lobkovsky, E. B. *Inorg. Chem*. **2013**, *52*, 3295−3312. (b) Frazier, B. A.; Bartholomew, E. R.; Wolczanski, P. T.; DeBeer, S.; Santiago-Berrios, M.; Abruña, H. D.; Lobkovsky, E. B.; Bart, S. C.; Mossin, S.; Meyer, K.; Cundari, T. R. *Inorg. Chem*. **2011**, *50*, 12414−12436.

16) (a) Gloaguen, Y.; Jacobs, W.; de Bruin, B.; Lutz, M.; van der Vlugt, J. I. *Inorg. Chem*. **2013**, *52*, 1682−1684. (b) Tejel, C.; Ciriano, M. A.; del Río, M. P.; van den Bruele, F. J.; Hetterscheid, D. G. H.; Spithas, N. T.; de Bruin, B. *J. Am. Chem. Soc*. **2008**, *130*, 5844−5845. (c) Hetterscheid, D. G. H.; Klop, M.; Kicken, R. J. N. A. M.; Smits, J. M. M.; Reijerse, E. J.; de Bruin, B. *Chem. Eur. J*. **2007**, *13*, 3386−3405.

17) (a) Puschmann, F. F.; Harmer, J.; Stein, D.; Rüegger, H.; de Bruin, B.; Grützmacher, H. *Angew. Chem., Int. Ed*. **2009**, *49*, 385−389. (b) Büttner, T.; Geier, J.; Frison, G.; Harmer, J.; Calle, C.; Schweiger, A.; Schönberg, H.; Grützmacher, H. *Science* **2005**, *307*, 235−238.

18) Niwa, T.; Nakada, M. *J. Am. Chem. Soc*. **2012**, *134*, 13538−13541.

19) (a) Liddle, B. J.; Wanniarachchi, S.; Hewage, J. S.; Lindeman, S. V.; Bennett, B.; Gardinier, J. R. *Inorg. Chem*. **2012**, *51*, 12720−12728. (b) Wanniarachchi, S.; Liddle, B. J.; Kizer, B.; Hewage, J. S.; Lindeman, S. V.; Gardinier, J. R. *Inorg. Chem*. **2012**, *51*, 10572−10580. (c) Wanniarachchi, S.; Liddle, B. J.; Lindeman, S. V.; Gardinier, J. R. J. *Organomet. Chem*. **2011**, *696*, 3623−3636. (d)

Wanniarachchi, S.; Liddle, B. J.; Toussaint, J.; Lindeman, S. V.; Bennett, B.; Gardinier, J. R. *Dalton Trans.* **2011**, *40*, 8776−8787. (e) Wanniarachchi, S.; Liddle, B. J.; Toussaint, J.; Lindeman, S. V.; Bennett, B.; Gardinier, J. R. *Dalton Trans.* **2010**, *39*, 3167−3169.

20) CrysAlisPro, Agilent Technologies,Version 1.171.34.46 (release 25-11-2010 CrysAlis171.NET), compiled Nov 25 2010,17:55:46.

21) SAINT+ Version 7.23a and SADABS Version 2004/1; Bruker Analytical Xray Systems, Inc.: Madison, WI, 2005.

22) Sheldrick, G. M. SHELXTL Version 6.12; Bruker Analytical Xray Systems, Inc.: Madison, WI, 2001.

23) SCALE3 ABSPACK - An Oxford Diffraction program (1.0.4,gui:1.0.3) (C); Oxford Diffraction Ltd., 2005.

24) As per a reviewer's query, it has not yet proven possible to isolate pure heteroleptic (X,Y)NiCl complexes from the dark green reaction mixtures obtained when using equimolar quantities of $NiCl_2$, pincer ligand, and base. Instead, the orange symmetrized product, $Ni(X,Y)_2$, is recovered from such attempts after solvent removal. Further efforts in this vein, using sterically encumbered pincer variants, are underway, and results will be reported in due course.

25) The single-crystal diffraction study of $3{\cdot}CH_2Cl_2$ shows a layered supramolecular structure where molecules of 3 are held together by CH···π and π···π noncovalent interactions. The solvate molecules are retained between sheets with [(solvate)CH···π (aryl) and (pz)CH···Cl] noncovalent interactions. It can be speculated that similar noncovalent interactions may be involved in the capture and retention of water molecules. Unfortunately, we were unsuccessful at completely removing solvent from $3{\cdot}CH_2Cl_2$, and because adventitious water replaces CH_2Cl_2 in dried samples, it is simply easier to work with the hemihydrate.

26) Lever, A. B. P. *Inorg. Chem*. **1965**, *4*, 763−764.

27) (a) Renger, T. *Phys. Rev. Lett.* **2004**, *93*, 188101-1−188101-4. (b) Holmes, O. G.; McClure, D. S. J. *Chem. Phys*. **1957**, *26*, 1686−1694.

28) (a) Patra, A. K.; Mukherjee, R. *Inorg. Chem*. **1999**, *38*, 1388−1393. (b) Mueller, H.; Bauer-Siebenlist, B.; Csapo, E.; Dechert, S.; Farkas, E.; Meyer, F. *Inorg. Chem*. **2008**, *47*, 5278−5292. (c) Michaud, A.; Fontaine, F.-G.; Zargarian, D. *Acta Crystallogr*. **2005**, E61, m784−m786. (d) Hirotsu, M.; Tsukahara, Y.; Kinoshita, I. Bull. *Chem. Soc. Jpn*. **2010**, *83*, 1058−1066. (e) Baker, A. T.; Craig, D. C.; Rae, A. D. *Aust. J. Chem*. **1995**, *48*, 1373−1378. (f) Astley, T.; Gulbis, J. M.;

Hitchman, M. A.; Tiekink, E. R. T. *J. Chem. Soc., Dalton Trans*. **1993**, 509−515. (g) Reimann, C. W. *J. Phys. Chem*. **1970**, *74*, 561−568.

29) Kasha, M.; Rawls, R. *Photochem. Photobiol*. **1968**, *7*, 561.

30) Hansch, C.; Leo, A.; Taft, R. W. *Chem. Rev*. **1991**, *91*, 165−195.

31) (a) McDaniel, A. M.; Rappé, A. K.; Shores, M. P. *Inorg. Chem*. **2012**, *51*, 12493−12502. (b) Sasaki, Y. Bull. *Inst. Chem. Res.*, Kyoto Univ. **1980**, *58*, 187−192. (c) Robinson, M. A.; Curry, J. R.; Busch, D. B. *Inorg. Chem*. **1963**, *2*, 1178−1181.

32) (a) DeAlwis, D. C. L.; Schulz, F. A. *Inorg. Chem*. **2003**, *42*, 3616−3622. (b) Nolet, M. C.; Michaud, A.; Bain, C.; Zargarian, D.; Reber, C. *Photochem. Photobiol*. **2006**, *82*, 57−63.

33) The independence of lowest energy NIR transition and the nature of para-aryl substituents indicate that the LUMO must also contain substantial ligand character.

34) (a) Crutchley, R. J. *Adv. Inorg. Chem*. **1994**, *41*, 273−325. (b) Zanello, P. Inorganic Electrochemistry: Theory, Practice and Applications; Royal Society of Chemistry: Cambridge, 2003; pp 174−178. (c) Astruc, D. Electron Transfer and Radical Processes in Transition-Metal Chemistry; VCH Publishers, Inc.: New York, 1995; pp 34−36.

35) Winter, R. F. *Organometallics* **2014**, Article ASAP, DOI: 10.1021/om500029x.

36) (a) Luo, S.; Averkiev, B.; Yang, K. R.; Xu, X.; Truhlar, D. G. *J. Chem. Theory Comput.* **2014,** *10*, 102−121. (b) Neese, F. J. *Phys. Chem. Solids* **2004**, *65*, 781−785. (c) Ruiz, E.; Cano, J.; Alvarez, S.; Alemany, P. *J. Comput. Chem*. **1999**, *20*, 1391−1400. (d) Caballol, R.; Castell, O.; Illas, F.; Moreira, I.; de, P. R.; Malrieu. *J. Phys. Chem*. *A* **1997**, *101*, 7860−7866. (e) Noodleman, L. *J. Chem. Phys*. **1981**, *74*, 5737−5743.

37) (a) Hush, N. S. Prog. *Inorg. Chem*. **1967**, *8*, 391−444. (b) Hush, N. S. Coord. *Chem. Rev*. **1985**, *64*, 135−157.

38) A reviewer noted that the N···N distance might not be the best distance to describe the electronic coupling because the charge was delocalized over the ligand via the quinoidal distortion. If the d value is changed to 8.425 Å, which is an estimate of the longest aryl−aryl centroid−centroid distance in $(1)^{+}$ from experimental structures of 1 and $(1)^{2+}$, then H_{ab} of 1 is reduced to 226 cm^{-1}, and this value would represent a lower limit of electronic coupling strength. A similar calculation on the gallium complex gives H_{ab} = 125 cm^{-1}. Regardless, the conclusions derived from calculations using either d value remain the same.

39) These values are slightly different than those reported in ref 19a.There was a typographical error in the $E_{1/2}(1)$ entry of Table 1 of the previous publication, which should read 0.989(3) instead of 0.939(3).

40) Brunschwig, B. S.; Creutz, C.; Sutin, N. *Chem. Soc. Rev*. **2002**, *31*, 168−184.

41) Marcus, R. A.; Sutin, N. *Biochim. Biophys. Acta* **1985**, *811*, 265−322. (b) Sutin, N. *Prog. Inorg. Chem*. **1983**, *30*, 441−499.

42) Stoll, S.; Schweiger, A. *J. Magn. Reson*. **2006**, *178*, 42−55.

43) (a) Mann, J. B.; Meek, T. L.; Knight, E. T.; Capitani, J. F.; Allen, L. C. *J. Am. Chem. Soc*. **2000**, *122*, 5132−5137. (b) Mann, J. B.; Meek,T. L.; Allen, L. C. *J. Am. Chem. Soc*. **2000**, *122*, 2780−2783.

44) Zhao, Y.; Truhlar, D. G. *Theor. Chem. Account* **2008**, *120*, 215-241.

45) (a) Luo, S.; Averkiev, B.; Yang, K. R.; Xu, X.; Truhlar, D. G. *J. Chem. Theory Comput.* **2014**, *10*, 102−121. (b) Khobragade, D. A.; Mahamulkar, S. G.; Pospíšil, L.; Císarová, I.; Rulíšek, L.; Jahn, U. *Chem. Eur. J.* **2012**, *18*, 12267 – 12277. (c) Kulkarni, A. D.; Truhlar, D. G. *J. Chem. Theory Comput.* **2011**, 7, 2325-2332. (d) Zhao, Y.; Truhlar, D. G. *Acc. Chem. Res.* **2008**, *41*, 157-167.

46) Rulíšek, L. *J. Phys. Chem. C* **2013**, *117*, 16871−16877.

47) Weigend, F. and Ahlrichs, R. *Phys. Chem. Chem. Phys.*, **2005**, *7*, 3297-3305.

48) Scalmani G., Frisch, M. J. *J. Chem. Phys.*, **2010**, *132*, 114110-114124.

49) Gaussian 09, Revision B.01, Frisch, M. J.; Trucks, G. W.; Schlegel, H. B.; Scuseria, G. E.; Robb, M. A.; Cheeseman, J. R.; Scalmani, G.; Barone, V.; Mennucci, B.; Petersson, G. A.; Nakatsuji, H.; Caricato, M.; Li, X.; Hratchian, H. P.; Izmaylov, A. F.; Bloino, J.; Zheng, G.; Sonnenberg, J. L.; Hada, M.; Ehara, M.; Toyota, K.; Fukuda, R.; Hasegawa, J.; Ishida, M.; Nakajima, T.; Honda, Y.; Kitao, O.; Nakai, H.; Vreven, T.; Montgomery, Jr., J. A.; Peralta, J. E.; Ogliaro, F.; Bearpark, M.; Heyd, J. J.; Brothers, E.; Kudin, K. N.; Staroverov, V. N.; Kobayashi, R.; Normand, J.; Raghavachari, K.; Rendell, A.; Burant, J. C.; Iyengar, S. S.; Tomasi, J.; Cossi, M.; Rega, N.; Millam, J. M.; Klene, M.; Knox, J. E.; Cross, J. B.; Bakken, V.; Adamo, C.; Jaramillo, J.; Gomperts, R.; Stratmann, R. E.; Yazyev, O.; Austin, A. J.; Cammi, R.; Pomelli, C.; Ochterski, J. W.; Martin, R. L.; Morokuma, K.; Zakrzewski, V. G.; Voth, G. A.; Salvador, P.; Dannenberg, J. J.; Dapprich, S.; Daniels, A. D.; Farkas, Ö.; Foresman, J. B.; Ortiz, J. V.; Cioslowski, J.; Fox, D. J. Gaussian, Inc., Wallingford CT, 2009.

50) (a) Casida, M. E.; Jamorski, C.; Casida, K. C.; Salahub, D. R. *J. Chem. Phys.*, **1998**, *108*, 4439-4449. (b) Scalmani, G.; Frisch, M. J.; Mennucci, B.; Tomasi, J.; Cammi, R.; Barone, V. *J. Chem. Phys.*, **2006**, *124*, 094107: 1-15.

51) Noodleman, L. *J. Chem. Phys.* **1981**, *74*, 5737-5743.

52) (a) Kelly, C. P.; Cramer, C. J.; Truhlar, D. G. *J. Phys. Chem. B* **2007**, 111, 408−422 (b) Winget, P.; Cramer, C. J.; Truhlar, D. G. *Theor. Chem. Acc.* **2004**, *112*, 217−227.

53) Underhill, A. E.; Billing, D. E.; *Nature* **1966**, *210*, 834-835.

CHAPTER 3

1) Elmisz, J.; Herrmann, C. *Chem. Commun*., **2013**, *49*, 10456.

2) Barbara, P. F.; Meyer, T. J.; Ratner, M. A. *J. Phys. Chem*. **1996**, *100*, 13148.

3) *Chem. Rev*. **1992**, *92*, 369. Themed issue for ET process in biologically relevant systems.

4) Tolbert, L. M.; Zhao, X.; Ding, Y.; Bottomley, L. A. *J. Am. Chem. Soc.* **1995**, *117*, 12891.

5) Jiang, B.; Yang, S. W.; Bailey, S. L.; Hermans, L. G.; Niver, R. A.; Bolcar, M. A.; Jones, W. E. *Coord. Chem. Re*v. **1998**, *171*, 365.

6) Tour, J. M.; Kozaki, M.; Seminario, J. M. *J. Am. Chem. Soc.***1998**, *120*, 8486.

7) Davies, W. B.; Svec, W. A.; Ratner, M. A.; Wasielewski, M. R. *Nature* **1998**, *396*, 60.

8) Liddle, B. J.; Wanniarachchi, S.; Hewage, J. S.; Lindeman, S. V.; Bennett, B.; Gardinier, J. R. *Inorg. Chem*. **2012**, *51*, 12720.

9) Hewage, J. S.; Wanniarachchi, S.; Morin, T. J.; Liddle, B. J.; Banaszynski, M.; Lindeman, S. V.; Bennett, B; Gardinier, J. R. *Inorg. Chem*. **2014**, *53*, 10070.

10) Wanniarachchi, S.; Liddle, N. J.; Toussaint, J.; Lindeman, S. V.; Bennett, B.; Gardinier, J. R. *Dalton Trans*., **2010**, *39*, 3167.

11) Wanniarachchi, S.; Liddle, N. J.; Toussaint, J.; Lindeman, S. V.; Bennett, B.; Gardinier, J. R. *Dalton Trans*., **2011**, *40*, 8776.

12) Wanniarachchi, S.; Liddle, B. J.; Kizer, B.; Hewage, J. S.; Lindeman, S. V.; Gardinier, J. R, *Inorg. Chem*. **2012**, *51*, 10572.

13) Cao, Z.; Xi, B.; Jodoin, D. S.; Zhang, L.; Cummings, S. P.; Gao, Y.; Tyler, S. F.; Fanwick, P. E.; Crutchley, R. J.; Ren, T. *J. Am. Chem. Soc*. **2014**, *136*, 12174.

14) Fitzgerald, E. C.; Brown, N. J.; Edge, R.; Helliwell, M.; Roberts, H. N.; Tuna, F.; Beeby, A.; Collison, D.; Low, P. J.; Whiteley, M. W. *Organometallics* **2012**, *31*, 157.

15) Wang, L.; Yang, W. W.; Zheng, R.; Shi, Q.; Zhong, Y.; Yao, J. *Inorg. Chem.* **2011**, *50*, 7074.

16) Zhang, D.; Wang, J.; Wen, H.; Chen, Z. *Organometallics* **2014**, *33*, 4738.

17) Xiao, X.; Liu, C. Y.; He, Q.; Han, M. J.; Meng, M.; Lei, H.; Lu.X. *Inorg. Chem.* **2013**, *52*, 12624.

18) Brunschwig, B. S.; Creutz, C.; Sutin, N. *Chem. Soc. Rev*., **2002**, *31*, 168.

19) Rathore, R.; Burns, C. L.; Deselinescu, M. I.; Denmark, S. E.; Bui, T. *Org. Synth*. **2005**, *82*, 1.

20) (a) Hush, N. S. *Prog. Inorg. Chem*. **1967**, *8*, 391. (b) Hush, N. S. *Coord. Chem. Rev*. **1985**, *64*, 135.

21) Robin, M.; Day, P. *Adv. Inorg. Radiochem*. **1967**, *10*, 247.

22) (a) Crutchley, R. J. *Adv. Inorg. Chem*. **1994**, *41*, 273. (b) Brunschwig, B. S.; Creutz, C.; Sutin, N. *Chem. Soc. Rev*. **2002**, *31*, 168.

23) (a) Marcus, R. A.; Sutin, N. *Biochim. Biophys. Acta*. **1985**, *811*, 265. (b) Sutin, N. *Prog. Inorg. Chem*. **1983**, *30*, 441.

CHAPTER 4

1) Ning, Z.; Tian, H. *Chem. Commun*. **2009**, 5483.

2) Kaim, W.; Sarkar, B. *Coord. Chem. Rev*. **2007**, *251*, 584.

3) Kaim, W.; Lahiri, G. K. *Angew. Chem. Int. Ed*. **2007**, *46*, 1778.

4) Launay, J. P. *Coord. Chem. Rev*. **2013**, *257*, 1544.

5) Terada, K.; Kanaizuka, K.; Iyer, V. M; Sannodo, M.; Saito, S.; Kobayashi, K.; Haga, M.A. *Angew. Chem., Int. Ed*. **2011**, *50*, 6287.

6) Lambert, C.; Noll, G. *Angew. Chem., Int. Ed.* **1998**, *37*, 2107.

7) Lambert, C.; Noll, G. *J. Am. Chem. Soc.* **1999**, *121*, 8434.

8) Lambert, C.; Noll, G. *Chem. Eur. J.* **2002**, *8*, 3467.

9) Barlow, S.; Risko, C.; Chung, S.; Tucker, N. M.; Coropceanu, V.; Jones, S. C.; Levi, Z.; Bredas, J. L.; Marder, S. R. *J. Am. Chem. Soc*. **2005**, *127*, 16900.

10) Zhou, G.;Baumgarten, M.; Mullen, K. *J. Am. Chem. Soc*. **2007**, *129*, 12211.

11) Barlow, S.; Risko, C.; Odom, S. A.; Zheng, S.; Coropceanu, V.; Beverina, L.; Bredas, J. L.; Marder, S. R. *J. Am. Chem. Soc*. **2012**, *134*, 10146.

12) Rak, S. F.; Miller, L. L. *J. Am. Chem. Soc.* **1992**, *114*, 1388.

13) Gautier, N.; Dumur, F.; Lloveras, V.; Vidal-Gancedo, J.; Veciana, J.; Rovira, C.; Hudhomme, P. *Angew. Chem. Int. Ed.* 2003, 42, 2765.

14) Nelsen, S. F.; Konradsson, A. E.; Weaver, M. N.; Telo, J. P. *J. Am. Chem. Soc.* **2003**, *125*, 12493.

15) Nelsen, S. F.; Weaver, M. N.; Zink, J. I. *J. Am. Chem. Soc.* **2005**, *127*, 10611.

16) Johnson, R.; Hupp, J. T. *J. Am. Chem. Soc.* **2001**, *123*, 2053.

17) Nelsen, S. F.; Trieber, D. A., II; Ismagilov, R. F.; Teki, Y. *J. Am. Chem. Soc*. **2001**, *123*, 5684.

18) Liddle, B. J.; Silva, R. M.; Morin, T. J.; Macedo, F. P.; Shuckla, R.; Lindeman, S. V.; Gardinier, J. R. *J. Org. Chem*. **2007**, *39*, 3167.

19) Hewage, J. S.; Wanniarachchi, S.; Morin, T. J.; Liddle, B. J.; Banaszynki, M.; Lindeman, S. V.; Bennett, B; Gardinier, J. R. *Inorg. Chem.* **2014**, *53*, 10070.

20) Wanniarachchi, S.; Liddle, B. J.; Toussaint, J.; Lindeman, S. V.; Bennett, B.; Gardinier, J. R. *Dalton Trans.* **2010**, *39*, 3167.

21) Wanniarachchi, S.; Liddle, B. J.; Toussaint, J.; Lindeman, S. V.; Bennett, B.; Gardinier, J. R. *Dalton Trans.* **2011**, *40*, 8776.

22) Wanniarachchi, S.; Liddle, B. J.; Lindeman, S. V.; Gardinier, J. R. *J. Organomet. Chem.* **2011**, *696*, 3623.

23) Radosevich, A. T.; Melnick, J. G.; Stoian, S. A.; Bacciu, D.; Chen, C.; Foxman, B. M.; Ozerov, O. V.; Nocera, D. G. *Inorg. Chem.* **2009**, *48*, 9214.

24) Chong, D.; Laws, D. R.; Nafady, A.; Costa, P. J.; Rheingold, A. L.; Calhorda, M. J.; Geiger, W. E. *J. Am. Chem. Soc.* **2008**, *130*, 2692.

25) Robin, M.; Day, P. *Adv. Inorg. Radiochem.* **1967**, *10*, 247.

26) Liddle, B. J.; Wanniarachchi, S.; Hewage, J. S.; Lindeman, S. V.; Bennett, B.; Gardinier, J. R. *Inorg. Chem.* **2012**, *51*, 12720.

27) Hush, N. S. *Prog. Inorg. Chem.* **1967**, *8*, 391.

28) Hush, N. S. *Coord. Chem. Rev.* **1985**, *64*, 135.

29) (a) Marcus, R. A. *J. Chem. Phys.* **1956**, *24*, 966–978. (b) Marcus, R. A.; Sutin, N. *Biochim. Biophys. Acta* **1985**, *811*, 265.

30) Heckmann, A.; Lambert, C. *Angew. Chem. Int. Ed*, **2012**, *51*, 326.

31) a) Xiao, X.; Liu, C. Y.; He, Q.; Han, M. J.; Meng, M.; Lei, H.; Lu, X. *Inorg. Chem.* **2013**, *52*, 12626. b) Xiao, X.; Meng, M.; Lei, H.; Liu, C. Y. *J. Phys. Chem. C* **2014**, *118*, 8308.

32) a) Banerjee, M.; Shukla, R.; Rathore, R. *J. Am. Chem. Soc.* **2009**, *131*, 1780. b) Talipov, M. R.; Boddeda, A.; Timerghazin, Q. K.; Rathore, R. *J. Phys. Chem. C.* **2014**, *118*, 21400.

33) Schmidt,S. P.; Trongler, W. C.; Basolo, F. *Inorg. Synth.*, **1990**, *28*,160.

34) Coulson; D. R.; Satek, L. C.; Grim, S. O. *Inorg. Synth.* **1990**, *28*, 107-109.

CHAPTER 5

1) Kitagawa, S.; Kiyaura, R.; Noro, S. *Angew. Chem. Int. Ed.,* **2004**, *43*, 2334.

2) Ferey, G.; *Chem. Soc. Rev*., **2008**, *37*, 191.

3) Tranchemontagne, D. J.; Mendoza-Cortes, J.; O'Keeffee, M.; Yaghi, O. M. *Chem. Soc. Rev*. **2009**, *38*, 1257.

4) Fujita, M.; Kwon, Y. J.; Washizu, S.; Ogura, K. *J. Am. Chem. Soc*. **1994**, *116*, 1151.

5) Yoshizawa, M.; Takeyama, Y.; Kusukawa, T.; Fujita, M. *Angew. Chem., Int. Ed.* **2002**, *41*, 1347.

6) Yaghi, O. M.; Li, G. M.; Li, H. L. *Nature.* **1995**, *378*, 703.

7) Li, H.; Eddaoudi, M.; O'Keeffe, M.; Yaghi, O. M. *Nature* **1999**, *402*, 276.

8) Eddaoudi, M.; Kim, J.; Rosi, N.; Vodak, D.; Wachter, J.; O'Keeffe, M.; Yaghi, O. M. *Science*. **2002**, *295*, 469.

9) Zaworotko, M. J. *Chem. Soc. Rev.* **1994**, *23*, 283.

10) Kitagawa, S.; Munakata, M.; Shimono, H.; Matuyama, S.; Masuda, H. *J. Chem. Soc*., *Dalton Trans*. **1990**, 2105.

11) Kitagawa, S.; Matsuyama, S.; Munakata, M.; Osawa, N.; Masuda, H. *J. Chem. Soc*., *Dalton Trans*. **1991**, 1717.

12) Gardner, G. B.; Venkataraman, D.; Moore, J. S.; Lee, S. *Nature* **1995**, *374*, 792.

13) Riou, D.; Roubeau, O.; Férey, G. *Micropor. Mater*. **1998**, *23*, 23

14) Shustova, N. B.; Dinca, M. *J. Am. Chem. Soc*. **2011**, *133*, 20126.

15) Wang, C.; Liu, D.; Lin, W. *J. Am. Chem. Soc*, **2013,** *135*, 13222.

16) Okubo, T.; Tanaka, N.; Kim, K. H.; Anma, H.; Seki, S.; Saeki, A.; Maekawa, M.; Kuroda-Sowa, T. *Dalton Trans.* **2011**, *40*, 2218.

17) Zhao, Y.; Hong, M.; Liang, Y.; Cao, R.; Li, W.; Weng, J.; Lu, S. *Chem. Commun*. **2001**, 1020.

18) Su, W.; Hong, M.; Weng, J.; Cao, R.; Lu, S. *Angew. Chem., Int. Ed.* **2000**, *39*, 2911.

19) Takaishi, S.; Hosoda, M.; Kajiwara, T.; Miyasaka, H.; Yamashita, M.; Nakanishi, Y.; Kitagawa, Y.; Yamaguchi, K.; Kobayashi, A.; Kitagawa, H. *Inorg. Chem.* **2008**, *48*, 9048.

20) Cook, T. R.; Zheng, Y.; Stang, P.J. *Chem. Rev.* **2013**, *113*, 734.

21) Zha, Q.; Ding, C.; Rui, X.; Xie, Y. *Cryst. Growth Des.* **2013**, *13*, 4583.

22) Burrows, A.D.; Mahon.,M. F. Renouf, C. L.; Richardson, C.; Warren, A. J.; Warren, J. E. *Dalton Trans.*, **2012**, *41*, 4153.

23) Alvaro, M.; Carbonell, E.; Ferrer, B.; Francesc, X.; Xamera, L.; Garcia, H. *Chem. Eur. J.* **2007**, *13*, 5106.

24) Coulson, D. R.; Satek, L. C.; Grim, S. O. *Inorg. Synth.* **1990**, *28*, 107.

25) Wanniarachchi, S.; Liddle, B. J.; Kizer, B.; Hewage, J. S.; Lindeman, S. V.; Gardinier, J. R. *Inorg. Chem.* **2012**, *51*, 10572.

CHAPTER 6

1) Cotton, F. A.; Feng, X.; Matusz, M.; Poli, R. *J. Am. Chem. Soc.* **1988**, *110*, 7077.

2) Archibald, S.; Alcock, N. W.; Busch, D. H.; Whitcomb, D. R. *Inorg. Chem.* **1999**, *38*, 5571.

3) Archibald, S.; Alcock, N. W.; Busch, D. H.; Whitcomb, D. R. *J. Cluster sci.* **2000**, *11*, 261.

4) Schier, A,; Schmidbaur, H. *Angew. Chem. Int. Ed*. **2015**, *54*, 746.

5) Ren, T.; Lin, C.; Amalberti, P.; Macikenas, D.; Protasiewicz, J. D.; Baum, J. C.; Gibson, T. L. *Inorg. Chem. Commun.* **1998**, *1*, 23.

6) Mohamed, A. A. *Coord. Chem. Rev*. **2010**, *254*, 1918.

7) Lane, A. C.; Vollmer, M. V.; Laber, C. H.; Megarejo, D. Y.; Chiarella, G. M.; Fackler, J. P.; Yang, X.; Baker, G. A.; Walensky, J. R. *Inorg. Chem*. **2014**, *53*, 11357.

8) Blakeslee, A. E.; Hoard, J. L. *J. Am. Chem. Soc.* **1956**, *78*, 3029.

9) Chen, X.-M.; Mak, T. C. W. *J. Chem. Soc., Dalton Trans.* **1991**, 1219.

10) Chen, X.-M.; Mak, T. C. W. *J. Chem. Soc., Dalton Trans.* **1991**, 3253.

11) Mak, T. C. W.; Yip, W.-H.; Kennard, C. H. L.; Smith, G.; O'Reilly,E. J. *J. Chem. Soc., Dalton Trans.* **1988**, 2353.

12) Smith, G.; Lynch, D. E.; Kennard, C.H. L. *Inorg. Chem.* **1996**, *35*, 2711.

13) Liddle, B. J.; Silva, R. M.; Morin, T. J.; Macedo, F. P; Shukla, R.; Lindeman, S. V.; Gardinier, J. R. *J. Org. Chem*. **2007**, *72*, 5637.

14) Gardinier, J.R.; Hewage, J. S.; Lindeman, S. V. *Inorg. Chem*. **2014**, *53*, 12108.

15) Chen, F.; Oh, S. W.; Wasilishen, R. E. *Can. J. Chem*. **2009**, *87*, 1090.

16) Geol, R. G.; Pilon, P. *Inorg. Chem*. **1978**, *17*, 2876.

17) Beck, J.; Stra¨hle, J. *Angew. Chem., Int. Ed. Engl.* **1986**, *25*, 95.

18) O'Connor, J. E.; Janusonis, G. A.; Corey, E. R. *J. Chem. Soc., Chem. Commun.* **1968**, 445.

19) Bondi, A. *J. Phys. Chem*. **1964**, *68*, 441.

20) Griffith, R.L. *J. Chem. Phys*. **1943**, *11*, 499.

21) VanSanten, R. A.; Kuipers, H. P. C. *Ad*v. *Catal.* **1987**, *35*, 265.

22) Stinson, S. *Chem. Eng. News* **1995**, *73*, 7.

23) Cui. Y.; He. C. *J. Am. Chem. Soc*. **2003**, *125*, 16202.

24) Wanniarachchi, S.; Hewage, J. S.; Lindeman, S. V.; Gardinier, J. R. *Organometallics* **2013**, *32*, 2885.

25) Yamaguchi, Y.; Yamanishi, K.; Kondo, M.; Tsukada, N. *Organometallics* **2013**, *32*, 4837.

26) Coulson, D. R.; Satek, L. C.; Grim, S. O. *Inorg. Synth*. **1990**, *28*, 107.

27) Yamada, Y.; Yamamoto, T.; Okawara, N. *Chem. Let*. **1975**, 361.

28) Uson, R.; Laguna, A.; Laguna, M.; Briggs, D. A.; Murray, H. H.; Fackler, J. P. *Inorg. Synth*. **1989**, *26*, 86.

29) Maestre, L.; Sameera, W. M. C.; Diaz-Requejo, M. M.; Maseras, F.; Perez, P. J. *J. Am. Chem. Soc.* **2013**, *135*, 1338.

30) Kulkarni, N. V.; Elkin, T.; Tumaniski, B.; Botoshansky, M.; Shimon, J. W.; Eisen, M. S. *Organometallics* **2014**, *33*, 3119.

31) Wanniarachchi, S.; Hewage, J. S.; Lindeman, S. V.; Gardinier, J. R. *Oraganometallics* **2013**, *32*, 2885.